

Development of AI based controller to improve performance of Wind Driven DFIG



Debirupa Hore

Department of Electrical and Instrumentation Engineering

Gauhati University

(Assam Engineering College)

Under Guidance of

Prof Dr.RunumiSarma

This thesis is submitted to

Gauhati University as requirement for the degree of

Doctor of Philosophy

Faculty of Engineering
January 2018

Dedication

*I would like to dedicate this thesis to my loving parents
and my dear husband and daughter*

Declaration

I hereby declare that this thesis is the result of my own research work which has been carried out under the guidance of Prof Dr.RunumiSarma of (Assam Engineering College, Jhalukbari), Gauhati University. I further declare that this thesis as a whole or any part thereof has not been submitted to any university (or institute) for the award of any degree or diploma. This thesis contains less than 90,000 (ninety thousand) words excluding bibliography and captions.

Debirupa Hore

January 2018

Certificate

This is to certify that the thesis titled “Development of AI based controller to improve performance of Wind Driven DFIG “is the result of research work of Debirupa Hore carried under my supervision, submitted to Gauhati University for the award of the degree of Doctor of Philosophy in Electrical Engineering under Faculty of Engineering. This thesis conforms to the standard of PhD Thesis under Gauhati University including the standard related to plagiarism and has a similarity index not more than 20% (twenty per cent), excluding the bibliography.

Prof Dr.RunumiSarma, Supervisor

January 2018

Members of the Research Advisory Committee (DRC):

- 1.
- 2.
- 3.

Acknowledgements

I would like to acknowledge my Supervisor Prof Dr.RunumiSarma Professor Electrical and Instrumentation Engineering Department, Assam Engineering College for her immense support, guidance and ideas for carrying my research work. I would also like to acknowledge our HOD Electrical Engineering Department Prof Dr.DamodarAgarwal Sir, Assam Engineering College for the support and encouragement provided during my research work. I would also like to thank Prof Dr D. Hazarika sir as well as all the faculties of Electrical Engineering Department, Assam Engineering College for showing path and for their support in carrying my research work.

I would also like to thank and acknowledge Librarian, Laboratory assistant and other staffs of Assam Engineering College for their immense support.

Abbreviation

DFIG	Double fed Induction generator
AI	Artificial Intelligence
PWM	Pulse width modulation
RSC	Rotor side converter
GSC	Grid Side converter
ANN	Artificial Neural Network
FL	Fuzzy Logic
ANFIS	Adaptive Neuro- Fuzzy System
WT	Wind Turbine
FIS	Fuzzy Inference System
THD	Total Harmonic Disorder
CEA	Central Electricity Authority
FFC	Feed Forward controller

Abstract

This research work proposes an innovative control strategy for a vector controlled wind turbine driven DFIG during dynamic conditions. The main objective of the presented system is to maximize the stator active power generation with least voltage and frequency disturbances during normal and fault conditions. For this the active and reactive power generation of the system is controlled with the aid of active power PI controller and reactive power PI controller with vector controlled scheme on both the converters for its decouple control along with hysteresis PWM current control method. The generated stator active power produced tracks the reference power from MPPT. The control strategy used during fault conditions is controlling the negative sequence stator flux during fault by controlling the d and q axis rotor current which can be controlled by using stator active and reactive power of the system. The Control scheme used is stator flux oriented control for rotor side converter control and grid voltage vector control for grid side converter control. Then an ANN and ANFIS based active and reactive power controller is also designed and used in lieu of the conventional PI controller. A comparative analysis shows that the performance of the DFIG improves significantly using AI based controllers. The design and training parameters of the two types of AI technique based controllers are also presented. The entire model is simulated in MATLAB/Simulink environment.

Table of Contents

Particular Page No.

List of figures VI

List of tables VII

Chapter 1: Introduction 1

1.1 Introduction to Wind Energy8

1.2 General 4

1.3 Wind Energy Scenario 5

1.4 Objective of the proposed work 7

1.5 Literature review 8

1.6 Motivation towards the work18

1.7 Outline of the Various Chapters of the Thesis19

Chapter 2: Modelling of overall wind energy conversion systems21

2.1 Modelling of Wind turbine21

2.1.1 The turbine equations21

2.1.1.1 Tip speed ratio21

2.1.1.2 Power extracted from the wind22

2.1.1.3 Performance coefficient22

2.1.2 Flow chart (s-function block) for

Maximum power point tracking	23	
2.2 Modelling of Double fed Induction Generator	23	
3.2.1 Fifth order Generator Model		24
2.3 Rotor side converter control strategy	30	
2.3.1 Rotor side converter control	30	
2.3.2 The active and reactive power equations	31	
2.3.3 Active power and reactive power control loop design	33	
2.3.4 Stator flux oriented vector control scheme	33	
2.4 Grid side converter control strategy	36	
2.4.1 Supply voltage oriented vector control scheme		37
2.5 Modelling of dc link voltage	38	
2.6 Modelling of overall system	39	
Chapter 3: Double fed Induction Generator Under fault conditions		41
3.1 Principle of operation of wind energy driven DFIG		41
3.2 Advantages of Variable Speed Wind driven DFIG	43	
3.3 Different modes of operation	43	
3.3.1: Sub-synchronous Motoring	44	
3.3.2: Sub-Synchronous Regeneration	44	
3.3.3 Super synchronous Motoring	44	
3.3.4 Super synchronous Regeneration	44	
3.4 Types of Conversion Systems	45	
3.4.1 Fixed speed operation	45	
3.4.2 Variable speed WECS with squirrel cage induction generator		46
3.4.3 Variable speed WECS with wound rotor induction generator		46
3.5 Study of Transients in Wind driven double fed Induction Generator	47	
3.5.1 After Clearance of the Fault	49	
3.5.2 Unbalanced Network Voltage Unbalanced Network Voltage	49	
3.6 Grid Codes for Wind Generating Station in India	50	
3.6.1 Grid behaviour of wind turbines	50	
3.6.2 The grid codes for wind, in general deal with the following issues	51	
3.6.1.1 Active power control		51
3.6.1.2 Frequency requirements		51
3.6.1.3 Fault / low voltage ride through		52
3.6.1.4 Data requirements	53	
3.6.1.5 Power quality issues like flicker, harmonics etc		53
3.6.3 Indian Wind Grid Code	53	
3.6.4 Connection code for wind farms	54	
3.6.4.1 Transmission voltage range	54	

3.6.4.2 Voltage unbalances	54	
3.6.4.3 Reactive Power Capability		55
3.6.4.4 Frequency tolerance limit		55
3.6.4.5 Active power control		55
3.6.4.6 Low Voltage ride through		56
Chapter 4: Control Strategy used for grid fault ride through		58
4.1 Control Strategy	58	
4.2 Controllers Used in the system	63	
4.3 Basic Real and Reactive Power control on GSC	64	
4.3.1: Sequence Impedance during fault	65	
4.4 Calculation of Total Harmonic distortion (THD)	66	
4.5 Design of PWM Inverter	66	
4.5.1 Hysteresis band current control PWM Technique		66
4.5.2 Converter output (AC side) considering isolated neutral		67
4.5.3 Flowchart for S-function coding of rotor and supply side converters	69	
Chapter 5: Design of Conventional Controllers		70
5.1 Design of PI controllers		70
5.1.1 Trial and Error method		70
5.1.2 Stability Criteria of PI controller		73
5.2 Design of Proportional Resonant Controller		74
5.2.1 Control of Rotor Side Converter	74	
5.2.2. Control of Grid Side Converter	77	
5.3 Design of PR Controller	79	
5.3.1 Stability Analysis	81	
Chapter 6: Design of AI Based Controller		88
6.1 Advantages of Neural Network	88	
6.1.1 Back Propagation Algorithm	88	
6.1.2. Local Minima	92	
6.1.3 Gradient Descent Learning	93	
6.1.4 The Levenberg–Marquardt algorithm	94	
6.1.4.1 Derivation of Levenberg–Marquardt algorithm		95
6.1.4.2 Calculation of Jacobian Matrix	98	
6.1.4.3 Algorithm of Levenberg Marquardt Method		99
6.1.5 Training Algorithms	100	
6.2 Design of Neural Network based controller	101	
6.2.1 ANN Controller Architecture	103	
6.2.1.1 ANN based Active Power controller		103
6.2.1.2 ANN based reactive power controller		104

6.2.1.3 Grid side ANN based DC Voltage controller	104
6.2.2 Steps used for design of ANN Controller	105
6.3 Design of ANFIS Controller	109
6.3.1 Fuzzy Inference Systems	110
6.3.2 Sugeno-Type Fuzzy Inference System	112
6.3.3 Adaptive Neuro-Fuzzy Inference System	113
6.4 Steps of ANFIS Controllers design	115
6.4.1. The steps incorporated in ANFIS MATLAB toolbox	118

Chapter: 7: Results and Simulations

7.1 Characteristics performance output of 5th order- Double fed Induction Generator Model at particular wind Speed	125
7.1.1 Performance output of DFIG at wind Velocity 6m/sec	125
7.1.2 Performance output of DFIG at rated wind velocity	126
7.1.3 Performance showing the Mechanical Power output from Wind Turbine	127
7.1.4 PWM Inverter Voltage output on Rotor Side Converter and torque angle delta	127
7.2 Results of DFIG Showing Synchronization of Grid Voltage and Stator Flux	128
7.3 Performance Showing the Harmonics (THD) in different waveforms using different types of Controller	129
7.3.1 Performance of DFIG Showing the Power Factor on the Stator side and GSC side and interaction factor	131
7.4 Performance of DFIG using conventional PI-Controller under Normal Operation	133
7.4.1 Performance of DFIG for constant wind velocity (6 m/sec)	133
7.4.2 Performance of DFIG for step change in wind velocity under normal condition (5m/sec to 7m/sec).	134
7.4.3 Performance of DFIG for ramp change in wind velocity under normal condition (5m/sec to 7m/sec)	136
7.4.4 Performance of DFIG from sub-synchronous mode to super synchronous mode of operation using conventional PI controller.	138
7.5 Performance of DFIG using ANN Controller under Normal operation	139
7.5.1 Performance of DFIG for constant wind Speed 6 m/sec	139
7.5.2 Performance of DFIG for Step Variation of wind Speed from (5 m/sec to 7m/sec)	141

7.5.3 Performance of DFIG for Ramp Variation of wind Speed from (5 m/sec to 7m/sec)	143
7.6 Performance Characteristics of DFIG during Unsymmetrical Faults for (Line to Line Fault)	148
7.6.1 Performance Characteristics of DFIG during Unsymmetrical Faults (Line to Line) fault using PI controller	146
7.6.2 Performance of DFIG Using ANN Controller	147
7.6.2.1 Performance of DFIG For constant Speed 6m/sec for Line to Line fault during Neural Network	147
7.6.2.2 Performance of DFIG for Step change in Speed 5m/sec to 7m/sec for Line to Line fault using Neural Network controller	149
7.6.2.3 Performance of DFIG for Ramp change in Speed 5m/sec to 7m/sec for Line to Line fault using Neural Network controller	150
7.6.3 Performance Characteristics of DFIG during Unsymmetrical Faults for (Line to Ground Fault)	152
7.6.3.1 Performance of DFIG during LG Fault for Constant Speed (6m/sec) using Neural Network Based Controller	154
7.6.3.2 Performance of DFIG during LG Fault for Step change in Speed using Neural Network Based Controller	155
7.6.3.3 Performance of DFIG during LG Fault for Ramp change in Speed using Neural Network Based Controller	156
7.7 Performance of DFIG Using ANFIS Controller	157
7.7.1 Performance of DFIG during (L-L) Fault for Constant wind Speed	157
7.7.2 Performance of DFIG during Line to Ground Fault for Constant wind Speed using ANFIS Controller	158
7.7.3 Performance of DFIG during Line to Line Fault for Step change in wind Speed using ANFIS Controller	159
7.7.4 Performance of DFIG during Line to Ground Fault for Step change in wind Speed using ANFIS Controller	160
7.7.5 Performance of DFIG during Line to Ground Fault for Ramp change in wind Speed using ANFIS Controller	161
7.7.6 Performance of DFIG during Line to Line Fault for ramp change in wind Speed using ANFIS Controller	162
7.8 Comparative Analysis of PI Controller and Neural Network	

Controller	163
7.8.1 During Line to Line Fault at Constant Wind Velocity (6m/sec)	163
7.8.2 Performance during Line to Line Fault for Step Change of Wind Velocity (5m/sec to 7m/sec)	164
7.8.3 Performance during (L-L) ramp change of Wind Velocity (5m/sec to 7m/sec)	165
7.9 Comparative Analysis of Performance between ANFIS Controller and Neural Network based Controller	167
7.9.1 Performance Comparison at Constant Wind Velocity (6m/sec) for (LL fault)	167
7.9.2 Performance Comparison of DFIG for Step change of Wind Velocity (5m/sec to 7m/sec) (L-L Fault)	168
7.9.3 Performance Comparison of DFIG for Ramp change of wind Velocity (5m/se to 7m/sec) (LL fault).	169
7.10 Performance Comparison between PI Controller and Neural Network based Controller (LG fault)	170
7.11 Performance of DFIG during Symmetrical Voltage dips of 15% using ANN controller.	171
7.12 Performance of DFIG for symmetrical voltage dips of 85% using PI controller.	172
7.13 Performance of DFIG for symmetrical Voltage dip of 85% using ANN controller.	173
7.14 Performance of DFIG for symmetrical Voltage dip of 85% using ANFIS controller	174
7.15 Performance Response of DFIG during Single Line to ground fault using PR Controller	175
7.12 Discussion	176
Chapter 8: Conclusion	
8.1 Conclusion	178
8.2 Future Scope	178
References	179
Appendixes	181

LIST OF NOMENCLATURE

The symbols used in the text have been defined at appropriate places, however, for easy reference, the list of common symbols are being given below. Some symbols used in a particular chapter have been defined in that chapter alone.

V_{as}, V_{bs}, V_{cs} : are the three phase supply voltages

V_s, V_r : are the RMS stator and rotor voltages

D, Q : are the Direct and quadrature axis Stationary reference frame
or stator natural reference frame.

α, β : are the Rotor natural reference frame rotating at a speed of ω_r

x, y : are the Stator flux oriented reference frames

ϕ_R : Rotor angular position

ϕ_s : Stator side Power factor angle

$\cos\phi_{sref}$: Stator side power factor

f_s : The Grid frequency

$[I_{ms}]$: Stator magnetizing current space phasor modulus.

I_{msD}, I_{msQ} : d and q axis stator magnetizing current Components respectively, expressed in the stationary reference frame.

I_{rd}, I_{rq} : The direct- and quadrature-axis rotor current components respectively, expressed in the stationary reference frame.

I_{rx}, I_{ry} : The direct- and quadrature-axis rotor current components respectively, expressed in the stator-flux-oriented reference frame.

I_{ra}, I_{ra} : The direct- and quadrature-axis rotor current components respectively, expressed in the rotor natural reference frame.

I_sD, I_sQ : The direct- and quadrature-axis stator current components respectively, expressed in the stationary reference frame.

I_{sx}, I_{sy} : The direct- and quadrature-axis stator current components respectively, expressed in the stator-flux-oriented reference frame.

K_P, K_I : The PI compensator parameters.

L_m : is the Magnetizing inductance

L_r, L_s : are the Rotor and stator inductances, respectively

L_r' : is the Rotor transient inductance

P_r, Q_r : Rotor side active and reactive powers, respectively

P_s, P_{sref} : Stator side active power actual and reference values, respectively

Q_s, Q_{sref} : Stator side reactive power actual and reference values, respectively

R_s, R_r : Stator and rotor phase winding resistances, respectively

V_{rx}, V_{ry} : Direct- and quadrature-axis rotor voltage components, respectively, expressed in the stator-flux-oriented reference frame.

$V_{r\alpha}, V_{r\beta}$: Direct- and quadrature-axis rotor voltage components respectively, expressed in the rotor natural reference frame.

$|V_s|$: is Stator voltage space phasor modulus.

$V_s D, V_s Q$: Direct- and quadrature-axis stator voltage components, respectively, expressed in the stationary reference frame

V_{sx}, V_{sy} : Direct- and quadrature-axis stator voltage components, respectively, expressed in the stator flux oriented reference frame.

$V_{r\alpha}, V_{r\beta}$: Direct- and quadrature-axis rotor voltage components respectively, expressed in the rotor natural reference frame.

θ_r : is the Rotor electrical angle.

ρ_s : is the phase angle of stator flux-linkage space phasor with respect to the direct-axis of the stationary reference frame.

ω_{sl} : Angular slip frequency.

ω_r : is the rotor electrical speed.

ω_r, ω_{rt} : Rotor angular speed referred to generator and Turbine side respectively.

ω_b : Rotor angular base speed (generator side).

ω_s : Grid/Supply side angular frequency.

$\lambda_{sD}, \lambda_{sQ}$: are d and q axis flux in stationary reference frame.

I_x, I_y : are d and q axis current between grid and grid side converter in supply voltage reference frame

V_x, V_y : are the d and q axis Supply voltage in supply voltage reference frame

T_{em} : Electromagnetic Torque
 T_{mech} : Mechanical Torque
 D : Damping Co-efficient
 ω_r : represents the rotational speed of the wind turbine.
 C_p, θ : are the Power coefficient, pitch angle
 V : Wind speed;
 λ : Tip speed ratio;
 ρ : The air density (in Kg/m^3);
 R : The radius of the turbine propeller;
 A_r : Blade swept Area of the wind turbine
 E : The DC link voltage
 R, L, C : is the Resistance, Inductance, capacitance of grid side converter filter. respectively.
 P_{dc} : is DC link Power
 I_{dc} : is DC current
 H, J : are inertia constant and moment of inertia
 P : is the Number of poles
 I_{as}, I_{bs}, I_{cs} : are the three phase current
 $I_{agrid}, I_{bgrid}, I_{cgrid}$: are the three phase current between grid and grid side converter
 V_{conx}, V_{cony} : The d and q axis Converter output voltage in supply voltage reference frame.
 I_{rxref}, I_{ryref} : are the reference values of the rotor current in stator-flux-oriented reference frame.

List of Figures

FigureTitle

- Figure: 1.1:** Pie diagram showing different Energy production
- Figure: 1.2:** World energy scenarios
- Figure 1.3:** India's Energy Basket

- Figure: 2. 1:** Modelling of wind turbine
- Figure 2.2:** Stator and rotor side reference frames for the “Quadrature phase Slip Ring” model
- Figure: 2.3:** Modelling of d axis stator current
- Figure 2.4:** Modelling of q axis stator current
- Figure 2.5:** Modelling of d-axis rotor current
- Figure 2.6:** Modelling of q-axis rotor current
- Figure 2.7:** Modelling of DFIG with stator and rotor quantities in natural reference frame
- Figure 2.8:** Block diagram of the stator flux oriented vector control scheme for rotor Side converter
- Figure 2.9:** Modelling of rotor side converter using conventional PI controller
- Figure 2.10:** Scheme for grid side converter control
- Figure 2.11:** Modelling of grid side converter
- Figure 2.12:** Modelling of dc link voltage
- Figure 2.13:** Modelling of overall system
- Figure 3.1:** Principle of operation of wind energy driven DFIG
- Figure 3.2:** Variable speed WECS with squirrel cage induction generator
- Figure 3.3:** Variable speed WECS with wound rotor induction generator
- Figure 3.4:** Variation of active power output of wind farms with respect to frequency
- Figure 3.5:** Fault ride through characteristics
- Figure: 4.1:** Control Strategy Scheme for DFIG
- Figure 4.2:** Control of rotor current
- Figure: 4.3:** Observation of components in stator-flux linkage
- Figure 4.4(a):** Scheme for Active Power Controller
- Figure 4.4(b):** Reactive Power Controller
- Figure 4.4 (C):** DC Voltage Controller
- Figure 4.5:** Single line diagram of GSC connected to the grid and phasor diagram showing load angle
- Figure 4.6:** Harmonics of different Order representation
- Figure 4.7:** Principle of operation of Hysteresis current controlled PWM Technique
- Figure 4.8:** Equivalent circuit indicating voltage between the neutral points

Figure 4.9:Simulation Model for extraction of Positive, Negative and Zero Sequence Flux

Figure 5.1: Schematic Showing PI Controllers

Figure 5.2: Closed Loop block diagram using PI controller

Figure 5.3: Bode plot for closed loop System using PI controller

Figure 5.4: Pole-Zero plots for closed loop System using PI controller

Figure 5.5:Conventional control scheme for the rotor side converter with FFC

Figure 5.6: Improved control scheme for the rotor side converter with transient FFC

Figure 5.7:Improved control scheme for the grid side converter with transient FFC

Figure 5.8: PR Current Controller

Figure 5.9: Bode Plot for Closed Loop PR Controller

Figure 5.10: Pole-Zero Plots for Closed Loop PR Controller

Figure 5.11: Root Locus Plot for Closed Loop PR Controller

Figure 5.12: Bode Plot for Closed Loop PR Controller

Figure 5.13: Pole-Zero Plots for Closed Loop PR Controller

Figure 5.14: Root Locus Plot for Closed Loop PR Controller

Figure 5.15: Schematic diagrams of the proposed current controllers for the GSC and RSC

Figure 6.1: Gradient Descent Learning

Figure 6.2: ANN Architecture

Figure 6.3: Neural Network Training in MATLAB showing hidden layers

Figure 6.4:Neural Network Training in MATLAB showing training parameters

Figure 6.5: Convergence of ANN network.

Figure 6.6:Simulation block of ANN

Figure 6.7(a): Active Power ANN Controller

Figure 6.7(b):Reactive Power ANN Controller

Figure 6.8:Simulation Model of Rotor Side Converter Using Neural Network Controller

Figure 6.9:Simulation Model of Grid Side Converter Using Neural Network Controller

Figure 6.10: Block diagram showing various parts of Fuzzy Logic System

Figure 6.11: ANFIS Architecture

Figure 6.12: ANFIS FIS System

- Figure 6.13:** ANFIS FIS system showing Inputs and output
- Figure 6.14:** ANFIS system showing membership functions for first input
- Figure 6.15:** ANFIS FIS system showing membership functions for Second Input
- Figure 6.16:** ANFIS FIS system showing output function
- Figure 6.17:** ANFIS FIS system Rules for Inputs and outputs
- Figure 6.18:** ANFIS FIS system showing convergence
- Figure 6.19:** ANFIS FIS Rule View
- Figure 6.19:** ANFIS FIS Rules
- Figure 6.20:** Training Data for AI controllers from PI Controller
- Figure 6.21:** Active Power ANFIS Controller.
- Figure 7.1:** Characteristics of Double fed Induction Generator a) Slip vs Time curve b) Slip vs Speed c) Rotor angle d) Stator Flux
- Figure 7.2:** Performance of DFIG during rated Generator Speed which is achieved at 8m/sec wind Velocity. a) Wind Velocity b) Rated generator Speed c) Rated active Power generated and reference Active Power c) Slip vs time curve.
- Figure 7.3:** Maximum Power Point Tracking of Wind Turbine under varying Wind Condition
- Figure 7.4:** Output Voltage waveform from PWM inverter on Rotor Side converter and Power angle “delta”.
- Figure 7.5:** a) Orientation of flux w.r.t Grid voltage and b) Stator voltage waveform
- Figure 7.6(a&b) :** Total Harmonic Disorder (THD) for the Stator current, Rotor Current, Stator Active Power, Generator Speed using a) PI controller b) ANN Controller
- Figure 7.6(c):** Total Harmonic Disorder (THD) for the Stator current, Rotor Current, Stator Active Power, Generator Speed using ANFIS Controller
- Figure 7.7:** The Power Factor of the DFIG on The stator Side and Grid Side of the Generator for various wind conditions.
- Figure 7.8:** Performance of DFIG during normal operation with constant wind velocity 6m/sec a) Wind Speed b) Reference Active Power c) Actual Active Power d) Actual Reactive Power.
- Figure 7.9:** Performance of DFIG during normal operation with constant wind velocity 6m/sec a) Generator rotor Speed b) DC Link Voltage.
- Figure 7.10:** Performance of DFIG during normal operation with constant wind velocity 6m/sec a) Stator Voltage b) Stator Current c) Rotor current in Stationary reference frame d) Rotor current in Natural reference frame.
- Figure 7.11:** Performance of DFIG during normal operation with Step change in wind velocity 5m/sec to 7m/sec a) Wind Speed b) Reference Active Power c) Actual Active Power d) Actual Reactive Power.

Figure 7.12: Performance of DFIG during normal operation with Step change in wind velocity 5m/sec to 7m/sec a) Generator rotor Speed b) DC Link Voltage.

Figure 7.13: Performance of DFIG during normal operation with Step change in wind velocity 5m/sec to 7m/sec a) Stator Voltage b) Stator Current c) Rotor current in Stationary reference frame.

Figure 7.14: a) Stator current in d axis b) Stator current in q axis c) Rotor current (r.m.s) d) rotor current in Natural reference frame.

Figure 7.15: Performance of DFIG during normal operation with Ramp change in wind velocity 5m/sec to 7m/sec a) Wind Speed b) Reference Active Power c) Actual Active Power d) Actual Reactive Power.

Figure 7.17: Performance of DFIG during normal operation with Ramp change in wind velocity 5m/sec to 7m/sec a) Generator rotor Speed b) DC Link Voltage.

Figure 7.18: Performance of DFIG during normal operation with Ramp change in wind velocity 5m/sec to 7m/sec a) Stator Voltage b) Stator Current c) Rotor current in Stationary reference frame.

Figure 7.19: Performance of DFIG during normal operation sub synchronous to super synchronous mode a) Wind Velocity b) Generator Speed c) Rotor current showing phase change

Figure 7.20: Performance of DFIG during constant wind velocity 6m/sec a) Wind Velocity b) Generator Speed c) DC link Voltage d) Reference stator Power e) Actual Stator power f) Reference Reactive Power g) Actual reactive Power

Figure 7.21: Performance of DFIG during constant wind velocity 6m/sec a) Supply Voltage b) Supply current c) Rotor Current

Figure 7.22: Performance of DFIG during step change in wind velocity 5m/sec to 7m/sec a) Wind Velocity b) Generator Speed c) DC link Voltage d) Reference stator Power e) Actual Stator power f) Reference Reactive Power g) Actual reactive Power

Figure 7.23: Performance of DFIG during constant wind velocity step change in wind velocity 5m/sec to 7m/sec a) Supply Voltage b) Supply current c) Rotor Current

Figure 7.24: Performance of DFIG during step change in wind velocity 5m/sec to 7m/sec a) Wind Velocity b) Generator Speed c) DC link Voltage d) Reference stator Power e) Actual Stator power f) Reference Reactive Power g) Actual reactive Power.

Figure 7.25: Performance of DFIG during constant wind velocity step change in wind velocity 5m/sec to 7m/sec a) Supply Voltage b) Supply current c) Rotor Current

Figure 7.26: Performance of DFIG showing a) Voltage magnitude b), c) d and q axis rotor current d) Power factor on GSC side e) Stator flux f), g) h) positive, negative and zero sequence Stator flux.

Figure 7.27: Performance of DFIG showing a) Wind Velocity b) Optimum Stator Power c) Actual Stator Power d) Actual reactive Power e) Generator Speed f) DC Link Voltage g) Rotor current h) Electromagnetic torque.

Figure 7.28: Performance of DFIG showing a) Voltage and Current magnitude b) d and q axis rotor current c) positive, negative sequence Stator flux.

Figure 7.29: Performance of DFIG showing a) Wind Velocity b) Generator Speed c) DC Link Voltage d) Rotor Current e) Optimum Power f) Actual Stator power g) Reference reactive power h) Actual reference power.

Figure 7.30: Performance of DFIG showing a) Wind Velocity b) Generator Speed c) DC Link Voltage d) Rotor Current e) Optimum Power f) Actual Stator power g) Reference reactive power h) Actual reference power.

Figure 7.31: Performance of DFIG showing a) Wind Velocity b) Generator Speed c) DC Link Voltage d) Rotor Current e) Optimum Power f) Actual Stator power g) Reference reactive power h) Actual reference power.

List of Tables

TableTitle

Table 3.1: Voltage withstand limits for wind farms

Table 3.2: Voltage unbalance limits for wind farms as per CEA

Table 3.3: Typical Parameters during Fault

Table 5.1: Ziegler Nichols Method

Table 5.2: Parameter for PR controller design

Table 6.1: ANN training Parameter and Architecture of the rotor side converters

Table 6.2: ANN training Parameter and Architecture of the Grid side converter

Table 6.3: ANFIS training Parameter and Architecture of the Rotor side converter controllers

Table 6.4: Hybrid Learning Algorithm

Table 7.1: Comparative data analysis

Chapter 1

Introduction

1.1 Introduction to Wind Energy

In the last few years, Nonconventional Energy sources are gaining much importance. Wind Energy sources are widely used now a day. Doubly fed induction generators (DFIGs) are widely used for power generations in Wind Turbine because of its variable speed operation. A DFIG consists of a rotor induction generator with its stator windings directly connected to the grid and its rotor windings are connected to the grid via ac/dc back-to-back PWM converters. This arrangement is cost effective as the converters are sized to handle only one third of the rated power of the Wind turbine as a result making it efficient for decoupled control of the active and reactive power. However, the major concerning factor of DFIGs is their operation during system grid faults. When the Voltage at the stator Winding drops suddenly due to grid fault there is a sudden change in the stator flux of the generator and can lead to an over current in the rotor windings. This over-current may cause severe damage to the semiconductor devices connected in the rotor side converter and large fluctuations of the dc-link voltage. If the unbalance is not taken seriously by the system, there will be high unbalance in stator current with a small amount of disturbance in stator voltage. The unbalanced currents in the windings can create unequal heating as well as disturbances in torque and power pulsation in the generator.

When DFIGs were started using in the field of wind energy systems, the penetration of Wind Turbines in the Grid System was relatively low. So their control during faults were mainly focused on the protection of the DFIG itself and no specific strategy was taken in order to provide the DFIG sufficient enough to contribute to network support during faults. So Crowbar circuits were used to protect the generator and its rotor circuit. This device consists of a bank of resistors, which is connected to the rotor windings through power electronic devices. After a fault is detected, the rotor windings are quickly connected to the crowbar resistors, and the rotor-side converter is disabled temporarily. Thus the short circuit current flows through the crowbar instead of the rotor-side converter. With this solution, the machine is effectively protected, but due to the fact

that the blocking of the rotor-side converter leads to the partial loss of power control during the crowbar action, large transients are generated after the fault, which may lead to the disconnection of the machines from the grid.

When the crowbar circuit is activated, the wind driven DFIG is converted to a conventional squirrel-cage induction generator, which can absorb a large amount of reactive power from the grid. Nowadays, as wind turbines represent a significant part of the total generation in electrical systems, system operators world-wide have revised their grid codes (GCs), making their requirements concerning the fault ride-through (FRT) capability of wind-turbines more stringent.

According to Grid code worldwide the Wind Turbine generator should provide low Voltage Ride through capability during grid faults for 85% voltage drop or more. It should be connected to the system and it contributes to the system Stability by providing reactive power to the grid during and after the faults. But this requirement cannot be fulfilled by the conventional crowbar system that was previously used for protection of DFIG. For this issue the researcher started taking the problem of FRT seriously and from several points of view.

Now a day, the control of wind turbines has been greatly improved by the introduction of power electronic device. Presently, the variable speed wind energy conversion system (WECS) equipped with doubly-fed induction generator (DFIG) with partial rated power electronic converters in the rotor circuit is the most popular and widely used scheme for the wind generation due to its several advantages. DFIG systems are conventionally controlled using either stator voltage-oriented or stator flux-oriented controls based on d-q decoupling. Most of the DFIG schemes have utilized conventional PI controllers ensuring proper functioning of its operation during the normal and abnormal conditions. However, these controllers do not perform satisfactorily under different operating conditions. Artificial intelligence (AI) techniques, such as fuzzy logic (FL), neural network (NN), and genetic algorithm (GA), ANFIS etc. are showing promising results in the different fields of engineering applications. Fuzzy logic (FL) applications to the control of power electronics and drive systems have been increasing exponentially in the past few years.

Power converter and drive systems possess inherent characteristics, such as nonlinearities, unavailability of a precise model or its excessive complexity, that make

them well suited for FL control. The fuzzy logic controller of a given system is capable of embedding in the control strategy, the qualitative knowledge and experience of an operator or field engineer about the process. In spite of its practical success, fuzzy logic has been criticized for its limitations, such as the lack of a formal design methodology, the difficulty in predicting stability and robustness of FL controlled systems. Further, in certain systems, it is difficult or sometimes impossible to define the crisp rules for control. In such situations, fuzzy rules can be used to control the system dynamics. However, sometimes, it is very difficult to define the fuzzy rules and the process of tuning the fuzzy system parameters requires long time, specifically, when the number of fuzzy rules are large.

Neural network based controllers have also been utilized as they require least computational time after training. However, to select optimal structure, parameter values and to minimize training set are some of the issues to be addressed in the neural network applications. Utilizing the advantages of both the neural network and fuzzy systems, researchers have tried to combine these two. A hybrid system can be obtained by combining fuzzy inference system and adaptive neural networks i.e. adaptive neuro-fuzzy inference system (ANFIS). ANFIS based controllers successfully implemented for several power systems and power electronics applications.

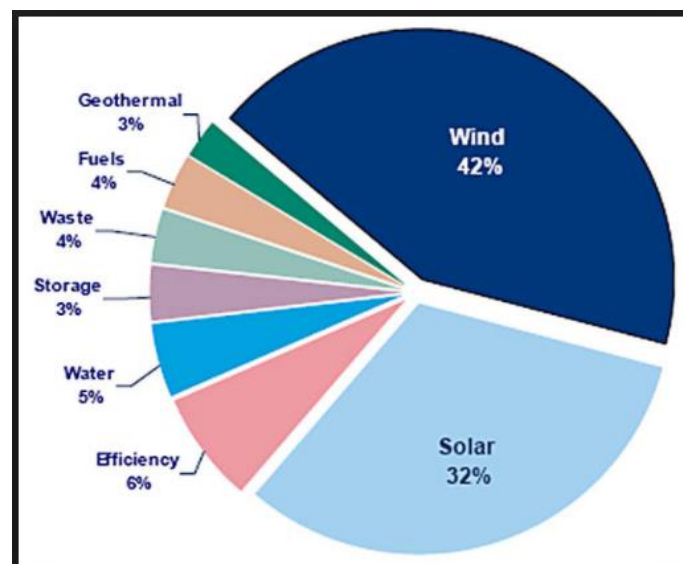


Figure: 1.1 Pie diagram showing different Energy production

1.2 General

Wind energy is one of the most important and promising extra ordinary sources of renewable energy all over the world, mainly because it is considered to be non-polluting and economically viable. At the same time, there has been a rapid development of related wind turbine technology. Nevertheless, this kind of electric power generation usually causes problems in the electrical system it is connected to, because of the lack or scarcity of control on the produced active and reactive powers. Several designs and arrangements have been implemented so as to cope with this difficulty .As far as variable-speed generation is concerned, it is necessary to produce constant-frequency electric power from a variable- speed source .This can be achieved by means of synchronous generators, provided that a static frequency converter is used to interface the machine to the grid. An alternative approach consists in using a wound-rotor induction generator fed with variable frequency rotor voltage. This allows fixed-frequency electric power to be extracted from the generator stator. Consequently, the use of DFIGs is receiving increased attention for wind generation purposes. One of the main advantages of these generators is that, decoupled control of stator side active and reactive powers is possible.

Because of several technical benefits,the modern wind turbines always use variable speed operation along with converter systems for power generations.

Double-fed Induction generator is one of the most popular wind turbines driven drive except Synchronous generator which includes an Induction generator with slip ring, an electronic converter and a DC link capacitor. Power electronic converter comprises of a back to back AC- DC -AC Voltage source converter and has two main parts: grid side converter (GSC that rectifies grid voltage) and rotor side converter (which feed rotor circuit). Power converter is designed in partial scale and just about 30% of the generator rated power which makes it attractive from economical point of view. Many different control methods can be used for control of power converter. One of the most common control techniques is using decouple active and reactive power PI controller to improve dynamic behaviour of wind turbine. But tuning of PI parameters is one of the main challenges in these control methods.

Using fuzzy logic controller, more reliable controller outputs can be produced. This is due to the fact that the need of the detailed mathematical model of the system can be avoided and just by using the knowledge of the total operation and behaviour of the system, tuning of the parameter can be done more easily. However research is going on to use Neural Network based controller and ANFIS based controllers are also used for smooth control of DFIG during dynamic conditions as well as varying wind conditions.

1.3 Wind Energy Scenario

First Wind Power station was installed in Ratnagiri (Maharashtra), Okha (Gujarat) and Tuticorin (Tamil Nadu). Wind power potential in India is 49,130 MW to 302,000 MW at 100m Hub height. As of 31st August the installed capacity of wind power in India was 27,676.55 MW. India is the fourth largest in production of wind power energy in the world after China USA and Germany/Spain. CHINA produces 145.1 GW (planning-250 GW by 2020) USA produces 75,000 MW and Germany produces 30,000 MW.

Wind power generation capacity in India has significantly increased in the last few years and as of 31st January 2017 the installed capacity of wind power was 28,871.59 MW, mainly spread across the South, West and North regions. The tariff of wind power reached a record low of 3.46 (5.1¢ US) per kWh (without any direct or indirect subsidies) during auctions for wind projects in February 2017.

In India the development of wind power generation began in 1986. The first wind farms was set up in coastal areas of Maharashtra (Ratnagiri), Gujarat (Okha) and Tamil Nadu (Tirunelveli) with 55 kW Vestas wind turbines. These demonstration projects were also supported by the Ministry of New and Renewable Energy (MNRE).

The potential for wind farms in the country was predicted to be more than 2,000 GW by 2011. The National Institute of Wind Energy has announced a revised estimation of the potential wind resource in India from 49,130 MW to 302,000 MW assessed at 100 m hub height. The wind- energy resource at higher hub heights that are prevailing is even more. The target for Wind Power generation capacity in India by the year 2022 is 60,000 MW as set by MNRE. Practically East and North east regions have no grid connected wind power plant as of March 2015.

As of the end of 2016, the worldwide total cumulative installed electricity generation capacity from wind power amounted to 486,790 MW, an increase of 12.5% compared

to the previous year. Installations increased by 54,642 MW, 63,330 MW, 51,675 MW and 36,023 MW in 2016, 2015, 2014 and 2013 respectively.

Since 2010 more than half of all new wind power was added outside of the traditional markets of Europe and North America, mainly driven by the continuing boom in China and India. At the end of 2015, China had 145 GW of wind power installed. In 2015, China installed close to half of the world's added wind power capacity.

Several countries have achieved relatively high levels of wind power penetration, such as 39% of stationary electricity production in Denmark, 18% in Portugal, 16% in Spain, 14% were Ireland and 9% in Germany in 2010. As of 2011, 83 countries around the world are using wind power on a commercial basis. Wind power's share of worldwide electricity usage at the end of 2014 was 3.1%.

A new 25 Km off the coast of Peterhead in north-east Scotland, 5 wind turbines, each measuring 253 metres in height, are installed in waters across the North Sea. Each turbine is designed to generate 6MW of electricity, and expected to power 20,000 households from October 2017.

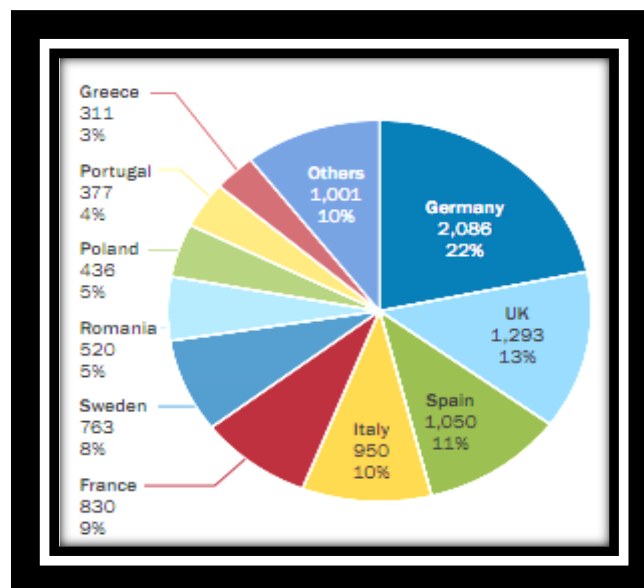


Figure: 1.2 World energy scenarios

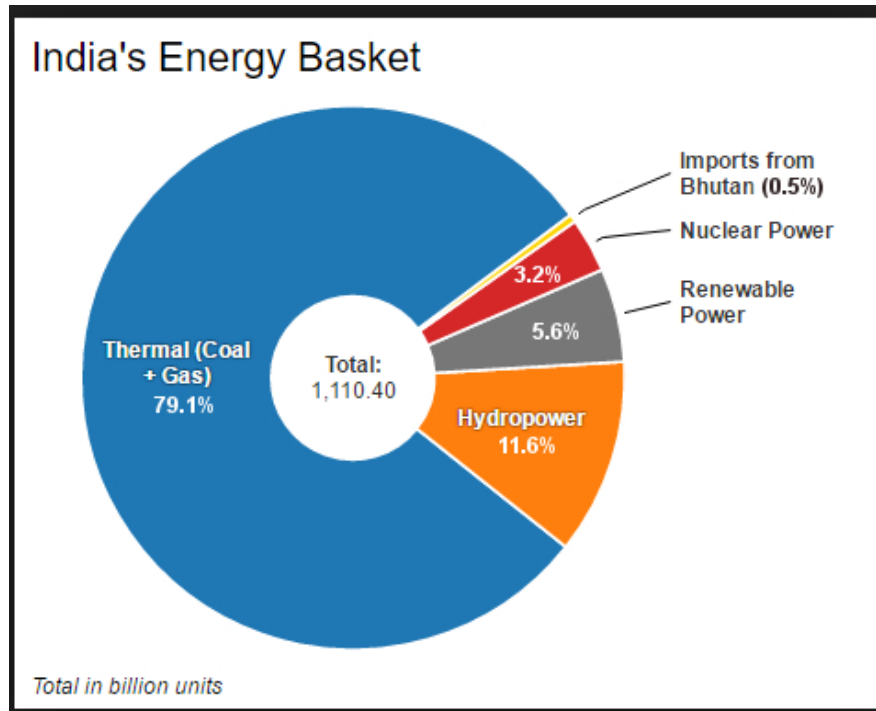


Figure 1.3 India's Energy Basket

1.4 Objective of the proposed work

Modern variable speed wind turbines offer the possibility of controlling active and reactive power separately. However, variable speed generators need a power electronic converter interface for interconnection with the grid. There are several other advantages of using variable speed generation such as mechanical stress reduction of turbine and acoustic noise reduction. With recent developments in power electronic converters, variable speed generation looks entirely feasible and cost effective. The main components of the proposed variable speed wind turbine electrical system consists of DFIG, whose stator winding is directly connected to the grid and rotor winding is connected to the grids through bidirectional PWM converter. The stator flux oriented vector control is adopted for rotor side converter control and the grid voltage oriented vector control is adopted for grid side Converter control. Direct and quadrature current components allow decoupled control of active and reactive power. Such an arrangement provides flexibility of operation in both synchronous and super synchronous generating modes. Quadrature rotor current is used to control the generator active power to achieve the desired rotational speed in the variable speed operation. The active power controller has to ensure power generation up to the rated value i.e., the optimum power output

from the wind turbine should be restricted within the range of rated value as the wind velocity increases. However, the active power produced by the DFIG should be in tune with the optimum power obtained from the wind turbine under varying wind speed up to rated power generation. The grid side converter should keep the dc voltage almost constant which ensures the reactive power control. With the increase of the wind velocity, the increase of reference power ensures the increase of active power generation using the active power PI controller within the range of rated power which ultimately ensures the tracking of optimum rotor speed of DFIG corresponding to a particular wind velocity. Also the operation of DFIG during grid fault condition (FRT) is a challenge. According to Grid code worldwide the Wind Turbine generator should provide low Voltage Ride through capability during grid faults for 85% voltage drop or even more. It should be connected to the system and contribute to the system Stability by providing reactive power to the grid during and after the faults. During Voltage drop there is over currents in rotor and Stator Windings. The DC link Voltages increases and there is large pulsations in generated Active Power Generator and Speed. The main objective of my research work is to reduce such disturbances in DFIG and its smooth operation. A complete simulation model has been developed for control of the active and reactive powers of the doubly fed generator under variable speed operation.

1.5 Literature Survey

(Pena et al., 1996) described the design of a vector controlled doubly-fed induction generator (DFIG), with back to back PWM voltage source converters (VSI) on the rotor side. The control scheme proposes an independent control of active and reactive power drawn from the supply, while ensuring sinusoidal AC supply currents. It also provides operation in wide speed range speed. The embedded control loops enable optimal speed tracking for maximum power point tracking from the wind.

(Tapia et al. 2003) present a comparison of simulation results of a grid-connected wind driven doubly-fed induction machine with real machine performance results. The machine parameters are simulated in natural reference frames i.e rotor reference frame for rotor parameters and Stationary reference frame for Stator parameters. It was also tested that the variable speed DFIG can operate below and above synchronous speed, which can be achieved by connecting rotor to grid via a back to back PWM converter. For decoupled control of the active and reactive powers generated by the machine,

stator-flux-oriented vector control is used. The mathematical model developed in this paper shows how the control strategy offers the possibility of controlling the power-factor also.

(**Hu et al. 2005**) presents a dynamic model using controllers to control both positive and negative sequence components for wind turbine driven DFIG under fault conditions. The modified control design using PWM Voltage source Converter presented for the grid side converter is a voltage PI-controller in the Stationary “ $\alpha\beta$ ” frames which diminishes the pulsations in DC link Voltage. Whereas on the rotor side converter two PI-controllers are used in stationary reference frame to improve the fault ride capability (FRT) of the wind driven DFIG by controlling the rotor over-current. The rotor current control scheme is based on the positive(+) and negative(-) synchronously rotating reference frame for providing precise and fast control of rotor current.

(**Xiang et al. 2006**) propose a control strategy that produces a component of the rotor current which will counteract the dc and negative sequence components of stator flux linkage. Experimental results show that under certain circumstances, the rotor current is limited; therefore, the use of the crowbar can be avoided. However, this method has disadvantage of dependency on the exact knowledge of the parameters of the DFIG and estimation of stator flux linkage.

(**Chowdhury and Chellapilla, 2006**) have described a vector control method of a doubly-fed induction generator drive for variable speed wind power generation. A wound rotor induction machine is connected with back-to-back three phase power converter on rotor and the grid side. The control scheme uses stator flux-oriented control for the rotor-side converter and grid voltage vector control for the grid-side converter bridge. A complete simulation model is developed for the control of the active and reactive powers of the doubly fed generator under variable speed operation. Several tests were performed to observe its operation under different wind conditions and is compared with performance of laboratory test setup consisting of a wound rotor induction machine driven by a variable speed dc motor. This paper has proved the control of both active and reactive power and stated that such a strategy will work well under various wind conditions. Also, that the hysteresis PWM current control method appears to be fast and accurate control.

(Wang and Xu 2007) develops a dynamic model and a control scheme for wind turbine DFIG to improve the performance and stability criteria during unbalanced grid conditions. In this scheme both positive and negative sequence components of currents during fault are extracted and controlled using positive and negative sequence controller. Here a control strategy is presented to control Active power, Reactive power Electromagnetic torque oscillations during asymmetrical fault conditions. The positive sequence controller controls the active and reactive power and a negative sequence controller reduces torque or power oscillations. That is by reducing the negative sequence component during asymmetrical fault system oscillations is reduced. The proposed scheme works very well under unbalance system Voltage.

(Hu et al. 2007) presents a dynamic model using controllers to control both positive and negative sequence components for wind turbine driven DFIG under fault conditions. The modified control design using PWM Voltage source Converter presented for the grid side converter is a voltage PI-controller in the Stationary “ $\alpha\beta$ ” frames which diminishes the pulsations in DC link Voltage. Whereas on the rotor side converter two PI-controllers are tuned in stationary reference frame to improve the fault ride capability (FRT) of the wind driven DFIG by controlling the rotor over-current. The rotor current control scheme is based on the positive(+) and negative(-) synchronously rotating reference frame for providing precise and fast control of rotor current.

(Xu and Wang 2007) present a control strategy and analysis of wind power based DFIG during unbalanced voltage conditions. The system is modelled using positive (+) and negative (-) synchronously reference frame. It shows that Network analysis using conventional vector control method of DFIG results in excessive oscillations in stator active and reactive power and electro-magnetic torque. Because of its sensitive nature oscillations occur in stator and rotor currents even with a small deviation in terminal voltage. A rotor current control strategy based on positive and negative reference frames is used to provide precise control of rotor positive and negative sequence currents. Due negative rotor current sequence component current increases so the DC link voltage which may damage the converter circuit which is designed for low voltage ratings.

(Xu and Wang 2007) presents a control strategy involving a design of proportional-resonant controller which tuned at grid frequency f_s & oriented in the stator stationary-reference frame without involving decomposition of the positive and negative sequence

currents components. The resonant controller controls the sequence component altogether thus reducing the oscillation in electromagnetic torque, Stator active power and frequency. Three selective control targets for RSC and GSC are developed to reduce the pulsations in stator active power. Rotor side converter is controlled to reduce the oscillations of the electro-magnetic torque.

(Hu and He 2007) presented a proportional integral plus multi-frequency resonant current controller for grid connected voltage source converter (VSI) under unbalance voltage conditions. The control scheme is implemented on positively synchronously rotating reference frame ($+\omega_s$) and is composed of PI plus MFRC controller tuned at frequency of $2\omega_s$ and $6\omega_s$ respectively. The scheme works well under unbalance voltage conditions by eliminating 5th, 7th order current harmonics and hence reducing active power oscillations and supply voltage imbalances.

(He and Hu 2008) presents the modelling and analysis of wind driven DFIG of a network under unbalanced voltage conditions, unsymmetrical fault associated with negative sequence currents and voltages which disturbs the system parameter. Here a new current-controlled scheme consisting of Proportional-Integral (PI) controller plus Proportional-Resonant controller is presented. It controls the rotor current without decomposition of positive and negative sequence. Hence the need of multiple controllers and use of notch filters are avoided. Under unbalance or low stator terminal voltage of wind driven DFIG the fluctuations in electromagnetic torque and output active power must be carefully removed. For the RSC the main focus is to reduce oscillations in stator active power generated by controlling the rotor current and for the GSC the to maintain dc link capacitor voltage at a constant value which assures the fact that the extra energy generated by rotor current is pumped out of the system.

(Flannery and Venkataramanan, 2008) have proposed a control strategy using a series grid-side converter is proposed. Although these last two arrangements are promising in some cases, the complexity and the additional cost impair their applicability.

(Hu et al. 2009) in their paper presented an overall new concept and mathematical modelling of generated active & reactive power along with a voltage sourced PWM converter. To avoid the use of band stop or notched filter obtaining decomposition of the negative and positive sequence “dq” component of currents and voltages a new

intrigue is proposed. A multi- frequency proportional resonant controller tuned in stationary “ $\alpha\beta$ ” frame is employed to improve the steady state and dynamic response under faulty conditions. The proposed control scheme tuned in the stationary reference frame provides better steady-state tracking capability for alternating-component and better transient response in compensation for wide range operation of unbalanced conditions. By reducing oscillating terms or harmonics from DC link voltage and stator powers the ratings of the capacitor and converters can be kept low.

(Zhou et al. 2009) provides the benefits of variable speed operation cost-effectively, and can control its active and reactive power independently. Crowbar protection is often adopted to protect the rotor-side voltage source converter (VSC) from transient over current during grid voltage dip. But under un-balanced grid voltage condition the electric torque transients occur and dc link voltage increases. This paper investigates on the dynamic behaviour of WTDFIG during unbalanced voltage operations and proposes new controllers to attenuate s positive and negative sequence separately. Scheme to extract positive and negative sequence components in real-time is also developed and the responses are compared with conventional scheme during unsymmetrical fault. It is seen that it is much faster than the “low-pass filter,” which makes the system sluggish. Equations of instantaneous active power and reactive power, and voltage equations of DFIG and grid VSC in positive (+) dq and negative (-) dq sequence are derived.

(Karimi-Davijani et al. 2009) suggests that a properly optimistically designed fuzzy controller (FC) can give better performance in dynamic conditions considering all uncertainties than a conventional proportional integral (PI) controller. Comparative results between the two controllers showed that the Fuzzy logic Controller can limit the generator currents during the fault, avoiding the use of the crowbars in rotor circuit.

(Lopez et al. 2009) propose the grid fault ride-through capability of DFIGs with the aid of crowbar circuit. There are disturbances in the machine parameter with little disturbances in the system voltage. To prevent this damages caused by overcurrent due to that voltage dips, the converter, are equipped with a crowbar circuit that short circuited the rotor. When the crowbar is activated, the rotor converter is disconnected hence the power generated from the turbine is no longer controlled. This paper proposes a control strategy which reduces the crowbar activation time which results in the control

of the turbine in short time and the turbine can supply a reactive power fulfilling the new grid requirement.

(Wang et al., 2009) propose control methods for FRT without any auxiliary external devices using the controllers. They show that if the DFIG speed and voltage controllers are suitably designed, it is possible to limit the rotor overcurrent during faults. The control system used in the DFIG systems to compensate the effect of grid voltage unbalance is by injecting negative sequence current into the Alternating system. The injected negative-sequence current can be provided by either rotor side or grid side converters. Various strategies for coordinating these two converters are discussed with their respective impacts on power and torque oscillations

(Phan and Lee, 2010) presented a control system applied to converter on rotor side to eliminate stator parameter imbalance. A proportional resonant (PR) based current-controller developed, which is implemented in the stator (dq) stationary reference frame. The PR controller is tuned at stator frequency f_s to achieve zero steady-state errors between actual and reference rotor currents without decomposing the positive (+) and negative (-) sequence components. The nonlinearity and complexity of the proposed control system is greatly reduced and control performance is significantly improved. The negative sequence components in unbalanced stator voltages are removed with the proposed controllers. As the negative sequence component is reduced the transients are also attenuated during faults giving more precise and efficient control of the Strategy.

(Lima et al. 2010) presents a new control scheme for the rotor-side converter (RSC) of wind turbines based doubly-fed induction generators (DFIG) to improve its low-voltage ride through capability. The main objective of this work is to design a control algorithm that would control the initial rotor over-currents that appear in the circuit during voltage drops. Unlike classical system, installation of crowbar circuits keeps the inverter connected to the generator that would permit the injection of power to the grid during the fault. This strategy is based on using the measured stator current values as the set point for the rotor current controller during the fault. The strategy proposes to synthesize a current in the stator in opposition to the currents generated during the fault, preventing the stator/rotor windings from the over-currents, without using crowbar circuits.

(Zheng and Guo, 2011) suggested that new grid codes are defined for the system requirement during low voltage ride through for increasing wind generation in power systems. Accordingly there is requirement of injecting reactive current into the grid. This paper presents an optimized control system with a combination of double vector PWM control along with crowbar circuit in series with the stator windings. The use of this additional circuit provides the wind farm with reactive power requirement thereby reducing the stator and rotor over-current and keeps the dc bus capacitor voltage stable, which prevent the damages that the consequences of voltage dips cause on the converter circuit and power system. The system performances during three-phase symmetrical fault were studied. The analysis and simulations results showed that the system can ride through fault satisfactorily by maintaining the stable operation of the wind farm.

(Hu et al. 2011) presents a control scheme by the use of virtual resistance in a crow bar circuit on the rotor side converter to limit the rotor overcurrent. Since the stator of a wind turbine DFIG is directly connected to a grid, the machine becomes very sensitive to grid fault disturbance. Grid voltage sag causes over-currents and over-voltages in rotor windings, which can damage the rotor-side converter (RSC). In order to protect the RSC, a classical solution based on installation of the crowbar is adopted. However as the DFIG absorbs reactive power from the grid, this type of solution deteriorates grid voltage sags and cannot meet the requirements of a new grid code.

(Yang et al. 2012) propose control methods for FRT without the use of any auxiliary device in case of asymmetrical grid faults. The proposed control strategy is based on the optimal coordination between the two converters aiming the attenuation of the disturbances in the rotor current and generated active power caused by the fault and also ensures the system stability. In order to handle the difficulties created due to the uncertainties of the system, the modelling is done considering the nonlinearity of the system. The controllers were designed based on fuzzy logic (FL) and GAs, which are more efficient AI techniques to handle nonlinearity and uncertainties. By using this AI based controllers it was observed that over currents at the rotor windings and the dc link over voltages are sufficiently attenuated. Even during faults reactive power requirement is also sufficed.

(Mokryani et al. 2012) presents a fuzzy logic based controller to increase fault ride through capability of variable speed wind turbine DFIG. The controller is designed in

order to compensate Voltages by regulating the stator active and reactive power of DFIG. Here the oscillations of stator active and reactive power are compensated simply by tuning the fuzzy controller rule base without using any filter circuits.

(**Yan et al. 2012**) presents a novel control strategy is proposed in this paper for the rotor side converter (RSC) of doubly-fed induction generator (DFIG)-based wind power generation systems. It is supposed to enhance the low-voltage ride-through (LVRT) capability of DFIGs during great-level grid voltage dips. The strategy consists of a proportional-resonant (PR) controller and auxiliary PR controllers. The auxiliary controllers compensate the output voltage of the RSC in case of grid faults, thus limiting the rotor inrush current of DFIG and meeting the requirements of LVRT. Sequential-component decompositions of current are not required in the control system to improve the response of system. Since the resonant compensator is a double-side integrator, the auxiliary controllers can be simplified through coordinate transformation. With limited RSC voltage ratings, the rotor fault currents of specified frequencies are eliminated to a great extent. The controller performs well, even when the angular frequency detection is not accurate. Simulations have been presented under symmetric and asymmetric grid fault conditions to confirm the analysis and verify the proposed control method.

(**Yasa et al. 2013**) presented detailed analysis of doubly-fed induction generator (DFIG) wind turbine and their electrical components during normal and asymmetrical fault conditions. Wind turbine components are individually modelled and then combined in a simulation process which is called coupled simulation. The simulation results show that during Line to ground fault the grid frequency oscillation occurs which results in oscillations in “q” and “d” axis rotor currents. An experimental-based study shows the adverse effects of these unsymmetrical faults on rotor currents.

(**Zarei and Asaei, 2013**) proposed a new control method for rotor side converter (RSC) and grid side converter (GSC) of doubly fed induction generator (DFIG). A combined vector control and direct power control for RSC and direct current control for GSC have been introduced. The RSC directly controls the stator d-q axis currents (rotating at synchronous speed ω_s) by applying an optimal voltage vector from a switching table. Under the unbalanced and distorted grid voltage conditions, the new control strategy injects a pure sinusoidal and balanced stator and GSC current without any need of extracting the negative sequence and 5th and 7th voltage harmonics. Only a modified

phase locked loop (PLL) to extract the positive sequence of the fundamental phase angle, is added to this situation.

(Wu et al. 2013) present an improved control strategy for both the rotor side converter (RSC) and grid side converter (GSC) of a doubly fed induction generator (DFIG)-based wind turbine (WT) system to enhance the low voltage ride through (LVRT) capability. Within the proposed control strategy, the RSC control introduces transient feed-forward compensation terms to mitigate the high frequency harmonic components and reduce the surge in the rotor currents. The proposed GSC control scheme also introduces a compensation term reflecting the instantaneous variation of the output power of the rotor side converter with consideration of the instantaneous power of grid filter impedance to keep the dc-link voltage nearly constant during the grid faults. To provide precise control, non-ideal proportional resonant (PR) controllers for both the RSC and GSC current regulation are employed to further improve dynamic performance. Further DC link Voltage equation is modified by modifying the rotor power equation in terms of grid side parameter.

(Vrionis et al. 2014) propose a new genetic algorithm based control strategy in fuzzy logic, to improve the LVRT capability of grid-connected wind turbines (WTs) with doubly-fed induction generators (DFIGs). The grid codes world-wide requires that WTs should supply reactive power to the grid during fault and after fault in order to support the grid voltage. The conventional crowbar systems initially used to protect the rotor-side converter during faults hence it don't fulfil this requirement as it draws reactive power from the grid. To avoid this drawback a control systems is designed that eliminate the use of the crowbar circuit. This paper proposes a FRT control scheme for the DFIG during fault in grid, without the use of any auxiliary hardware. The control strategy make note of Voltage and rotor current parameter and controls them. The coordination of the two controllers is achieved via a fuzzy controller which is properly tuned using genetic algorithms. Using the proposed control Strategy, with relatively weak grid the DFIG can successfully ride-through the fault. The over-currents at the rotor windings and the dc link over-voltages are reduced and the DFIG can continuously supply with reactive power during and after the faults contributing to the support of the ac- voltage.

(Feng et al., 2015) presents that for doubly fed induction generator (DFIG)- based wind energy conversion systems (WECSs), large electromotive force will be induced in the rotor circuit during grid faults. Without proper protection scheme, the rotor side of DFIG will suffer from over-currents, which may even destroy the rotor-side converter (RSC). To mitigate this problem, a new flux-linkage tracking-based low-voltage ride-through (LVRT) control strategy is proposed to suppress the short-circuit rotor current. Under the proposed control strategy, the rotor flux linkage is controlled to track a reduced fraction of the changing stator flux linkage by switching the control algorithm of RSC during grid faults.

(Ling, 2016) presents a comparative study on the FRT techniques for wind turbine driven DFIG based on three broad subcategories including control algorithms, external hardware circuit, and control strategies to achieve the uninterrupted operation during grid faults which will provide voltage stability and hence reactive power supply to the system during faults.

(Le et al., 2016) presents a creative control strategy for improving FRT capability of a wind energy driven DFIG. Here passivity theory is applied on the current based control loops of the rotor side converter (RSC). Two-term approach control scheme is used for the grid side converter (GSC) to keep the DC-link capacitor voltage almost constant. Here active and reactive power component is controlled to achieve the proposed control strategy.

(Lopez and Gubia) have proposed an improved version of the crowbar circuit, eliminating the duration of the crowbar action for the wind turbine driven DFIG. As the time of action is reduced the DFIG parameters return to its initial conditions faster.

(Zhang et al.) Present a method to limit the rotor short current of doubly-fed induction generator (DFIG) was limited by introducing a rotor side protection circuit. Second, the voltage of DC bus was limited by a DC energy absorb circuit. Third, STATCOM was used to increase the low level voltages of the wind farm. Simulation under MATLAB was studied and the corresponding results were given and discussed. The methods proposed in this paper can limit the rotor short current and the DC voltage of the DFIG WT to some degree, but the voltage support to the power system during the fault largely depend on the installation place of STATCOM. New FRT needs not only the WTs keep

on grid but also can provide voltage support or generator reactive power to the power system.

(Suresh and Prasad) present a mathematical model of a doubly fed induction generator (DFIG) in the positive synchronous reference frame under distorted grid voltage conditions with the help of fuzzy logic controller. The oscillations of the DFIG's electromagnetic torque and the instantaneous stator active and reactive powers are fully described when the grid voltage is harmonically distorted. Four alternative control targets are proposed to improve the system responses during grid harmonic distortions. A new rotor current control scheme implemented in the positive synchronous reference frame is developed. The control scheme consists Fuzzy logic controller and a resonant controller consequently, the fundamental and the fifth- and seventh-order components of rotor currents are directly regulated by the Fuzzy-R controller without sequential-component decompositions.

1.6 Motivation towards the work

As a result of increasing environment concern, more and more electricity is generated from renewable sources .To meet the power demand, taking into account the economical and environment factors, wind energy conversion is gradually gaining interest as a suitable source of renewable energy where wind turbines are used. Now a days wind driven DFIG is used for electromagnetic conversion system. A tendency to erect more numbers of wind turbines can be observed. But due to the continuous change in the wind velocity the power produced also fluctuates to great extent. This kind of electrical power generation usually causes problems in the electrical system it is connected to because of the lack or scarcity of control on the produced active and reactive power. As far as variable speed generation is concerned, it is necessary to produce constant frequency electrical power from variable speed source. Therefore adequate model to study the impact of wind turbine on electrical power system behaviour are needed. This can be very efficiently done by vector control of Wind driven DFIG. One of the advantages of these generators is that decoupled control of stator active and reactive power can be done. When connected to constant frequency network, the induction generator runs at near synchronous speed drawing the magnetizing current from the mains therefore, resulting in constant speed constant frequency operation (CSCF). However, the power captured due to fluctuating wind

speed can be substantially improved if there is flexibility in varying the shaft speed. In such variable speed constant frequency (VSCF) application rotor side control of grid connected wound rotor induction machine is an attractive solution. In the system under consideration, the stator is directly connected to the three phase grid and the rotor is supplied by two back to back PWM converters. Such an arrangement provides flexibility of operation in both sub synchronous and super synchronous generating modes. The rating of the power converters used in the rotor circuit is substantially lower than the machine rating and is decided by the range of the operating speed. One of the two converters, the function of the line side converter is to regulate the dc bus voltage. The machine side converter has to control the active power generation and generator speed and reactive power of the machine. Also there is requirement for low voltage ride through according to grid codes now a day. During Grid fault conditions the Voltage at PCC drops down. There might be over current in Rotor winding which may damage the rotor circuit. Also the DC link Voltage may also increase. The protection of DFIG and power electronic device is of prime importance. Also there should be uninterrupted power generation up to 85% drop of Stator Voltage without disconnecting DFIG from the grid. This motivated this research work.

1.7 Outline of the Various Chapters of the Thesis:

CHAPTER 1: This chapter gives a brief Introduction of Wind Power energy, overview about the World wind energy scenario, Motivation towards the work and objectives of the proposed work.

CHAPTER 2: In this chapter brief literature survey is presented on various papers on Wind driven DFIG under dynamic conditions.

CHAPTER 3: This chapter presents the different types of wind energy systems, Principle of operation of doubly fed Induction generator and different modes of operation of Induction machines.

CHAPTER 4: This chapter explains the detailed mathematical modelling of Wind Energy System driven DFIG scheme. This includes the modelling of Wind turbine, the modelling of DFIG, The modelling of Stator flux oriented Rotor side converter control. The modelling of Supply voltage oriented Grid side converter, the modelling of DC link

voltage. It also contains the Principle of operation of Hysteresis current controlled PWM technique and its modelling.

CHAPTER 5: This chapter presents the Control Strategy used in the present system for controlling DFIG under fault conditions and also the design of Hysteresis current controlled PWM inverter.

CHAPTER 6: This chapter includes the design of conventional PI and PR controller.

CHAPTER 7: In this Chapter the design of AI technique based controllers are discussed. This includes the design of Neural Network based controller and ANFIS based controller.

CHAPTER 8: In this chapter the Simulation results which include the performance of DFIG using conventional PI controller, Neural Network controller and ANFIS Controller for various wind condition as well as various fault condition are presented. A comparative Analysis of performance with various types of controllers is observed.

CHAPTER 9: This chapter provides the closure of the present work and conclusion and the scope for future work in this field.

Chapter 2

Modelling of overall wind energy conversion systems

2.1 Modelling of Wind Turbine

2.1.1 The turbine equations

2.1.1.1 Tip speed ratio

Tip speed ratio (λ) is defined as the ratio between linear velocity of the blade tip ($R \cdot \omega$) and the wind velocity (V_w).

$$\lambda = \omega r * \frac{R}{V} \quad 2.1$$

Where, R is the radius of the turbine.

2.1.1.2 Power extracted from the wind

The rotor converts the kinetic energy contained by the wind into mechanical energy. The Wind turbine is connected to the rotor shaft via gear box to increase the speed of rotation.

The equation of Power from wind energy i.e. mechanical power P_{mech} , in terms of ρ the air density [kg/m^3], C_p the performance coefficient or power coefficient, λ the tip speed ratio, the ratio between blade tip speed and wind speed upstream the rotor V [m/s], θ the pitch angle of rotor blades [deg], and A_r is the area covered by the rotor [m^2] is given by-

$$P_{mech} = \frac{\rho}{2} * C_p(\lambda, \theta) * A_r * V^3 \quad 2.2$$

2.1.1.3 Performance coefficient

The performance coefficient C_p is a function of the tip speed ratio λ and the pitch angle θ . The calculation of the performance coefficient requires the use of blade element theory.

$$C_p(\lambda, \theta) = 0.22 \left(\left(\frac{116}{\lambda_i} \right) - 0.4 * \theta - 5 \right) e^{-(12.5)/\lambda_i} 2.3$$

Where, $\frac{1}{\lambda_i} = \frac{1}{\lambda + 0.08 * \theta} - \frac{0.035}{\theta^3 + 1} 2.4$

The blade pitch angle θ is considered to be 0 in this case.

An S function code is prepared to design maximum power point tracking (MPPT) system to extract the maximum power by varying the rotational speed of turbine.

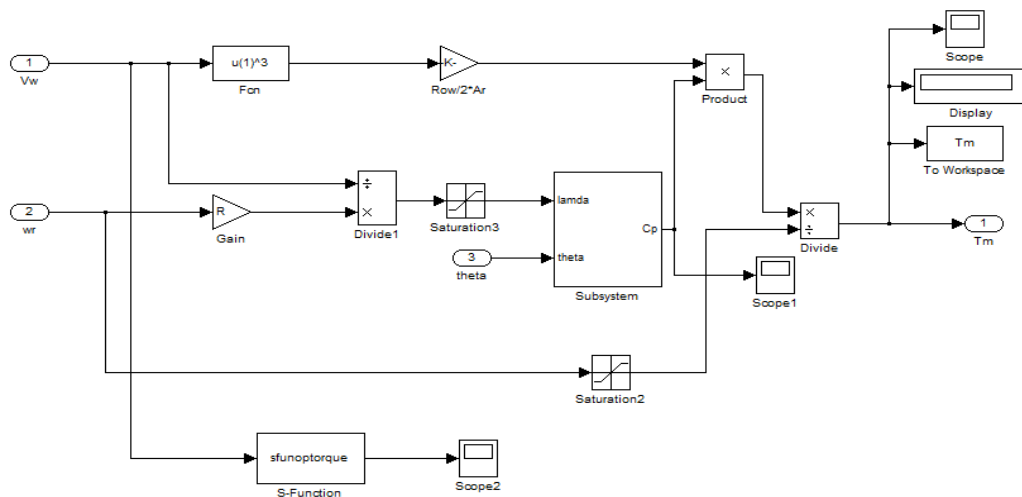
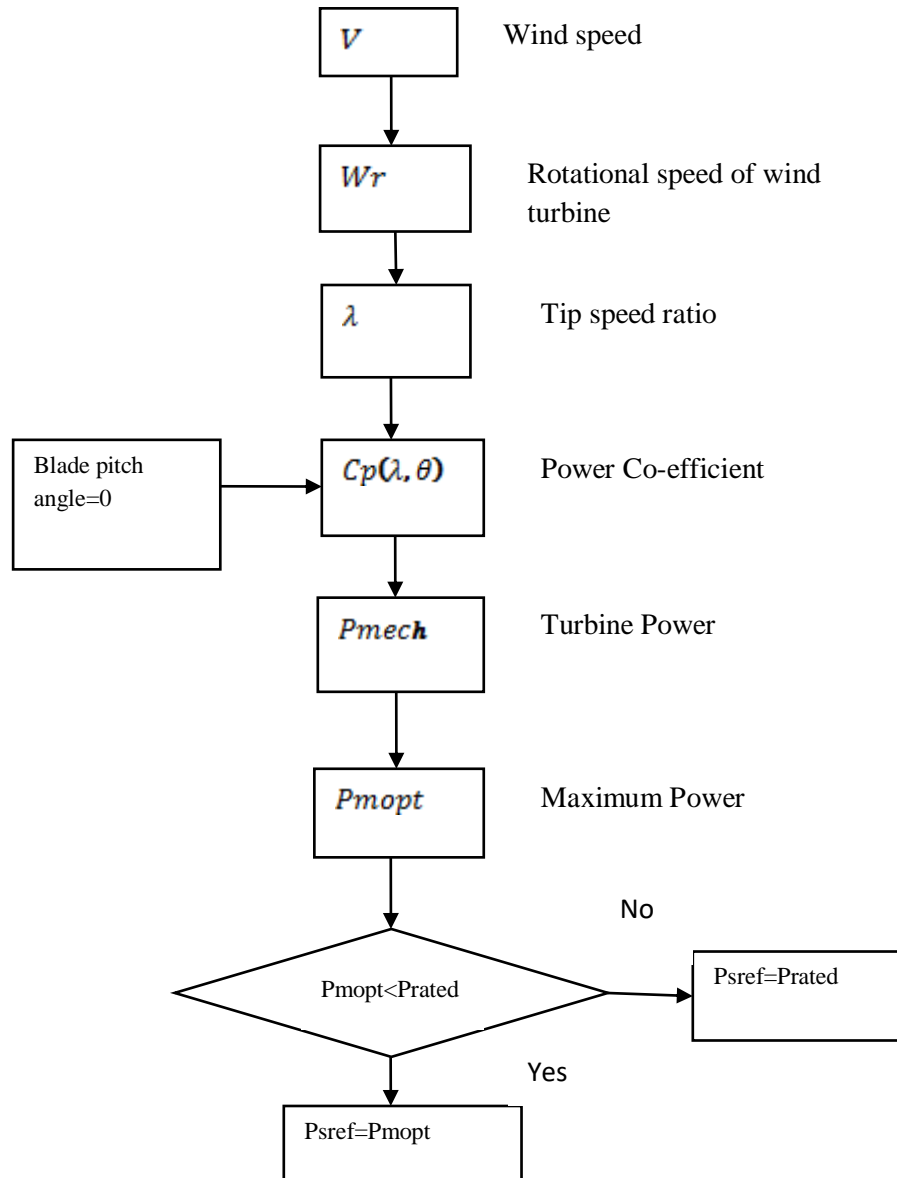


Figure: 2. 1 Modelling of wind turbine

2.1.2 Flow chart (s-function block) for maximum power point tracking



2.2 Modelling of doubly fed induction generator

Doubly fed Induction machines can be operated in generating as well as a motoring mode both sub synchronous and super synchronous speeds depending on the direction of power flow. But only the generating modes at sub synchronous and super synchronous speeds are of interest for wind power generations. The remarkable feature of variable speed wound-rotor machine is that it is doubly fed i.e fed from both stator and rotor side. Normally, the stator is directly connected to the grid and the rotor is interfaced through a variable frequency power converter. In order to

cover a wide operation range from sub synchronous to super synchronous speeds, the power converter placed on the rotor side operates with power flowing in both the directions. This is achieved by means of a back-to-back PWM converter configuration. The operating principle of a DFIM can be analysed using the classic theory of rotating fields and the well-known d-q model, as well as both three-to-two and two to three axes transformations using Clarke's equation.

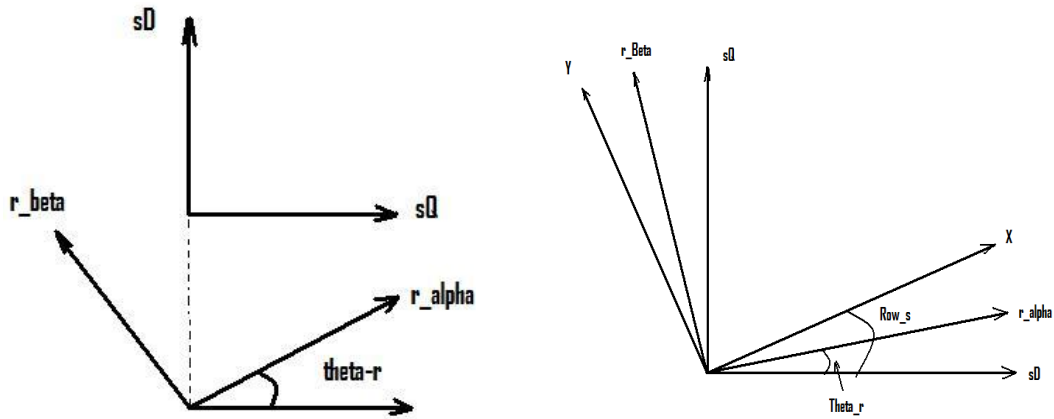


Fig: 2.2 Stator and rotor side reference frames for the “Quadrature phase Slip Ring” model

2.2.1 Fifth order Generator Model

Generator Voltage equations in dq reference frame are given by:

$$V_{SD} = R_S I_{SD} + \frac{d\lambda_{sD}}{dt} - \omega_S \lambda_{sQ} \quad 2.5$$

$$V_{SQ} = R_S I_{SQ} + \frac{d\lambda_{sQ}}{dt} + \omega_S \lambda_{sD} \quad 2.6$$

$$V_{rD} = R_r I_{rD} + \frac{d\lambda_{rD}}{dt} - (\omega_S - \omega_r) \lambda_{rQ} \quad 2.7$$

$$V_{rQ} = R_r I_{rQ} + \frac{d\lambda_{rQ}}{dt} + (\omega_S - \omega_r) \lambda_{rD} \quad 2.8$$

In order to deal with the machine dynamic behaviour in the most realistic possible way, both stator and rotor variables are referred to their corresponding natural reference frames in the developed model. In other words, the stator side current and voltage components are referred to a stationary reference frame, while the rotor side current and voltage components are referred to a reference frame rotating at rotor electrical speed of, ω_r . The machine electrical model expressed in such reference frames is referred to as the “Quadrature-Phase Slip-Ring” model. There is a quadrature phase stator winding (sD, sQ) and a quadrature phase rotor winding r_α, r_β the rotor winding r_α is displaced from stator winding sD by the angle θ_r .

The Voltage and the current equations are-

$$\begin{bmatrix} V_s D \\ V_s Q \\ V_{r\alpha} \\ V_{r\beta} \end{bmatrix} = \begin{bmatrix} R_s + sL_s & 0 & sL_m \cos\theta_r - sL_m \sin\theta_r \\ 0 & R_s + sL_s & sL_m \sin\theta_r + sL_m \cos\theta_r \\ sL_m \cos\theta_r & sL_m \sin\theta_r & R_r + sL_r \\ -sL_m \sin\theta_r & sL_m \cos\theta_r & 0 \end{bmatrix} \begin{bmatrix} I_s D \\ I_s Q \\ I_{r\alpha} \\ I_{r\beta} \end{bmatrix} \quad 2.9$$

Three phase stator and rotor voltage equations are-

$$\begin{bmatrix} V_{sA} \\ V_{sB} \\ V_{sC} \\ V_{rA} \\ V_{rB} \\ V_{rC} \end{bmatrix} = \begin{bmatrix} R_s + sL_s & SM_s & SM_s & SM_{sr} \cos\theta_r & SM_{sr} \cos\theta_1 & SM_{sr} \cos\theta_2 \\ SM_s & R_s + sL_s & SM_s & SM_{sr} \cos\theta_2 & SM_{sr} \cos\theta_r & SM_{sr} \cos\theta_1 \\ SM_s & SM_s & R_s + sL_s & SM_{sr} \cos\theta_1 & SM_{sr} \cos\theta_2 & SM_{sr} \cos\theta_r \\ SM_{sr} \cos\theta_r & SM_{sr} \cos\theta_2 & SM_{sr} \cos\theta_1 & R_r + sL_r & SM_r & SM_r \\ SM_{sr} \cos\theta_1 & SM_{sr} \cos\theta_r & SM_{sr} \cos\theta_2 & SM_r & R_r + sL_r & SM_r \\ SM_{sr} \cos\theta_2 & SM_{sr} \cos\theta_1 & SM_{sr} \cos\theta_r & SM_r & SM_r & R_r + sL_r \end{bmatrix} \begin{bmatrix} I_{sA} \\ I_{sB} \\ I_{sC} \\ I_{rA} \\ I_{rB} \\ I_{rC} \end{bmatrix} \quad 2.10$$

Where, $S = d/dt$

The Stator flux linkage space phasor in the stationary reference frame

$$\lambda_{sA} = L_s I_{sA} + M_s I_{sB} + M_s I_{sC} + M_{sr} \cos\theta_r I_{rA} + M_{sr} \cos\left(\theta_r + 2 * \frac{\pi}{3}\right) I_{rB} + M_{sr} \cos\left(\theta_r + 4 * \frac{\pi}{3}\right) I_{rC}$$

$$\lambda_{sB} = L_s I_{sB} + M_s I_{sA} + M_s I_{sC} + M_{sr} \cos\left(\theta_r + 4 * \frac{\pi}{3}\right) I_{rA} + M_{sr} \cos\theta_r I_{rB} + M_{sr} \cos\left(\theta_r + 2 * \frac{\pi}{3}\right) I_{rC}$$

$$\lambda_{sC} = L_s I_{sC} + M_s I_{sB} + M_s I_{sA} + M_{sr} \cos\left(\theta_r + 2 * \frac{\pi}{3}\right) I_{rA} + M_{sr} \cos\left(\theta_r + 4 * \frac{\pi}{3}\right) I_{rB} + M_{sr} \cos\theta_r I_{rC} \quad 2.11$$

The Rotor flux linkage space phasor in the rotating reference frame fixed to the rotor-

$$\lambda_{rA} = L_r I_{rA} + M_r I_{rB} + M_r I_{rC} + M_{sr} \cos\theta_r I_{sA} + M_{sr} \cos\left(\theta_r + 4 * \frac{\pi}{3}\right) I_{sB} + M_{sr} \cos\left(\theta_r + 2 * \frac{\pi}{3}\right) I_{sC}$$

$$\lambda_{rB} = L_r I_{rB} + M_r I_{rC} + M_r I_{rA} + M_{sr} \cos\left(\theta_r + 2 * \frac{\pi}{3}\right) I_{sA} + M_{sr} \cos\theta_r I_{sB} + M_{sr} \cos\left(\theta_r + 4 * \frac{\pi}{3}\right) I_{sC}$$

$$\lambda_{rC} = L_r I_{rC} + M_r I_{rA} + M_r I_{rB} + M_{sr} \cos\left(\theta_r + 4 * \frac{\pi}{3}\right) I_{sA} + M_{sr} \cos\left(\theta_r + 2 * \frac{\pi}{3}\right) I_{sB} + M_{sr} \cos\theta_r I_{sC} \quad 2.12$$

The direct and quadrature axis flux linkage components-

$$\lambda_{sD} = L_s I_{sD} + L_M I_{rD} \quad 2.13$$

$$\lambda_{sQ} = L_s I_{sQ} + L_M I_{rQ} \quad 2.14$$

$$\lambda_{rD} = L_r I_{rD} + L_M I_{sD} \quad 2.15$$

$$\lambda_{rQ} = L_r I_{rQ} + L_M I_{sQ} \quad 2.16$$

The torque equations

$$T_{em} = -\frac{3}{2} * \frac{P}{2} * \frac{L_M}{L_S} (\lambda_{SQ} * I_{rd} - \lambda_{SD} * I_{rq}) \quad 2.17$$

Generator equation of motion

$$P \left(\frac{\omega_r}{\omega_b} \right) = \frac{1}{2H} * (T_{mech} - T_{em} - D * \omega_m) \quad 2.18$$

Concept of Slip

The difference between the synchronous speed of the magnetic field, and the shaft rotating speed is slip - measured in RPM or frequency. Slip increases with increasing load providing a greater torque.

$$s = \frac{N_s - N_r}{N_s}$$

Where, N_s and N_r are the synchronous speed and the mechanical speed of the rotor respectively. The synchronous speed is given by- $60f_s/P$. Where, P = number of pole pairs and f_s is the electrical frequency of the applied stator voltage. The Voltage and the current equations are-

$$\frac{d}{dt} \begin{pmatrix} I_{sD} \\ I_{sQ} \\ I_{r\alpha} \\ I_{r\beta} \end{pmatrix} = \begin{cases} \left\{ \begin{array}{l} R_s L_r I_{sD} - L_m (L_r \omega_r \sin \theta_r + R_r \cos \theta_r) I_{r\alpha} - L_r V_{sD} + L_m \cos \theta_r V_{r\alpha} - L_m \sin \theta_r V_{r\beta} \\ -L_m^2 \omega_r I_{sQ} + L_m (R_r \sin \theta_r - L_r \omega_r \cos \theta_r) I_{r\beta} \end{array} \right\} / (L_m^2 - L_s L_r) \\ \left\{ \begin{array}{l} L_m^2 \omega_r I_{sD} + L_m (L_r \omega_r \cos \theta_r - R_r \sin \theta_r) I_{r\alpha} - L_r V_{sQ} + L_m \sin \theta_r V_{r\alpha} + L_m \cos \theta_r V_{r\beta} \\ + R_s L_r I_{sQ} - L_m (L_r \omega_r \sin \theta_r + R_r \cos \theta_r) I_{r\beta} \end{array} \right\} / (L_m^2 - L_s L_r) \\ \left\{ \begin{array}{l} -L_m (L_s \omega_r \sin \theta_r + R_s \cos \theta_r) I_{sD} + R_r L_s I_{r\alpha} + L_m \cos \theta_r V_{sD} + L_m \sin \theta_r V_{sQ} - L_s V_{r\alpha} \\ + L_m^2 \omega_r I_{r\beta} + L_m (L_s \omega_r \cos \theta_r - R_s \sin \theta_r) I_{sQ} \end{array} \right\} / (L_m^2 - L_s L_r) \\ \left\{ \begin{array}{l} L_m (R_s \sin \theta_r - L_s \omega_r \cos \theta_r) I_{sD} + R_r L_s I_{r\beta} + L_m \cos \theta_r V_{sQ} - L_m \sin \theta_r V_{sD} - L_s V_{r\beta} \\ -L_m^2 \omega_r I_{r\alpha} - L_m (R_s \cos \theta_r + L_s \omega_r \sin \theta_r) I_{sQ} \end{array} \right\} / (L_m^2 - L_s L_r) \end{cases} \quad 2.19$$

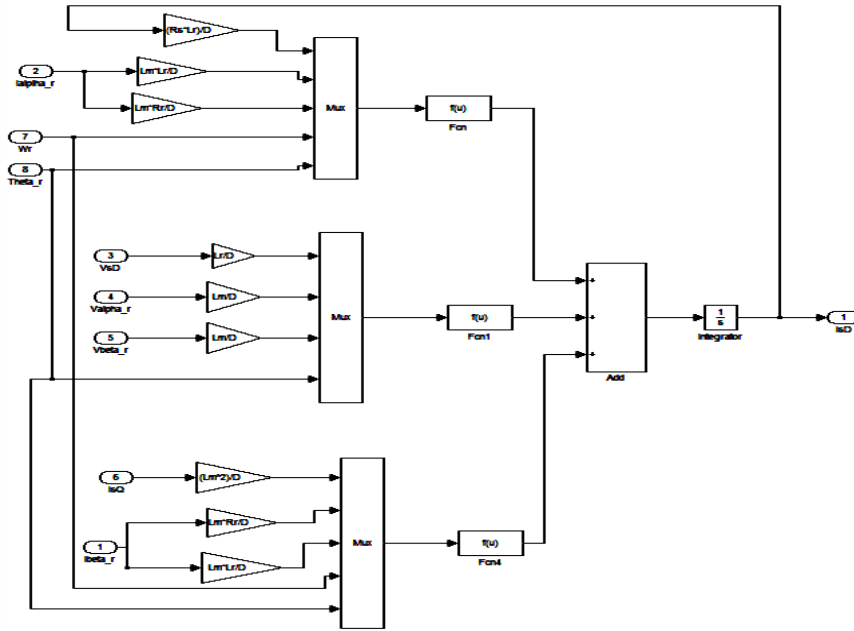


Figure: 2.3 Modelling of d axis stator current

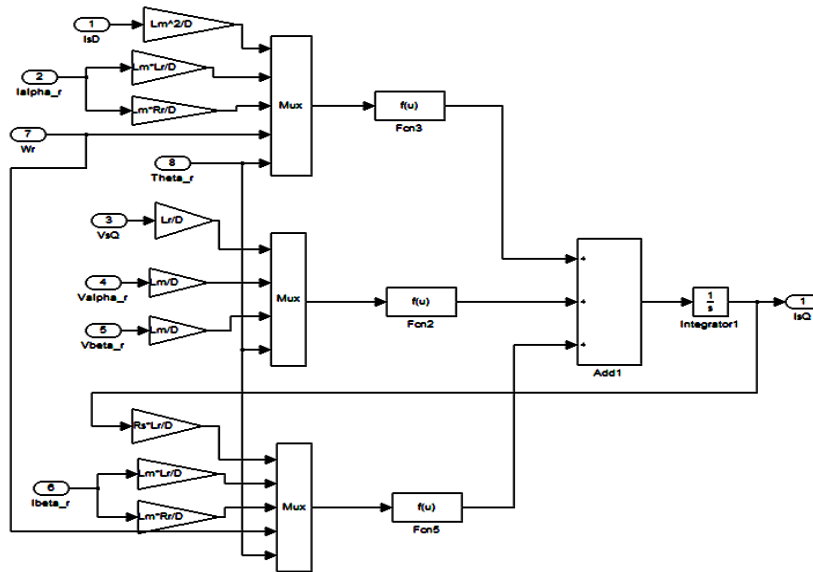


Figure 2.4: Modelling of q axis stator current

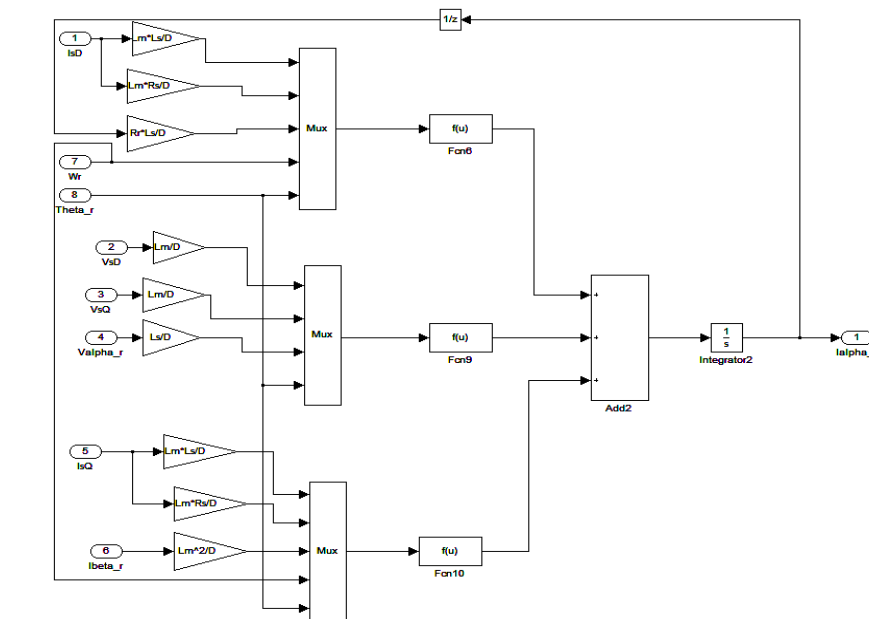


Figure 2.5: Modelling of d-axis rotor current

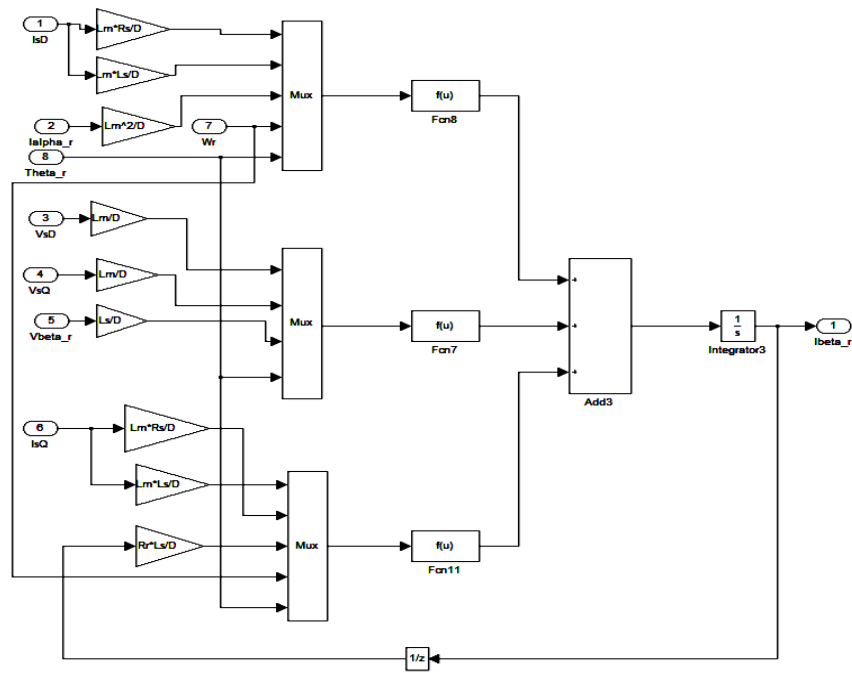


Figure 2.6: Modelling of q-axis rotor current

Magnetizing inductance in $=Lm = Xm / (2 * pi * fs * n)$ (in mH);

Stator inductance in $Ls = Xls / (2 * pi * fs) + (n * Lm)$ (in mH);

Stator inductance in $Lr = Xlr / (2 * pi * fs) + (Lm / n)$ (in mH);

Leakage factor $\sigma = 1 - (Lm^2 / Ls * Lr)$

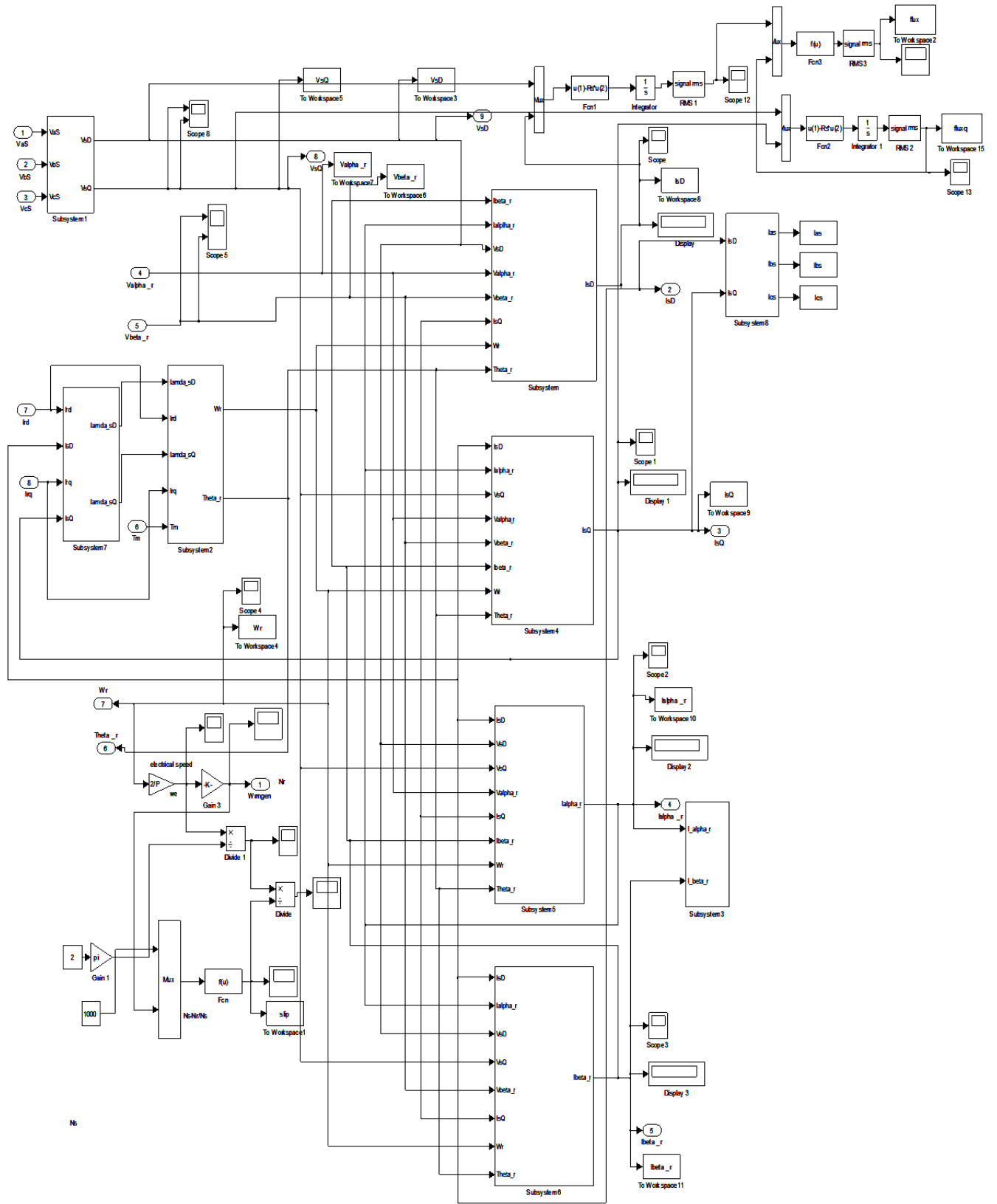


Figure 2.7: Modelling of DFIG

2.3 Rotor side converter control strategy

2.3.1 Rotor side converter control

Vector control method is used to control the rotor side converter. The main feature of the rotor side converter is to control the generated active power or the generator speed or Electromagnetic torque. For this a maximum power point tracker is used to be made to capture the maximum power of wind energy by operating them at a rotational speed corresponding to the optimum tip speed ratio and using wind turbine equations. An S function program is written to track reference active power from MPPT. This active power is set as a reference active power or optimum active power, P_{opt} .

A control strategy is presented wherein the rotor current I_{ry} in the stator flux oriented reference frame is controlled to get the desired active power and correspondingly getting desired values of speed and torque. The reactive power set point can also be calculated from active power set point using a desired power factor. The reactive power can be controlled by controlling the I_{rx} in the stator flux oriented reference frame. The control uses the principle that in the stator flux oriented frame the rotor current variation will reflect in stator current variations and hence by controlling the rotor current, the stator active and reactive powers can be controlled.

A reference current I_{ryref} is derived from the error between the active power reference and the actual active power by tuning an active power PI controller. Similarly a reference current I_{rxref} is obtained from reactive power reference and actual reactive power by tuning a reactive power PI controller. Both the reference currents are then transformed to their natural reference frame that is in the rotor reference frame. These rotor current references after dq to *abc* transformation using Clarkes transformation equations are used for implementing hysteresis PWM modulation on the rotor side three phase converters.

In stator flux oriented control, both stator and rotor quantities are transformed to a special reference frame that rotates at an angular frequency identical to the stator flux linkage space phasor with the real axis of the reference frame aligned to the stator flux vector. At steady state, the reference frame speed equals the synchronous speed.

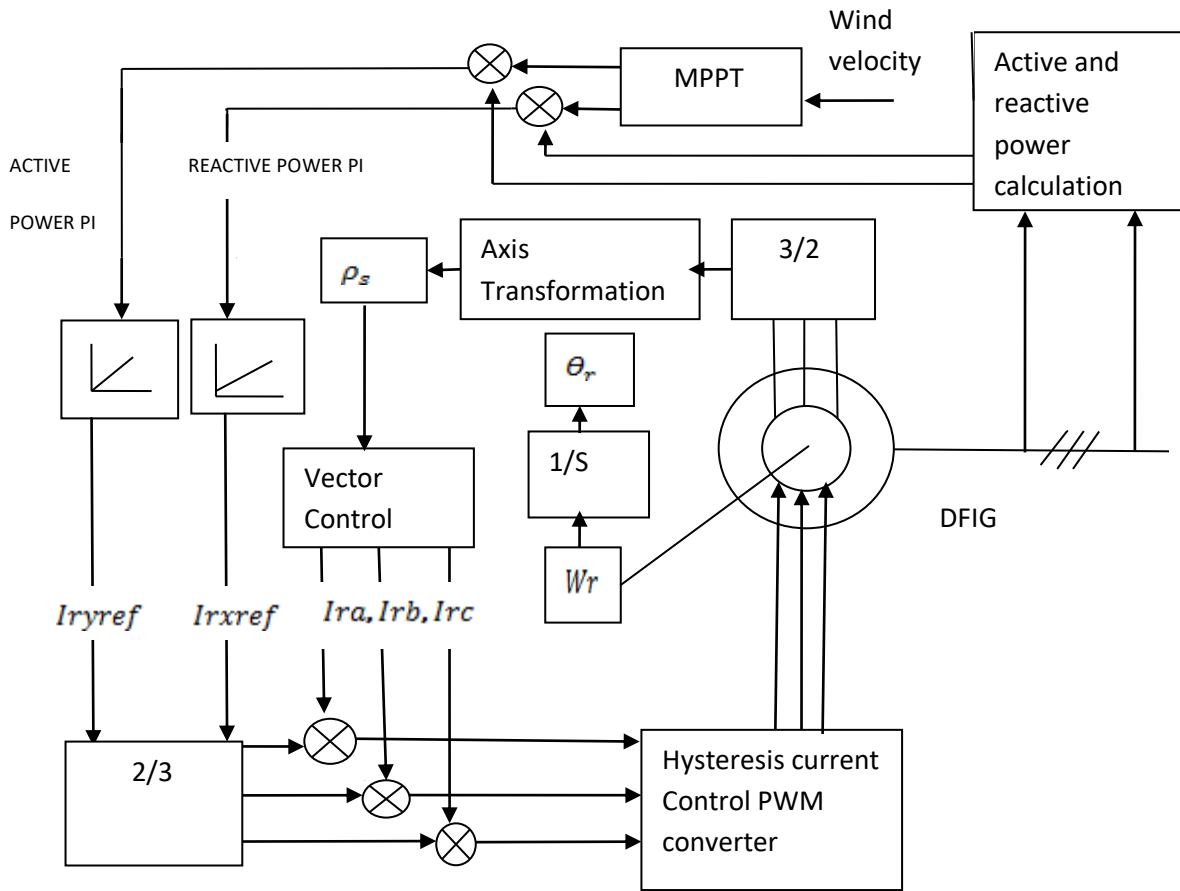


Figure 2.8 Block diagram of the stator flux oriented vector control scheme for RSC

2.3.2 The active and reactive power equations

The scheme makes use of the stator flux angle, which is determined dynamically to map the stator and rotor quantities into new reference frame. It can be shown that the choice of stator flux-oriented reference frame results in a decoupled control of stator side active and reactive powers as follows:

Stator flux linkages expressed in the new reference frame are:

$$\lambda_{sX} = L_S I_{sX} + L_M I_{rX} \quad 2.20$$

$$\lambda_{sY} = L_S I_{sY} + L_M I_{rY} \quad 2.21$$

Since the real axis (x) of the new reference frame is aligned with the stator flux linkage vector, $\lambda_{sY} = 0$ thus,

$$L_S I_{sY} + L_M I_{rY} = 0 \quad 2.22$$

$$I_{sY} = -(L_M/L_S)I_{rY} \quad 2.23$$

The stator Magnetizing Current is-

$$I_{ms} = (\lambda_{sX} + j\lambda_{sY})/L_M \quad 2.24$$

But since $\lambda_{sY} = 0$

$$I_{ms} = \lambda_{sX}/L_M \quad 2.25$$

$$I_{sX} = (\lambda_{sX} - L_M I_{rX})/L_S \quad 2.26$$

$$I_{sX} = L_M/L_S(I_{ms} - I_{rX}) \quad 2.27$$

In stator flux-oriented reference frame, since, we have $V_{sy} = |V_s|$. Thus,

$$P_s = \left(\frac{3}{2}\right) * |V_s| * I_{sY} \quad 2.28$$

$$Q_s = \left(\frac{3}{2}\right) * |V_s| * I_{sX} \quad 2.29$$

Therefore, substituting the above values in the equation 2.26 and 2.27 in equation 2.28 and 2.29 we get

$$P_s = -\left(\frac{3}{2}\right) * |V_s| * L_m/L_s * I_{rY} \quad 2.30$$

$$Q_s = \left(\frac{3}{2}\right) * |V_s| * L_m/L_s(I_{ms} - I_{rX}) \quad 2.31$$

Therefore, the d-axis component of the rotor current can be controlled to regulate the stator reactive power while the q-axis component of the rotor current can be controlled to control the stator active power and the generator speed. As a result, the control of stator active power via I_{qr} and stator reactive power via I_{dr} are essentially decoupled, and so a separate decoupler is not necessary to implement field orientation control for the slip power recovery. Flux control is generally unnecessary, since it would maintain a constant level, restricted by the constant magnitude and frequency of the line voltage, while the control of the reactive power becomes possible.

2.3.3 Active power and reactive power control loop design

It can be seen that, for any given wind speed, there is a rotational speed, ω_r which generates a maximum power $P_{mech} = P_{opt}$, It is important to consider that when wind

speed changes, the rotational speed varies so as to follow the change. But as a reliable measurement of the wind speed hitting the blades of the generator cannot be ensured, the equation for obtaining the target power P_{opt} can be modified eliminating the dependence on wind speed.

$$P_{sref} = P_{opt} \quad 2.32$$

$$Q_{sref} = -P_{sref} * \tan\phi_{sref} \quad 2.33$$

$$Q_{sref} = (P_{sref} + P_r) * \tan\phi_{sref} - Q_r \quad 2.34$$

The rotor side Active or reactive power are –

$$P_r = 3/2(V_{rX} * I_{rX} + V_{rY} * I_{rY}) \quad 2.35$$

$$Q_r = 3/2(V_{rY} * I_{rX} - V_{rX} * I_{rY}) \quad 2.36$$

The difference between the reference and the actual values of the stator active power is the input to the active power PI controller and the output of which is the q –axis reference current component established in stator flux oriented reference frame. Similarly, the reference values of the stator reactive power is compared with the actual reactive power and their difference serves as a input to the reactive power PI controller and the output of which is the d-axis rotor reference current.

The active and the reactive power controllers are so tuned that the DFIG assures power within the rated value. The actual Active and reactive power tracks the reference active and reactive power keeping the DC voltage almost constant.

2.3.4 Stator flux oriented vector control scheme

The steps followed to model and implement this vector control algorithm are

1. Three-to-two phase Clarke's transformation of measured stator and rotor side currents in their corresponding natural reference frames.

$$I_\alpha = \frac{2}{3}(I_a) - \frac{1}{3}(I_b - I_c)$$

$$I_\beta = \frac{2}{\sqrt{3}}(I_b - I_c)$$

2. Estimation of the stator flux-linkage space phasor^s angular position with respect to the stationary direct axis. Since the rotor side current components need to be changed first from their natural axes to the stationary reference frame, it is necessary to measure the rotor angle. The equations to be followed are given below.

$$I_{rd} = I_{r\alpha}\cos\theta_r - I_{r\beta}\sin\theta_r \quad 2.37$$

$$I_{rq} = I_{r\alpha}\sin\theta_r + I_{r\beta}\cos\theta_r \quad 2.38$$

$$I_{msD} = (L_s/L_m) * I_{sD} + I_{rD} \quad 2.39$$

$$I_{msQ} = (L_s/L_m) * I_{sQ} + I_{rQ} \quad 2.40$$

$$I_{ms} = \sqrt{I_{msD}^2 + I_{msQ}^2} \quad 2.41$$

$$\rho_s = \tan^{-1}(\lambda_{sQ}/\lambda_{sD}) \quad 2.42$$

$$\rho_s = \tan^{-1}\left(\frac{I_{msQ}}{I_{msD}}\right) \quad 2.43$$

3. The stationary rotor current is transformed to stator flux oriented reference frame by the following transformation equations.

$$I_{rX} = I_{rd}\cos\rho_s + I_{rq}\sin\rho_s \quad 2.44$$

$$I_{rY} = -I_{rd}\sin\rho_s + I_{rq}\cos\rho_s \quad 2.45$$

4. The rotor currents in the stator flux oriented reference frame are transformed into three phase currents. The reference rotor current which is the output from active and reactive power controller is also transformed to three phases and is applied to hysteresis current controller to be compared with actual rotor currents

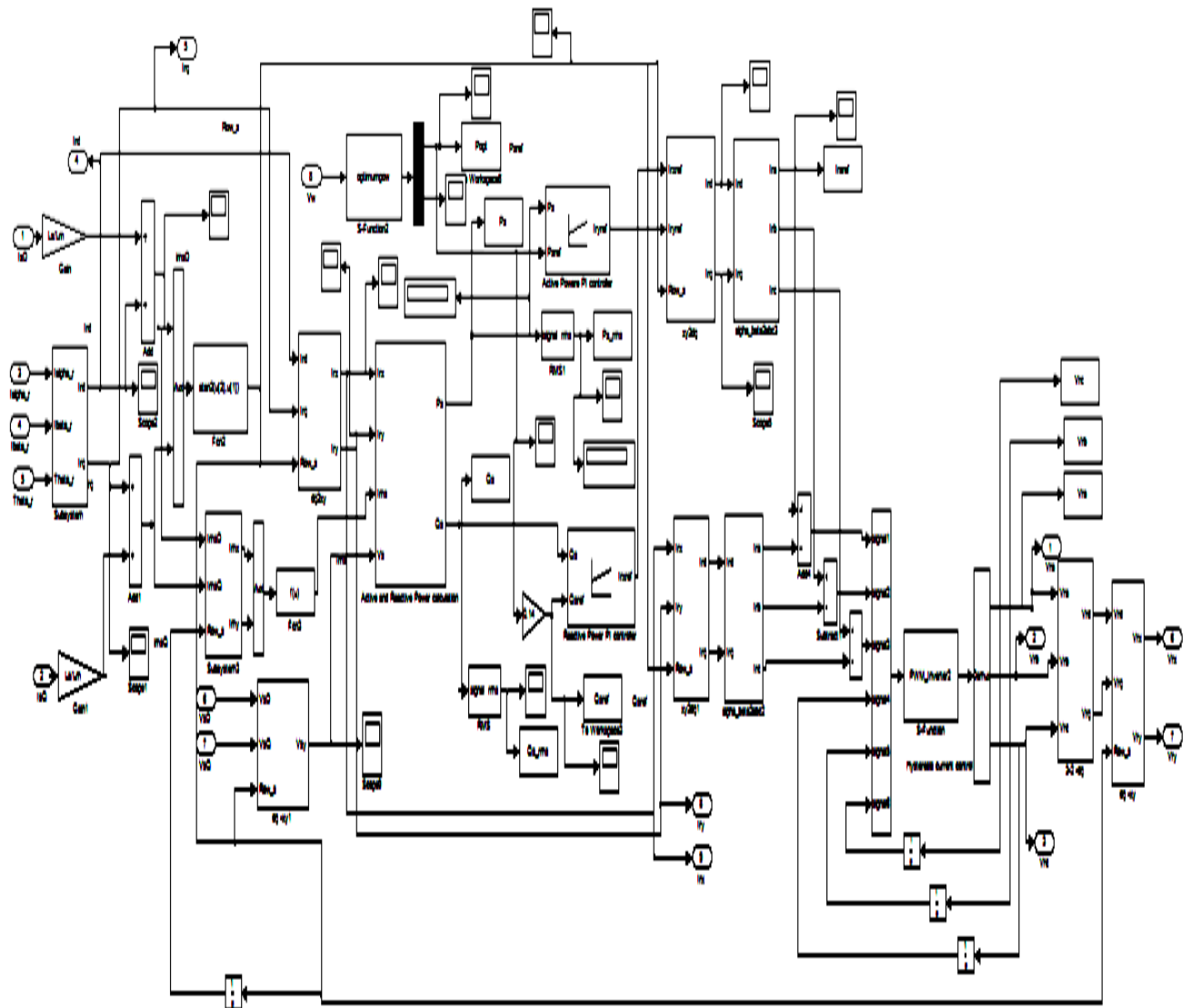


Figure2.9 Modelling of rotor side converter using conventional PI controller

2.4 Grid side converter control strategy:

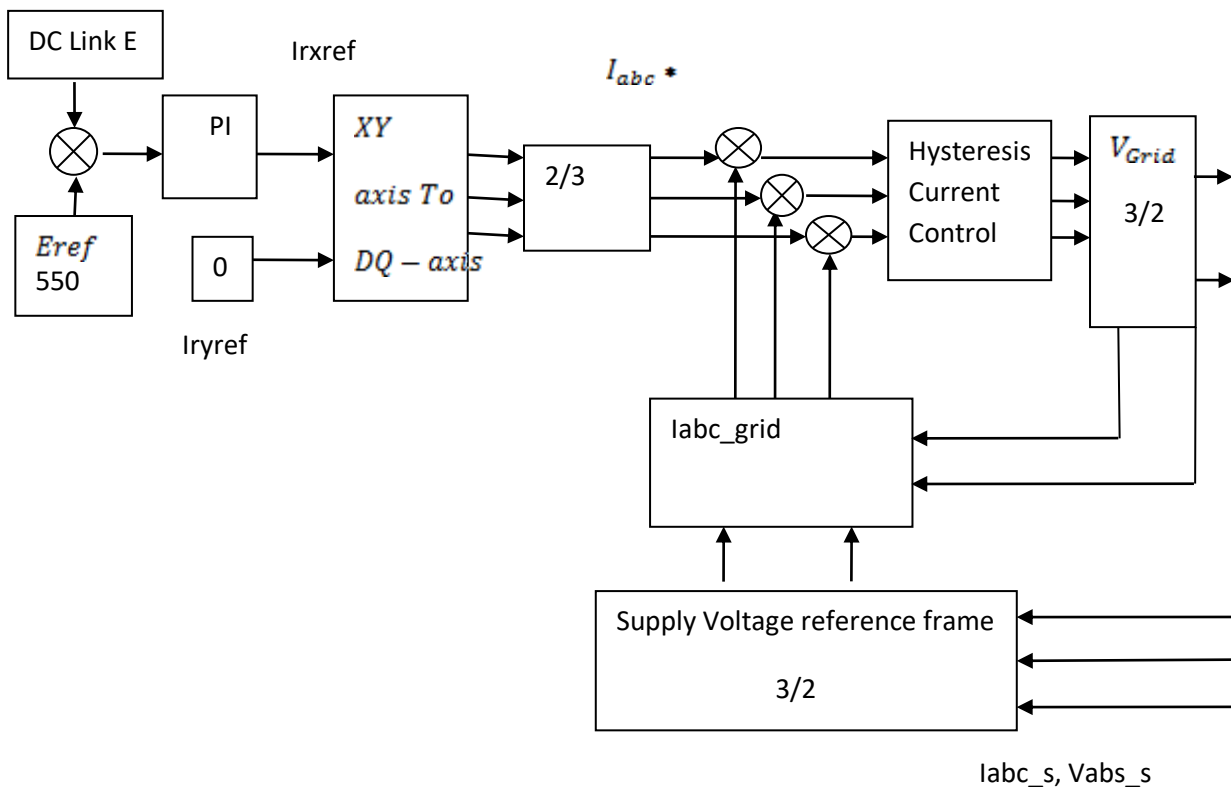


FIG 2.10 Scheme for grid side converter control

The main purpose of GSC is to keep the dc link voltage constant irrespective of the flow of rotor power. The grid side converter control scheme starts with transforming the grid voltages to the stationary reference frame and the voltage vector angle is calculated using D and Q axis stationary reference frame grid Voltage. The dc link voltage can be controlled by controlling the direct axis current I_x in the voltage vector oriented reference frame. Thus, a reference current I_{xref} is derived from the DC link voltage error i.e. the error between the actual dc link voltage and the reference dc link voltage of the converter bridge by tuning a Voltage PI controller. The current I_{yref} was forced to make zero so as to make the displacement equal to zero.

The reference currents in the grid voltage vector oriented frame were then transformed to their natural frame of reference i.e the stationary frame. Then from the stationary frame it is converted to three phase to implement hysteresis modulation. The actual line current is calculated by considering the inductance drop of the line.

The objective of the grid side converter is to keep the dc link voltage constant irrespective of the direction of rotor power flow. Decoupled control of active and reactive powers flowing between rotor and grid is done by using supply voltage vector oriented control. In such a scheme, current I_x is controlled to keep the dc link voltage constant and current I_y is used to obtain the desired value of reactive power flow between supply side converter and the supply.

2.4.1 Supply voltage oriented vector control scheme

All voltage and current quantities are transformed to a special reference frame that rotates at the same speed as the supply voltage space phasor with the real axis (x-axis) of the reference frame aligned to the supply voltage vector. The real axis (x) is aligned with the supply voltage phasor. The supply voltage angle should be in orientation with the supply voltage. The grid side converter terminal voltage and the phase currents are also referred to new reference frame. First the supply voltage angle (θ_s) has to be determined. By definition, the Supply voltage angle is-

$$\theta_s = \tan^{-1} \frac{V_s Q}{V_s D} \quad 2.46$$

The real axis (x) is aligned with the supply voltage phasor. Thus, $V_y = 0$. Hence, the powers between the grid side converter and the grid are:

$$P_s = \left(\frac{3}{2}\right) * (V_x * I_x + V_y * I_y) = \left(\frac{3}{2}\right) * (V_x * I_x) \quad 2.47$$

$$Q_s = \left(\frac{3}{2}\right) * (V_y * I_x + V_x * I_y) = \left(\frac{3}{2}\right) * (V_x * I_y) \quad 2.48$$

Then the current flowing between the grid and the converter can be obtained from-

$$V_x = R * I_x + L * \frac{d}{dt}(I_x) - \omega_s * L * I_y + V_{conX} \quad 2.49$$

$$V_y = R * I_y + L * \frac{d}{dt}(I_y) - \omega_s * L * I_x + V_{conY} \quad 2.50$$

Therefore, it is seen that in supply voltage reference frame the x-axis current controls the active power and the y-axis current controls the reactive power.

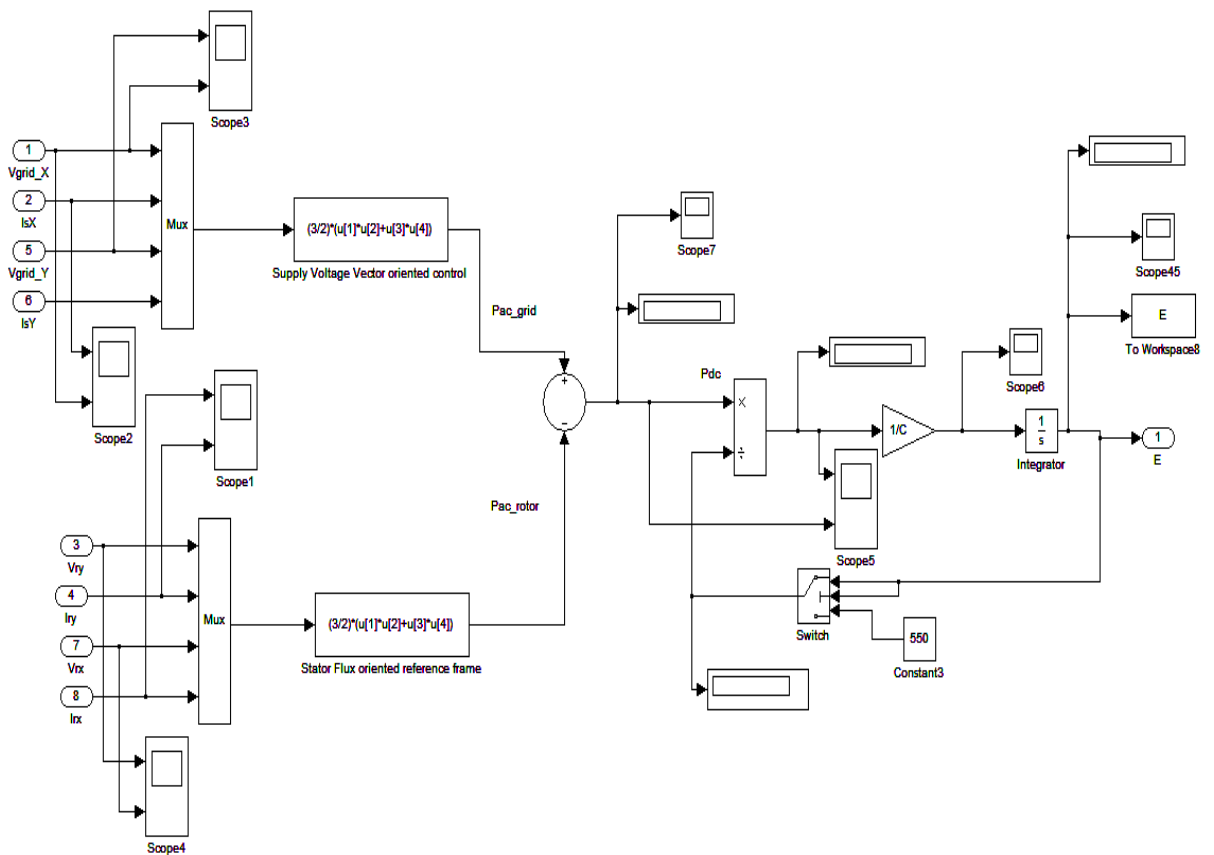


Figure2.12 Modelling of dc link voltages

2.6 Modelling of overall system:

The overall system modelling contains the modelling of wind turbine, and an S function coded block for maximum power point tracking from the wind turbine. It also contains the vector control of rotor side converter and grid side converter and the modelling of DC link voltage along with an s-function coded block of Hysteresis current control PWM switching of pulses. The scheme also contains active and reactive power fuzzy PI controllers along with the fuzzy active and reactive power controllers.

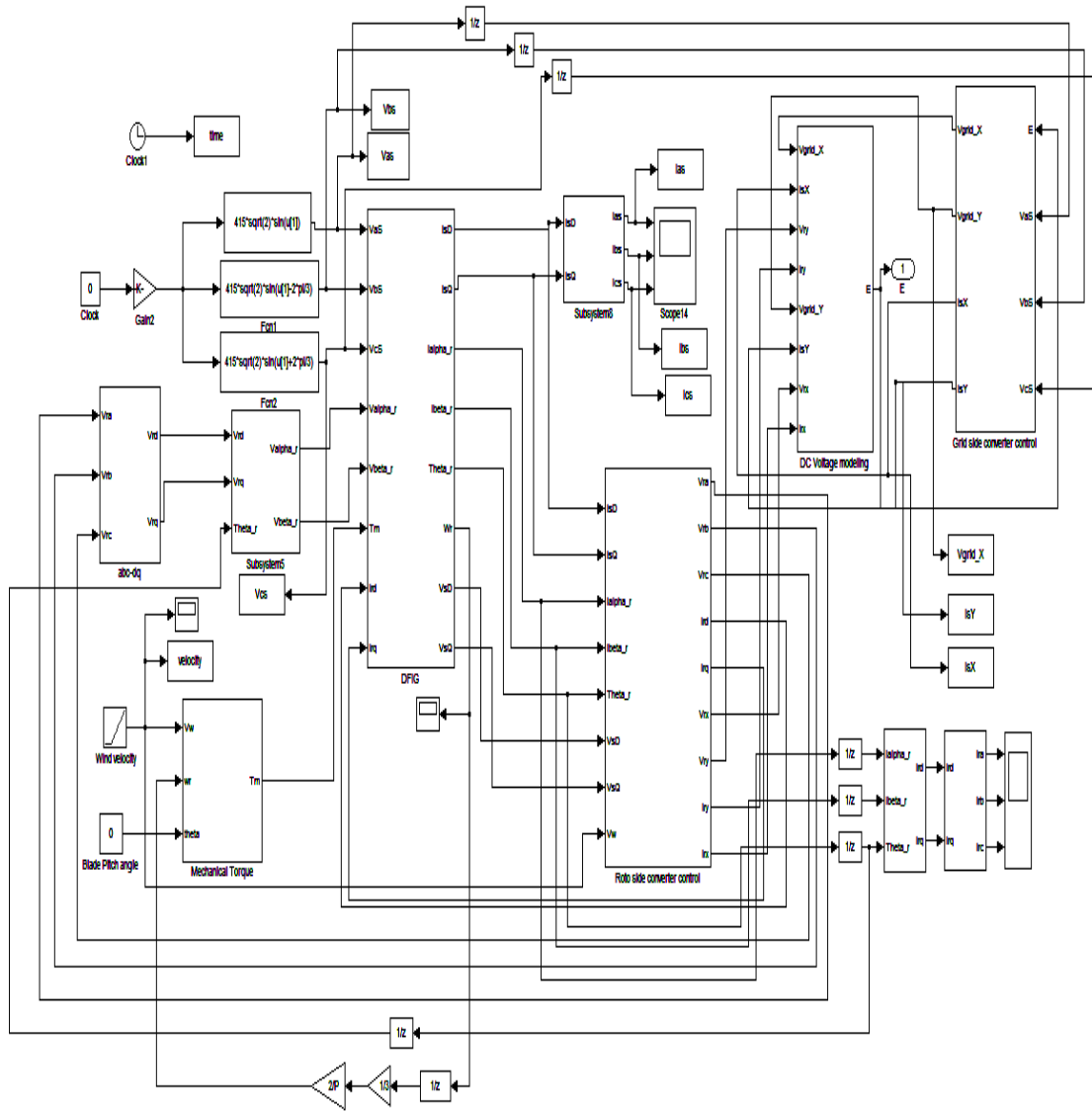


Figure2.13 Modelling of overall system

Chapter 3

Doubly fed Induction Generator Under fault conditions

3.1 Principle of operation of wind energy driven DFIG

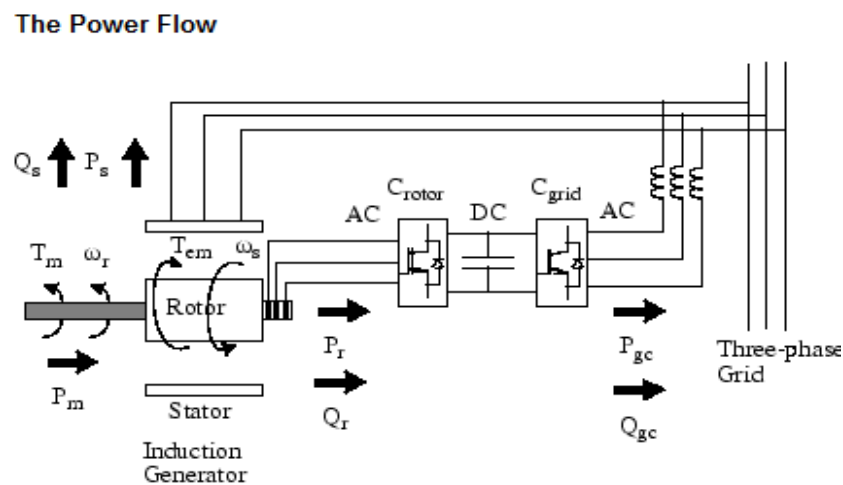


Fig 3.1 Principle of operation of wind energy driven DFIG

In this Wind Energy generation scheme, the stator side is connected to the AC grid, and the wound rotor is fed from the power electronics back to back PWM converter through slip rings to allow variable speed DFIG to operate at a variable speed in response to changing wind velocity. The basic concept of this scheme is to insinuate a frequency converter between the variable frequencies doubly fed induction generator and the fixed frequency grid. The DC capacitor linked between the stator and rotor side converter allows the storage of power from induction generator for further generation. The slip power depending on the speed of machine can flow in both directions. It can flow from the supply to the rotor and from the rotor to the supply. This scheme can operate well on both sub-synchronous and super-synchronous modes of operation. The generator can be controlled as a generator or as a motor in both sub-synchronous and super-synchronous speed modes of operation. The rotor side converter operates as a rectifier and stator side converter as inverter below the synchronous speed in the motoring mode and above the

synchronous speed in the generating mode, where the slip power is returned to the stator. Again rotor side converters operates as an inverter and stator side converter as a rectifier below the synchronous speed in the generating mode and above the synchronous speed in the motoring mode, where slip power is supplied to the rotor. At the synchronous speed, machine behaves as a synchronous machine by taking slip power to excite the rotor windings. The mechanical power and the stator electric power output are computed as follows:

$$P_m = T_m \omega_r \quad 3.1$$

$$P_s = T_{em} \omega_s \quad 3.2$$

For a loss less generator the mechanical equation is:

$$J \frac{d\omega_r}{dx} = T_M - T_{em} \quad 3.3$$

In steady-state at fixed speed for a loss less generator and

$$T_m = T_{em} \quad 3.4$$

$$P_m = P_s + P_r \quad 3.5$$

It follows that:

$$P_r = P_m - P_s \quad 3.6$$

$$= T_m \omega_r - T_{em} \omega_s \quad 3.7$$

$$= T_m \left(\frac{\omega_s - \omega_r}{\omega_s} \right) \omega_s = -s T_m \omega_s = -s P_s \quad 3.8$$

Where, S is defined as the slip of the generator

Generally the absolute value of slip is much lower than 1 and, consequently, P_r is only a fraction of P_s . Since T_m is positive for power generation and since P_s is positive and constant for a constant frequency grid voltage, the sign of P_r is a function of the slip sign. P_r is positive for negative slip (speed greater than synchronous speed) and it is negative for positive slip (speed lower than synchronous speed). For super-synchronous speed operation of DFIG, the rotor power P_r is transmitted to DC bus capacitor which happens to raise the DC voltage. During sub-synchronous speed operation of DFIG,

power is taken from the DC bus capacitor which tends to decrease the DC link capacitor voltage. Grid side converter is used to generate or absorb the power P_{gc} in order to keep the DC voltage constant. In steady-state for a loss less AC/DC/AC converter P_{gc} is equal to P_r and the speed of the wind turbine is determined by the power P_r absorbed or generated by Rotor converter.

It can be considered that if the phase-sequence of the alternating voltage generated by rotor side converter is positive for sub-synchronous speed then it will be negative for super-synchronous speed. The frequency of this voltage is equal to the product of the grid frequency (f) and the absolute value of the slip(s) i.e sf . At synchronous speed there is no flow of rotor current and only dc excitation is applied to the rotor which makes it to behave like a synchronous machine.

3.2 Advantages of Variable Speed Wind driven DFIG

The advantages of the above scheme are as follows-

- DFIG can be operated below, above and at synchronous speed. The speed range is restricted only by the rotor voltage rating of the DFIG.
- With DC currents injected into the rotor circuit operation of DFIG at synchronous speed is possible with the inverter working in chopping.
- Comparatively low distortion stator, rotor and supply currents flow
- Independent and decouple control of active and reactive power can be achieved.
- Control of the displacement factor between the voltage and the current in the supply converter, and hence control over the system power factor can be obtained.
- The power converters need only to handle the low rated rotor power which is very less compared to the Stator power. So, the ratings of the power converters are also reduced and correspondingly became more cost effective.

3.3 Different modes of operation

There are four modes of operation of this scheme. They are as follows-

- Sub-synchronous Motoring
- Sub-synchronous Regeneration.
- Super -Synchronous Motoring.

➤ Super-Synchronous Regeneration.

3.3.1: Sub-synchronous Motoring

In the Sub-synchronous Motoring mode, the stator input or air gap power is positive and remains constant and the slip power which is proportional to slip is returned back to the line through the converter. Therefore the line supplies the net mechanical power output consumed by the shaft. The slip frequency current in the rotor creates a rotating magnetic field in the same direction as in the stator and the rotor speed corresponds to the difference between these two frequencies. At true synchronous speeds ($\omega = \omega_s$), the converter supplies DC excitation to the rotor and the machine behaves like a standard synchronous motor.

3.3.2: Sub-Synchronous Regeneration

In Sub-Synchronous Regeneration mode, the shaft is driven by the load and the mechanical energy is converted into the electrical energy and pumped out of the stator. With negative rated torque, the mechanical power input to the shaft increases with speed and this equals the electrical power fed to the line. In the sub-synchronous speed range, the slip is positive and the air gap power is negative. Therefore negative slip power is fed to the rotor from the converter so that the total air gap power is constant. The rotor current has positive phase sequence. At synchronous speed converter supplies DC excitation current to the rotor and the machine behaves as a synchronous generator.

3.3.3 Super synchronous Motoring

In Super synchronous Motoring mode, the shaft speed increases beyond the synchronous speed, the slip becomes negative and the slip power is absorbed by the rotor. The slip power supplements the air gap for the total mechanical power output. The line therefore supplies slip power in addition to stator input power. At this condition, the phase sequence of the slip frequency is reversed so that the slip current induced rotating magnetic field is opposite to that of the stator.

3.3.4 Super synchronous Regeneration-

In Super-synchronous regeneration mode the stator power output remains constant, and the additional mechanical power input is also added as a slip power output. The converter phase- sequence is now reversed so that the rotor field rotates in opposite direction. The variable speed wind generation mentioned for mode 3 can also be used in this mode.

3.4 TYPES OF WIND CONVERSION SYSTEMS

A wind energy conversion system can be operated using three types of Induction Machines. These three types of Induction machines are as follows:

1. Conventional fixed speed systems
2. Variable speed WECS with squirrel cage induction generator
3. Variable speed WECS with wound rotor induction generator

3.4.1 Fixed speed operation

Fixed speed wind electric conversion systems (WECS) generally use squirrel cage induction generators with direct grid connection so as to maintain a fixed speed that matches the electrical frequency of the grid. Pole changing method is generally employed in order to operate the fixed speed systems at low and high wind velocities efficiently. Smaller number of pole pairs is used at high wind speeds and higher number at lower wind speeds. This allows the generator or the machine to operate at a different mechanical speed without affecting its actual electrical frequency. The advantage of this scheme is that a cost effective aerodynamic control like stall control can be used. However, certain drawbacks in fixed speed systems are observed. They are:

- It cannot optimally use the available wind power due to constant speed operation.
- Since there is no inherent reactive power control method in this configuration, it must use capacitor banks instead of drawing the reactive power from the grid.
- Since the generator is made to run at a constant speed in spite of fluctuations in wind speed, it will result in fluctuation of generated voltage as well as output power.

In variable speed systems, the turbine rotor absorbs the mechanical power fluctuations by changing its speed. So the output power curve is smoother which greatly enhances the quality of power. However, since variable speed operation produces a variable frequency voltage, a power electronic converter must be used to connect to the constant frequency grid.

3.4.2 Variable speed WECS with squirrel cage induction generator:

In this setup the stator of the squirrel cage induction generator will be connected to the grid by means of back-to-back connected power electronic converter bridges as shown in Fig. 4.2. The converter is needed because the variable speed generator produces a variable frequency voltage that has to be converted to match the constant grid frequency. Since the power converter has to convert all the stator power, the converter size depends on the stator power rating. The advantages of this configuration are:

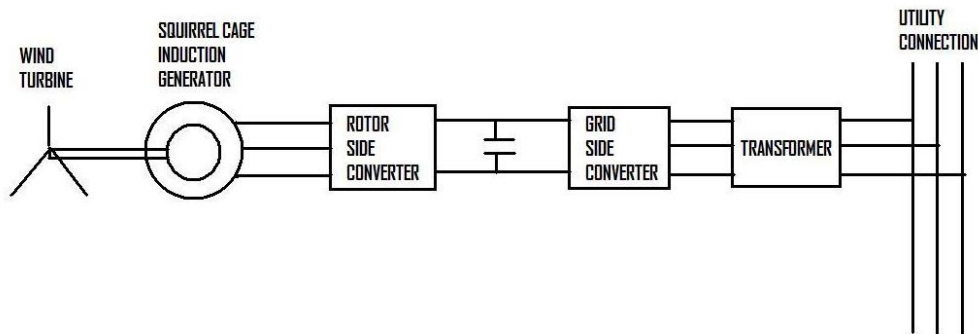


Figure 3.2 Variable speed WECS with squirrel cage induction generator

- Its ability to make the best use of available wind power and
- The fact that it eliminates the need for a capacitor bank since it is able to draw its required reactive power from the grid.
- However, the cost of the power converter can be high due to its large size.

3.4.3 Variable speed WECS with wound rotor induction generator:

Although a squirrel cage induction generator may be used in variable speed WECS, the power converter size in the earlier system can be reduced by using it on the rotor side of a wound rotor induction generator. Fig. 4.3 shows a variable speed system using a wound rotor generator. The power converter is now connected between the rotor and grid. So it needs to carry only the slip power, the magnitude of which will be the machine slip times the stator power. In general though wound rotor induction generators cost more than the squirrel cage type, however, for large ratings the cost becomes comparable. So, the net advantages of using a wound rotor generator outweigh that of a squirrel cage machine for utility scale wind power generation. This scheme is the most used and recommended scheme now days for WECS.

The advantages of this system are-

- Reduced converter cost due to low level inverter rating compared to system rating.
- Reduced cost of inverter filter due to low power level.
- Independent control of active and reactive power of the generator.

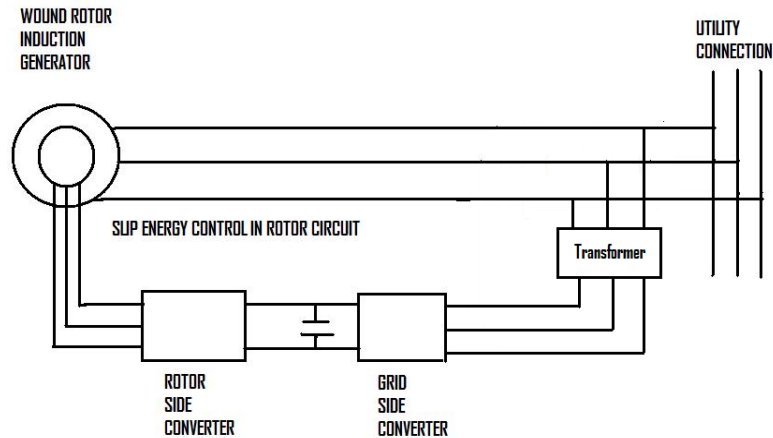


Figure 3.3 Variable speed WECS with wound rotor induction generator

3.5 Study of Transients in Wind driven doubly fed Induction Generator

Power system transient stability is the ability of the system to return to its stable operating condition after the occurrence of a disturbance that changes its topology.

Examples of changes of the topology of a power system are

- (i) Sudden Tripping of the generator or the line,
- (ii) Sudden change in load.
- (iii) A short circuit fault symmetrical or unsymmetrical.

Unwanted transients occur in the Stator and rotor currents whenever a fault occurs at the PCC i.e point of common coupling in the power grid. The transmission of generated Active power into the grid from Wind Driven DFIG is also effected due to the Voltage drop. The DC link Voltage fluctuation also increases. When an Unsymmetrical fault occurs the positive sequence negative and Zero sequence currents come into scenario. The negative sequence currents are responsible for the over current appearing in the rotor circuit. A clockwise rotating magnetic motive force (MMF) is formed in the generator air gap. This MMF will then induce a clockwise rotating flux in the gap, which induces an electromotive force (EMF) in the rotor circuit with a frequency of $(2 -$

$s)\omega_s$. So, the induced rotor current components has a frequency of $(2 - s)fs$ as well, where s is the slip.

For more severe unsymmetrical fault condition at the stator side, the magnitude of the rotor current harmonics will be higher which can lead to higher harmonics in the generated electromagnetic torque.

During the Fault instant, due to short circuit, the voltage at the generator terminal drops down. Due to this phenomenon several consequences takes place.

- Generator Stator and rotor flux decreases which aids the demagnetizing process in the generator. The consequent of the demagnetizing process is that the generated active power and the Electromagnetic torque of the machine also decrease. The Mechanical torque from the wind turbine gets higher as compared to the electromagnetic torque and therefore the generator starts to accelerate.
- High amount of current transients start appearing in the stator and rotor windings.
- The Grid Side Converter is unable to transfer the excess power from the rotor through the Rotor side converter further to the grid. As a result, the excess energy rather than going back to the connected grid goes into charging the dc-Link capacitor connected between the Rotor and Grid Side converter rapidly.
- A part of the potential energy stored in the rotating shaft of the Wind Turbine DFIG cannot transfer the energy to the system suddenly due to the mass of the shaft. This delays the restoration of the grid frequency. As a result of consequence there appear oscillations in the rotating mass of the machine shaft which can be even more with high time constant and damping ratio.

During the occurrence of fault the rotor current of the doubly fed Induction generator rises to a high level which can affect the converter circuit. The converters are relatively of lower power rating as they are required to handle the rotor circuit power i.e the rotor slip power. So they are designed to handle 30% of the DFIG rating, and are primarily used in order to supply active power to the grid. The two major issues to be addressed during fault in a wind driven DFIG is firstly the over current in the rotor circuit and secondly DC link Voltage fluctuation. Typically, the rotor current limit is twice the rated value and the dc-link voltage limit is about 1.2 times its rated value.

3.5.1 After Clearance of the Fault

The instant after the fault is cleared, the voltage cannot be recovered immediately completely because Rotor Side Converter cannot provide the necessary reactive power to the generator for its magnetization process. The generator thus absorbs the required reactive power directly from the grid and delays the recovering process of the grid voltage. The dc-Link voltage is brought back to its nominal value successfully by the grid side converter. The generator currents and voltages start to incline or rather converge to their pre fault values gradually from that moment. The Rotor Side Converter regains its decoupled control over the generated active and reactive power.

3.5.2 Unbalanced Network Voltage

Under Unbalance Network and assuming no zero sequence components, the three-phase parameters such as voltages, currents, and flux may be decomposed into positive and negative sequence components. In the stationary reference frame (DQ), the voltages, currents, and flux can be decomposed into positive and negative sequence components as

$$F_{DQ}(t) = F_{DQ+}(t) + F_{DQ-}(t) \quad 3.9$$

$$F_{DQ}(t) = F_{DQ+}(t).e^{j(\omega_s t + \varphi^+)} + F_{DQ-}(t).e^{-j(\omega_s t + \varphi^-)} \quad 3.10$$

Where φ^+ and φ^- are the respective phase shift for positive and negative sequence components. For positive (dq)+reference frame the d+ axis is fixed to the positive stator flux rotating at speed of ω_s . While for the negative (dq) – reference frames its d– axis rotating at an angular Speed of $-\omega_s$ with the phase angle to the D axis being $-\theta_s$.

The transformation between and reference frames are given by

$$F_{dq^+}(t) = F_{DQ+}(t).e^{-j\omega_s t} \quad 3.11$$

$$F_{dq^+}(t) = F_{DQ+}(t).e^{-j2\omega_s t} \quad 3.12$$

$$F_{dq^-}(t) = F_{DQ+}(t).e^{j\omega_s t} \quad 3.13$$

$$F_{dq^-}(t) = F_{DQ+}(t).e^{j2\omega_s t} \quad 3.14$$

Using above two equations the stator and rotor current, voltage, and flux vectors can be expressed using their respective positive and negative sequence components as:

$$F_{sdq} + (t) = F_{sdq+} + (t) + F_{sdq-} + (t) \quad 3.15$$

$$= F_{sdq+} + (t) = F_{sdq+} + F_{sdq-} - (t). e^{-j2\omega st} \quad 3.16$$

$$F_{rdq} + (t) = F_{rdq+} + (t) + F_{rdq-} + (t) \quad 3.17$$

$$= F_{rdq+} + (t) = F_{rdq+} + F_{rdq-} - (t). e^{-j2\omega st} \quad 3.18$$

The active and reactive power in terms of oscillating components are given by

$$P_S = P_{SO} + P_{SSin2} \cdot Sin(2\omega st) + P_{SCos2} \cdot Cos(2\omega st) \quad 3.19$$

$$Q_S = Q_{SO} + Q_{SSin2} \cdot Sin(2\omega st) + Q_{SCos2} \cdot Cos(2\omega st) \quad 3.20$$

3.6 Grid Codes for Wind Generating Station in India

3.6.1 Grid behaviour of wind turbines

Important aspects which determine the grid behaviour of wind turbines are that majority of these are fixed speed turbines consisting of induction generators. This is unlike the conventional generators which are synchronous generators / alternators and have characteristics different from the induction generators. Machines with induction generators need capacitor banks for VAR support, otherwise reactive power will be drawn from the grid. The drawl of reactive power affects the voltage profile at the point of connection to the grid. However, wind turbines of variable type, which use wound rotor or permanent magnet synchronous generators, do not need a reactive power support. They may have to deal with issues like harmonics generated by the power converters, which has to be kept under control. Another major characteristic is the behaviour of the wind turbine during system faults/ disturbances. The wind turbines are designed to disconnect from the grid during system faults, when the voltage at the point of connection drops beyond a certain percentage of the nominal value. If wind turbines are to remain connected to the grid during system fault, a source of reactive power must be able to sustain the wind turbine in the generation mode during such fault conditions.

3.6.2 The grid codes for wind, in general deal with the following issues:

- Active power control
- Frequency
- Voltage and reactive power issues
- Fault ride through capability
- Protection
- Power quality issues like flicker, harmonics etc.

3.6.1.1 Active power control

This is the ability of the wind turbine generators to regulate the active power output of the wind turbine according to system requirements. Active power control of wind turbines is to ensure a stable frequency in the system, to prevent overloading of transmission lines, to avoid large voltage steps and in-rush currents during start up and shut down of wind turbines. In a wind turbine, the power output is a function of the wind speed and the power fed into the grid by the turbine irrespective of the frequency of the grid. However, with this feature the active power controller will take into account not only the wind speed, but also the requirements of the grid. The wind turbines will also have to regulate the in rush currents during start up.

During a fault, if the turbine were to stay on line, the active power output has to be reduced in a controlled manner to prevent tripping of the generator. All the same, the active power output should be brought back to the pre fault value after the fault is cleared.

The rate at which the power is ramped up after a system fault or during start up should not cause significant power surges.

3.6.1.2 Frequency requirements

System frequency is a major indicator of the power balance in the system. A decrease in generation vis-a-vis the demand causes the frequency to drop below the nominal frequency and vice versa. In India, the frequency varies from 48.5- 51.5 Hz due to the power imbalance. This imbalance can be mitigated by primary control and secondary control of conventional synchronous generators. During an increase of load, the energy stored in these synchronous generators can balance the power for 1- 30 s, this is the primary control. The secondary control, employed with time span of 10 – 15 min. is by

governor action which increases the input to the generator and stabilizes the system frequency.

Low penetration of wind turbines does not affect the system frequency. High penetration of wind turbines can have a significant impact on the grid. Even so, the wind turbines may not be able to contribute to primary control. The power output of the wind turbine can be regulated during high frequency, if needed. However, during low frequencies the output of the wind turbine cannot be controlled to contribute more power to the grid.

3.6.1.3 Voltage and reactive power issues

Wind turbines with induction generators need reactive power support. Capacitor banks are the preferred method of reactive power compensation in wind farms, though dynamic VAR support devices like the STATCOM are available. If not properly compensated reactive power drawl from the system can cause increased losses, overheating and de- rating of the lines. Doubly fed induction generators and synchronous generator based wind turbines do not have any constraints with respect to reactive power. Thus, the behavior of different types of wind turbines can be standardized by means of the grid code.

3.6.1.4 Fault / low voltage ride through

This refers to the ability of the wind turbine to remain connected to the grid without tripping from the grid for a specified period of time during a voltage drop at the point of connection. The period of fault ride through depends on the magnitude of voltage drop at the Point of Common Coupling (PCC) during the fault and the time taken by the grid system to recover to the normal state.

During system disturbances, if generators of large generating capacity connected to the grid continue their operation, this aids the system in returning to normal operation. On the other hand, disconnection of such a generator would further aggravate the disturbance and may lead to a system collapse. If the fault causes loss of a conventional generating unit, the system would need sufficient spinning reserve to cover the loss of the generator. Hence the need for fault rides through capability.

During a fault that causes a voltage drop at the wind turbine terminals, the reactive power demand of induction generators increases. Unless a reactive power support is available at the generator terminals, the reactive power will be drawn from the grid.

This will reduce the thermal capacity of the conductors connecting the turbine to the grid, to transfer active power and cause further drop in voltage at the point of common coupling.

➤ **Wind farm protection**

In case of large wind farms connected to the grid, wind turbines are required to remain connected to the grid within specified voltage and frequency limits. High short circuit currents, under voltages and over voltages during and after the fault can damage the wind turbine. The relay protection system of the wind turbine should take in to account:

- Normal operation of the system and support to network during and after the fault.
- Secure wind farms from damage originating from faults in the network.

Wind turbines are required to be equipped with under frequency and over frequency protection, differential protection of the generator transformer, and back up protection. The protection system requirements have been mentioned in some of the grid codes. Grid codes require that wherever low voltage ride through schemes and frequency protection schemes are applied on the wind turbines, the settings should be done in proper coordination with the transmission system protection relaying.

3.6.1.5 Data requirements

Monitoring of large wind farms to obtain up-to-date information on the real time status of the wind farm is essential. This will help in tracking the dynamic changes that the wind farms will undergo. The system operator can change the set point according to the operating conditions.

3.6.1.6 Power quality issues like flicker, harmonics etc

Flicker is defined as the visual fluctuations in the light intensity as a result of voltage fluctuations and is caused by wind turbines, both during continuous operations and switching operations. Human eye is most sensitive to frequencies in the range 1- 10 Hz. Power fluctuations due to wind speed fluctuations lie in the frequency range of < 0.1 Hz and hence are less critical to flicker. Flicker in variable speed turbines is found to be lower than that of fixed speed wind turbines due to smoothening of the power fluctuations.

3.6.3 Indian Wind Grid Code

Planning Code for transmission systems evacuating wind power

Wind power evacuation shall feature as a part and parcel of the overall grid planning.

The transmission utility / transmission system operator have to consider both short term and long term expected wind generation in the region. The planning criterion should consider the following scenarios:

- i. System peak load with high wind generation
- ii. System light load with high wind generation
- iii. Local light load with high wind generation

The high wind generation have to be classified as a percentage of the overall wind farm capacity, based on the voltage level to which it is connected. For instance, wind farms connected below 66 kV levels may reach their peak capacity during the windy months as wind turbines see the same wind over a smaller geographical spread; this must be taken care of during the transmission planning.

3.6.4 Connection code for wind farms

Wind farms have to maintain certain minimum technical standards for grid connection with respect to the following:

3.6.4.1 Transmission voltage range

The wind farms must be capable of normal operation for the following voltage ranges.

Table: 3.1: Voltage withstand limits for wind farms

Voltage (kV)			
Nominal	% Limit of variation	Maximum	Minimum
400	+5% to -10%	420	360
220	+11% to -9%	245	200
132	+10% to -9%	145	120
110	+10% to -12.5%	121	96.25
66	+10% to -9%	72.5	60
33	+5% to -10%	34.65	29.7

3.6.4.2 Voltage unbalance

Voltage unbalance, defined as the ratio of the deviation between the highest and lowest line voltage to the average of the three line voltages, can cause negative sequence current to flow in the rotor of the wind turbine. As per the Grid Standard (CEA) followed, the following limits have been specified:

Table 3.2 Voltage unbalance limits for wind farms as per CEA

Voltage level (kV)	Unbalance (%)
400	1.5
220	2
<220	3

3.6.4.3 Reactive power capability

The wind farms should be able to maintain a power factor of 0.95 lagging to 0.95 leading at the grid connection point. At system voltages higher than nominal, the requirement is a lagging power factor, whereas at lower voltages, the wind farm can operate at leading power factor injecting reactive power to the grid.

3.6.4.4 Frequency tolerance range

The frequency tolerance range for wind farms is 47.5 – 51.5 Hz. Beyond this, the frequency tolerance should be manufacturer specific. Wind farms should be able to withstand change in frequency up to 0.5 Hz/sec.

3.6.4.5 Active power control

For wind farms at high voltage levels active power control of the wind farm output shall be possible on system operator's request.

The active power response of wind farms to frequency should be such that the power injection into the grid is limited at frequencies above nominal.

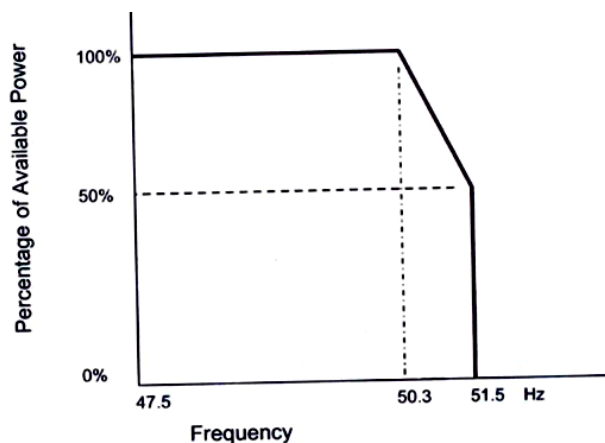


Figure 3.4 Variation of active power output of wind farms with respect to frequency

3.6.4.6 Low voltage ride through

Wind farms should have low voltage ride through capabilities.

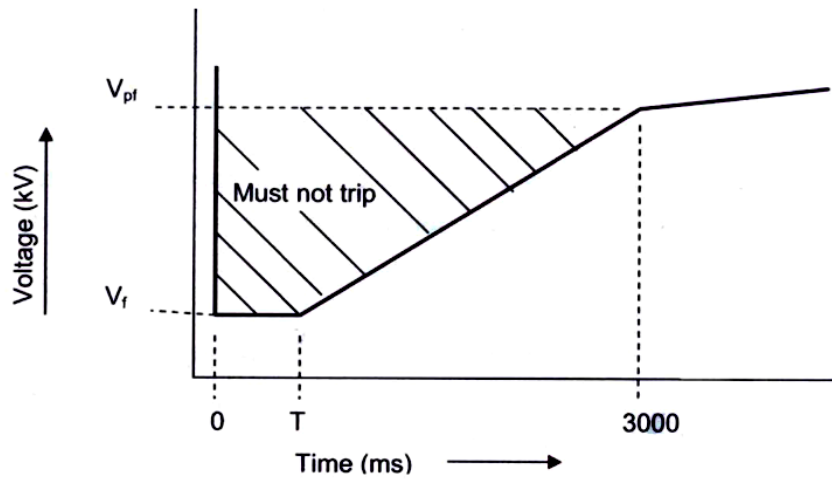


Figure 3.5: Fault ride through characteristics

V_f : 15% of nominal system voltage

V_{pf} : Minimum Voltage for normal operation of the wind turbine

Table 3.3 Typical Parameters during Fault

Nominal system voltage (kV)	Fault clearing time, T(ms)	V_{pf} (kV)	V_f (kV)
400	100	360	60.0
220	160	200	33.0
132	160	120	19.8
110	160	96.25	16.5
66	300	60	9.9

Protection schemes for wind farm protection:

The minimum requirement with respect to wind farm protection is:

- i) under/over voltage protection
- ii) under/over frequency protection
- iii) over current and earth fault protection
- iv) load unbalance (negative sequence) protection
- v) differential protection for the grid connecting transformer
- vi) capacitor bank protection

vii) tele-protection channels (for use with distance protection) between the grid connection point circuit breaker and user connection point circuit breaker.

During fault ride-through, the Wind turbine generators (WTGs) in the wind farm should have the capability to meet the following requirements:

- a) Should minimize the reactive power drawl from the grid.
- b) The wind turbine generators should provide active power in proportion to retained grid voltage as soon as the fault is cleared.

Chapter 4

Control Strategy used for grid fault ride through

4.1 Control Strategy

The main objective of the control strategy in our Wind driven DFIG system design is to

1. Maximise power generation in Wind Turbine driven DFIG.
2. Limit Active power production in case of high wind speed.
3. Reactive Power Control during faults by controlling reactive power exchange between the grid and the machine.
4. Minimize the transients in rotor and stator current, stator active power, DC link Voltage etc during unsymmetrical faults
5. To reduce the negative sequence stator flux in DFIG during unsymmetrical faults without using external device.

An innovative control strategy is used in this project to increase the stability of the wind driven DFIG during fault conditions as well as normal conditions. The main objective is to give a smooth operation and maximize active power output during fault and normal operations. Unsymmetrical fault is associated with positive, negative and zero sequence components of voltage, current and flux. As the Voltage at the PCC drops, demagnetizing occurs to keep the flux constant, negative sequence flux increases which rotates at synchronous speed in the opposite direction of that of the rotating magnetic field and hence cut the rotor conductors at relatively twice the speed. The negative sequence currents are responsible for the over current appearing in the rotor circuit. As the rotor current transients appear in the circuit this leads to transients in the stator active power using equation (4.1).

$$P_S = -\left(\frac{3}{2}\right) * |V_S| * L_m/L_s * I_{rY} \quad 4.1$$

As the rotor current increases the GSC cannot pump out all currents towards the grid side and hence DC link voltage also increases. The negative sequence flux causes an adverse effect on the entire circuit.

We know that-

$$V_{rabc} = R_r I_{rabc} + \frac{d\lambda_{rabc}}{dt} - \omega_s \lambda_{sabc} \quad 4.2$$

$$\lambda_{sabc} = L_S I_{sabc} + L_M I_{rabc} \quad 4.3$$

$$\lambda_{rabc} = L_S I_{rabc} + L_M I_{sabc} \quad 4.4$$

Using above equations we get:

$$\lambda_{rabc} = \frac{L_M}{L_S} \lambda_{sabc} + \frac{L_S L_r - L_M^2}{L_S} I_{rabc} \quad 4.5$$

$$\sim \lambda_{sabc} + (L_{ls} + L_{lr}) I_{rabc} \quad 4.6$$

$$\text{And } I_{sabc} = \frac{L_r \lambda_{sabc} - L_M \lambda_{rabc}}{(L_r L_S + L_M^2)} \quad 4.7$$

Also

$$\lambda_{sabc} = \lambda_{1_sabc} + \lambda_{2_sabc} + \lambda_{0_sabc} \quad 4.8$$

$$L_S = L_{lS} + L_M \quad 4.9$$

$$L_r = L_{lr} + L_M \quad 4.10$$

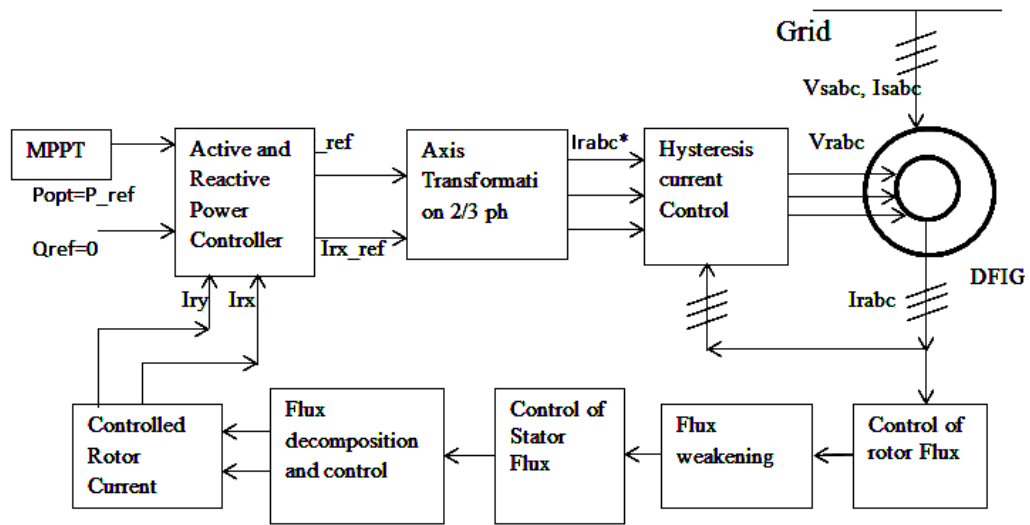


Figure: 4.1 Control Strategy Scheme for DFIG

After unsymmetrical fault occurs the Stator flux has three components viz positive sequence component rotating at ω_s and negative sequence component rotating at $-\omega_s$. So the relative speed of the negative sequence stator flux w.r.t to the rotor winding is $\omega_s + \omega_r$. So the EMF induced is more as more flux is cut by rotor windings. If the negative sequence flux component is reduced EMF induced will be less hence the rotor current will be attenuated during fault.

The rotor current is jointly decided by the injected rotor voltage and the EMF induced $\frac{d\lambda_{s_abc}}{dt}$. To constrain the rotor overcurrent it is desirable that the voltage applied from the rotor converter to the rotor winding should be used to weaken the effect of dc and negative sequence component in the stator flux linkage.

The control scheme implemented in simulation model is vector control algorithm for terminal voltage regulation and MPPT. The rotor side converter act as a controlled voltage source to produce voltage proportional to the amount which is sufficient to counteract the effect of negative and DC sequence component without any additional equipment.

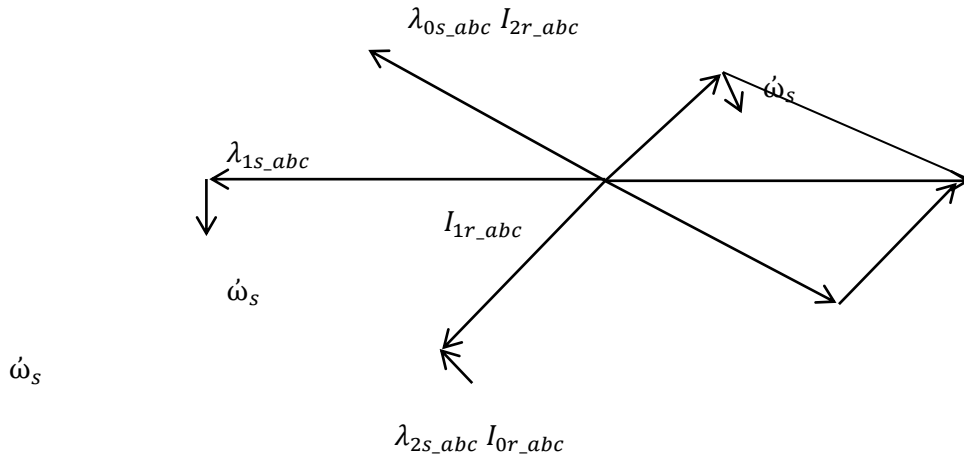


Figure 4.2: Control of rotor current

From equation 4.6 we can get:

$$\frac{\lambda_{rabc} - \lambda_{sabc}}{(L_{ls} + L_{lr})} = I_{rabc} \quad 4.11$$

It can be observed from the above equation that the rotor current is dependent on the interaction of the Stator and rotor flux. If the difference between the Stator and rotor flux increases then the rotor current increases. The rotor overcurrent can be suppressed if the rotor and stator flux changes synchronously at the time of Voltage drop. The relationship between the stator and rotor flux can be given by-

$$\lambda_{rabc} = I * \lambda_{sabc} \quad 4.12$$

I is the proportional or Interaction factor

Rotor current can be obtained from using 4.10 and 4.11 that

$$\frac{I*\lambda_{Sabc}-\lambda_{Sabc}}{(L_{lS}+L_{lr})} = I_{rabc} \quad 4.13$$

Using equation 4.7 and 4.13 we get

$$I = \frac{L_r}{L_m} - \frac{I_{sabc}(L_r L_s - L_m^2)}{L_m \lambda_{sabc}} \quad 4.14$$

I also show the interaction between the rotor and stator flux. During normal operation both the stator and rotor flux is rotating at synchronous speed. When voltage across stator drops the stator flux gradually decreases and rotor overcurrent appears. Thus if we can control or reduce the rotor flux gradually overcurrent in rotor circuit can be controlled during fault. Equation 4.6 shows that the rotor current can be controlled to counter the undesired component in the Stator flux linkage. Also equation 5.6 shows that the DFIG machine design with increased rotor or stator leakage inductance it will increase the effectiveness of rotor current control and ability to ride through grid fault.

The rotor current is controlled using Active and reactive power controller and using Hysteresis PWM inverter controlled voltage is generated by PWM voltage converter which will control the rotor and stator flux and thereby attenuate the rotor overcurrent.

The waveform of Interaction factor “I” is shown with PI as well as ANN controller. It is seen that during voltage dip the interaction between the rotor flux and stator flux increases. As a result using 4.11 we can see that the rotor current increases. But with the aid of ANN controller the Interaction factor I decreases and hence rotor overcurrent also reduces which further reduced the transients in Stator active power, generator speed and DC link voltage.

The rotor flux linkage can be expressed in terms of stator flux linkage. Equation (4.6) shows that if the rotor current is controlled to counter the effect of undesired components in the stator-flux linkage then overcurrent can be reduced. Also stator active and reactive power can be controlled as per equation (4.1). Also from equation (4.6) it can be noticed that if the DFIG is designed with increased rotor stator leakage inductance, it will increase the effectiveness of rotor current control and hence the ability to ride through grid faults. The Scheme to decompose the stator-flux into positive, negative, and zero sequence (dc) components appeared during unsymmetrical fault is:

The proposed controller includes three parts:

- 1) Stator-flux linkage estimation and decomposition;
- 2) Calculation of d and q rotor current reference;
- 3) Active and reactive power controller based rotor current control.

Fig.4.3 shows the Scheme to decompose the stator-flux linkage vector into positive, negative, and zero sequence (dc) components. The stator voltage and current are used to calculate the total flux linkage as shown. A second-order band-pass filter, with gain and phase response set to unity and zero degree, respectively, at stator frequency of (50 Hz), is used to remove the dc component. It should be noted that in Fig. 4.3, the derivative operation has the effect of phase shifting the positive and negative sequence flux linkage components by $\Pi/2$ and $-\Pi/2$ rad respectively separating positive and negative sequence components. We can express it as:

$$= 1/2[\lambda_{ac_sabc} - (-j) * \frac{d\lambda_{sabc}}{dt}] \quad 4.15$$

$$= 1/2[(\lambda_{1_sabc} + \lambda_{2_sabc}) - (-j) * \frac{dy}{dx}(\lambda_{0_sabc} + \lambda_{1_sabc} + \lambda_{2_abc})] \quad 4.16$$

$$= 1/2[(\lambda_{1_sabc} + \lambda_{2_sabc}) - (-j) * (j\lambda_{1_sabc} - \lambda_{s_abc})] \quad 4.17$$

$$= \lambda_{2_sabc}$$

Similarly,

$$= 1/2[\lambda_{ac_sabc} - (-j) * \frac{d\lambda_{sabc}}{dt}] \quad 4.18$$

$$= 1/2[(\lambda_{1_sabc} + \lambda_{2_sabc}) - (-j) * \frac{dy}{dx}(\lambda_{0_sabc} + \lambda_{1_sabc} + \lambda_{2_abc})] \quad 4.19$$

$$= 1/2[(\lambda_{1_sabc} + \lambda_{2_sabc}) - (-j) * (j\lambda_{1_sabc} - \lambda_{s_abc})] \quad 4.20$$

$$= \lambda_{1_sabc}$$

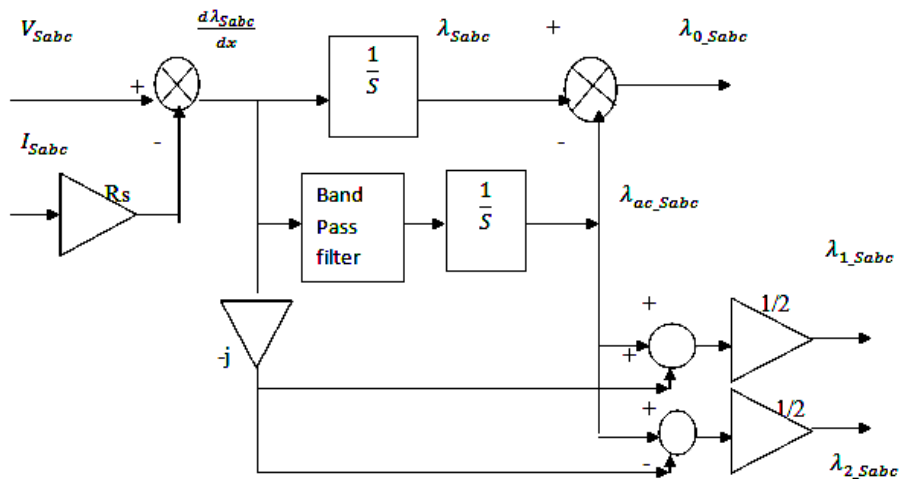
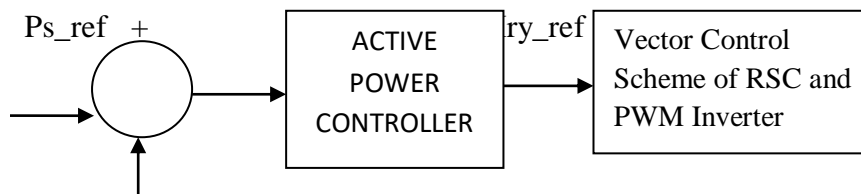


Figure: 4.3 Observation of components in stator-flux linkage

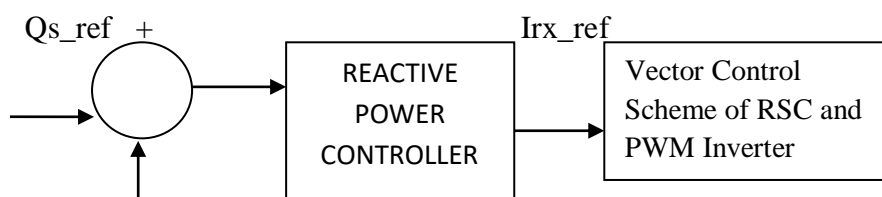
4.2 Controllers Used in the system

Two types of controllers are used in the rotor side converter and one controller is used in the grid side converter. The Active power PI controller and reactive power PI controller is used on the RSC. The DC link voltage controller is used in the GSC. The scheme is tested with four varieties of controllers:

1. PI controllers
2. Proportional resonant controller
3. Neural network controller
4. ANFIS controller



Ps -Figure 4.4(a): Scheme for Active Power Controller



Qs- Figure 4.4(b): Reactive Power Controller

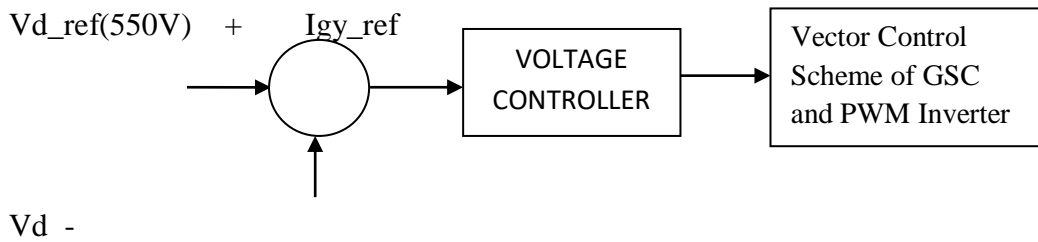


Figure 4.4 (C): DC Voltage Controller

The active power and reactive power controller controls the actual active and reactive power of the system hence controlling the d and q axis rotor current. We know that the q axis rotor current controls the stator active power and d axis rotor current controls the stator reactive power. So if the stator active and reactive power is controller with the aid of Active and reactive power controllers the rotor currents are controlled and hence the rotor flux is controlled controlling the stator flux during normal and fault conditions.

4.3 Basic Real and Reactive Power control on GSC

The grid side converter is used to control the flow of real and reactive power from the Wind turbine system to the grid. The grid-side converter is connected to the grid through inductors. The grid-side converter (VSI) generates balanced three-phase voltages at the 50 Hz frequency which is of controllable magnitude and phase angle. Load angle, which is the phase angle between the sending end voltage and receiving end voltage, can be controlled by controlling the real and reactive power flow between the grid and wind generation system. Load angle control uses the angle, δ , between the voltage generated by the grid-side converter, E , and the grid voltage, V and the real power, P , injected on to the grid. Likewise, reactive power, Q , is controlled using the magnitude of the voltage generated by the grid-side converter. The steady-state equations governing the real and reactive power flow from the grid-side converter to the grid are:

$$P = \frac{E*V}{X_s} \sin \delta \quad 4.16$$

$$Q = \frac{V^2}{X_s} - \frac{V*E}{X_s} \cos \delta \quad 4.17$$

Where, X_s is the reactance of the line between the grid and the GSC. If δ is small then the equations are simplified to:

$$P = \frac{E*V}{X_s} \delta$$

4.18

$$Q = \frac{V^2}{X_s} - \frac{V*E}{X_s} \delta$$

P can be controlled using load angle, δ , and Q can be controlled by controlling Voltage. The overall control scheme uses vector control scheme, Controllers and PWM inverter for generation of controlled rotor voltage and power electronics enables the grid-side converter to produce the necessary voltage magnitude and load angle, δ , to meet a required Pc and Qc demand. The controller output should synchronise to the grid frequency and phase. This can be done using phase-locked loop. The power exported to grid by the GSC is determined by the the DC link voltage. The grid-side converter controller regulates the DC link voltage. If the DC link voltage rises, the grid-side converter can export more amount of real power by increasing the load angle so that the DC link voltage return to its rated value. If more power is exported by the GSC than is currently generated by the RSC, the DC link voltage will fall below its rated value. The DC link voltage thereby indicates power flow balance between the generated power and the exported power in the rotor side.

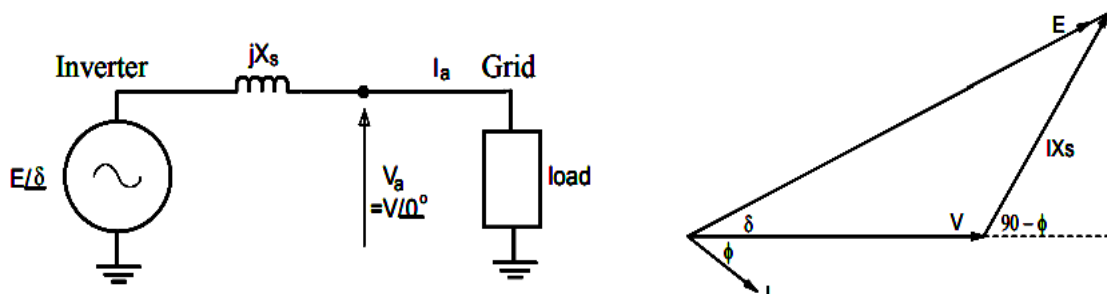


Figure 4.5: Single line diagram of GSC connected to the grid and phasor diagram showing load angle

4.3.1: Sequence Impedance during fault

During the fault the speed of the wind turbine exceeds the synchronous speed and the slip ratio changes. This change in slip ratio affects the turbine's positive sequence impedance. The zero sequence impedance is almost unchanged. During the fault the positive and negative sequence impedances are decreased.

4.4: Calculation of Total Harmonic distortion (THD)

Total Harmonic Distortion (THD) is expressed as the Root-Sum-Square (RSS) in percentage. The THD is usually calculated by taking the root sum of the squares of the first five or six harmonics of the fundamental frequency.

Equations for THD Calculation

If the measurement data is in volt,

$$THD(\%) = \frac{\sqrt{V_1^2 + V_2^2 + V_3^2 + \dots + V_n^2}}{V_1}$$

Where V_n is in RMS voltage

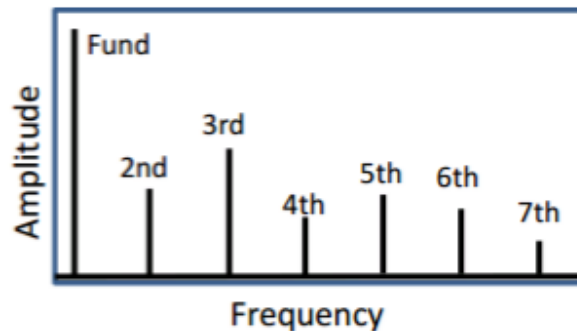


Figure 4.6: Harmonics of different Order representation

4.5 Design of PWM Inverter

4.5.1 Hysteresis band current control PWM Technique

Hysteresis band PWM technique is an instantaneous feedback current controlled PWM technique where the actual current continually tracks the reference or command current within the hysteresis band. A control circuit is designed to generate a sinusoidal reference current waveform of desired magnitude and frequency and it is compared with the actual phase current waveform generated from the circuit network. As the current exceeds a certain prescribed hysteresis band or limit (say 0.001) the upper switch in the three phase half bridge inverter circuit is turned off and the lower switch is turned on. As a result, the output voltage from the inverter transits from +0.5V_d to -0.5V_d and consequently the current starts to decay. As the current crosses the lower band limit (-0.001), the lower switch is turned off and the upper switch is turned on. The actual current wave is thus forced to track the sine reference wave within the hysteresis band by back and forth switching of the upper and lower switches.

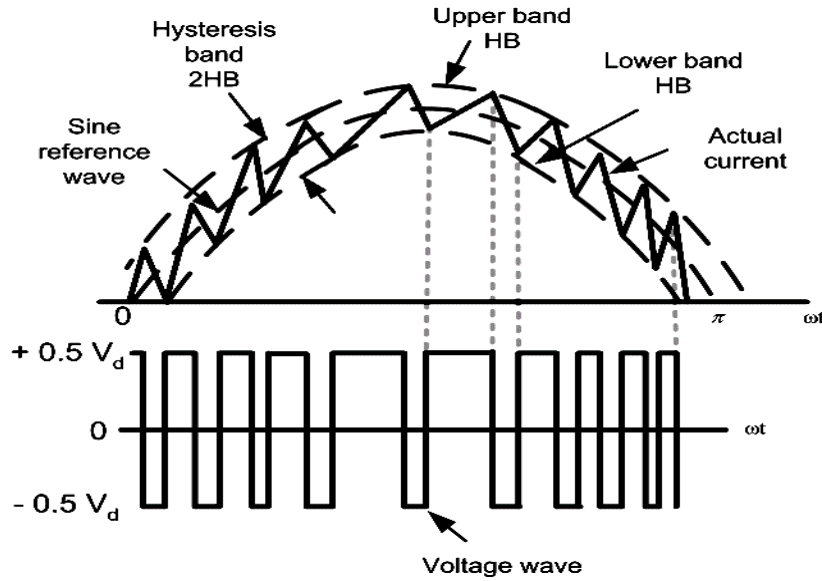


Fig 4.7 Principle of operation of Hysteresis current controlled PWM Technique

4.5.2 Converter output (AC side) considering isolated neutral

Upper Switch on-

$$(I^* - I) > 0.1 \text{ and } V_{ao} = \frac{1}{2} * V_d$$

Lower switch on-

$$(I^* - I) < -0.1 \text{ and } V_{ao} = -\frac{1}{2} * V_d$$

Three phase bridge Converter equations considering Isolated Neutral

$$V_{ao} = V_{an} + V_{no}$$

$$V_{bo} = V_{bn} + V_{no}$$

$$V_{co} = V_{cn} + V_{no}$$

$$V_{no} = \frac{1}{3} (V_{ao} + V_{bo} + V_{co})$$

Therefore,

$$V_{an} = \frac{2}{3} * V_{ao} - \frac{1}{3} * V_{bo} - \frac{1}{3} * V_{co}$$

$$V_{bn} = \frac{2}{3} * V_{bo} - \frac{1}{3} * V_{ao} - \frac{1}{3} * V_{co}$$

$$V_{cn} = \frac{2}{3} * V_{co} - \frac{1}{3} * V_{ao} - \frac{1}{3} * V_{bo}$$

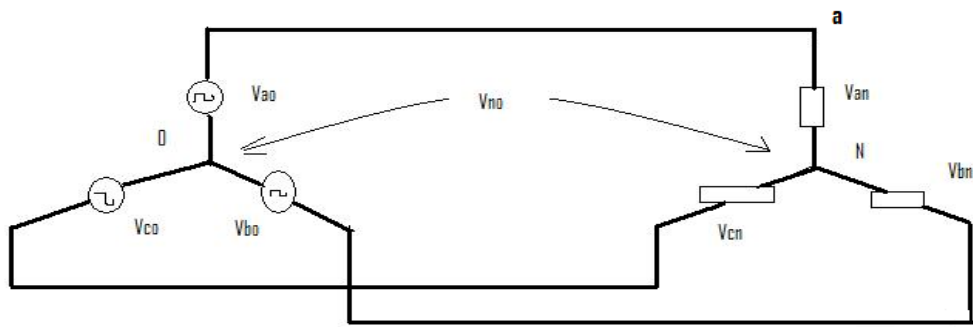


**Figure: 4.8 Equivalent circuit indicating voltage between the neutral points
Simulation Model for Extraction of Flux sequence**

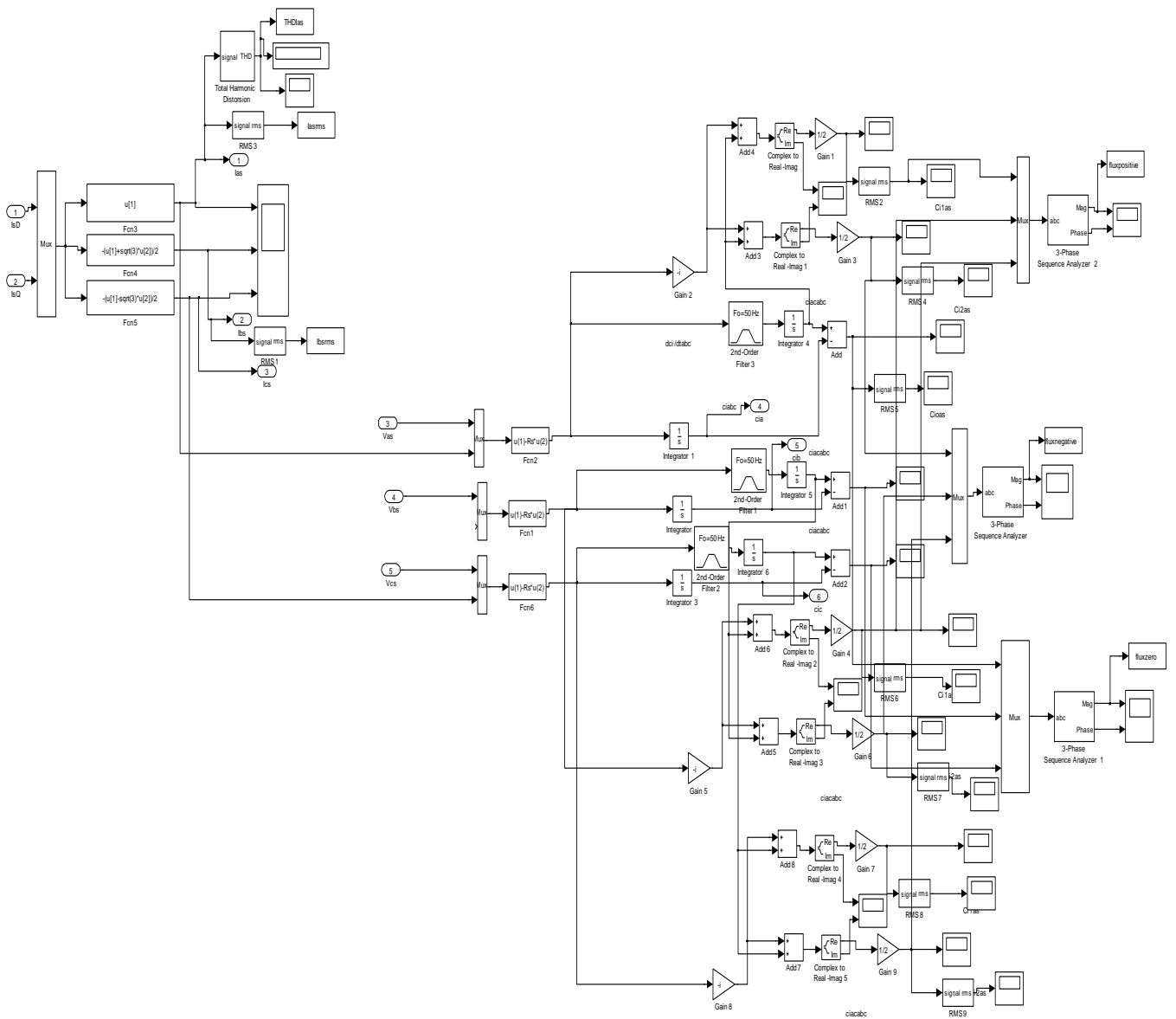
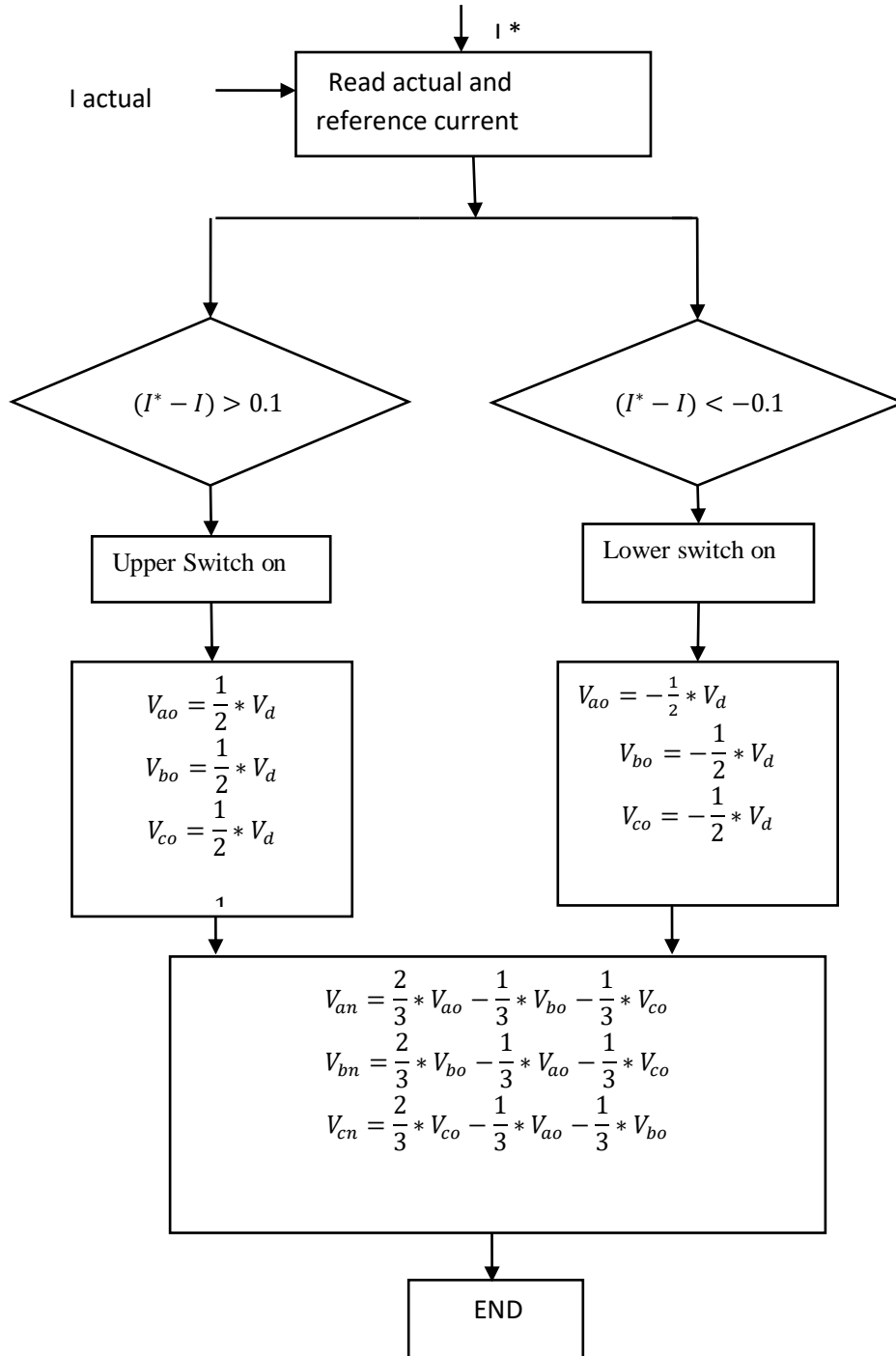


Figure 4.8 Simulation Model for extraction of Positive, Negative and Zero Sequence Flux

4.5.3 Flowchart for S-function coding of rotor and supply side converters



Chapter 5

Design of Conventional Controllers

5.1 Design of PI controllers

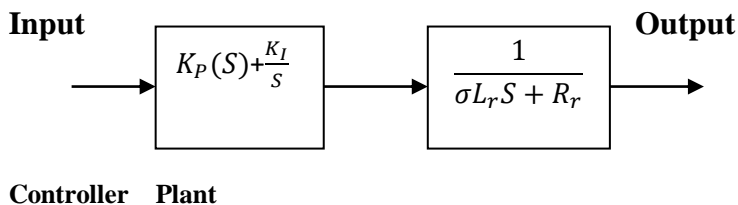


Figure: 5.1 Schematic Showing PI Controllers

The advantages of PI controllers are:

- As they are proportional controller they help in reducing the steady state error, thus make the system more stable.
- Slow response of the over damped system can be made faster with the help of these controllers.
- Due to their unique ability they can return the controlled variable back to the exact set point following a disturbance and that's why these are known as reset controllers.

The equation governing PI controller is given by-

$$u(t) = K_p \cdot e(t) + K_i \int e(t) \cdot dt \quad 5.1$$

$$u(S) = K_p(S) + \frac{K_i}{S} \quad 5.2$$

$$= K_p(S + a)/S = a = \frac{K_i}{K_p}$$

The designing parameter includes the value of K_p and K_i .

5.1.1 Trial and Error Method

In this method, first we have to set K_i and K_d values to zero and increase proportional term (K_p) until system reaches the oscillating behaviour. Once it is oscillating, Integral term should be adjusted so that oscillations stops and finally D is adjusted to get fast response.

The Ziegler-Nichols method is another popular method of tuning a PID controller. It is very similar to the trial and error method wherein I is set to zero and P is increased until the loop starts to oscillate. Once oscillation starts, the critical gain K_c and the period of oscillations P_c are noted.

The second method targets plants that can be rendered unstable under proportional control. The technique is designed to result in a closed loop system with 25% overshoot. This is rarely achieved as Ziegler and Nichols determined the adjustments based on a specific plant model.

Steps for using only proportional feedback control:

1. Reduce the integrator and derivative gains to 0.
2. Increase K_p from 0 to some critical value $K_p=K_{cr}$ at which sustained oscillations occur. If it does not occur then another method has to be applied.
3. Note the value K_{cr} and the corresponding period of sustained oscillation, P_{cr}

The P and I are then adjusted as per the tabular column shown below

Table 5.1: Ziegler Nichols Method

PID Type	K_p	T_i	T_d
P	$0.5 K_{cr}$	∞	0
PI	$0.45 K_{cr}$	$\frac{P_{cr}}{1.2}$	0
PID	$0.6 K_{cr}$	$\frac{P_{cr}}{2}$	$\frac{P_{cr}}{8}$

Using the voltage, flux and active and reactive power equations in chapter 3 we derive

$$V_{rd} = R_r I_{rd} + \left(L_r - \frac{L_M^2}{L_s} \right) \frac{dI_{rd}}{dt} - \sigma \omega_s \left(L_r - \frac{L_M^2}{L_s} \right) I_{rq} \quad 5.3$$

$$V_{rq} = R_r I_{rq} + \left(L_r - \frac{L_M^2}{L_s} \right) \frac{dI_{rq}}{dt} - \sigma \omega_s \left(L_r - \frac{L_M^2}{L_s} \right) I_{rd} \quad 5.4$$

The transfer function of doubly fed Induction Generator derived from voltage equation and flux equations is:

$$G(S) = \frac{L_M V_s}{L_S R_r + s L_S (L_r - \frac{L_M^2}{L_S})} \quad 5.5$$

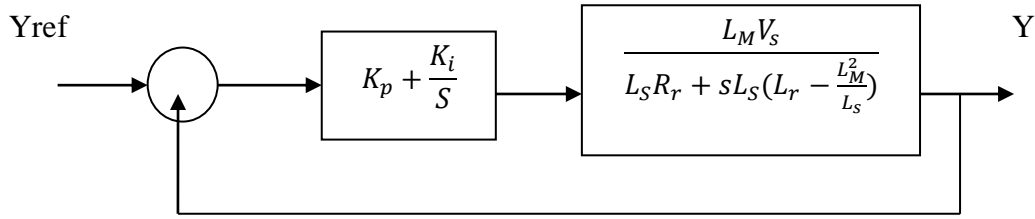


Figure: 6.2: Closed Loop block diagram using PI controller

$$\text{Open loop Transfer function is: } \left(\frac{s + \frac{K_i}{K_p}}{\frac{s}{K_p}} \right) * \frac{\frac{L_M V_s}{L_S (L_r - \frac{L_M^2}{L_S})}}{s + (L_r - \frac{L_M^2}{L_S})} \quad 5.6$$

Using compensation method to eliminate the zero in the transfer function we use:

$$\frac{K_i}{K_p} = (L_r - \frac{L_M^2}{L_S})$$

Putting the values in equation 6.6 we get:

$$\text{OLTF, } G(s) = \frac{K_p * \frac{L_M V_s}{L_S (L_r - \frac{L_M^2}{L_S})}}{s} \quad 5.7$$

The Closed loop transfer function is given by $\frac{G(s)}{1 + G(s)H(s)}$

$$\text{We get CLTF} = \frac{1}{1 + s \tau_r} \quad 5.8$$

$$\tau_r = \frac{1}{K_p} \frac{L_S (L_r - \frac{L_M^2}{L_S})}{L_M V_s} \quad 5.9$$

τ_r is the system time response

Therefore we derive the values of K_p and K_i in terms of machine parameter as:

$$K_p = \frac{1}{\tau_r} \frac{L_S (L_r - \frac{L_M^2}{L_S})}{L_M V_s} \quad 5.10$$

$$K_i = \frac{1}{\tau_r} \frac{R_r L_S}{L_M V_s} \quad 5.11$$

5.1.2 Stability Criteria of PI controller

The bode plot diagram and Pole Zero plot are plotted for the closed loop transfer function derived for the machine and PI controller in MATLAB using the values of K_p and K_i . It can be observed from the bode plot that the gain margin is infinite and phase margin is positive. Infinite gain margin (GM) denotes that the controller will remain stable for larger values of K_p . The value of phase margin (PM) obtained is also within the stability criteria value. The value of PM and GM indicates that the system is inherently stable. The pole zero plots also shows that the poles lay on the negative half of S-plane which indicates a stable system.

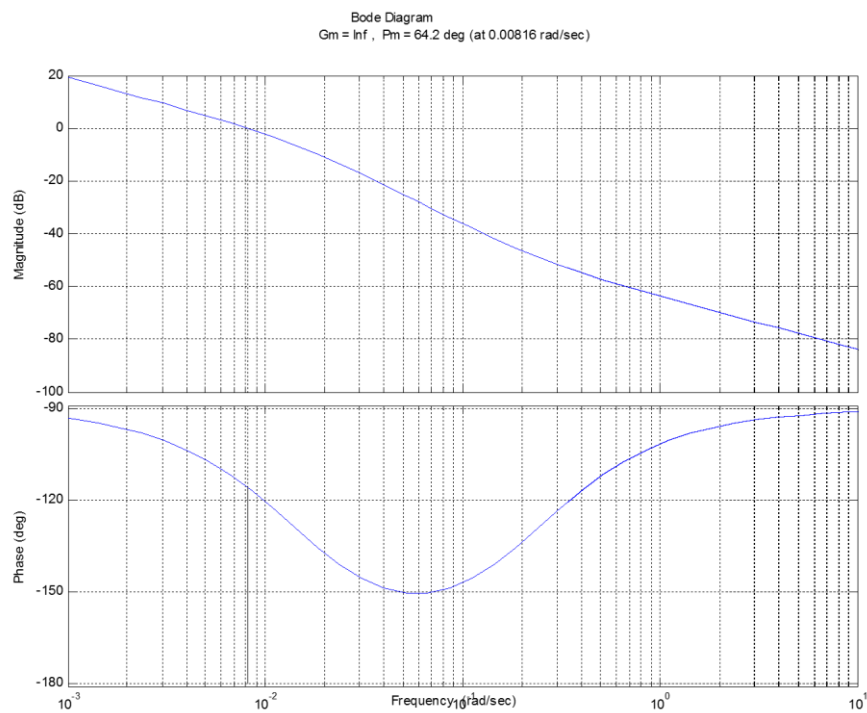


Figure 5.3: Bode plot for closed loop System using PI controller

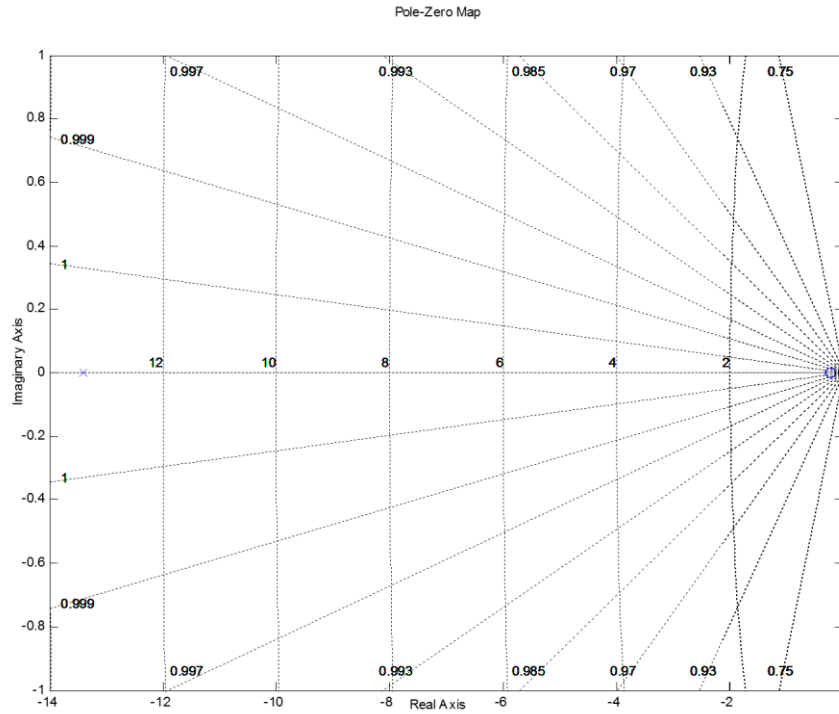


Figure 5.4: Pole-Zero plots for closed loop System using PI controller

5.2 Design of Proportional Resonant Controller

5.2.1 Control of Rotor Side Converter

The rotor current control strategy is to extenuate the impact of negative sequence and dc component of the stator flux under unsymmetrical faults. These two components will accord to the large magnitudes of the rotor currents which will damage the power converters for going beyond loading capability.

The relationship between voltages and current i.e. u_{qr} , u_{dr} and i_{qr} , i_{dr} in the rotating “dq” reference frame can be described as-

$$\begin{bmatrix} U_{dr} \\ U_{qr} \end{bmatrix} = \begin{bmatrix} R_r + L_r'P & -(\dot{\omega} - \dot{\omega}_r)L_r' \\ (\dot{\omega} - \dot{\omega}_r)L_r' & R_r + L_r'P \end{bmatrix} \begin{bmatrix} i_{dr} \\ i_{qr} \end{bmatrix} + \frac{L_m}{L_s} [U_{qs} - \dot{\omega}_r \Psi_{ds}] \quad 5.12$$

Where, L_r' is the rotor transient inductance, $L_r' = \sigma L_r$ with $\sigma = 1 - \frac{L_m^2}{L_m L_r}$

In the conventional RSC vector control scheme, the synchronous rotating dq reference frame with the d -axis oriented with the stator-flux vector is employed, where $\omega = \omega_s$, $u_{ds} = 0$ and $u_{qs} = \omega_s \psi_{ds}$. Thus, the relationship between u_{qr} , u_{dr} and i_{qr} , i_{dr} in the synchronous

rotating dq reference frame with the d -axis oriented with the stator-flux vector can be derived from Equation (5.3):

$$U_{dr} = R_r i_{dr} + \sigma L_r \dot{i}_{dr} - (\dot{\omega}_s - \dot{\omega}_r) \sigma L_r i_{qr}$$

$$U_{qr} = R_r i_{qr} + \sigma L_r \dot{i}_{qr} - (\dot{\omega}_s - \dot{\omega}_r) \sigma L_r i_{dr} + (\dot{\omega}_s - \dot{\omega}_r) \frac{L_m}{L_s} \Psi_{ds} \quad 5.13$$

There is a “cross-coupling” term in RSC control loop. To decouple the effect of d -, q -axis rotor currents control, the feed-forward compensation (FFC) terms u_{qr2} and u_{dr2} are introduced and added to the output of the current regulator:

$$U_{dr2} = -\dot{\omega}_{slip} \sigma L_r i_{qr}$$

$$U_{qr2} = \dot{\omega}_{slip} \sigma L_r i_{dr} + \dot{\omega}_{slip} \frac{L_m}{L_s} \Psi_{ds} \quad 5.14$$

Where $\omega_{slip} = \omega_s - \omega_r$

In the conventional control loops system for RSC with FFC, also the stator output active power (or electromagnetic torque) ally with the q -axis rotor current and the stator output reactive power (or terminal voltage) ally with the d -axis rotor current. Typically the active and reactive power control is used in the outer loop , and in the inner loops the rotor currents regulation is done. Both the outer loops and inner loops apply negative feedback control.

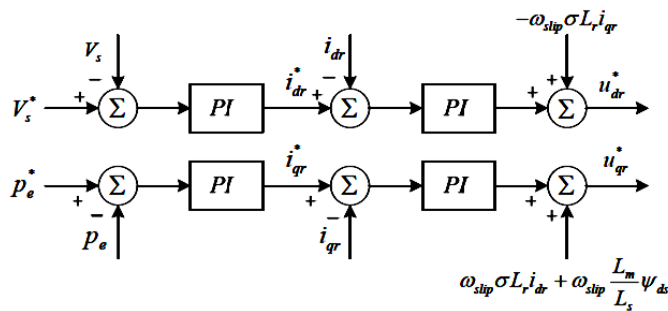


Figure 5.5. Conventional control scheme for the rotor side converter with FFC.

The aforestated in the control scheme on RSC, the parameters are assumed to be oriented with the stator flux reference frame rotating with speed of synchronous speed ω_s . However, during stator voltage transients or disturbances, the rotating speed of the

stator flux vector is different from that of the stator voltage space vector. Hence, ω is not necessarily equal to the synchronous speed ω_s .

Considering the stator flux transient during grid voltage dips, the DFIG transient model given by Equation (5.6) should be used instead of Equation (5.5). Therefore, for more precise control, the transient feed-forward compensation terms u_{qr2} and u_{dr2} should be introduced as:

$$U_{dr2} = -(\dot{\omega} - \dot{\omega}_r)\sigma L_r i_{qr} + \frac{L_m}{L_s} U_{ds}$$

$$U_{qr2} = -(\dot{\omega} - \dot{\omega}_r)\sigma L_r i_{dr} + \frac{L_m}{L_s} (U_{qs} - \dot{\omega}_r \Psi_{ds}) \quad 5.15$$

In the conventional control scheme of DFIG using PI controllers on RSC, dual current regulators, were used. One for the positive and the other for the negative sequence along with multiple low pass filters and reference frames transformations to extract the dc signals and negative sequence components. The multiple filters and the transformations between reference frames will make the system sluggish with amplitude and phase errors making the system less dynamic and less stable.

To further improve the dynamical performance of the control scheme on RSC, a non-ideal Proportional-Resonant Controller tuned at the grid frequency f_s is used. Compared to ideal PR controller, the gain of non-ideal PR controller is finite, and relatively high for enforcing steady-state error to become small. Its bandwidth can be widened by setting $\dot{\omega}_c$ appropriately, which will help in reducing sensitivity towards slight frequency change in a typical utility grid fault.

The PR controller is implemented in the “ $\alpha\beta$ ” stationary reference frame. In the “ $\alpha\beta$ ” stationary reference frame, the positive and negative sequence rotor currents are assumed to be as ac components with the frequency of $+\dot{\omega}_s$ and $-\dot{\omega}_s$ and the dc stator flux related component as dc component. A resonant controller tuned at frequency $\dot{\omega}_s$ regulates the both positive and negative sequence currents at $+\dot{\omega}_s$ and $-\dot{\omega}_s$ in the “ $\alpha\beta$ ” reference frame, and providing zero steady-state error. As a result, the proposed PR current-controller in the “ $\alpha\beta$ ” reference frame can directly regulate the negative sequence components as precisely as the positive sequence without using a notch filter

for current decomposition, which leads to a better transient response and a simple RSC control design.

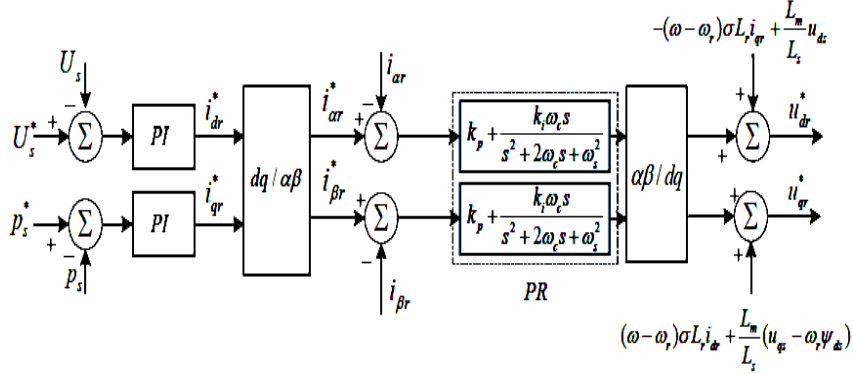


Figure 5.6. Improved control scheme for the rotor side converter with transient FFC.

5.2.2. Control of Grid Side Converter

The grid side converter control is to keep the dc-link voltage constant. When the grid voltage dips, the dc-link voltage may fluctuate due to the instantaneous unbalanced power flow between the grid and rotor side converter. The parameters in the grid side are implemented in synchronously rotating reference frame with its x -axis aligned in the direction of the grid voltage vector reference frame. For decouple control of active and reactive power flow between the grid and the grid-side converter, control scheme used dc-link voltage and grid reactive power control for outer loop and grid side inductor current regulation for the inner control loops.

In normal operation, the power flowing through the GSC and RSC is balanced, i.e. P_r is equal to P_g so the dc-link voltage is constant. When the grid voltage dips, P_r is not equal to P_g due to the unbalanced power flow between the GSC and RSC, and therefore the dc-link voltage may fluctuate. A control modified strategy for limiting the dc-link voltage fluctuation during fault has already been proposed on the GSC. The Voltage and current equations on the grid side are given by:

$$U_{dg} = U_{ds} + R_g i_{dg} + L_g \frac{di_{dg}}{dt} - \omega_s L_g i_{qg}$$

$$U_{qg} = U_{qs} + R_g i_{qg} + L_g \frac{di_{qg}}{dt} - \omega_s L_g i_{dg} \quad 5.16$$

Where R_g and L_g are the grid side filter resistor and inductor, respectively and $U_{ds}, U_{qs}, U_{dg}, U_{qg}$ and i_{dg}, i_{qg} are d -axis, q -axis components of the DFIG terminal

voltage and grid side filter voltage and current respectively. U_g is the control voltage provided by the GSC.

According to Equation (6.16), there is a cross-coupling item $\dot{\omega}_s L_g i_{dg}$ in the q -axis GSC control loop while there is another cross-coupling item $\dot{\omega}_s L_g i_{qg}$ in the d -axis GSC control loop. To decouple the q -axis and d -axis current control in the GSC control loop, the feed-forward compensation terms U_{dg2} and U_{qg2} are introduced as follows:

$$U_{dg2} = U_{ds} - \dot{\omega}_s L_g i_{qg}$$

$$U_{qg2} = U_{qs} - \dot{\omega}_s L_g i_{dg} \quad 5.17$$

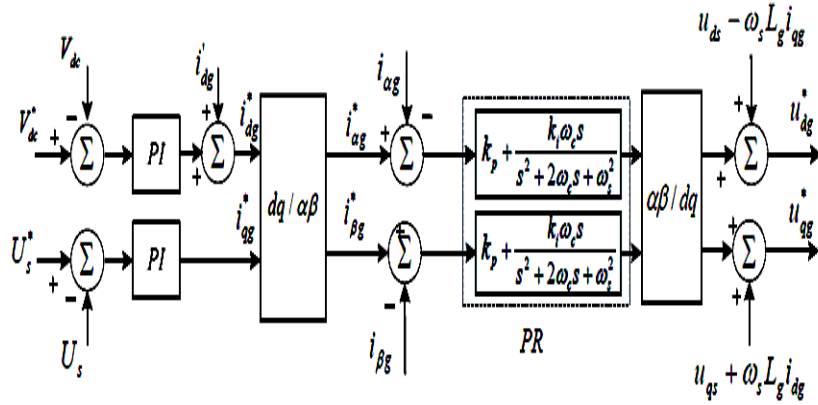


Figure 5.7: Improved control scheme for the grid side converter with transient FFC
Also, the dynamics of the capacitor in the dc-link between the rotor and stator side converters are described by:

$$C_{dc} V_{dc} \frac{dV_{dc}}{dt} = P_r - P_g \quad 5.18$$

$$P_r = \frac{1}{2} (U_{qr} i_{qr} + U_{dr} i_{dr}) \quad 5.19$$

$$P_g = \frac{1}{2} (U_{qg} i_{qg} + U_{dg} i_{dg}) \quad 5.20$$

Where C_{dc} is the dc capacitor; V_{dc} is the voltage of the capacitor; P_r and P_g are the instantaneous active power at the RSC and GSC side, respectively.

The terminal voltage u_s of the DFIG is aligned with the d -axis grid voltage vector, therefore the voltages become: $U_{ds} = U_s$ and $U_{qs} = 0$ Substituting Equation (6.16) into Equation (5.20) yields the instantaneous grid side converter active power as:

$$P_g = U_{ds}i_{dg} + R_g i_{dg}^2 + R_g i_{qg}^2 + \frac{1}{2}L_g \frac{di_{dg}^2}{dt} + \frac{1}{2}L_g \frac{di_{qg}^2}{dt} \quad 5.21$$

Also, from Equations (5.18) and (5.20), the dc-link voltage dynamic equation, in terms of grid side filter current and terminal voltage, can be expressed as:

$$\frac{1}{2}C_{dc} \frac{dV_{dc}^2}{dt} = P_r - (U_{ds}i_{dg} + R_g i_{dg}^2 + R_g i_{qg}^2 + \frac{1}{2}L_g \frac{di_{dg}^2}{dt} + \frac{1}{2}L_g \frac{di_{qg}^2}{dt}) \quad 5.22$$

During grid voltage dips, the output power of the rotor side converter varies which leads to the imbalance of the power equation and dc link voltage fluctuates.

If sum of instantaneous active powers output from the GSC and the grid filter is nearly equal to the instantaneous output power from the RSC, the dc-link voltage will remain nearly constant. So the DC link Voltage equation is modified in terms of the rotor side power and grid side power given in above equation.

$$P_r = U_{ds}i_{dg} + R_g i_{dg}^2 + \frac{1}{2}L_g \frac{di_{dg}^2}{dt} \quad 5.23$$

Proportional-Resonant controllers are also used in the GSC control loop to improve dynamic response. The improvised Grid side control scheme shows that the “d” axis (*active current component*) reference current of the grid side converter is set as the output of the dc-link voltage controller. Also, the “q” axis (*reactive current component*) reference current is used to control terminal voltage.

5.3 Design of PR Controller

The PR controller applied to the RSC of a DFIG was employed in this study to improve the accuracy of the control system. One of the most important features of the resonant controller is that it is capable of sufficiently tracking the AC reference current, and therefore, can eliminate steady-state control variable errors at the chosen (resonant) frequencies. The s-domain open-loop transfer function of the proposed PR current controller is defined as:

$$G_o(S) = K_1 + \frac{K_2(s)}{s^2 + \omega_s^2} \quad 5.24$$

Where K_1 is the proportional gain that has the same function in the PI controller; K_2 denotes the resonant gain, which provides the infinite gain for AC component tracking; and $s \omega_s$ is the resonant frequency equal to the synchronous frequency of the stator voltage outputs.

The magnitude and phase characteristics of the open loop transfer functions for PR controllers w.r.t different values of the resonant gain K_2 has been observed. The large gain produced at the resonant frequency ensures that the steady-state errors in the rotor currents can be completely eliminated. Furthermore, the selection of resonant gain values determines the cross-over frequency and dynamic response of the control system. A low K_2 gives a very narrow bandwidth, whereas a high K_2 leads to larger bandwidth. The bode-diagram of the closed-loop transfer functions of the PR current controller are shown. The gains used in both bode diagrams were determined based on the Naslin polynomial technique.

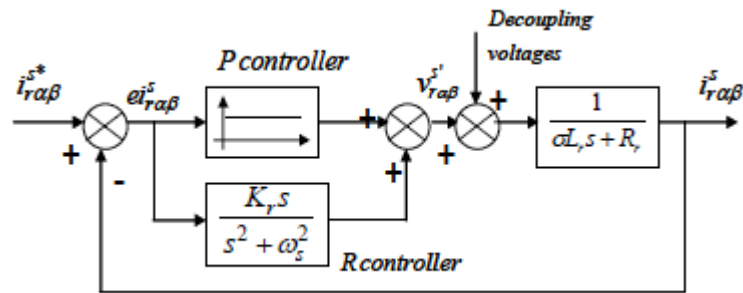


Figure-5.8: PR Current Controller

Open-Loop Transfer Function: Transfer function of the resonant controller can be expressed as follows:

$$G_o(S) = K_1 + \frac{K_2(s)}{S^2 + \omega_s^2} = \frac{C_0 + C_1(s) + C_2(S^2)}{S^2 + \omega_s^2} \quad 5.25$$

Where $C_0 = K_1 \omega_s^2$, $C_1 = K_2$, $C_2 = K_1$

The open-loop transfer function is given by-

$$G_o(S) = \frac{C_0 + C_1(s) + C_2(S^2)}{S^2 + \omega_s^2} * \frac{1}{R_r + \sigma L_r(S)} \quad 5.26$$

For controller design based on Naslin Polynomial, the characteristic polynomial of the closed-loop transfer function can be calculated as-

$$D(s) = C_0 + C_1(s) + C_2(S^2) + R_r + \sigma L_r(S) * (S^2 + \omega_s^2) \quad 5.27$$

The parameters of the controller can be computed based on the third-order Naslin polynomial:

$$P_N(S) = a_o(1 + \frac{s}{\omega_o} + \frac{s^2}{\alpha\omega_o^2} + \frac{s^3}{\alpha^3\omega_o^3}) \quad 5.28$$

From the last two equations we obtain:

$$C_o = \sigma L_r \alpha^3 \omega_o^3 - R_r \omega_s^2$$

$$C_1 = \sigma L_r \alpha^3 \omega_o^2 - \sigma L_r \omega_s^2 \quad 5.29$$

$$C_2 = \sigma L_r \alpha^2 \omega_o - R_r \quad \text{Or in the form}$$

$$K_1 = \sigma L_r \alpha^2 \omega_o - R_r \quad 5.30$$

$$K_2 = \sigma L_r \alpha^3 \omega_o^2 - \sigma L_r \omega_s^2 \quad 5.31$$

Calculation-

Selecting the Naslin polynomial parameter $\alpha=2$

$$\omega_o = \frac{1}{\sqrt{\alpha}} \omega_s = \frac{1}{\sqrt{2}} * 314 = 222 \text{ rad/s}$$

Table: 5.2 Parameter for PR controller design

Lr=0.052;	Rr=0.0399;
D=0.9974;	$\omega_s=314;$
Wo=222;	$\alpha=2$
We get-	
K1=46	K2=15335

5.3.1 Stability Analysis

A closed-loop current control scheme in the RSC is described in Fig 6.9. An analytical investigation regarding its frequency response when operating in a closed-loop system was conducted in order to determine if the proposed controller could achieve zero steady-state control error. The closed-loop transfer function of the control scheme is given by:

$$G_C(s) = \frac{i_{r\alpha\beta}^S}{i_{r\alpha\beta}^{S*}} = \frac{G_O(S)}{R_r + \sigma L_r(S) + G_O(S)}$$

$$\frac{K_1(S^2 + \omega_s^2) + K_2(S)}{(S^2 + \omega_s^2)(R_r + \sigma L_r(S)) + K_1(S^2 + \omega_s^2) + K_2(S)} \quad 5.32$$

MATLAB PROGRAM-

```

num1=[Kp Kr Kp*Ws*Ws ];
den1=[1 0 Ws*Ws];
G1=tf(num1,den1);
num2=1;
den2=[D*LrRr];
G2=tf(num2,den2);
Sys1=series(G1,G2);
Sys_final=feedback(Sys1,1,-1);
Sys_final
bode (Sys_final);
grid on;
margin (Sys_final);
Transfer function:

```

46 s^2 + 15335 s + 4.535e006

0.05186 s^3 + 46.04 s^2 + 2.045e004 s + 4.539e006

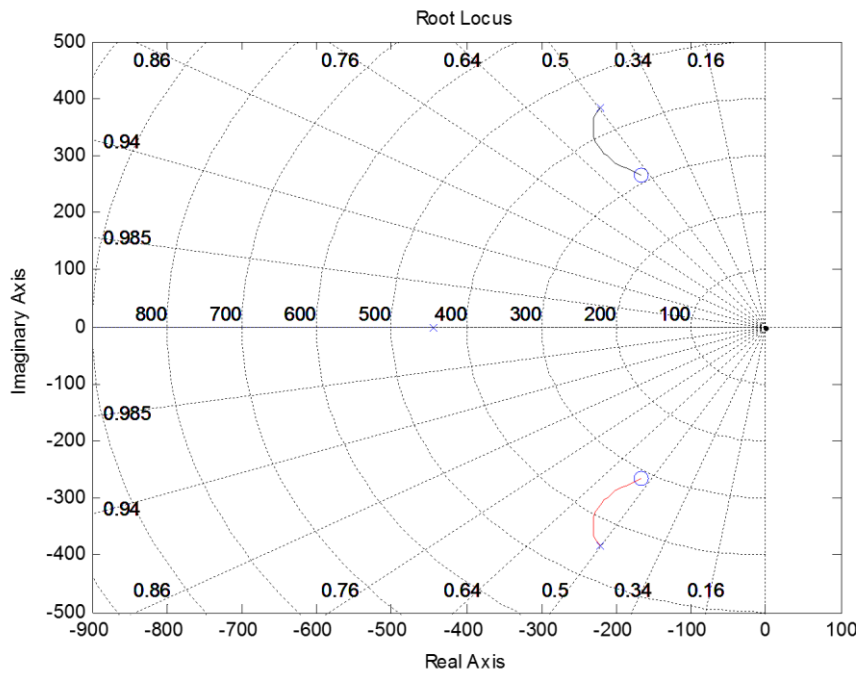


Figure5.9: Bode Plot for Closed Loop PR Controller

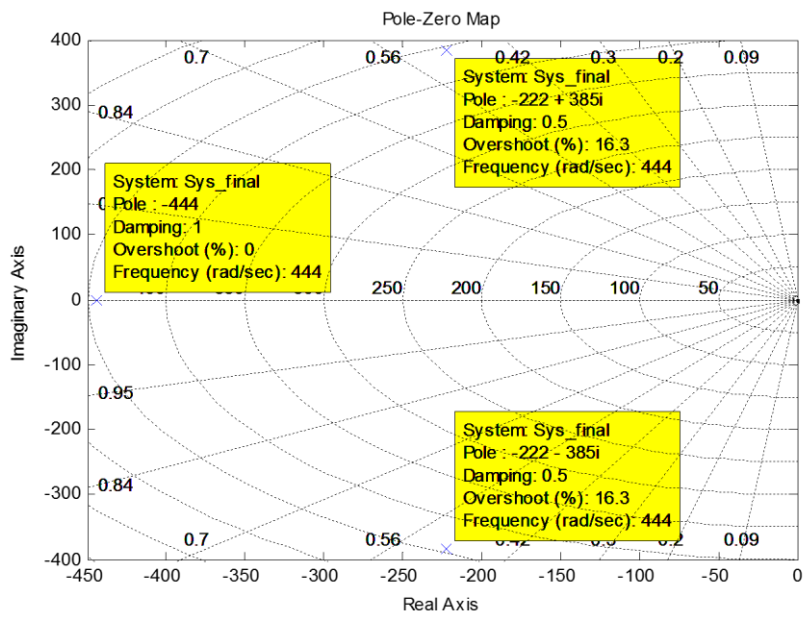


Figure5.10: Pole-Zero Plots for Closed Loop PR Controller

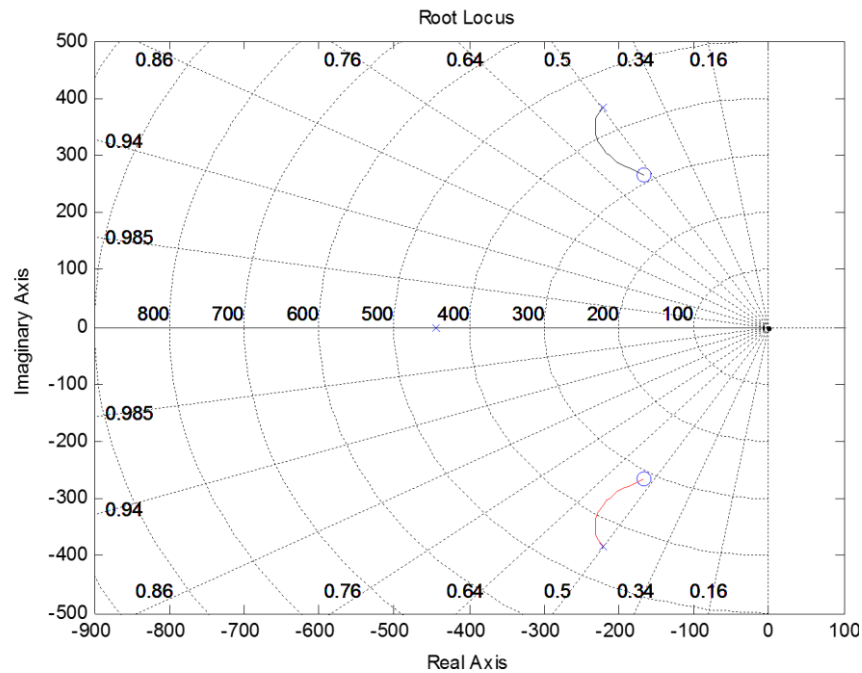


Figure5.11: Root Locus Plot for Closed Loop PR Controller

Equation (5.24), gives the ideal PR controller with an infinite gain at the AC frequency of 0, and no phase shift and gain at other frequencies. For K_1 , it is tuned in the same way as for a PI controller, and it basically determines the dynamics of the system in terms of bandwidth, phase and gain margin. To avoid stability problems associated with an infinite gain, (5.33) can be used instead of (5.24) to give a non-ideal PR controller its gain is now finite, but still relatively high for enforcing small steady-state error. Another feature of (5.33) is that, unlike (5.24), its bandwidth can be widened by setting ω_c appropriately, which can be helpful for reducing sensitivity towards slight frequency variation in a typical utility grid (for (5.24), K_i can be tuned for shifting the magnitude response vertically, but this does not give rise to a significant variation in bandwidth.

$$G_{AC}(S) = K_1 + \frac{2\omega_c K_2(s)}{s^2 + 2\omega_c(s) + \omega_s^2} \quad 5.33$$

MATLAB PROGRAM

$K_p=46;$

$K_r=15335;$

$D=0.9974;$

```

Lr=0.052;
Rr=0.0399;
Ws=314;
Wc=5;
num1=[Kp 2*Wc*(Kp+Kr) Kp*Ws*Ws ];
den1=[1 2*WcWs*Ws];
G1=tf(num1,den1);
den2=[D*LrRr];
G2=tf(num2,den2);
Sys1=series(G1,G2);
Sys_final=feedback(Sys1,1,-1);
Sys_final
bode(Sys_final);
grid on;
margin(Sys_final);
pzmap(Sys_final);
rlocus(Sys_final);

```

Transfer function:

$$\frac{46 s^2 + 153810 s + 4.535e006}{0.05186 s^3 + 46.56 s^2 + 1.589e005 s + 4.539e006}$$

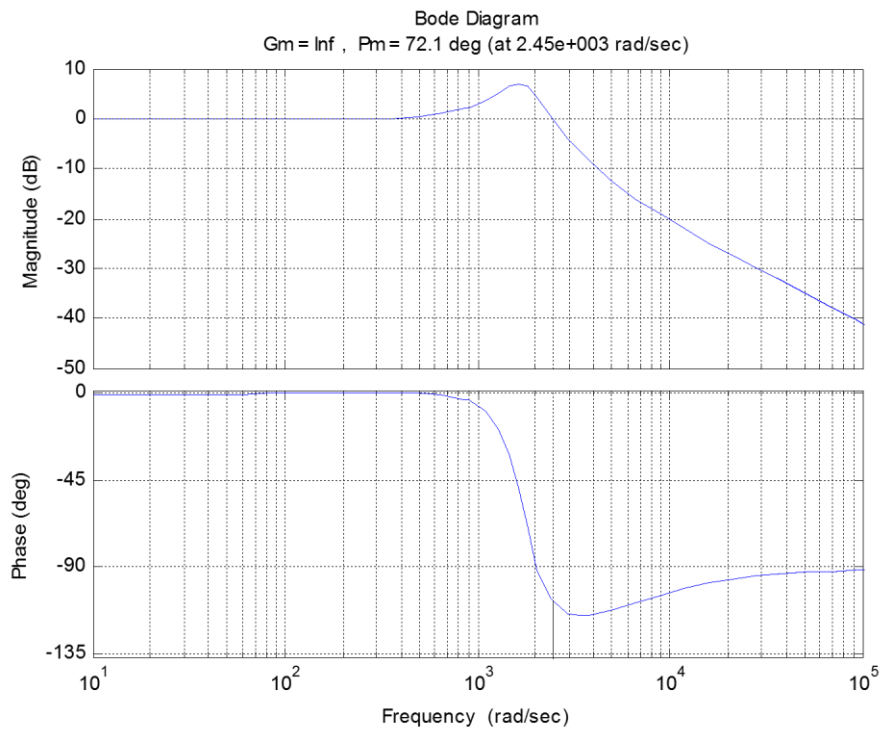


Figure5.12: Bode Plot for Closed Loop PR Controller

The bode plot shows that the Gain Margin is Infinite and phase Margin is Positive for the closed loop systems that means the system is Stable.

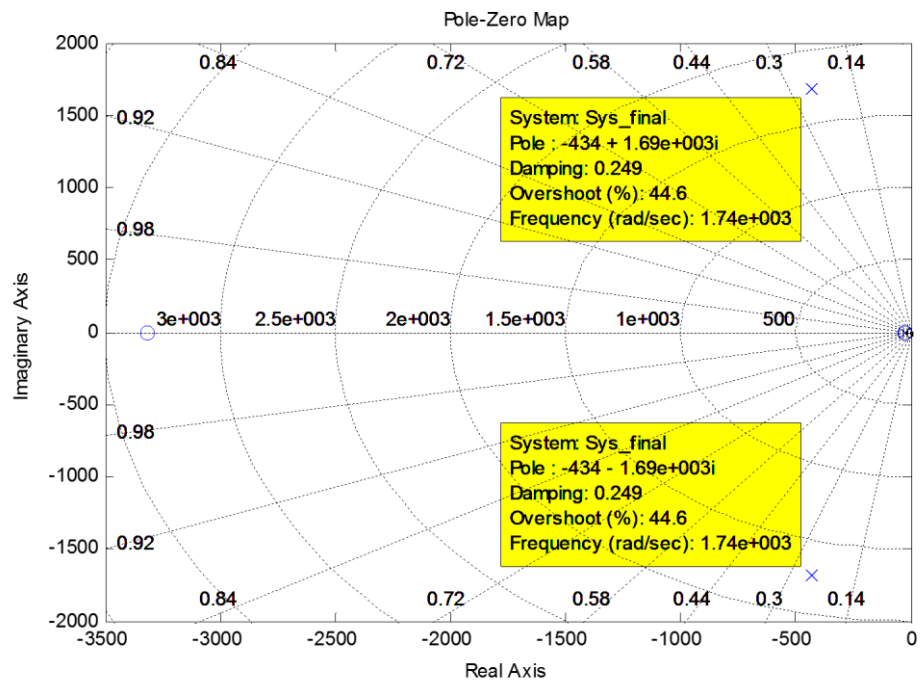


Figure5.13: Pole-Zero Plot for Closed Loop PR Controller

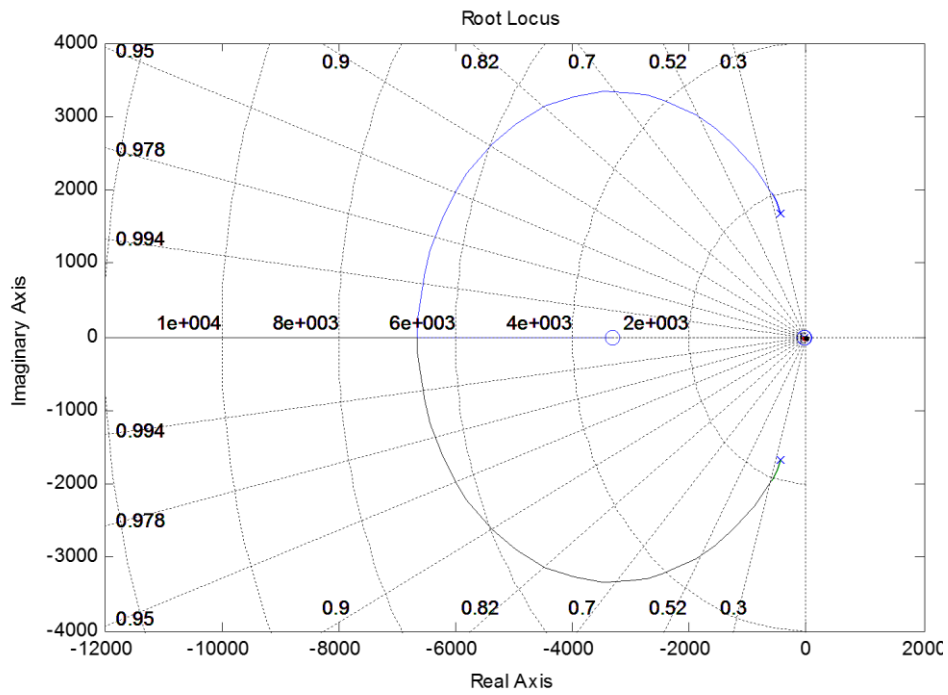


Figure 5.14: Root Locus Plot for Closed Loop PR Controller

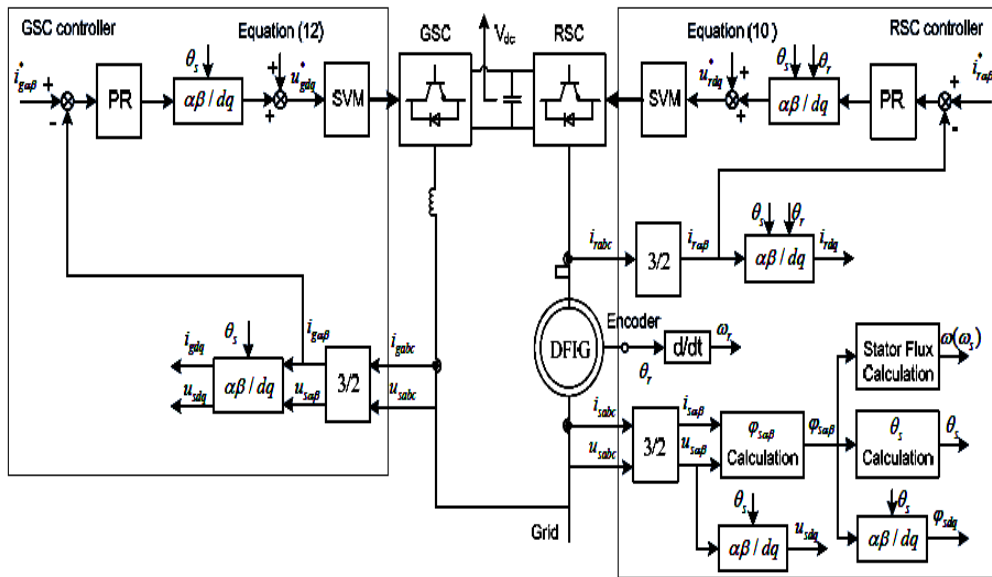


Figure 5.15 schematic diagrams of the proposed current controllers for the GSC and RSC

Chapter 6

Design of AI Based Controller

6.1 Advantages of Neural Network

The design and analysis of the two Artificial intelligence based controllers are discussed in this unit.

The active and reactive power PI controller used in vector controlled rotor side converter and the DC voltage controller used in the grid side converter are replaced by the ANN based controller and ANFIS controller successively one by one and the performance was studied and tested during the fault conditions. Both the Artificial based controller were developed using MATLAB/Simulink code.

Artificial Neural Network is relatively easier to use and understand compared to other optimization techniques and statistical methods. Error Back propagation Learning Algorithm is widely used now a days for various problems. ANN can be used to perform nonlinear statistical modelling. It consists of a black box between input and output. The black box generally consists of number of hidden layers which contains numerous numbers of neurons. Back Propagation method has slow convergence but output is mostly accurate. It has the capability to solve complex problems like regression classification and forecasting problems.

6.1.1 Back Propagation Algorithm

Back propagation is one of the systematic training and learning method which provides a efficient method for changing the synaptic weights in the neural network and error correction learning. The error back propagation algorithm is a kind of supervised learning. Here the recorded set of observations or training set are provided. i.e. inputs and the desired outputs/Targets are fed, and then the error (difference between actual and expected results) is computed. These differences in output are back propagated in the different layers of the neural networks and the algorithm adjusts the synaptic weights in between the neurons of successive layers such that overall error energy of the network, E is minimized. The idea of the back propagation algorithm is to reduce this error, until the ANN is trained with available the training data. Training of network i.e. error

correction is stopped when the value of the error energy function has become sufficiently small and as desired in the required limits. Error: $e_j(n) = d_j(n) - y_j(n)$

For this error signal at the output of neuron j at iteration n is:

$$e_j(n) = d_j(n) - y_j(n) \quad 6.1$$

$d_j(n)$ is the desired output

$y_j(n)$ is the actual output

Neuron j is the output node.

$$\text{Instantaneous error is } \xi(n) = \frac{1}{2} \sum_{j \in C} e_j^2(n) \quad 6.2$$

$$\text{The average error is: } \xi_{av} = \frac{1}{N} \sum_{n=1}^N \xi(n) \quad 6.3$$

$V_j(n)$ Produced at the input of the activation function is.

$$V_j(n) = \sum_{i=0}^m w_{ji}(n) y_i(n) \quad 6.4$$

Where, m is total no. of input applied to jth neuron excluding bias.

Hence the function signal $y_j(n)$ appearing at the output of the neuron j at iteration n is

$$y_j(n) = \phi_j(v_j(n)) \quad 6.5$$

The back Propagation algorithm applies a correction $\Delta w_{ji}(n)$ to the synaptic weight $w_{ji}(n)$ which is proportional to the partial derivative $\frac{\partial \xi(n)}{\partial w_{ji}(n)}$. According to chain rule of calculus we can express this gradient as:

$$\frac{\partial \xi(n)}{\partial w_{ji}(n)} = \frac{\partial \xi(n)}{\partial e_j(n)} \frac{\partial e_j(n)}{\partial y_j(n)} \frac{\partial y_j(n)}{\partial v_j(n)} \frac{\partial v_j(n)}{\partial w_{ji}(n)}$$

The partial derivative $\frac{\partial \xi(n)}{\partial w_{ji}(n)}$ represents a sensitivity factor determining the direction of search in weight space for the synaptic weight w_{ji} .

Differentiating w.r.t $e_j(n)$ we get

$$\frac{\partial \xi(n)}{\partial e_j(n)} = e_j(n) \quad 6.6$$

Differentiating equation (6.1) w.r.t $y_j(n)$

$$\frac{\partial e_j(n)}{\partial y_j(n)} = -16.7$$

Differentiating equation (6.5) w.r.t $V_j(n)$

$$\frac{\partial y(n)}{\partial v_j(n)} = \phi'_j(v_j(n))6.8$$

Differentiating equation (6.4) w.r.t $w_{ji}(n)$

$$\frac{\partial v_j(n)}{\partial w_{ji}(n)} = y_j(n)6.9$$

Using above equations we get:

$$\frac{\partial \xi(n)}{\partial w_{ji}(n)} = -e_j(n) \phi'_j(v_j(n))y_j(n)6.10$$

The correction $\Delta w_{ii}(n)$ applied to $w_{ii}(n)$ is defined by the delta rule

$$\Delta w_{ji}(n) = -\eta \frac{\partial \xi(n)}{\partial w_{ji}(n)}6.11$$

Where η is the learning rate parameter of the back propagation algorithm

$$\Delta w_{ji}(n) = -\eta \delta_j(n) y_i(n)6.12$$

Where the local gradient $\delta_j(n)$ is defined by

$$\begin{aligned} \delta_j(n) &= -\frac{\partial \xi(n)}{\partial v_j(n)}6.13 \\ &= -\frac{\partial \xi(n)}{\partial e_j(n)} \frac{\partial e_j(n)}{\partial y_j(n)} \frac{\partial y_j(n)}{\partial v_j(n)} \end{aligned}$$

$$= e_j(n) \phi'_j(v_j(n))6.14$$

The local gradient $\delta_j(n)$ for output neuron j is equal to the product of the corresponding error signal $e_j(n)$ for that neuron and the derivative $\phi'_j(v_j(n))$ of the associated activation function.

Case 1: Neuron j is an Output Node

When neuron “j” is located at the output node or layer of the neural network it is supplied with a desired response of its own. We use equation 1 to compute the error signal $e_j(n)$ associated with this neuron. And then compute $\delta_j(n)$

Case 2: Neuron j is a Hidden Node

When neuron j is located in a hidden layer of the network there is no specified desired response for that neuron. The error signal for a hidden neuron have to be determined recursively in terms of the error signals of all the neurons to which that hidden neuron is directly connected to .This is where the development of the back propagation algorithm gets complicated. We can redefine the local gradient $\delta_j(n)$ for hidden neuron j as:

$$\delta_j(n) = -\frac{\partial \xi(n)}{\partial y_j(n)} \frac{\partial y_j(n)}{\partial v_j(n)} \quad 6.15$$

$$= -\frac{\partial \xi(n)}{\partial y_j(n)} \phi'_j(v_j(n)) \quad 6.16$$

To calculate $\frac{\partial \xi(n)}{\partial y_j(n)}$ we may use $\xi(n) = \frac{1}{2} \sum_{j \in C} e_k^2(n)$

If neuron “k” is an output node. Index “k” is used in place of index “j”

Differentiating above equation w.r.t function signal $y_j(n)$ we get:

$$\frac{\partial \xi(n)}{\partial y_j(n)} = \sum_k e_k \frac{\partial e_k(n)}{\partial y_j(n)} \quad 6.17$$

We use the Chain rule for the partial derivative $\frac{\partial e_k(n)}{\partial y_j(n)}$ and rewrite the above equation

$$\frac{\partial \xi(n)}{\partial y_j(n)} = \sum_k e_k \frac{\partial e_k(n)}{\partial v_k(n)} \frac{\partial v_k(n)}{\partial y_j(n)} \quad 6.18$$

We Know, $e_k(n) = d_k(n) - y_k(n) = d_k(n) - \phi_k(v_k(n))$

Neuron k is output node

$$\frac{\partial e_k(n)}{\partial v_k(n)} = -\phi'_k(v_k(n)) \quad 6.19$$

$$v_k(n) = \sum_{j=0}^m w_{kj}(n) y_j(n) \quad 6.20$$

Where m is the total number of inputs (excluding the bias) applied to the neuron k the synaptic weight $w_{ko}(n)$ is equal to the bias $b_k(n)$ applied to neuron k corresponding input is fixed at the value 1

Differentiating w.r.t $y_j(n)$

$$\frac{\partial v_k(n)}{\partial y_j(n)} = w_{kj}(n) \quad 6.21$$

$$\frac{\partial \xi(n)}{\partial y_j(n)} = -\sum_k e_k(n) \phi'_k(v_k(n)) w_{kj}(n) \quad 6.22$$

$$= -\sum_k \delta_k(n) w_{kj}(n)$$

$$\delta_j(n) = \phi'_j(v_j(n)) \sum_k \delta_k(n) w_{kj}(n) \quad 6.23$$

If neuron j is hidden

Weight correction $\Delta w_{ji}(n) = (\text{Learning Rate } \eta) * (\text{Local Gradient } \delta_j(n)) * (\text{Input Signal of neuron } j \ y_j(n))$

Algorithms for Error Back Propagation Learning Method are:

1. We initialize random weight and choose learning rate η .
2. For each input patterns and target outputs forward Pass is done. Assuming j hidden layer nodes and N input for a 2 Layer MLP $Y_k = f(\sum_{j=0} w_{jk} O_j)$. Where O_j is output from each hidden node $j: O_j = f(\sum_{i=0} w_{ij} x_i)$.
3. For each output unit $k: \delta_k = (y_{target} - y_k) y_k (1 - y_k)$ is to be computed.
4. For hidden units j (from last to first hidden layer, for the case of more than 1 hidden layer): $\delta_j = O_j (1 - O_j) \sum_k w_{jk} \delta_k$ is to be computed.
5. For all weights change weight by gradient descent $\Delta w_{ji}(n) = \eta \delta_j(n) y_j(n)$.
6. For weight from input layer unit i to hidden layer unit j the weight changes by: $\Delta w_{ji}(n) = \eta \delta_j x_j$
7. For weight from hidden layer unit j to output layer unit k weight changes: $\Delta w_{jk}(n) = \eta \delta_k O_j$

6.1.2. Local Minima

Since back propagation uses a gradient descent procedure, a back propagation network follows the contour of an error surface with weight updates moving it in the direction of steepest descent. For simple two layer networks (without a hidden layer), the error surface is bowl shaped and using gradient descent to minimize error is not a problem. The network will always find an errorless solution (at the bottom of the bowl). Such errorless solutions are called global minima. However, when an extra hidden layer is added to solve more difficult problems, the possibility arises for complex error surfaces

which contain many minima. Since some of the minima are deeper, there is possibility that gradient descent method will not find global minima. Instead, the network may fall into local minima which represent suboptimal solutions. Obviously, we would like to avoid local minima when training a Back Propagation network. In some case this may be difficult to implement. However, in practice it is important to try to assess how frequently and under what conditions local minima occur and to examine possible strategies for avoiding them. As a general rule of thumb, the more hidden units we have in a network the less likely we are to encounter a local minimum during training. Although additional hidden units increase the complexity of the error surface the extra dimensionality increases the number of possible escape routes.

6.1.3 Gradient Descent Learning

Training the neural network involves finding the minimum of a complicated nonlinear function (called "error function"). This function describes the error, the neural network makes in approximating or classifying the training data, which is a function of the weights of the network. We want the error to become as small as possible and should try to move towards the point of minimum error area. For that we use gradient descent method is used. Gradient descent means going downhill in small steps until we reach the bottom of error surface. This is the learning technique used in back propagation. In back propagation weight update is equal to the slope of the energy function which is further scaled by a learning rate " η ", (thus, the steeper the slope, the bigger the update but may cause a slow convergence)

$$\text{We know the error equation: } E = \frac{1}{2} \sum_{j \in C} (T_j^P - Y_j^P)^2 \quad 6.24$$

Where set $\{C\}$ includes all the neurons in the output layer of the network. For " P^{th} " observation " T_j " represents the desired output and " Y_j " represents actual output from the system, for j th neuron in the output layer. Square of the error energy is taken so that the error of opposite signs doesn't cancel out each other. The objective of this learning process is to adapt the ANN parameters to minimize the overall error energy. Weights are updated on pattern by pattern basis until complete set of training data is utilised i.e one epoch. We need to find out a new weight value so that the E becomes minimum and also we know that the changing the weight value either takes us away from minima point or closer to it, so to tune for that weight value, we need to find the

direction that will guide us to local minima of the curve i.e opposite to the direction of the gradient of error (GE) .Gradient means change of error energy w.r.t weight value.

$GE = \frac{dE}{dW_{ji}} = \frac{dE}{dY_j} \frac{dY_j}{dW_{ji}}$, Where W_{ji} represents the synaptic weight to j^{th} neuron in the output layer from the i^{th} neuron in the previous layer.

Derivative of the error equation we get $\frac{dE}{dY_j} = -(T_j - Y_j)$ 6.25

We also know from neural network $Y_j = \sum_i W_{ji} X_i$ 6.26

Therefore, $\frac{dY_j}{dW_{ji}} = \frac{d \sum_i W_{ji} X_i}{dW_{ji}} = X_i$ 6.27

Therefore using above two equation we get: $GE = -(T_j - Y_j) X_i$

Correction weight is opposite to the gradient. So we can write $\Delta W_{ji} = -(T_j - Y_j) X_i$

Updated new value of synaptic weight is $W_{j_{i\text{new}}} = W_{j_{i\text{old}}} + \Delta W_{ji}$ 6.28

To speed up the convergence method learning rate is used and we can write:

$W_{j_{i\text{new}}} = W_{j_{i\text{old}}} + \eta(T_j - Y_j) X_i$ 6.29

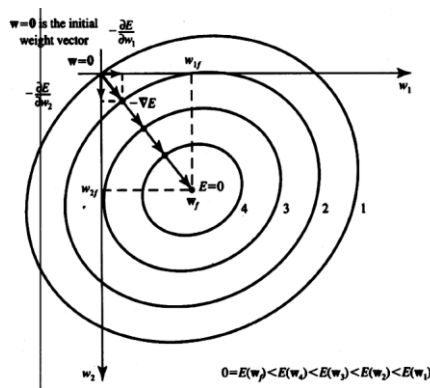


Figure 6.1 Gradient Descent Learning

6.1.4 The Levenberg–Marquardt algorithm

The Levenberg–Marquardt algorithm developed by Kenneth Levenberg and Donald Marquardt, provides a fast and stable convergence and solutions to optimize non linear function. This algorithm is suitable for small- and medium-sized training problems. Many different methods are developed for ANN training. The steepest descent algorithm, also commonly known as the error backpropagation (EBP) algorithm was like a light in the darkness on the field of artificial neural networks and could be considered as one of the most important breakthroughs for neural network training. The

major drawback of error backpropagation algorithm is its slow convergence. The two major reasons for such slow convergence is that firstly its step sizes should be adequate to the gradients. Logically, small step sizes should be taken where the gradient is steep so as not to skip out of the required minima (because of oscillation). So, if the step size is chosen constant and small value, the portion where the gradient is shallow, the training process would be very slow. Secondly, the curvature of the error surface may not be the same in all directions, which may result in the slow convergence. The slow convergence of the steepest descent method is greatly improved by the Gauss–Newton algorithm . Using second-order derivatives of error function to “naturally” evaluate the curvature of error surface, The Gauss–Newton algorithm is able to find proper step sizes for each direction and converge very fast; especially, if the error function has a quadratic surface, it can converge directly in the first iteration. The Levenberg–Marquardt algorithm uses both the steepest descent and the Gauss–Newton algorithm. It inherits the speed advantage of the Gauss–Newton algorithm and the stability of the steepest descent method. It’s more robust than the Gauss–Newton algorithm, due to the fact that it can converge fast even if the error surface is in much more complex quadratic situation.

The Levenberg–Marquardt algorithm performs a combined training process. It switches to the steepest descent algorithm, when the local curvature is proper and becomes the Gauss–Newton algorithm to speed up the convergence significantly.

6.1.4.1 Derivation of Levenberg–Marquardt algorithm

Sum square error (SSE) is defined in back propagation algorithm to evaluate the entire training process. For all training patterns and network outputs, it is calculated by:

$$E(x, w) = \frac{1}{2} \sum_{p=1}^p \sum_{m=1}^M E_{p,m}^2 \quad 6.30$$

$$E_{p,m} = d_{p,m} - o_{p,m}$$

Where “x” is the input vector

“W” is the weight vector

“d” is desired output vector

“o” is actual output vector

The steepest gradient descent algorithm is a first-order algorithm. It uses the first-order derivative of total error function to find the minima in error space. Normally, the gradient “g” is defined as the first-order derivative of total error function.

$$g = \frac{dE(x,w)}{dw} = \left[\frac{dE}{dW_1} \frac{dE}{dW_2} \frac{dE}{dW_3} \frac{dE}{dW_N} \right]^T \quad 6.31$$

$$W_{K+1} = W_k + \eta G_K \quad 6.32$$

In Newton’s method all the gradient components G_1, G_2, \dots, G_N are functions of weights and all weights are linearly independent

$$G_1 = F_1(W_1, W_2, \dots, W_N)$$

$$G_2 = F_2(W_1, W_2, \dots, W_N) \quad 7.33$$

$$G_N = F_N(W_1, W_2, \dots, W_N)$$

Taking Taylor series and first-order approximation we get:

$$G_1 = G_{1,0} + \frac{\partial G_1}{\partial W_1} \Delta W_1 + \frac{\partial G_1}{\partial W_2} \Delta W_2 \dots \dots \frac{\partial G_1}{\partial W_N} \Delta W_N$$

$$G_2 = G_{2,0} + \frac{\partial G_2}{\partial W_1} \Delta W_1 + \frac{\partial G_2}{\partial W_2} \Delta W_2 \dots \dots \frac{\partial G_2}{\partial W_N} \Delta W_N$$

$$G_N = G_{N,0} + \frac{\partial G_N}{\partial W_1} \Delta W_1 + \frac{\partial G_N}{\partial W_2} \Delta W_2 \dots \dots \frac{\partial G_N}{\partial W_N} \Delta W_N$$

Using equation (6.31) we get $\frac{\partial G_i}{\partial w_j} = \frac{\partial \frac{\partial E}{\partial W_i}}{\partial w_j} = \frac{\partial^2 E}{\partial W_j \partial W_i} \quad 6.34$

Therefore, using equation (6.31) and (6.34) we get

$$G_1 = G_{1,0} + \frac{\partial^2 E}{\partial W_1^2} \Delta W_1 + \frac{\partial^2 E}{\partial W_1 \partial W_2} \Delta W_2 \dots \dots \frac{\partial^2 E}{\partial W_1 \partial W_N} \Delta W_N$$

$$G_2 = G_{2,0} + \frac{\partial^2 E}{\partial W_2 \partial W_1} \Delta W_1 + \frac{\partial^2 E}{\partial W_2^2} \Delta W_2 \dots \dots \frac{\partial^2 E}{\partial W_2 \partial W_N} \Delta W_N$$

$$G_N = G_{N,0} + \frac{\partial^2 E}{\partial W_N \partial W_1} \Delta W_1 + \frac{\partial^2 E}{\partial W_N \partial W_2} \Delta W_2 \dots \dots \frac{\partial^2 E}{\partial W_N^2} \Delta W_N \quad 6.35$$

For objective function to be minimum derivative of gradient should be equals Zero,

$$\frac{dG}{dw} = 0$$

$$0 = G_{1,0} + \frac{\partial^2 E}{\partial W_1^2} \Delta W_1 + \frac{\partial^2 E}{\partial W_1 \partial W_2} \Delta W_2 \dots \dots \frac{\partial^2 E}{\partial W_1 \partial W_N} \Delta W_N$$

$$0 = G_{2,0} + \frac{\partial^2 E}{\partial W_2 W_1} \Delta W_1 + \frac{\partial^2 E}{\partial W_2^2} \Delta W_2 \dots \dots \frac{\partial^2 E_1}{\partial W_2 W_N} \Delta W_N \quad 6.36$$

$$0 = G_{N,0} + \frac{\partial^2 E}{\partial W_N W_1} \Delta W_1 + \frac{\partial^2 E}{\partial W_N W_2} \Delta W_2 \dots \dots \frac{\partial^2 E_1}{\partial W_N^2} \Delta W_N$$

$$-\frac{\partial E}{\partial W_1} = -G_{1,0} = \frac{\partial^2 E}{\partial W_1^2} \Delta W_1 + \frac{\partial^2 E}{\partial W_1 W_2} \Delta W_2 \dots \dots \frac{\partial^2 E_1}{\partial W_1 W_N} \Delta W_N$$

$$-\frac{\partial E}{\partial W_2} = -G_{2,0} = \frac{\partial^2 E}{\partial W_2 W_1} \Delta W_1 + \frac{\partial^2 E}{\partial W_2^2} \Delta W_2 \dots \dots \frac{\partial^2 E_1}{\partial W_2 W_N} \Delta W_N \quad 6.37$$

$$-\frac{\partial E}{\partial W_N} = -G_{N,0} = \frac{\partial^2 E}{\partial W_N W_1} \Delta W_1 + \frac{\partial^2 E}{\partial W_N W_2} \Delta W_2 \dots \dots \frac{\partial^2 E_1}{\partial W_N^2} \Delta W_N$$

In matrix form we get:

$$\begin{bmatrix} -G_{1,0} \\ -G_{2,0} \\ -G_{3,0} \end{bmatrix} = \begin{bmatrix} -\frac{\partial E}{\partial W_1} \\ -\frac{\partial E}{\partial W_2} \\ -\frac{\partial E}{\partial W_3} \end{bmatrix} = \begin{bmatrix} \frac{\partial^2 E}{\partial W_1^2} & \frac{\partial^2 E}{\partial W_1 W_2} & \dots & \frac{\partial^2 E_1}{\partial W_1 W_N} \\ \frac{\partial^2 E}{\partial W_2 W_1} & \frac{\partial^2 E}{\partial W_2^2} & \dots & \frac{\partial^2 E_1}{\partial W_2 W_N} \\ \frac{\partial^2 E}{\partial W_N W_1} & \frac{\partial^2 E}{\partial W_N W_2} & \dots & \frac{\partial^2 E_1}{\partial W_N^2} \end{bmatrix} \times \begin{bmatrix} \Delta W_1 \\ \Delta W_2 \\ \vdots \\ \Delta W_N \end{bmatrix} \quad 6.38$$

$$\text{The Hessian Matrix } H = \begin{bmatrix} \frac{\partial^2 E}{\partial W_1^2} & \frac{\partial^2 E}{\partial W_1 W_2} & \dots & \frac{\partial^2 E_1}{\partial W_1 W_N} \\ \frac{\partial^2 E}{\partial W_2 W_1} & \frac{\partial^2 E}{\partial W_2^2} & \dots & \frac{\partial^2 E_1}{\partial W_2 W_N} \\ \vdots & \vdots & \vdots & \vdots \\ \frac{\partial^2 E}{\partial W_N W_1} & \frac{\partial^2 E}{\partial W_N W_2} & \dots & \frac{\partial^2 E_1}{\partial W_N^2} \end{bmatrix} \quad 6.39$$

Applying above equations we get

$$-G = H \Delta W \quad 6.40$$

$$\Delta W = H^{-1} G \quad 6.41$$

$$W_{k+1} = W_k - H_k^{-1} G_k \quad 6.42$$

To simplify the calculation of Hessian Matrix which is second order error derivative Jacobian matrix is introduced which is derivative of the error w.r.t biases and weights.

$$J = \begin{bmatrix} \frac{\partial E_{1,1}}{\partial W_1} & \dots & \frac{\partial E_{1,1}}{\partial W_N} \\ \frac{\partial E_{1,2}}{\partial W_1} & & \frac{\partial E_{1,2}}{\partial W_N} \\ \frac{\partial E_{1,M}}{\partial W_1} & & \frac{\partial E_{1,M}}{\partial W_N} \\ \vdots & \ddots & \vdots \\ \frac{\partial E_{P,M}}{\partial W_1} & \dots & \frac{\partial E_{P,M}}{\partial W_N} \end{bmatrix} \quad 6.43$$

Using equation 6.31 and 6.38 and 6.39 we get the relation between the gradient and the Jacobian Matrix J as:

$$G = JE \quad 6.44$$

Error Vector has the form $E = \begin{bmatrix} E_{1,1} \\ E_{1,2} \\ \cdot \\ \cdot \\ E_{1,M} \\ \cdot \\ E_{P,1} \\ E_{P,2} \\ \cdot \\ \cdot \\ E_{P,M} \end{bmatrix}$

The Hessian Matrix is calculated as:

$$h_{i,j} = \frac{\partial^2 E}{\partial W_j \partial W_i} = \frac{\delta^2 \frac{1}{2} \sum_{p=1}^P \sum_{m=1}^M E_{p,m}^2}{\partial W_1 \partial W_1} = \sum_{p=1}^P \sum_{m=1}^M \frac{\partial E_{p,m}}{\partial W_i} \frac{\partial E_{p,m}}{\partial W_j} + S_{i,j} \quad 6.45$$

$$\text{Where } S_{i,j} = \sum_{p=1}^P \sum_{m=1}^M \frac{\partial^2 E_{p,m}}{\partial W_i \partial W_j} E_{p,m} \quad 6.46$$

The relation between H and J can be written as $H = J^T J$

In Levenberg–Marquardt algorithm Hessian matrix is approximated as: $H = J^T J + \mu I$

Where μ is combination coefficient and I is identity matrix

$$\text{Therefore } W_{k+1} = W_k - H_k^{-1} G_k \quad 6.47$$

$$W_{k+1} = W_k - (J_k^T J_k)^{-1} J_k E_k \quad 6.48$$

$$\text{Where } G_k = \frac{dE_k(x,W)}{dw_i} = J_k E_k \quad 6.49$$

6.1.4.2 Calculation of Jacobian Matrix

For a feed forward Network with three Layers viz. input Layer, Hidden Layer and Output Layer we can define the output node of neuron j as-

$$Y_j = f_j(\text{net}_j) \quad 6.50$$

Where, f_j is the sigmoid activation function of neuron j and net_j is the sum of weighted inputs of neuron j:

$$\text{net}_j = \sum_{i=1}^{n_i} W_{j,i} y_{j,i} + b_{j,0} \quad 6.51$$

Where

$y_{j,i}$ is the i th input of neuron j, weighted by $W_{j,i}$

$b_{j,0}$ is the bias weight of neuron j

Derivation of equation 6.50 w.r.t weight we get: $\frac{\partial \text{Net}_j}{\partial W_{j,i}} = Y_{j,i}$ 6.52

And slope S_j of activation function f_j is $S_j = \frac{\partial Y_j}{\partial \text{Net}_j} = \frac{\partial f_j(\text{Net}_j)}{\partial \text{Net}_j}$ 6.53

Between the output node Y_j of a hidden neuron j and network output O_m , there is a complex nonlinear Relationship.

$$O_m = F_{m,j} Y_j \quad 6.54$$

O_m is the m^{th} output of the network.

The elements of the Jacobian Matrix can be calculated as:

$$\frac{\partial E_{p,m}}{\partial W_{j,i}} = \frac{\partial (d_{p,m} - O_{p,m})}{\partial W_{j,i}} = \frac{\partial O_{p,m}}{\partial W_{j,i}} \quad 6.55$$

$$= \frac{\partial O_{p,m}}{\partial Y_j} * \frac{\partial Y_j}{\partial \text{net}_j} * \frac{\partial \text{net}_j}{\partial W_{j,i}} \quad 6.56$$

Combining the above equations we get: $\frac{\partial E_{p,m}}{\partial W_{j,i}} = -F'_{mj} S_j Y_{j,i}$ 6.57

Where $\delta_j = S_j \sum_{m=1}^M F'_{mj} E_m$ 6.58

In the Levenberg–Marquardt algorithm, the δ parameters are calculated for each neuron j and each output m, separately.

$$\delta_{m,j} = S_j F'_{mj} \quad 6.59$$

Combining 6.57 and 6.59 we get-

$$\frac{\partial E_{p,m}}{\partial W_{j,i}} = -\delta_{m,j} Y_{j,i} \quad 6.60$$

7.1.4.3 Algorithm of Levenberg Marquardt Method

- Weights are randomly generated and forward pass calculation is done and finally SSE is evaluated using equation (6.30).
- The Jacobian matrix is calculated for ith layer using equation (6.43).
- Back propagation pass is evaluated and weights are adjusted according to new value using equation (6.48).
- With new weights again SSE error is calculated.
- If the total SSE is more the weight vector is reset and combination coefficient μ is increased by coefficient 10. Then go to step iii and again update weights.
- If the total SSE is less the weight vector is again reset and combination coefficient μ is decreased by coefficient 10. Then go to step iii and again update weights.
- Repeat step iii with the new updated weights till the total error is smaller than the requisite value.

6.1.5 Training Algorithms

There are many different training algorithms with back-propagation. There exists a range of computational and storage requirements as no single algorithm suits all locations. Training algorithms summarize the training algorithms included in MATLAB software. The few important terms have been briefed below:

Resilient Back-propagation (trainrp)

For the hidden layers of Multilayer networks sigmoid transfer functions are generally employed. Sigmoid transfer function creates issue for training of a multiple layer network especially when steepest descent algorithm is applied. This can be due to the fact that gradient of the function is small numerical value perpetuating low variations in weights and biases in spite of its favourable value at quite a distant. The resilient back-propagation training algorithm is used to avoid the harmful effects of the magnitudes in partial derivatives.

Scaled Conjugate Gradient (trainscg)

In the conjugate gradient algorithms, each and every iteration needs different search line. This makes it computationally expensive and tedious as for every search the

response of network is computed several times in all training inputs. Whereas scaled conjugate gradient algorithm (SCG) consumes less time for the line search but it is more complicated algorithm.

Levenberg-Marquardt (trainlm)

The Levenberg-Marquardt was designed to reach second order training speed without the utilization of the Hessian matrix. The Hessian matrix is approximated from the Jacobian matrix.

6.2 DESIGN OF NEURAL NETWORK BASED CONTROLLER

The neural network used in the system has input, output and hidden layers. The input and target training data pairs are generated from the simulations of the system using vector controlled method with PI controllers under various operating conditions such as:

1. Operation at different wind speed conditions.
 - I. Operation of DFIG during Constant Wind Conditions
 - II. Operation of DFIG for ramp increase in wind speed.
 - III. Operation at different step increases in wind speed.
2. Operation at different Unsymmetrical Conditions
 - I. Operation of DFIG during Single Line to ground fault.
 - II. Operation of DFIG during Line to Line fault
 - III. Operation of DFIG during Symmetrical Voltage dip of 85% and 15%

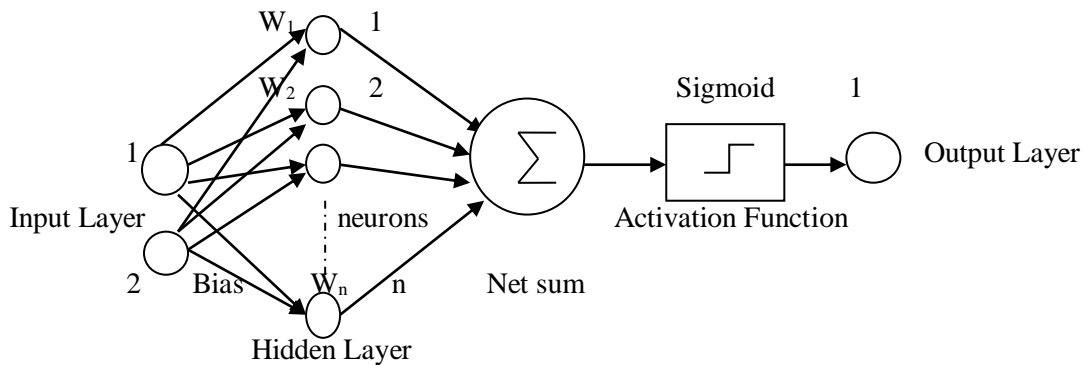


Figure 6.2: ANN Architecture

Sigmoidal activation function (σ) is taken in hidden layer ($1/(1+e^{-ax})$). Sigmoidal Activation function is the most common activation function used in the ANN as it is able to handle nonlinearity, easy computation and differentiable. The sigmoid activation function has smooth threshold. For comparison, a simple threshold produces a value of one when $x > 0$, and a value of zero when $x < 0$. The sigmoid performs this same basic threshold function, but is also differentiable. The derivative of sigmoid activation function is easy and is given by $f'_x = f_x(1 - f_x)$. The significance of being differentiable is that it is required to find the gradient vector for carrying out the back propagation algorithm.

The neural network will be more flexible if the sigmoid is adjusted left-or-right, making it centred on some other value than $x=0$. It is very simple to implement an additional node to the input layer, with its input always having a value of one. When this is multiplied by the weights of the hidden layer, it provides a bias (DC offset) to each sigmoid. This addition is called a bias node. It is treated as a node similar to the other nodes, except for the constant input. The output from sigmoid obtained is un-normalized probability, which simplifies the classification task.

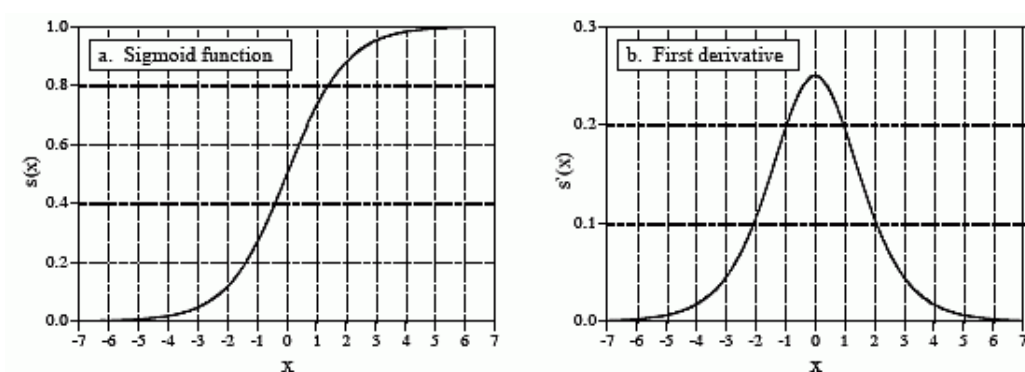


Figure 6.2.1 Sigmoid Activation function and its derivative

➤ **Selection of Input and output layers for the ANN controller**

The ANN Architecture has mainly three layers viz. the input layer, hidden layer and output layer. The input layer maps the input variable from outside of the net with the Hidden layers or nodes. For the design of the ANN based Active and reactive power controller, the first step is the selection of the number of input nodes. As the controller receives the error between the reference active and reactive power and actual active and reactive power of the DFIG so the number of input nodes selected is 1 for each

controller. The output from both the controller controlled d and q axis rotor currents. So the number of outputs selected is 1 for both the active and reactive power controller.

➤ **Selection of hidden layers and number of neurons in hidden layers**

For selection of hidden layers there is no fixed rule or no rule is suggested as “best” rule for this task. But the mainstream approach is mostly a trial and error process starting from a set of rules of thumb and a heavy cross validating attitude.

Generally the number of hidden layers selected is 1 or 2 which is appropriate for most of the cases. But there are some considerations for selection of hidden layers.

1. **Nonlinearity** –The input data collected for training the neurons are first examined whether it is linearly separable or not. If it is not linearly separable then hidden layer is required.
2. **The rules of thumb-** The most common rule of thumb is to choose a number of hidden neurons between 1 and the number of input variables. A slight variation of this rule suggests choosing a number of hidden neurons between one and the number of Inputs minus the number of outputs.

E.g. if there are 2 input and 1 output then hidden layer can be between 1 and 2.

3. **Cross Validation-**The basic idea to get the number of neurons is to cross validate the model by running simulations with different configurations and get the average MSE, then by plotting the average MSE vs the number of hidden neurons we can see which configurations are more effective at predicting the values of the test set.
4. The number of hidden neurons should be $2/3$ the size of the input layer, plus the size of the output layer.
5. The number of hidden neurons should be less than twice the size of the input layer.

The number of hidden layer selected is 1 and the number of neurons in the hidden layer is selected from cross validation by running simulation and plotting mean square error curve. The number of hidden layers is changed until a better result is obtained. The network training was done until the system undergoes 1000 iterations. A trained neural network control functional block was created and the PI controller was replaced by the neural network function block. The same procedure is done for all the controllers in the

system separately. The network is trained using Levenberg Marquart back propagation algorithm (trainlm) to actuate the values of the weights and biases.

6.2.1 ANN Controller Architecture

Two ANN based controllers are designed for the rotor side controller and one ANN based controller for the grid side controller.

6.2.1.1 ANN based Active Power controller

The architecture taken for the design of the neural network controller is (2-1-1) where inputs layers are reference active power(P_{sref}) and actual active power(P_s) and the output/target layer is the reference q axis rotor current in stator reference frame rotating at stator flux angle (I_{xref}). The number of hidden layer has 50 neurons. This controlled current output from the ANN controller regulates electromagnetic torque and hence the generated stator active power of the DFIG.

6.2.1.2 ANN based reactive power controller

The architecture taken for the design of the neural network controller is (2-1-1) where inputs layer are reference active power(Q_{sref}) and actual active power(Q_s) and the output/target layer is the reference d axis rotor current in stator reference frame rotating at stator flux angle (I_{yref}). The number of hidden layers has 70 neurons. This controlled component of the current controls the reactive power in the stator side of DFIG and the main flux in the Stator circuit in such a way that during faults it significantly reduces the negative sequence component of stator flux.

6.2.1.3 Grid side ANN based DC Voltage controller

The architecture taken for the design of the neural network controller is (2-1-1) where inputs layers are reference DC link Voltage ($V_{sref}=550V$) and actual DC link voltage (V_s) and the output/target layer is the reference d axis grid current in voltage vector reference frame rotating at voltage angle (I_{ygrid}). This current component regulates the grid voltage and current in such a way that the DC link voltage remains constant during any varying operating conditions. It also ensures that the power factor on the GSC side is almost 1 such that the reactive power exchange is only towards the stator side and there is no reactive power exchange in the grid side. The number of hidden layer has 70 neurons. The parameters of ANN controllers for RSC and GSC are given below

Table 6.1: ANN training Parameter and Architecture of the rotor side converters

	Inputs Layer	Hidden Layers	Outputs Layer
Activation Function(\emptyset)	Sigmoidal	Sigmoidal	Linear
Parameter $-\gamma$	2.0	2.0	-
Parameter-a	2.0	2.0	-
Parameter-c	-1.0	-1.0	-
No. of Inputs	1		
No. of Neurons	1	50	1
Input Target training pairs	10001		
No. of iterations	1000		
Error	10e-4		
Learning Coefficient, η	0.05		
Momentum, α	0.2		

Table6.2: ANN training Parameter and Architecture of the Grid side converter

	Inputs	Hidden Layers	Outputs
Activation Function(\emptyset)	Symmetric Sigmoidal	Symmetric Sigmoidal	Linear
Parameter $-\gamma$	2.0	2.0	-
Parameter-a	2.0	2.0	-
Parameter-c	-1.0	-1.0	-
No. of Inputs	1		
No. of Neurons	1	70	1
Input Target training pairs	10001		
No. of iterations	1000		
Error	10e-4		
Learning Coefficient, η	0.05		
Momentum, α	0.2		

6.2.2 Steps used for design of ANN Controller

Step 1: A feed forward three layered Neural Network is taken. The three layers are viz 1 the input, 1 hidden layer, 1 output layer. The number of neuron in the hidden layer is adjusted. The weights are assigned to a random value and then updated gradually using back propagation method. Large number of hidden layers can increase complexity of the system and less number of hidden layer chosen can give insufficient convergence.

Step 2: The input and Target (X-T) set pattern is determined and the data is saved in workspace by running the simulation model under various operating conditions using tuned PI controller. The data are saved in Matrix format.

Step 3: The training algorithm is chosen. There are many different training algorithms with back-propagation. One of the training algorithms is Levenberg-Marquardt (trainlm). Computation of the gradient is done with the Jacobian matrix through a standard technique of back-propagation.

Step 4: Training parameters such as number of epochs, goal of training are set and the network is trained using Levenberg-Marquardt back propagation Algorithm”.

Step 5: The network is trained upto 1000 epochs and the number of neurons are changed until the mean Square error reaches a minimum value. The Simulink model of the trained network is generated using “gensim” and replaced by the conventional PI controller.

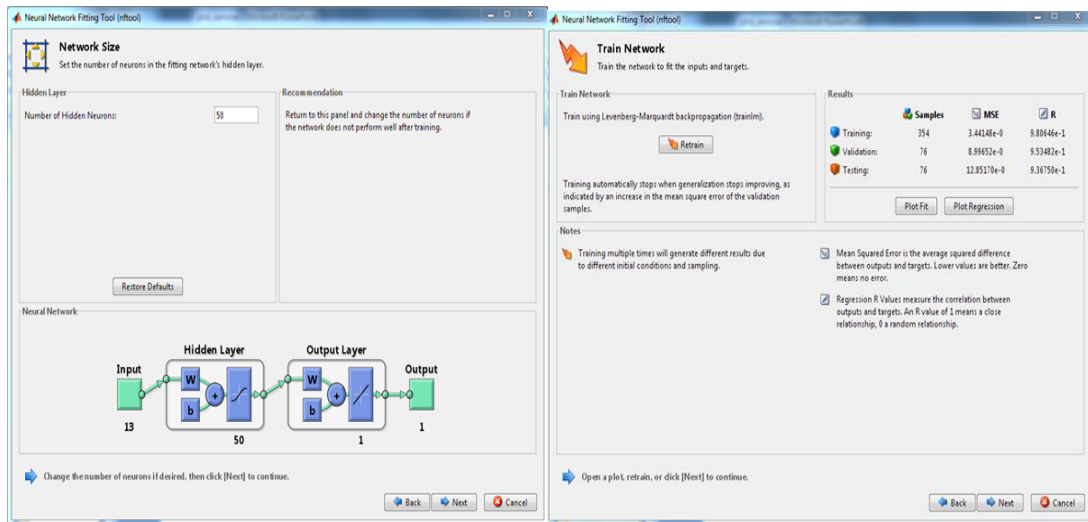


Figure 6.3 Neural Network Training in MATLAB showing hidden layers

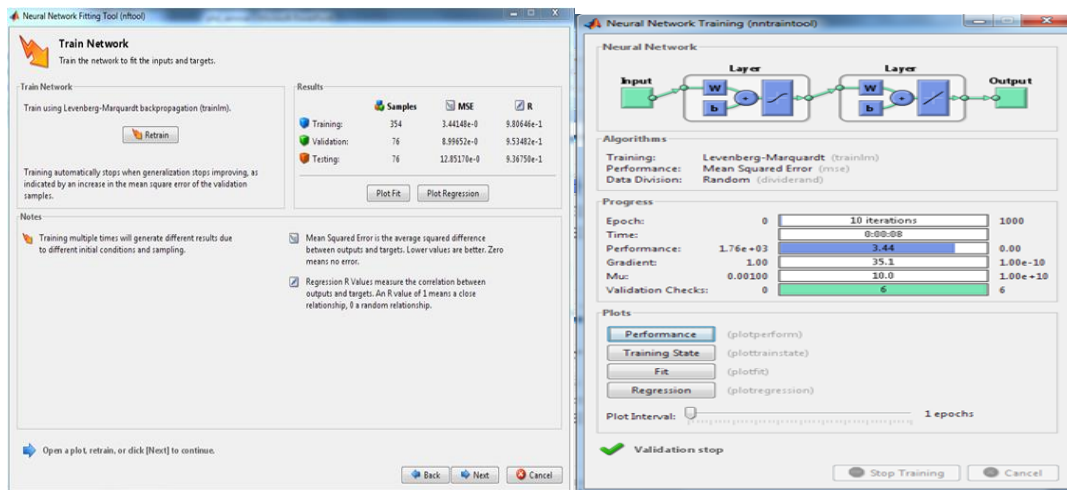


Figure 6.4 Neural Network Training in MATLAB showing training parameters

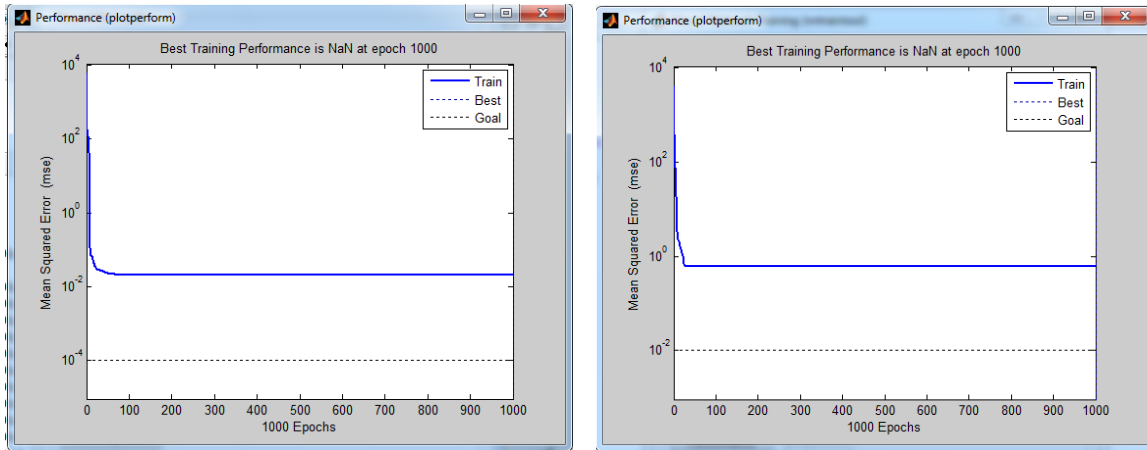


Figure 6.5 Convergence of ANN network

The Levenberg–Marquardt algorithm which was independently developed by Kenneth Levenberg and Donald Marquardt provides a numerical solution to the problem of minimizing a nonlinear function. It is fast and has stable convergence.

A Simulink block is created after the training of the Neural Network. This neural network block is placed instead of conventional PI controller. All the conventional PI controllers are replaced one by one after proper training and system is run.

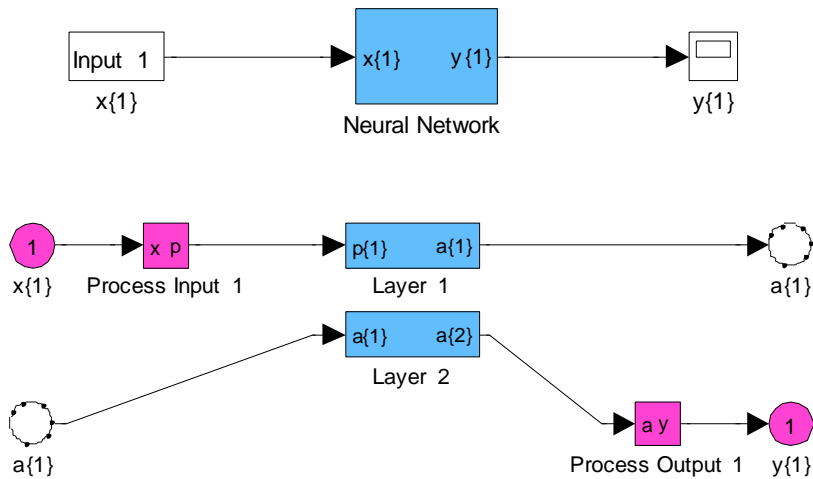


Figure 6.6 Simulation block of ANN

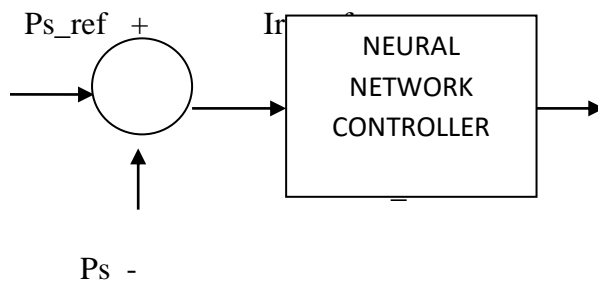


Figure 6.7 (a): Active Power ANN Controller

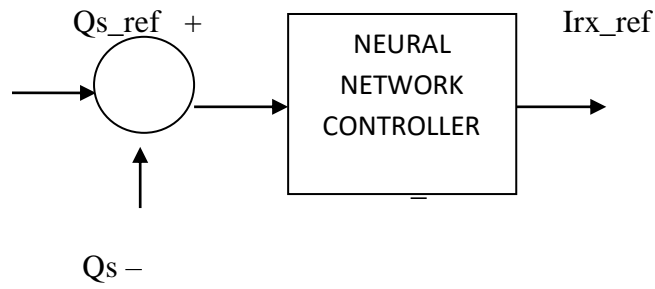


Figure 6.7 (b): Reactive Power ANN Controller

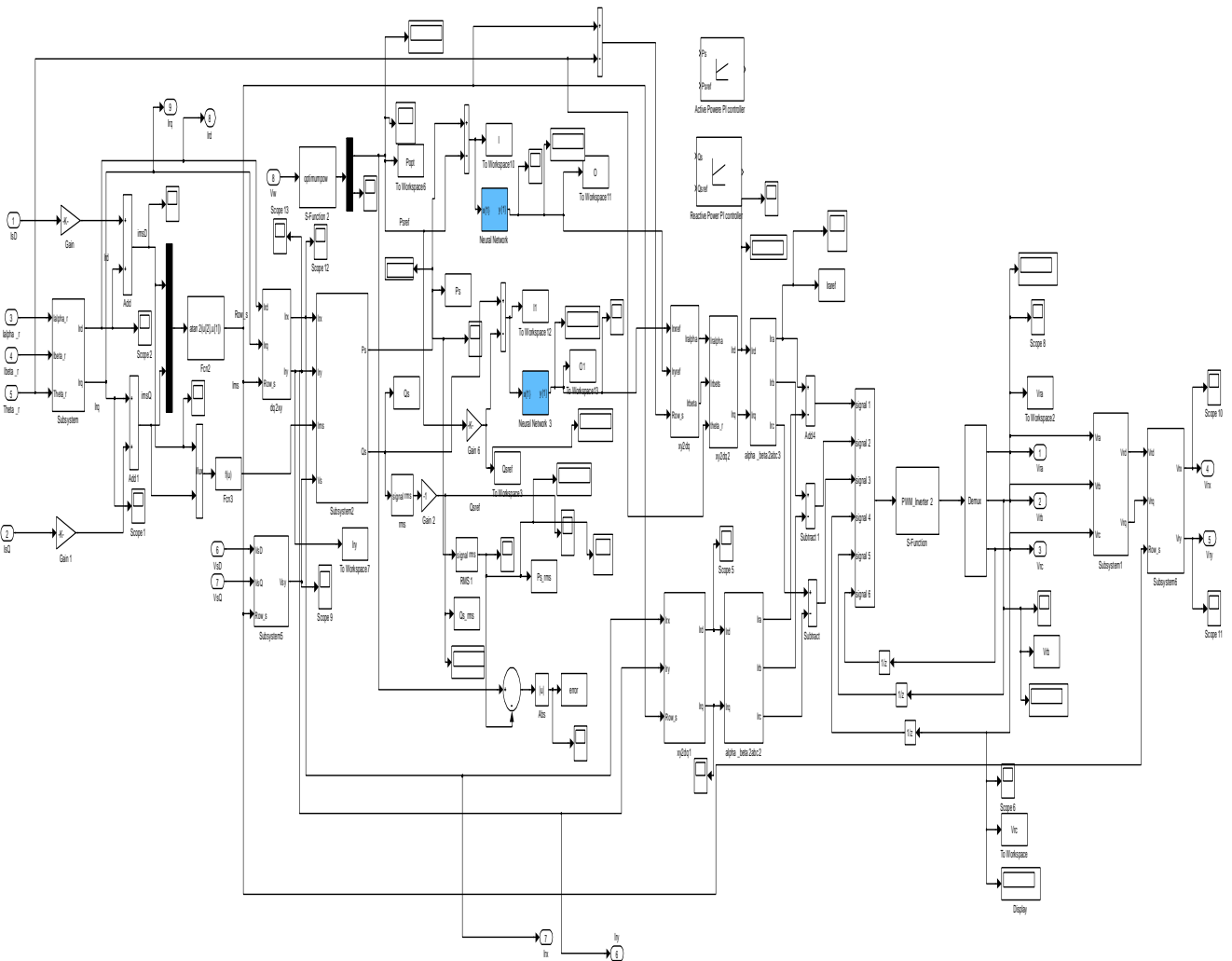


Figure 6.8: Simulation Model of Rotor Side Converter Using Neural Network Controller

Secondly, If Input 1= x and Input 2= y , then output : $Z=(\text{Constant})$ where $a=b=c=0$.

The Advantages of ANFIS Systems are

- An adaptive neuro-fuzzy inference system (ANFIS) is a Takagi-Sugeno inference system based artificial neural-network system.
- The ANFIS technique blends the property of both neural networks and fuzzy logic principles, by capturing the potential benefits of both in a single architecture.
- With the aid of fuzzy IF–THEN rules learning capability maximize to deal nonlinear functions.
- For using the ANFIS in a more efficient and optimal way genetic algorithm can also be used.
- It is a very powerful approach for building complex and nonlinear relationship between a set of input and output data.
- It can be trained without the need of any of the expert knowledge usually required for the standard fuzzy logic design. Both numerical and linguistic knowledge can be combined into a fuzzy rule base by using fuzzy methods.
- Fuzzy membership functions (MFs) can be tuned optimally by using optimization algorithms. Other advantages of the ANFIS include fast learning capability, fast adaptation and handling of nonlinear systems.

The ANFIS structure can also be implemented in real time.

6.3.1 Fuzzy Inference Systems

Fuzzy inference systems (FISs) are also known as fuzzy rule-based systems, fuzzy model, fuzzy expert system, and fuzzy associative memory. This is a major unit of a fuzzy logic system. The decision-making is an important part in the entire system. The FIS formulates suitable rules and based upon the rules the decision is made. This is mainly based on the concepts of the fuzzy set theory, fuzzy IF–THEN rules, and fuzzy reasoning. FIS uses “IF THEN” statements, and the connectors present in the rule statement are “OR” or “AND” to make the necessary decision. The basic FIS can take either fuzzy inputs or crisp inputs, but the outputs it produces are almost always fuzzy sets. Different defuzzification method is adopted to extract a crisp value when the FIS is used as a controller in any system.

Basically a FIS consists of five functional blocks:

- A rule base, containing a number (depends on input /output) of fuzzy if-then rules.
- A data base, which defines the membership functions of the fuzzy sets used in the fuzzy rules.
- A decision-making unit, which performs the inference operations on the rules.
- A fuzzification interface, which transforms the crisp inputs into degrees of match with linguistic values.
- A defuzzification method, which transforms the fuzzy results obtained into a crisp output.
- Generally, the rule base and data base are jointly referred to as the knowledge base.

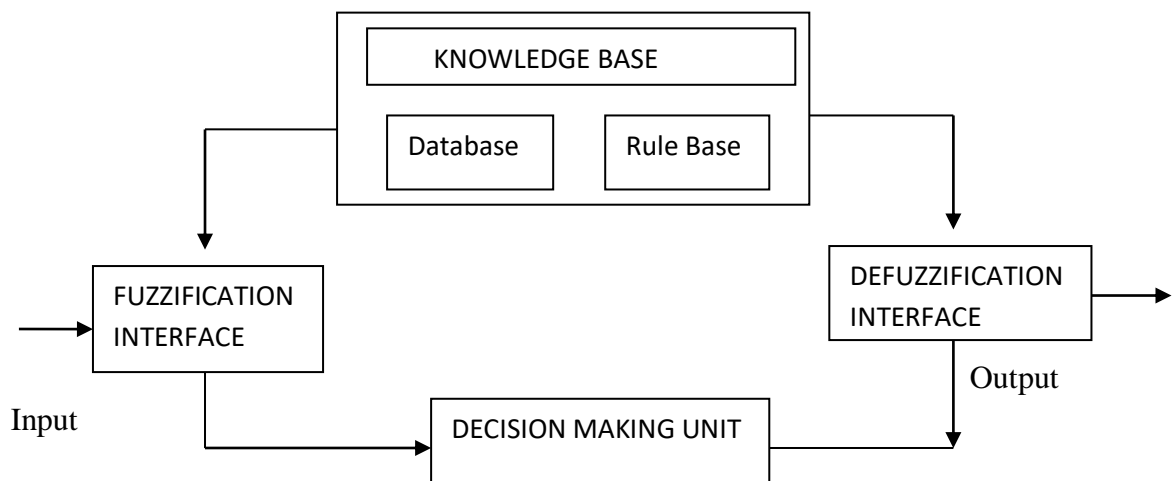


Figure 6.10 Block diagram showing various parts of Fuzzy Logic System

There are two types of fuzzy inference systems Mamdani type and Sugeno-type. These two types of inference systems vary, somewhat, in the way outputs are determined. Mamdani's fuzzy inference method is the most commonly used fuzzy methodology. Mamdani's method was among the first control systems built using fuzzy set theory. It was proposed in 1975 by EbrahimMamdani as an attempt to control a steam engine and boiler combination by synthesizing a set of linguistic control rules obtained from experienced human operators [16]. Mamdani-type inference expects the output membership functions to be fuzzy sets. After the aggregation process, there is a fuzzy

set for each output variable that needs defuzzification which is done by finding the centroid of a two-dimensional aggregate output function.

6.3.2 Sugeno-Type Fuzzy Inference System

Sugeno-Type Fuzzy Inference System was introduced by Takagi Sugeno Kang in 1985. It has similarity with Mamdani Method in many aspects. The main difference between Mamdani and Sugeno System is in the formation of rules, defuzzification method. In the Sugeno system Weighted Average method is used for defuzzification method. The first two parts of the fuzzy inference process, i.e. fuzzifying the inputs and applying the fuzzy operator, are exactly the same. The main difference between Mamdani's and Sugeno's methods is that the Sugeno output membership functions are either linear or constant.

The rule in a Sugeno fuzzy model takes the form: If Input-1 = x, and Input-2 = y, then, Output is $z = ax + by + c$.

For a zero-order Sugeno model, the output level z is a constant ($a=b=0$). The output level z_i of each rule is weighted by the firing strength W_i of the rule. For example, for an AND rule with Input-1 = x, and Input-2 = y, the firing strength is $W_i = \text{AND}(F1(x), F2(y))$, where, $F1(\cdot)$ and $F2(\cdot)$ are the membership functions for Inputs-1 and -2. The final output of the system is the weighted average of the outputs of all the rules, computed as

$$\text{Final output} = \frac{\sum_{i=1}^N W_i Z_i}{\sum_{i=1}^N W_i} = \sum_{i=1}^N \overline{W}_i Z_i, \overline{W}_i = \frac{W_i}{\sum_{i=1}^N W_i}$$

Since it is a more compact and computationally efficient representation than a Mamdani system, the Sugeno system lends itself to the use of adaptive techniques for constructing fuzzy models. These adaptive techniques can be used to customize the membership functions so that the fuzzy system accurately models the data. Some of the advantages of the Sugeno method are

- It is computationally efficient.
- It works well with linear techniques (e.g., PID control).
- It works well with optimization and adaptive techniques.
- It has continuity of the output surface plane.
- It is well-suited to mathematical analysis.

6.3.3 Adaptive Neuro-Fuzzy Inference System

The very basic architecture of Fuzzy Inference System includes a model which maps input to input membership functions as well as input membership functions to the rules and rules to output Membership functions and finally to defuzzified value or output. In Non-Adaptive Neuro Fuzzy System Rules are formed by expertise or human interpretation. The shape of the membership functions used also depends upon the system parameter. Adaptive Neuro Fuzzy inference system is easy and fast learning method where a method is provided to the fuzzy model to learn information about the data set available to compute the membership function. It is a process which combines both Fuzzy inference System and Neural Network to track input and output data.

In an adaptive neuro-fuzzy inference technique, a fuzzy inference system is designed, whose membership functions parameters are tuned or optimized using either a error back propagation algorithm method, or in combination with a least squares type of method using a given input and output data set. This helps fuzzy system to learn from data and formation of rule as per the system requirement.

The basic structure of the ANFIS algorithm for a first order Sugeno-type fuzzy system is shown in Fig. 7. The various layers are explained below:

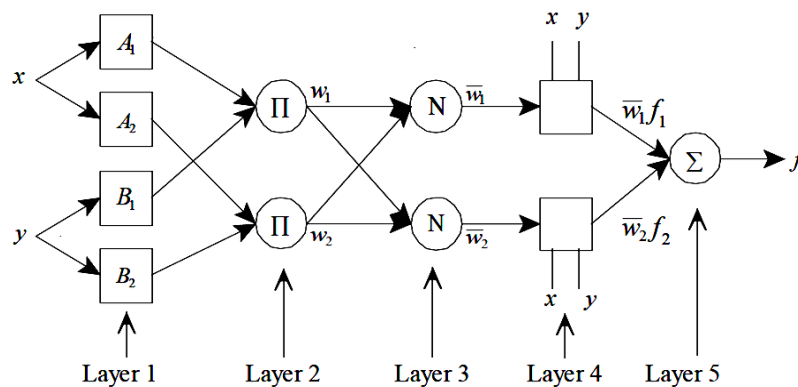


Figure 6.11 ANFIS Architecture

Layer 1:

Every node i , in this layer, is a square node with a node function $O_{i1} = \mu_{A_i}(x)$ where, x is the input to node i , and A_i is the linguistic label (small, large, etc.,) associated with this node function. In other words, O_{i1} is the membership function of A_i and it specifies the degree to which the given input “ x ” satisfies the quantifier A_i . Usually $\mu_{A_i}(x)$ is

selected to be bell shaped with maximum value equal to 1, and minimum value equal to 0, such as-

$$\mu_{A_i}(x) = \frac{1}{1 + \left[\left(\frac{x-c_i}{a_i}\right)^2\right]^{b_i}}$$

Where, $\{a_i, b_i, c_i\}$ is the parameter set. As the values of these variables changes, the bell-shaped membership functions change accordingly, thus, exhibiting various forms of membership functions on linguistic label A_i . The trapezoidal or triangularshaped membership function is generally used. Parameters in this layer are referred to as premise parameters.

Layer 2:

The node in this layer is a circle node, and labelled“ Π ”, which multiplies the incoming signals coming and sends the product in the output node. For example $W_i = \mu_{A_i}(x)X\mu_{B_i}(x)$, $i = 1, 2$. Each node output represents the firing strength of a rule. In fact, other T-norm operators that performs generalized AND can be used as the node function in this layer.

Layer 3:

Every node in this layer is symbolised as circle node, labelled “ N ”. The i^{th} node calculates the ratio of the i^{th} rule’s firing strength to the sum of all rule’s firing strengths, as given below.

$$\overline{W}_i = \frac{W_i}{W_1+W_2}, i=1,2$$

Outputs of this layer are known as normalized firing strengths.

Layer 4:

Every node i in this layer is a square node with a node function

$$O_i^4 = \overline{W}_i f_i = \overline{W}_i(p_i x + q_i y + r_i)$$

Where, \overline{W}_i is the output of layer 3, and $\{p_i, q_i, r_i\}$ is the parameter set. Parameters in this layer will be referred to as consequent parameters.

Layer 5:

The node in this layer is symbolised as circle node labelled “ Σ ” that computes overall output as the summation of all incoming signals, i.e,

$$O_i^5 = \text{overall output} \sum_i \overline{W}_i f_i = \frac{\sum_i W_i f_i}{\sum_i W_i}$$

The adjustment of modifiable parameters is a two-step process. First, information is propagated forward in the network until Layer-4, where the parameters are identified by a least-squares estimator. Then the parameters in Layer-2 are modified using gradient descent. The only user specified information is the number of membership functions in the universe of discourse for each input and output as training information. ANFIS uses two steps firstly the input patterns are propagated forward, and the optimal consequent parameters are estimated by an iterative least mean square procedure keeping premise parameters fixed for the current cycle through the training set. The pattern is propagated again, and in this epoch (iterations), back propagation is used to modify the premise parameters, while the consequent parameters remain fixed.

The parameters associated with the membership functions will change through the learning process by compilationsupported by a gradient vector which provides a measure of how excellently the fuzzy inference system is mapping the input/output data pairs for a given set of parameters. Once the gradient vector is obtained, some of the available optimization methods can be applied to adjust the parameters to reduce the error between desired and target value.

6.4 STEPS ANFIS CONTROLLERS DESIGN

The ANFIS (Adaptive Neuro fuzzy Controller) is designed with the help of MATLAB toolbox. Sugeno type Fuzzy Inference system is used. The following steps are followed to design the Fuzzy inference system.

1. Two inputs and one output are taken. First input is the error between the Reference and actual parameter fed to the controller and the second input is the derivative of the error signal that is fed to the Controller. The output is the output from conventional Controller i.e the controller action.

The inputs and outputs of the ANFIS controllers are as follows.

- a. ANFIS active power controller

Input 1: Error between reference and actual stator active power $P_{sref} - P_s$.

Input 2: The derivative of the error signal $\frac{d(P_{sref} - P_s)}{dt}$. To examine the change in error w.r.t time.

Output 1: q axis rotor current in stator flux oriented reference frame I_{ry_ref} .

b. ANFIS reactive power controller

Input 1: Error between reference and actual stator active power $Q_{sref} - Q_s$.

Input 2: The derivative of the error signal $\frac{d(Q_{sref} - Q_s)}{dt}$. To examine the change in error w.r.t time.

Output 1: d axis rotor current in stator flux oriented reference frame I_{rx_ref} .

2. The membership functions are assigned. Nine Trapezoidal Membership functions are taken to cover wide range of universe of discourse. The linguistic variables assigned for membership functions are VNB, NB, NM, NS, Zero, PS, PM, PB, VPB. Total number of rules formed is 81.
3. Triangular or trapezoidal shapes are simple to implement and fast for computation that's why these membership functions are widely used. The trapezoidal membership function and the number of membership function is selected based on the cross validation trial and error method by running the simulation and testing the output and inspecting the input variables.
4. In the ANFIS Editor training data are loaded in Array form. The data is fed by first running the system with conventional PI controller. The error of reference and actual values which is the input to PI Controller, the derivative of error and output from the PI controller is saved in MATLAB workspace. After that the data is imported from workspace to the ANFIS editor and trained until the error is reduced. The output of ANFIS can be of two types: Constant or Linear.
5. The trained FIS is exported to the Workspace. The Simulink block of Fuzzy System is used for simulation of the system with the same name as that of the FIS.
6. The system is trained for different numbers of Epochs until a satisfactory result is obtained. The conventional PI controllers used for RSC of DFIG. are replaced by ANFIS controller. Fuzzy logic tool box in MATLAB has been used for designing and testing of the ANFIS controllers.

The data required for training and testing the ANFIS are generated by designing and testing conventional PI controllers for a set of different operating conditions by utilizing vector control technique as discussed earlier.

Table 6.3: ANFIS training Parameter and Architecture of the Rotor side converter controllers

	Inputs Layer	Output Layer
Activation Function(\emptyset)	Bell Shaped	Constant
Parameter -a	2.0	2.0
Parameter-b	2.0	2.0
Parameter-c	-1.0	-1.0
No. of Inputs	2	
No. of Outputs	1	
No. of Epochs	60	
Error tolerance limit	0	
Membership functions No.	9	Constant
Membership function taken	Trapezoidal	Constant
Learning method	Hybrid algorithm	Grid Partition

After loading the generated data, the ANFIS structure gets generated by using grid partitioning method. For this work the input and the output selected is of Trapezoidal and linear type membership functions respectively.

While training the ANFIS model, the ranges and boundaries of trapezoidal membership functions are changed by using hybrid algorithm.

Hybrid learning algorithm consists of two passes:

1. Forward Pass: During forward pass up to Node 4 the consequent parameters are treated with the least squares method.
2. Backward Pass: The error signals then propagated backward and the premise parameters are updated by gradient descent method.

Table 6.4: Hybrid Learning Algorithm

	Forward Pass	Backward Pass
Premise Parameter	Fixed	Gradient descent
Consequent Parameter	LeastSquare estimator	Fixed
Signals	Node output	Error Signals

The overall output of the system is found using Weighted Average defuzzification, method by combining outputs of all the rules.

$$\text{Final output} = \frac{\sum_{i=1}^N W_i Z_i}{\sum_{i=1}^N W_i} \text{ where } z = ax + by + c$$

- Conventional Active PI controllers in rotor side converter as well as Grid side converter are replaced with the trained ANFIS based controllers.
- The performance of the ANFIS controllers has been observed and tested for various conditions and results are compared with conventional PI controllers.

6.4.1. The steps incorporated in ANFIS MATLAB toolbox

Step 1: A new FIS Sugeno type Inference system is formed.

Step 2: Two inputs and one output are taken.

Step 3: Trapezoidal Membership functions are taken and 9 linguistic variables are taken for each membership function.

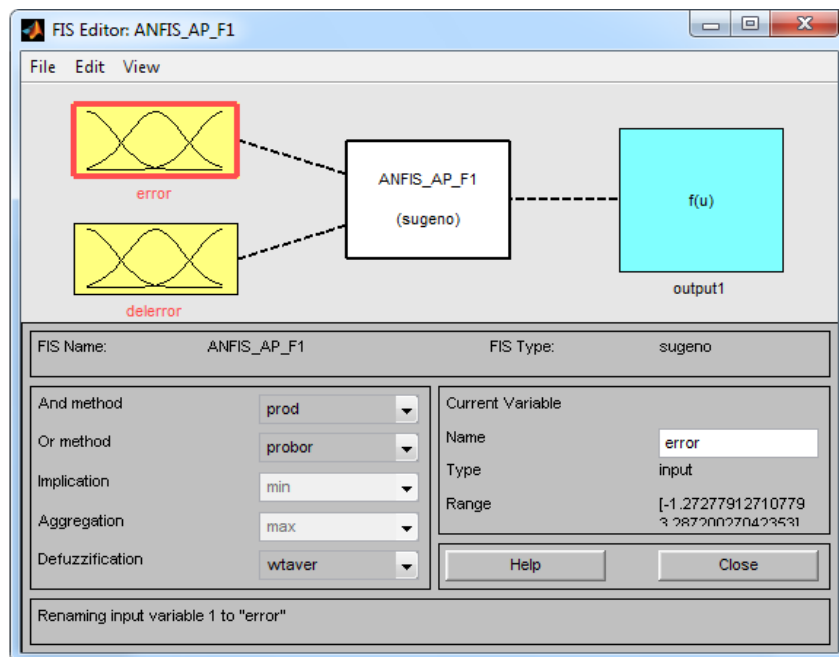


Figure 6.12 ANFIS FIS System

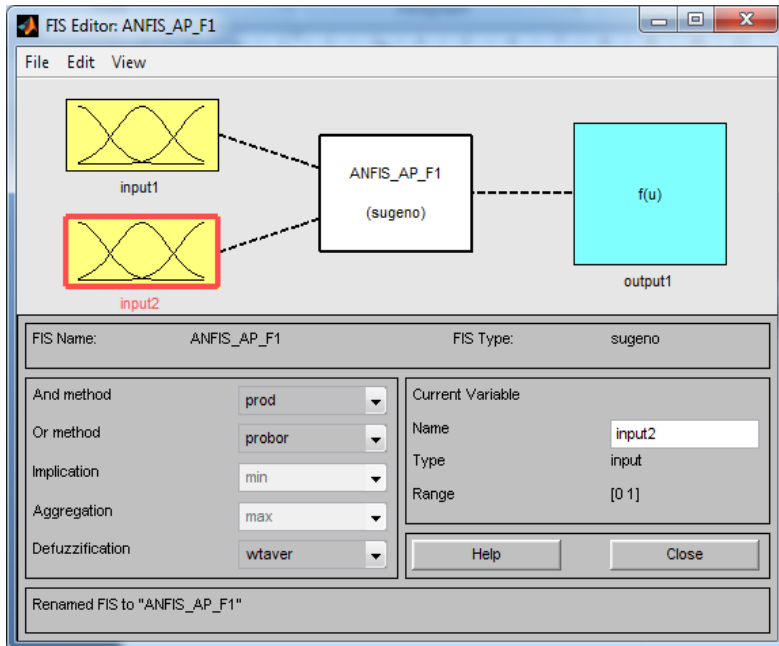


Figure 6.13 ANFIS FIS system showing Inputs and output

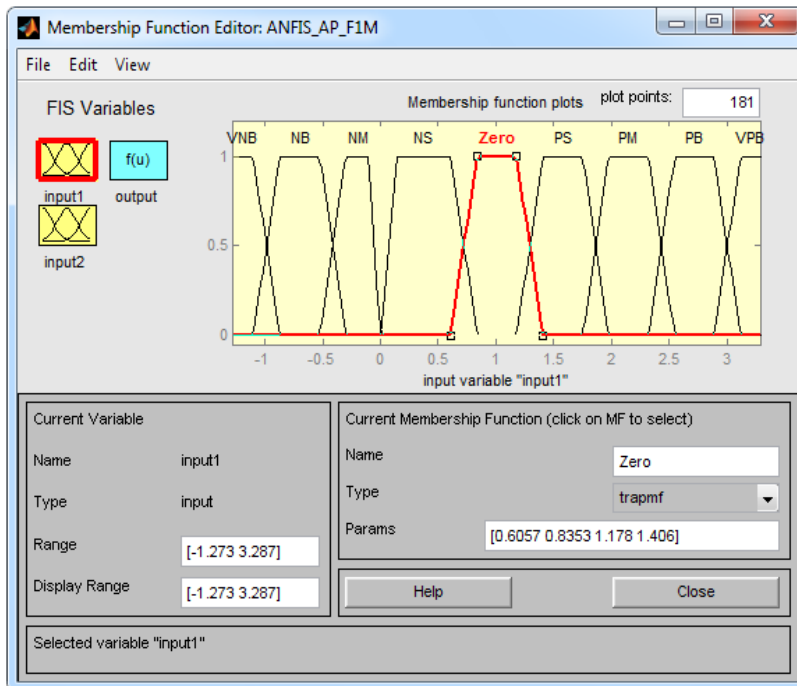


Figure 6.14 ANFIS FIS system showing membership functions for first Input

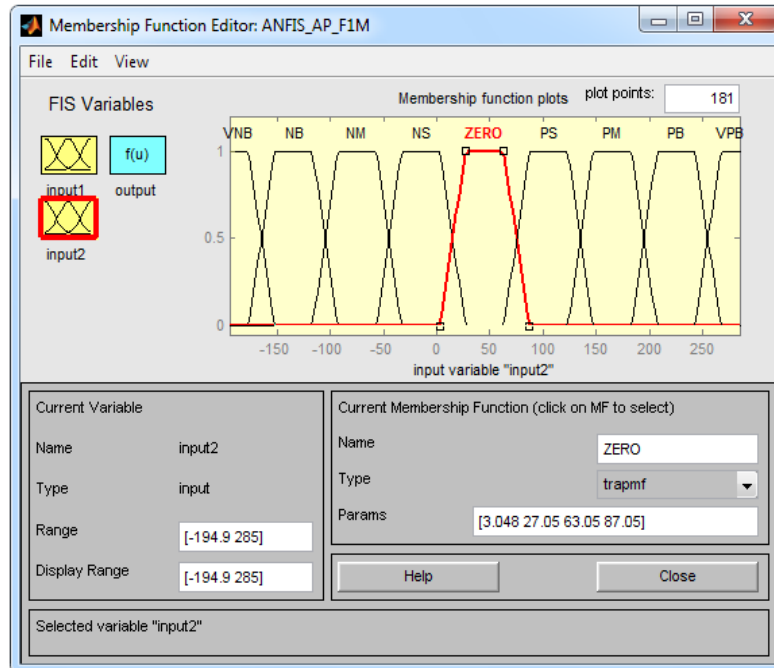


Figure 6.15 ANFIS FIS system showing membership functions for Second Input

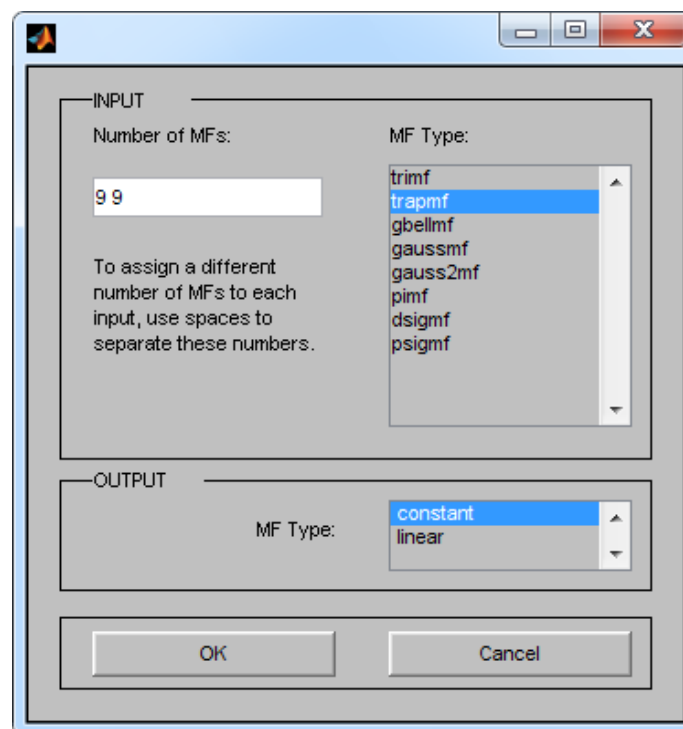


Figure 6.16 ANFIS FIS system showing output function

Output Membership Functions taken is Constant type.

Step 4: ANFIS model is formed using grid partition method with 2 input 1 output and 81 rules.

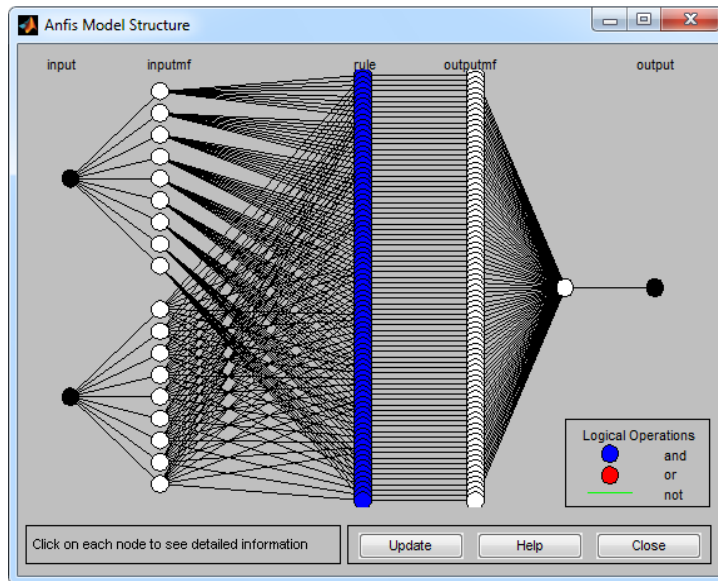


Figure 6.17 ANFIS FIS system Rules for Inputs and outputs

Step 5: Training and testing data set is loaded in FIS model which is obtained by running the Simulink main model using conventional PI controller under various conditions. Training process is continued until the error becomes minimum or equal to or near Zero.

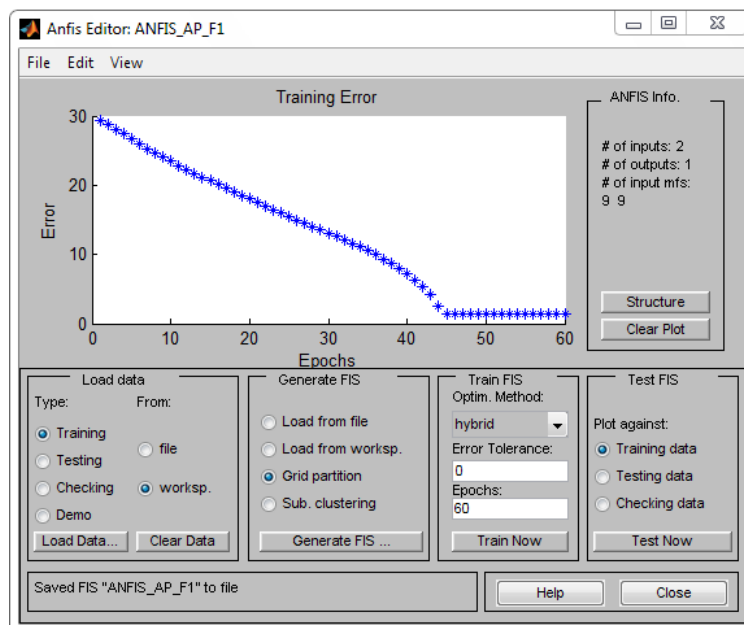


Figure 6.18 ANFIS FIS system showing convergence

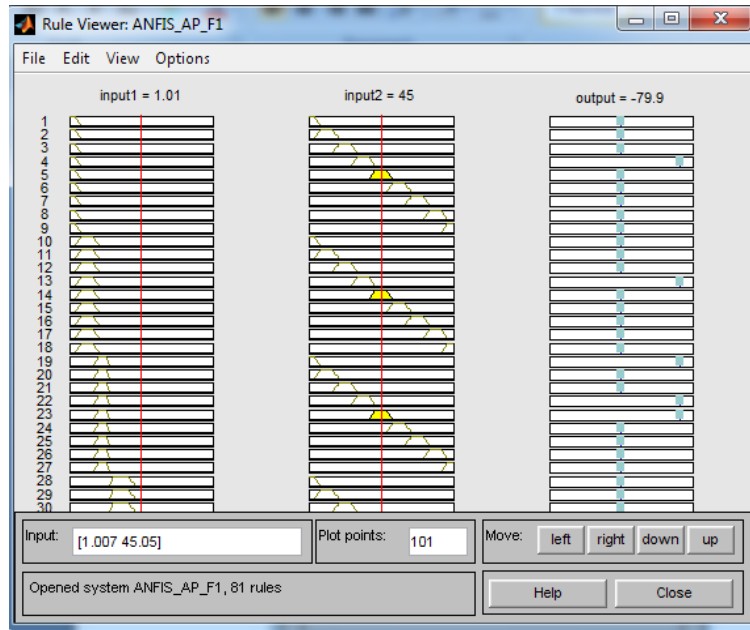


Figure 6.19 ANFIS FIS Rule View

No of Epochs taken are 60.

Step 6: Rules are formed automatically by learning process using data set feed.

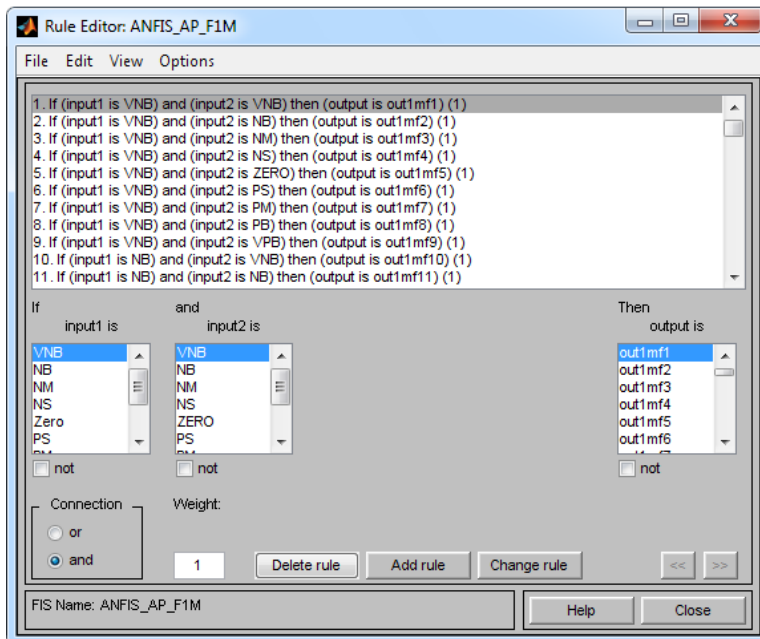


Figure 6.19 ANFIS FIS Rules

After proper tuning of ANFIS controller, the Active and Reactive Power PI controller is replaced by ANFIS based Active and reactive Power Controller respectively.

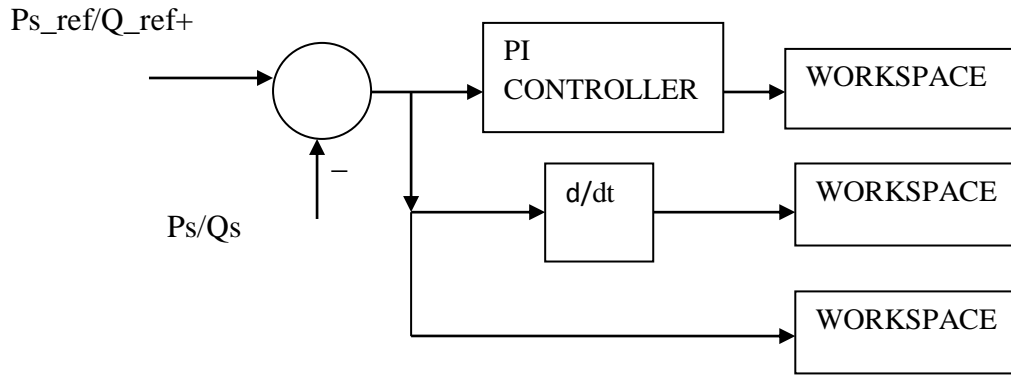


Figure 6.20: Training Data for AI controllers from PI Controller

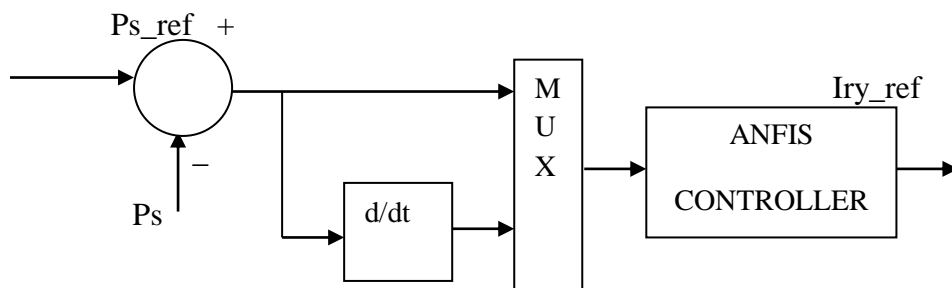


Figure 6.21: Active Power ANFIS Controller

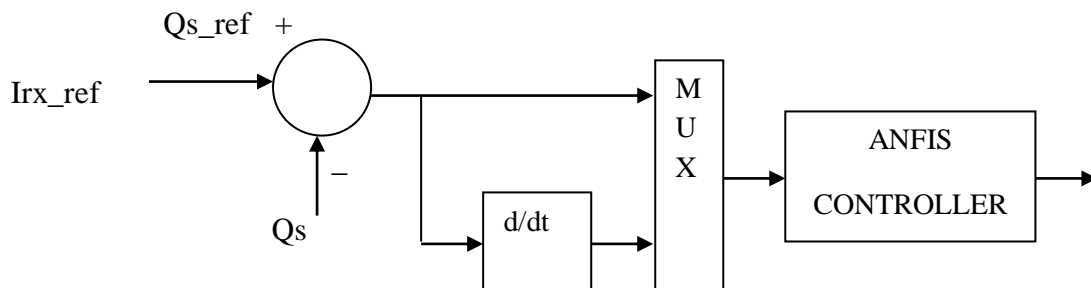


Figure 6.22: Reactive Power ANFIS Controller

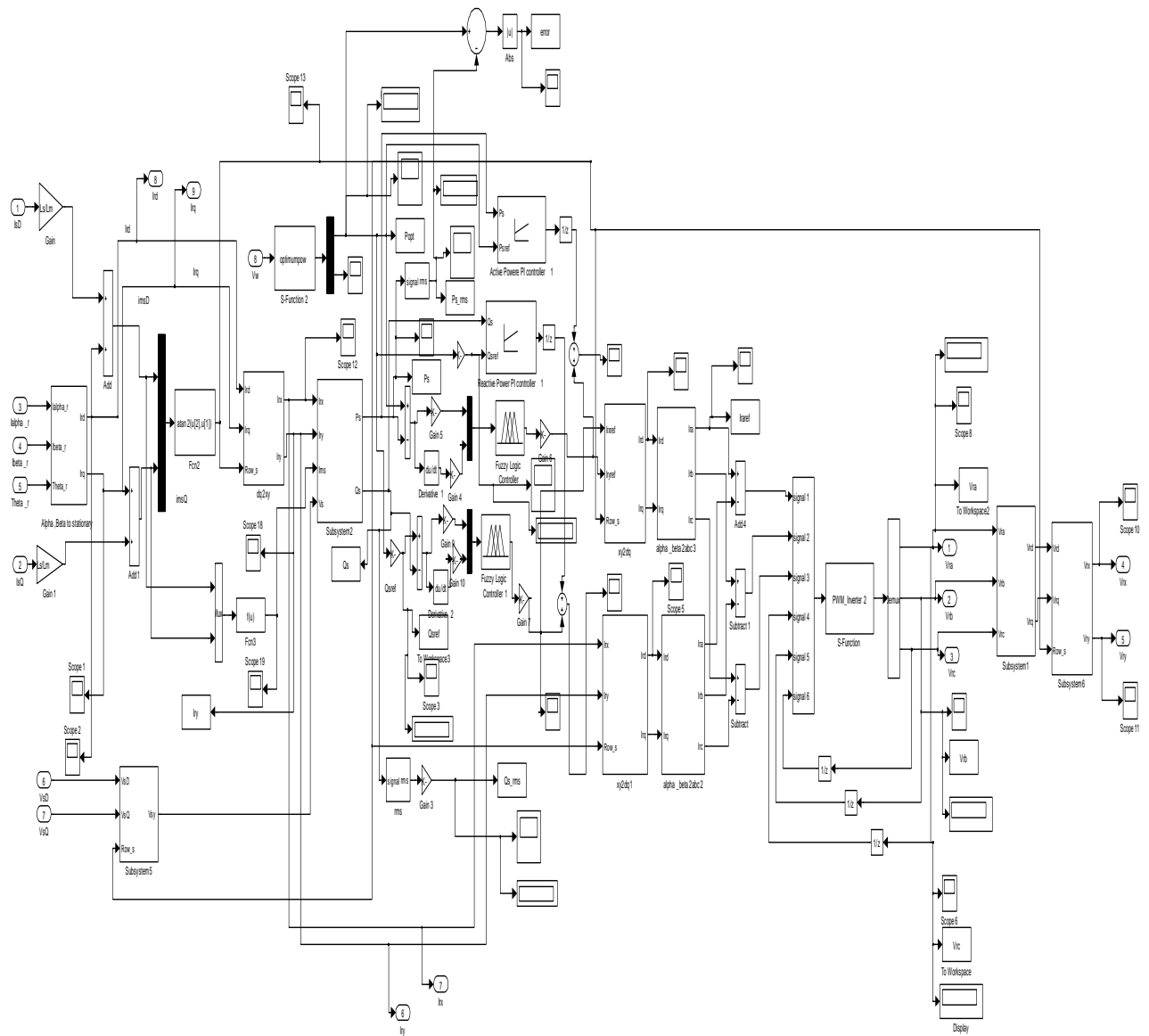


Figure6.23: Simulation Model of Rotor Side Converter using ANFIS Controller

Chapter : 7

Results and Discussions

7.1 Characteristics performance output of 5th order Doubly fed Induction Generator Model at particular wind Speed

7.11 Performance output of Doubly fed Induction Generator at wind Velocity 6m/sec.

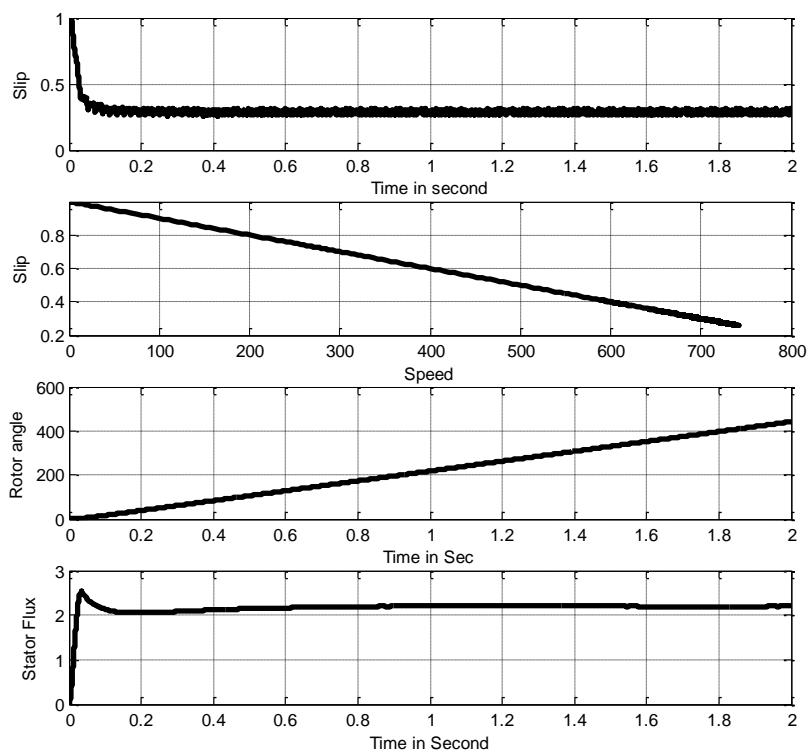


**Figure 7.1: Characteristics of Doubly fed Induction Generator a)Slip vs Time curve
b)Slip vs Speed c)Rotor angle d)Stator Flux**

Observation: The Slip vs time and slip vs speed are obtained in during sub synchronous speed of the DFIM. The machine is operating in Motoring Mode. The slip decreases gradually as the generator speed increases. The rotor angle increases gradually. The stator flux is fixed for constant wind velocity without any fault.

7.12 Performance output of Doubly fed induction generator at rated wind velocity

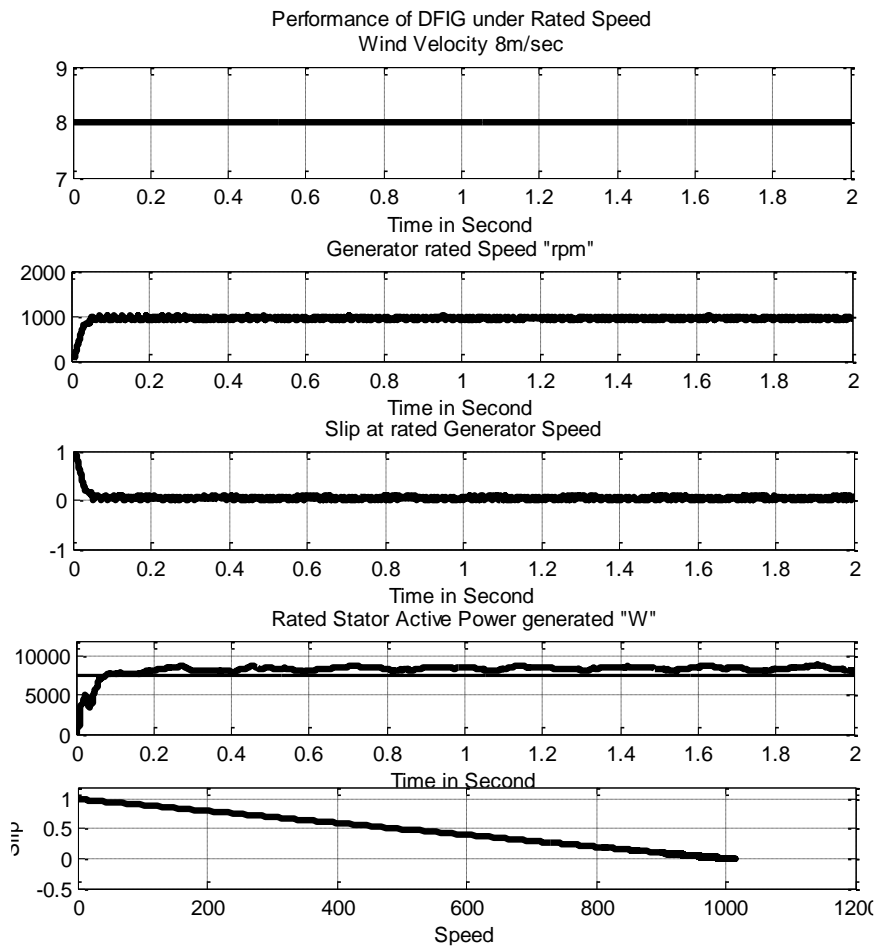


Figure 7.2: Performance of DFIG during rated Generator Speed which is achieved at 8m/sec wind Velocity. a) Wind Velocity b) Rated generator Speed c) Rated active Power generated and reference Active Power c) Slip vsspeed curve.

Observation: At wind velocity of 8m/sec the rated generation is obtained. The machine runs at rated speed. The slip is almost Zero. The speed of the rotor is almost equal to the synchronous speed of the generator. The Generator generates rated active power on the Stator side. The slip gradually reduces to Zero.

7.13 Performance showing the Mechanical Power output from Wind Turbine and PWM

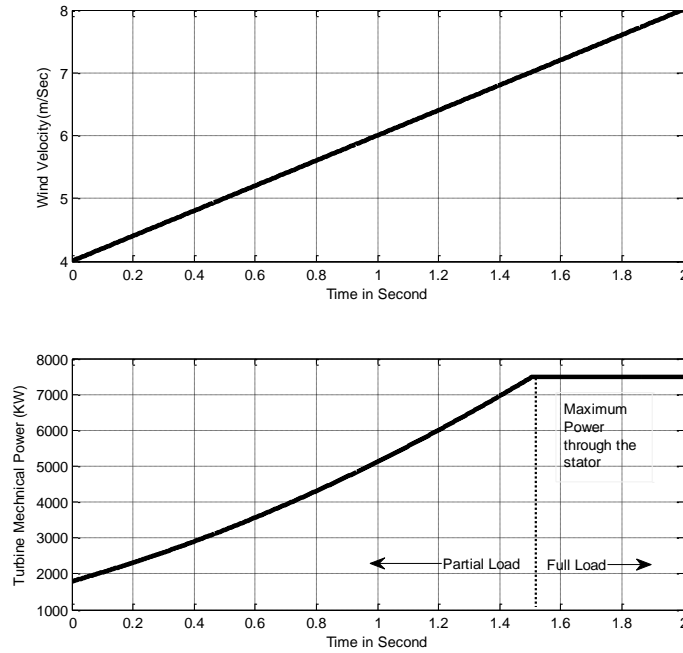


Figure 8.3: Maximum Power Point Tracking of Wind Turbine under varying Wind Condition

Observation: As the wind Speed is varied the mechanical Power obtained from the Wind turbine also varies and at rated Wind Velocity 8m/sec, it produces rated turbine power (7.5 KW).

7.14 PWM Inverter Voltage output on Rotor Side Converter and torque angle delta

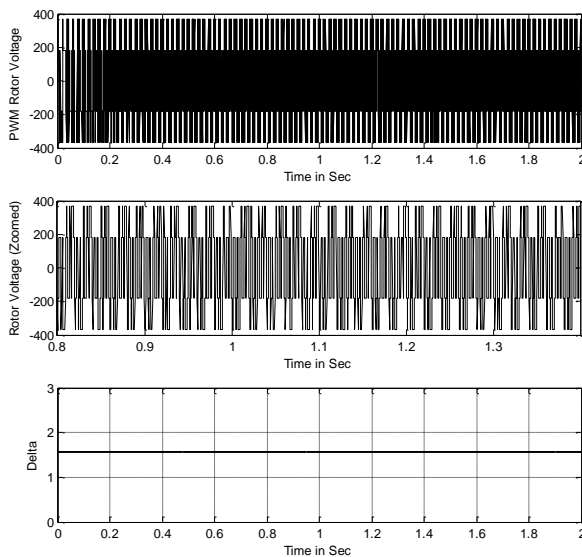


Figure 7.4: Output Voltage waveform from PWM inverter on Rotor Side converter and Power angle “delta”

7.2 Results of DFIG Showing Synchronization of Grid Voltage and Stator Flux

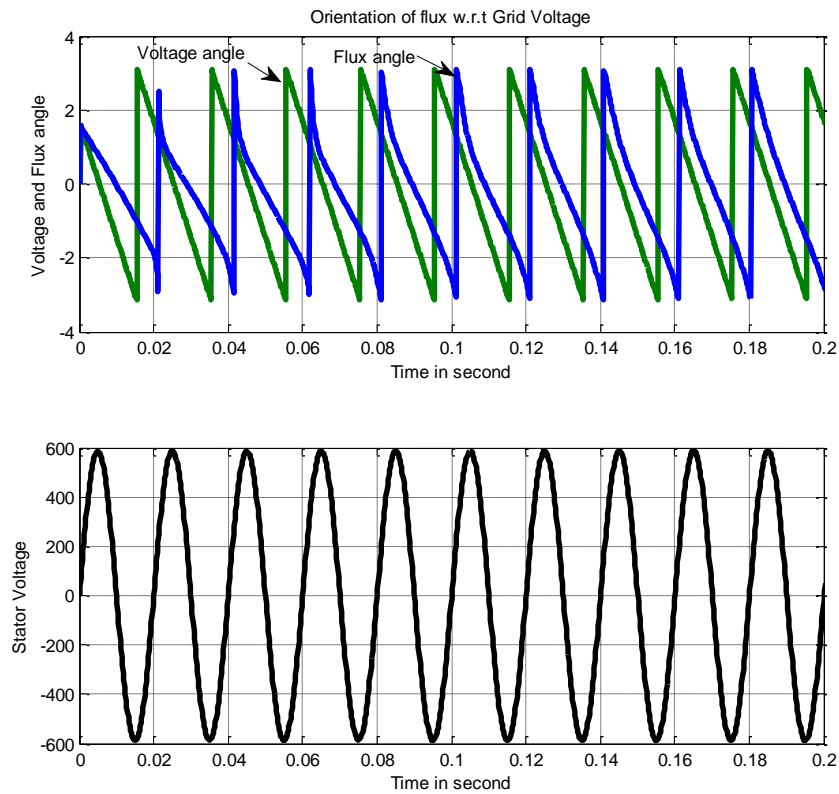


Figure 7.5: a) Orientation of flux w.r.t Grid Voltage and b) Stator Voltage Waveform

Observation: It is observed that the Stator flux angle is oriented along the Grid Voltage angle. Also the flux angle waveform seems to lead the Voltage angle.

7.3 Performance Showing the Harmonics (THD) in different waveforms using different types of Controller

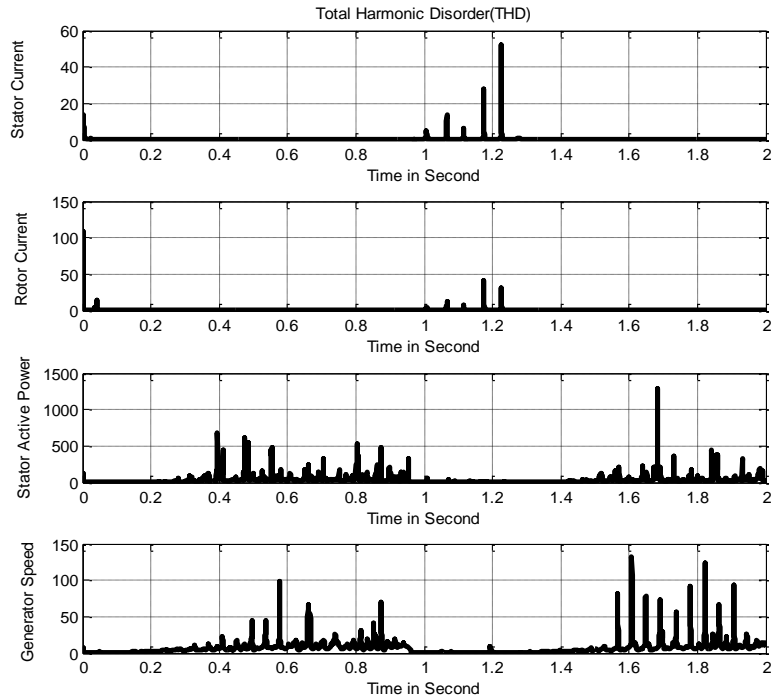


Fig (a) Using PI controller

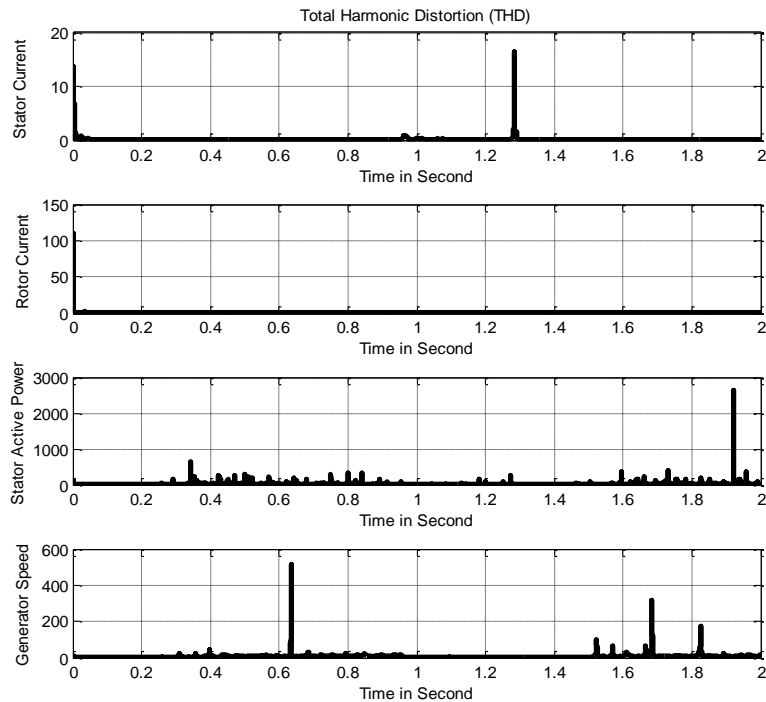


Fig (a) Using ANN controller

Figure 7.6: Total Harmonic Disorder (THD) for the Stator current, Rotor Current, Stator Active Power, Generator Speed using a) PI controller b) ANN Controller

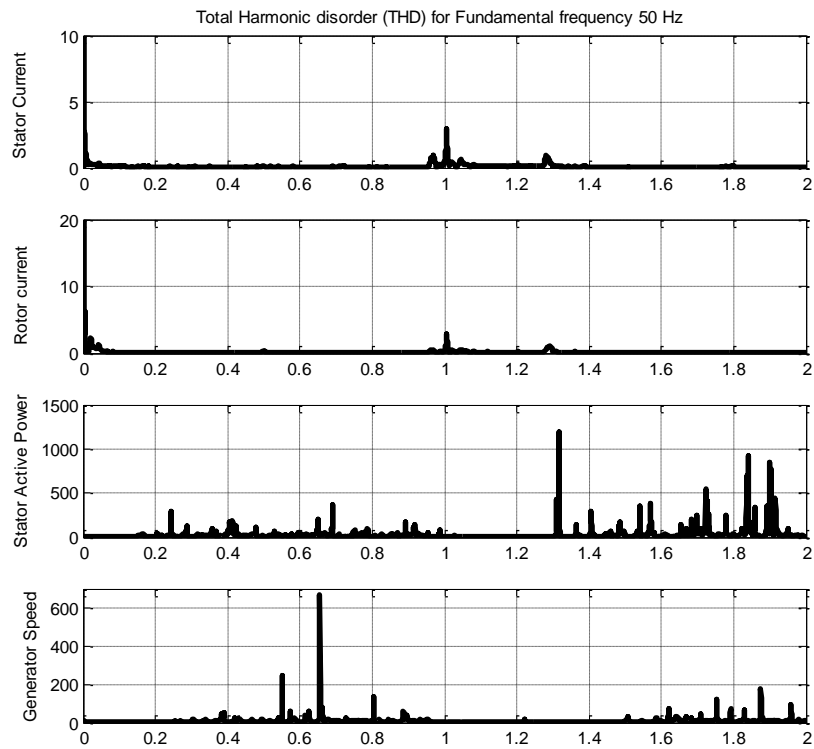


Fig (a) Using ANFIS controller

Figure7.6: Total Harmonic Disorder (THD) for the Stator current, Rotor Current, Stator Active Power, Generator Speed using ANFIS Controller

Observation: The Total Harmonic Disorder (THD) is reduced to a great extent using ANN controller during fault (L-L). Using ANFIS controller the rotor current and generator speed harmonics are further reduced.

7.3.1 Performance of DFIG Showing the Power Factor on the Stator side and GSC side

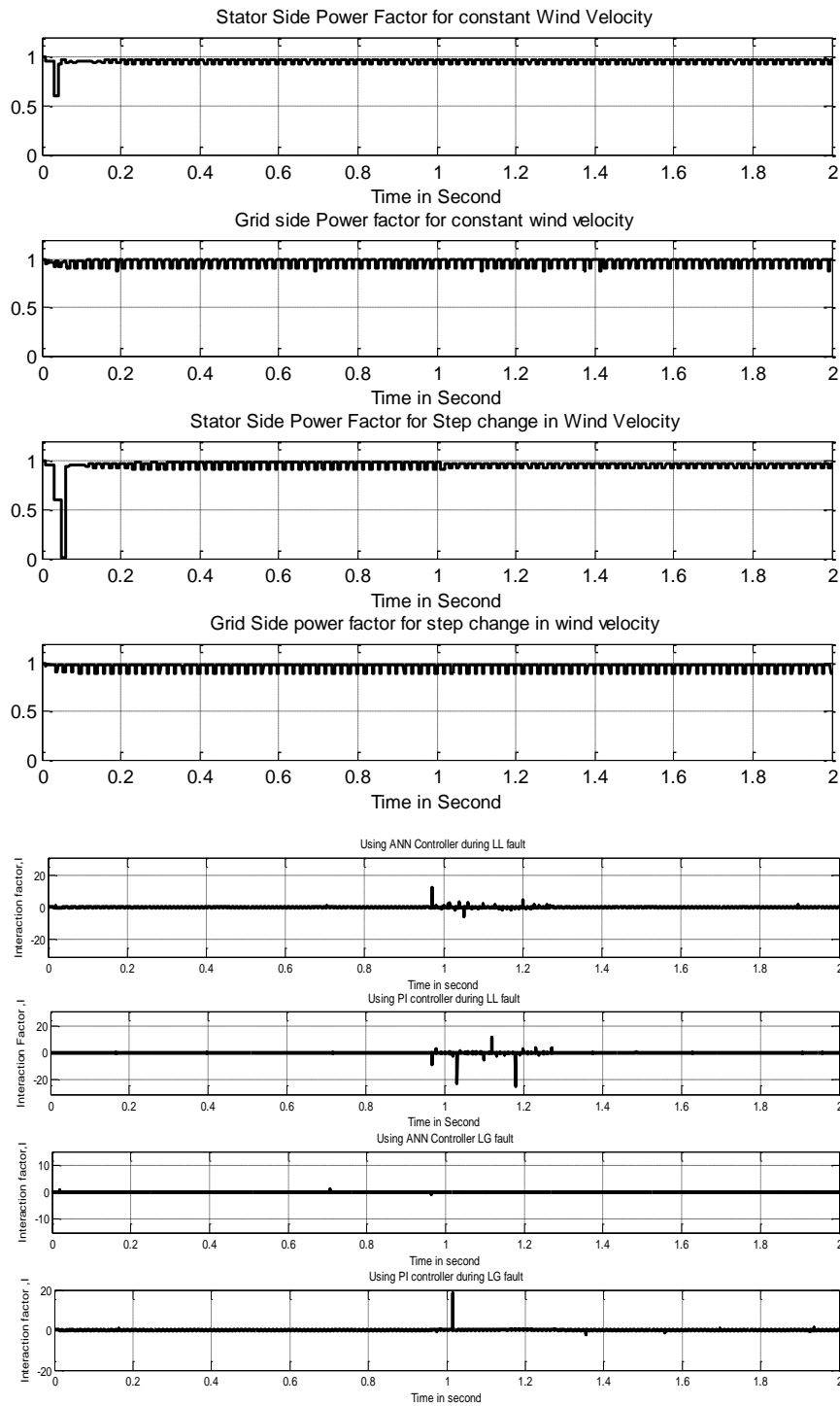


Figure 7.7: a) The Power Factor of the DFIG on The stator Side and Grid Side of the Generator for various wind conditions b) Interaction factor using PI and ANN controller

Observations: The Power factors on the Stator side and the Grid side are almost unity. It can also be seen from the Voltage and current Waveforms which are almost in phase with each other. It indicates the reactive power exchange. The reactive power exchange is only in the stator side. There is no reactive power drawn from the grid side converter. Even during the fault the Grid side converter does not draw reactive power from the grid thus maintaining the system stability.

7.4 Performance of DFIG using conventional PI-Controller under Normal Operation

7.4.1 Performance of DFIG for constant wind velocity (6 m/sec)

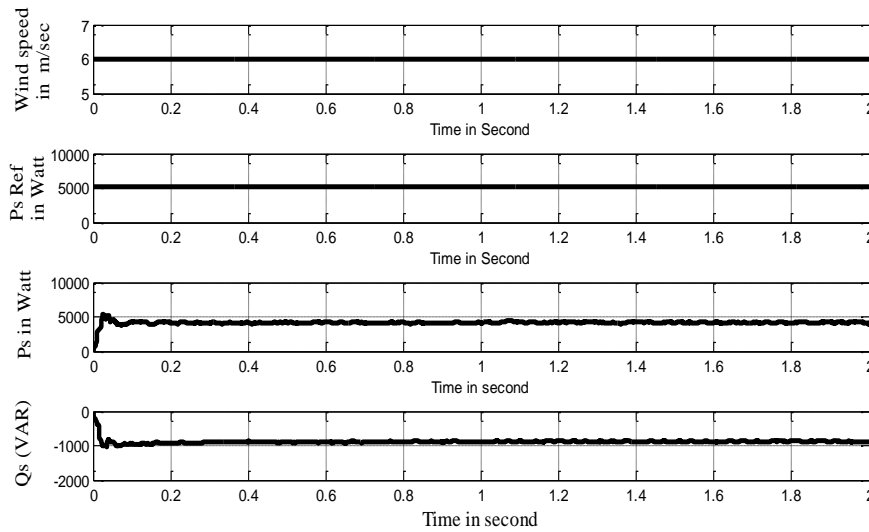


Figure 7.8: Performance of DFIG during normal operation with constant wind velocity 6m/sec a) Wind Speed b) Reference Active Power c) Actual Active Power d) Actual Reactive Power.

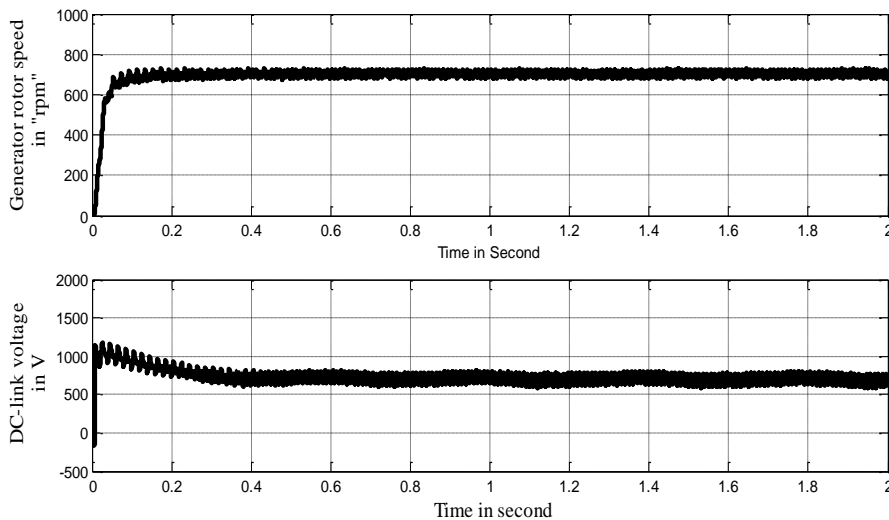


Figure 7.9: Performance of DFIG during normal operation with constant wind velocity 6m/sec a) Generator rotor Speed b) DC Link Voltage.

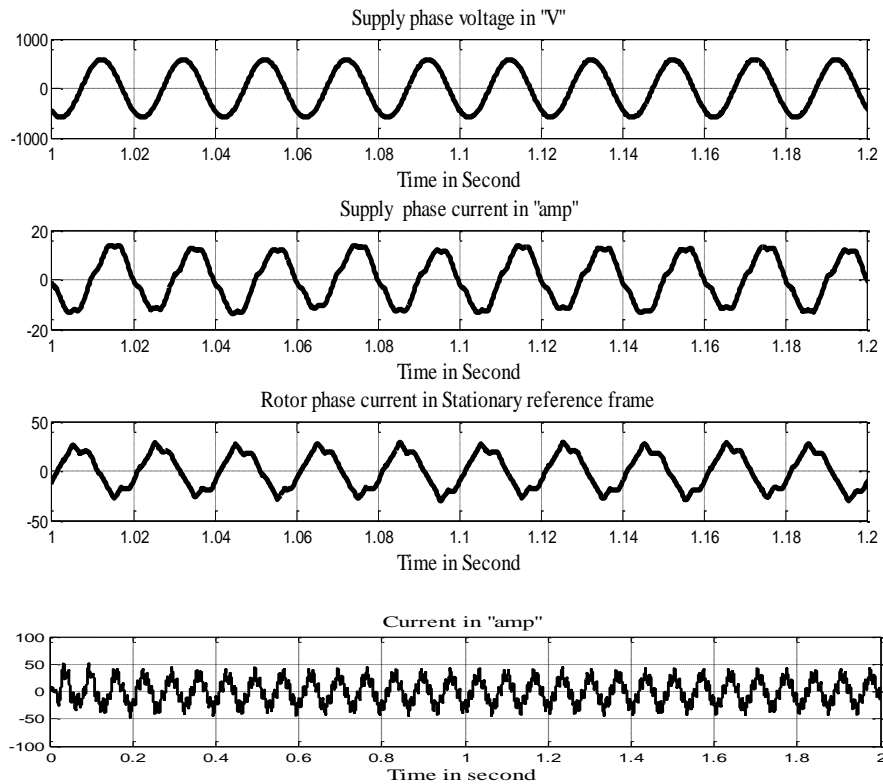


Figure 7.10: Performance of DFIG during normal operation with constant wind velocity 6m/sec a) Stator Voltage b) Stator Current c) Rotor current in Stationary reference frame d) Rotor current in Natural reference frame.

Observation: The actual active Power is almost approaching the reference power closely and Actual DC link voltage takes more time to stabilize to reference DC link value. Supply Voltage and current are almost in phase which corresponds to unity power factor at all operating conditions but the Rotor current output is sinusoidal but with some distortion.

7.4.2 Performance of DFIG for step change in wind velocity under normal condition (5m/sec to 7m/sec)

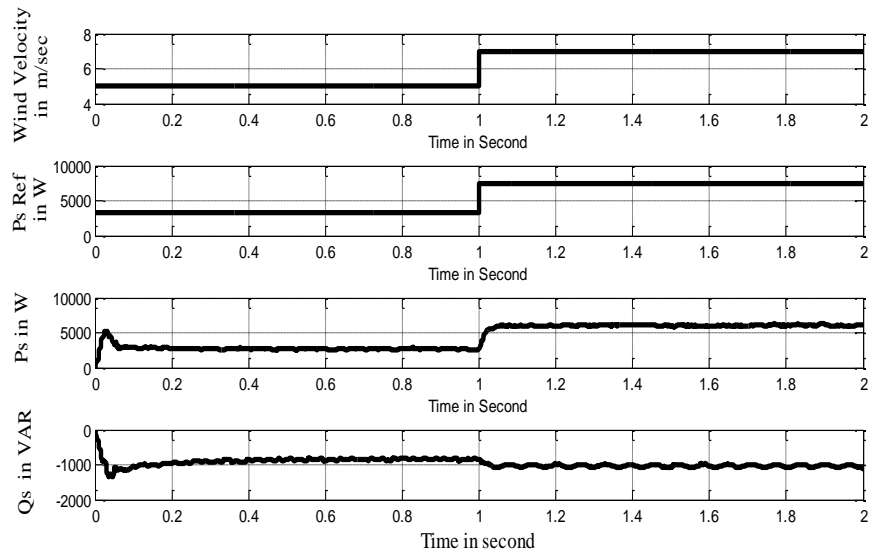


Figure 7.11: Performance of DFIG during normal operation with Step change in wind velocity 5m/sec to 7m/sec a) Wind Speed b) Reference Active Power c) Actual Active Power d) Actual Reactive Power.

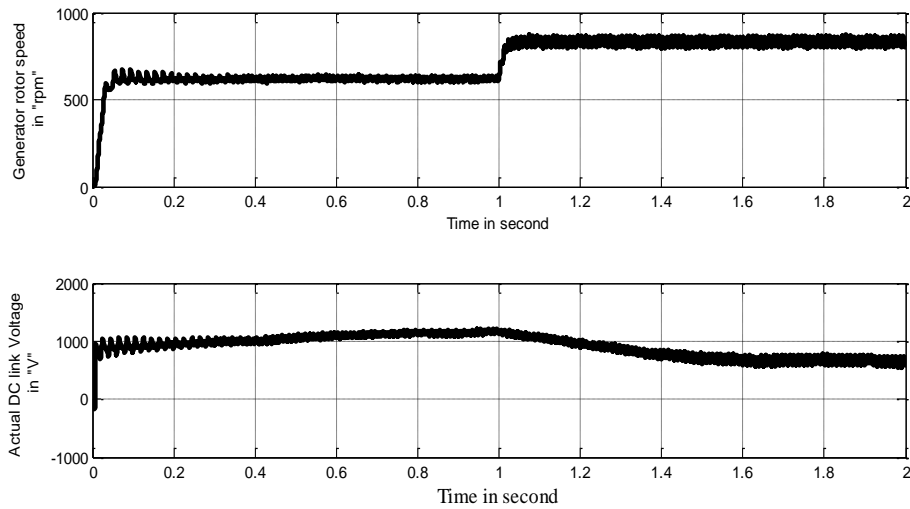


Figure 7.12: Performance of DFIG during normal operation with Step change in wind velocity 5m/sec to 7m/sec a) Generator rotor Speed b) DC Link Voltage.

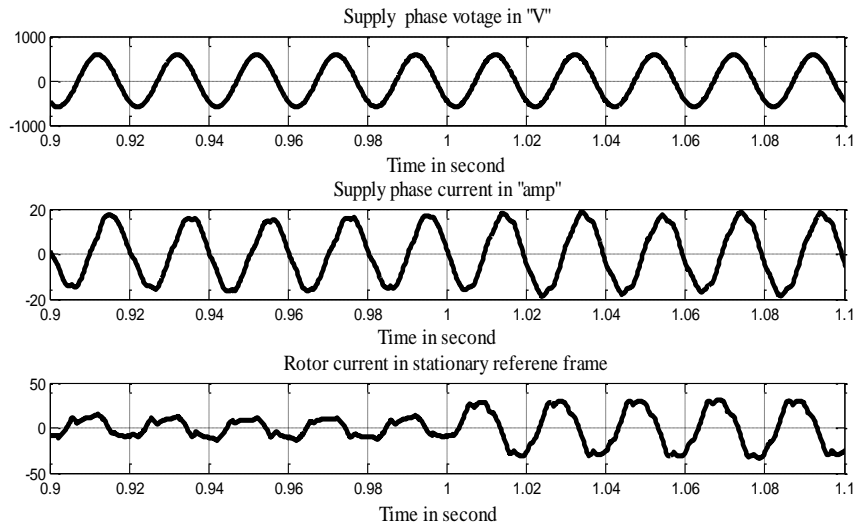


Figure 7.13: Performance of DFIG during normal operation with Step change in wind velocity 5m/sec to 7m/sec a) Stator Voltage b) Stator Current c) Rotor current in Stationary reference frame.

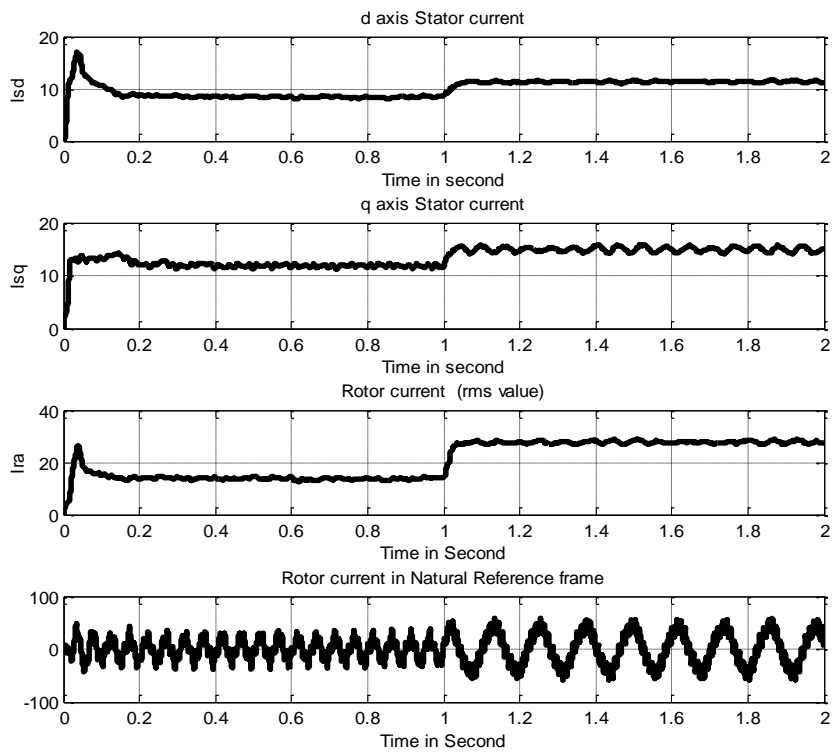


Figure 7.14:a) Stator current in d axis b)Stator current in q axis c)Rotor current(r.m.s) d)rotor current in Natural reference frame.

Observation: The actual active Power is almost approaching the reference power and Actual DC link voltage takes more time to stabilize to reference DC link value. Supply Voltage and current are almost in phase which corresponds to unity power factor at all operating condition but the Rotor current output is sinusoidal but with some distortion. But with PI controller it is also observed that there is a difference between active actual power and reference power. Reactive power requirement is little bit higher and the DC voltage stabilizes much late. Rotor current distortion is more. Rotor phase current frequency changes to suit change in the rotor speed i.e new value of slip.

7.4.3 Performance of DFIG for ramp change in wind velocity under normal condition (5m/sec to 7m/sec)

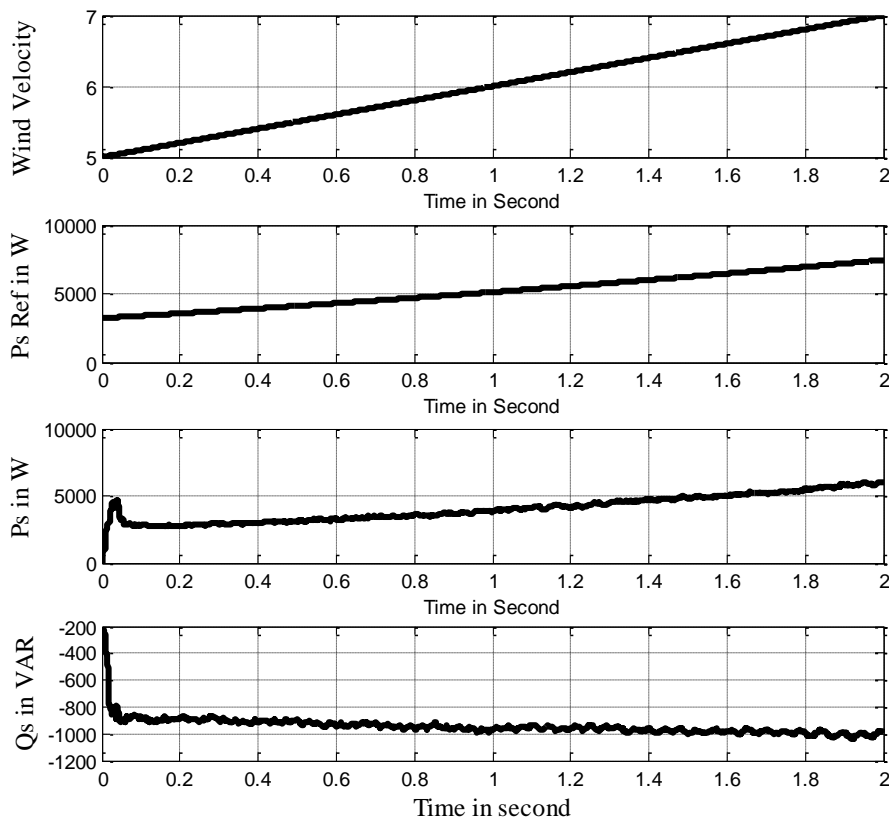


Figure 7.15: Performance of DFIG during normal operation with Ramp change in wind velocity 5m/sec to 7m/sec a) Wind Speed b) Reference Active Power c) Actual Active Power d) Actual Reactive Power

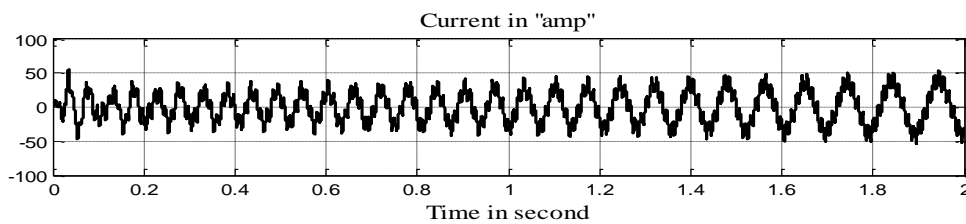


Figure 7.16: Rotor phase current in natural reference frame

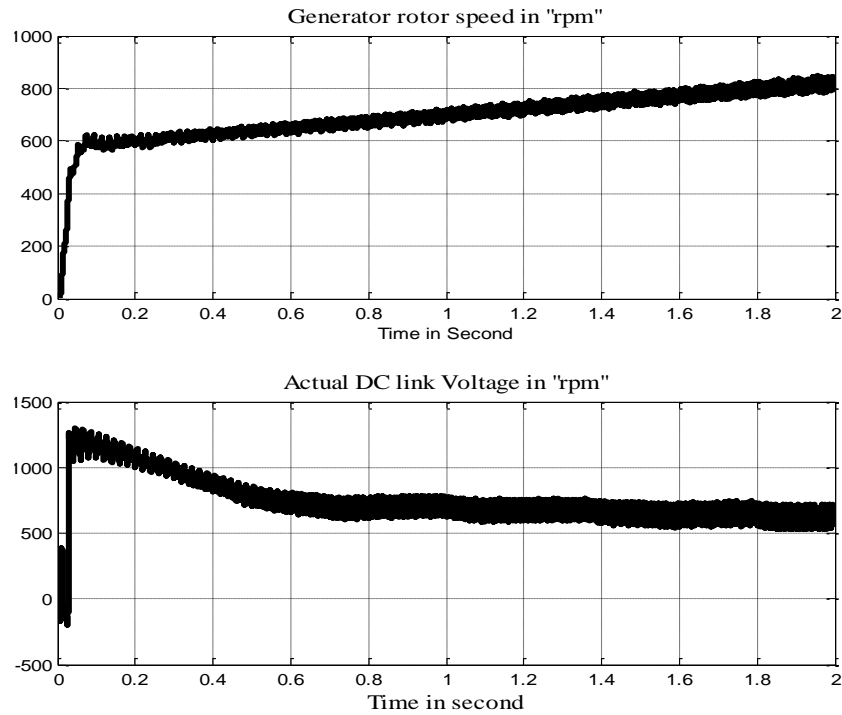


Figure7.17: Performance of DFIG during normal operation with Ramp change in wind velocity 5m/sec to 7m/seca) Generator rotor Speed b) DC Link Voltage.

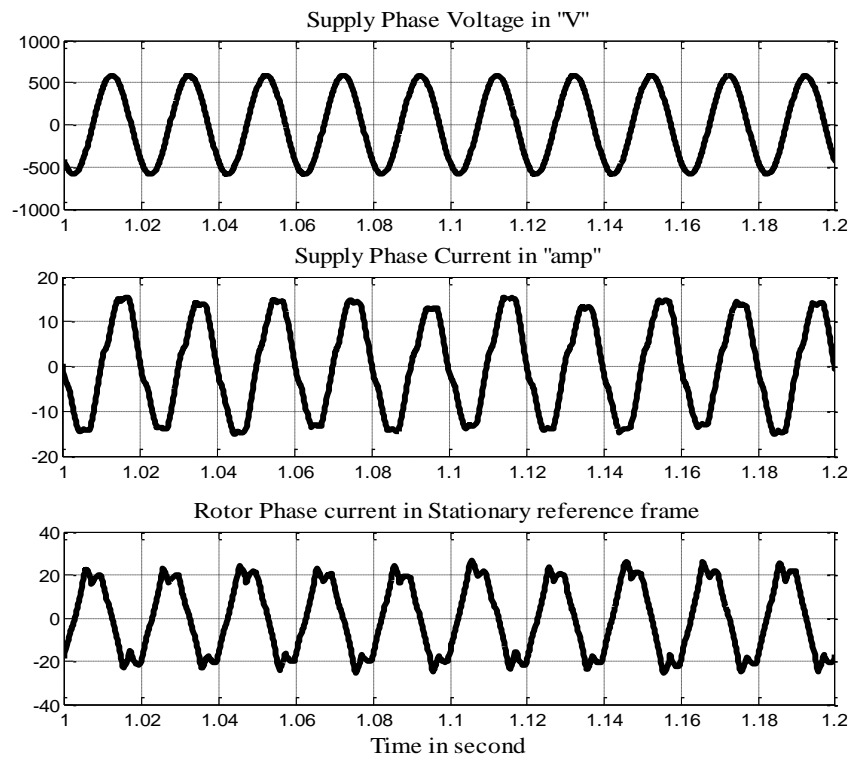


Figure7.18: Performance of DFIG during normal operation with Ramp change in wind velocity 5m/sec to 7m/seca) Stator Voltage b) Stator Current c) Rotor current in Stationary reference frame.

Observation: The actual active Power is almost approaching the reference power and Actual DC link voltage takes more time to stabilize to reference DC link value. Supply Voltage and current are almost in phase which corresponds to unity power factor at all operating condition but the Rotor current output is sinusoidal but with some distortion. But with PI controller it is also observed that there is a difference between active actual power and reference power. Reactive power requirement is little bit higher and the DC voltage stabilizes much late. Rotor current distortion is more. Rotor phase current frequency changes to suit change in the rotor speed i.e new value of slip.

7.4.4 Performance of DFIG from sub-synchronous mode to super synchronous mode of operation using conventional PI controller

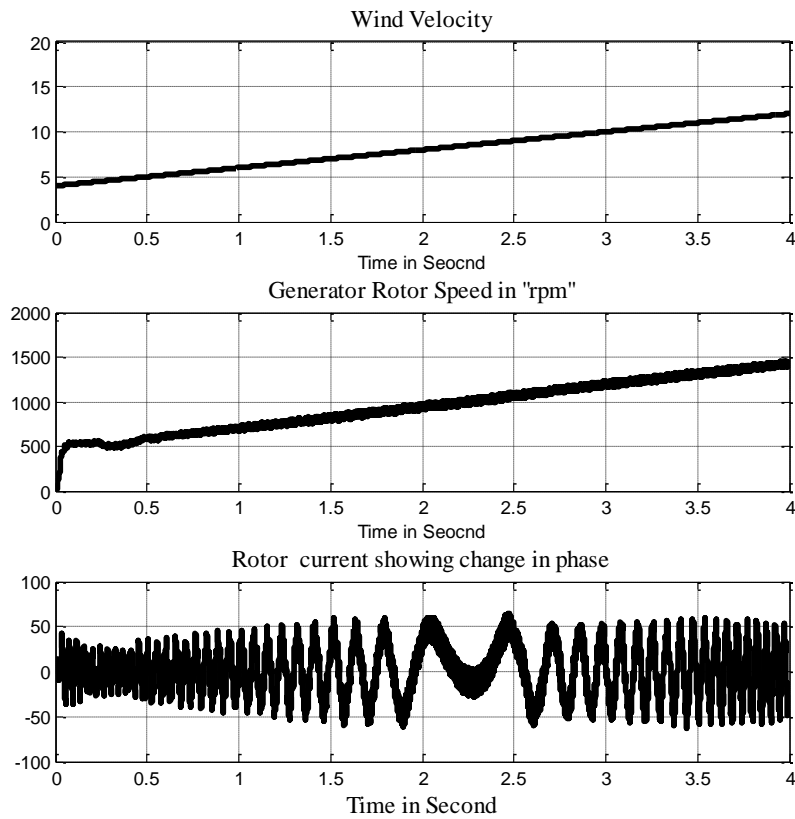


Figure 7.19: Performance of DFIG during normal operations sub synchronous to super synchronous mode a) Wind Velocity b) Generator Speed c) Rotor current showing phase change

Observation:

- Operates from sub synchronous to super synchronous mode
- Rotor current changes its phase while operating through synchronous speed

7.5 Performance of DFIG using ANN Controller under Normal operation

7.5.1 Performance of DFIG for constant wind Speed of (6 m/sec)

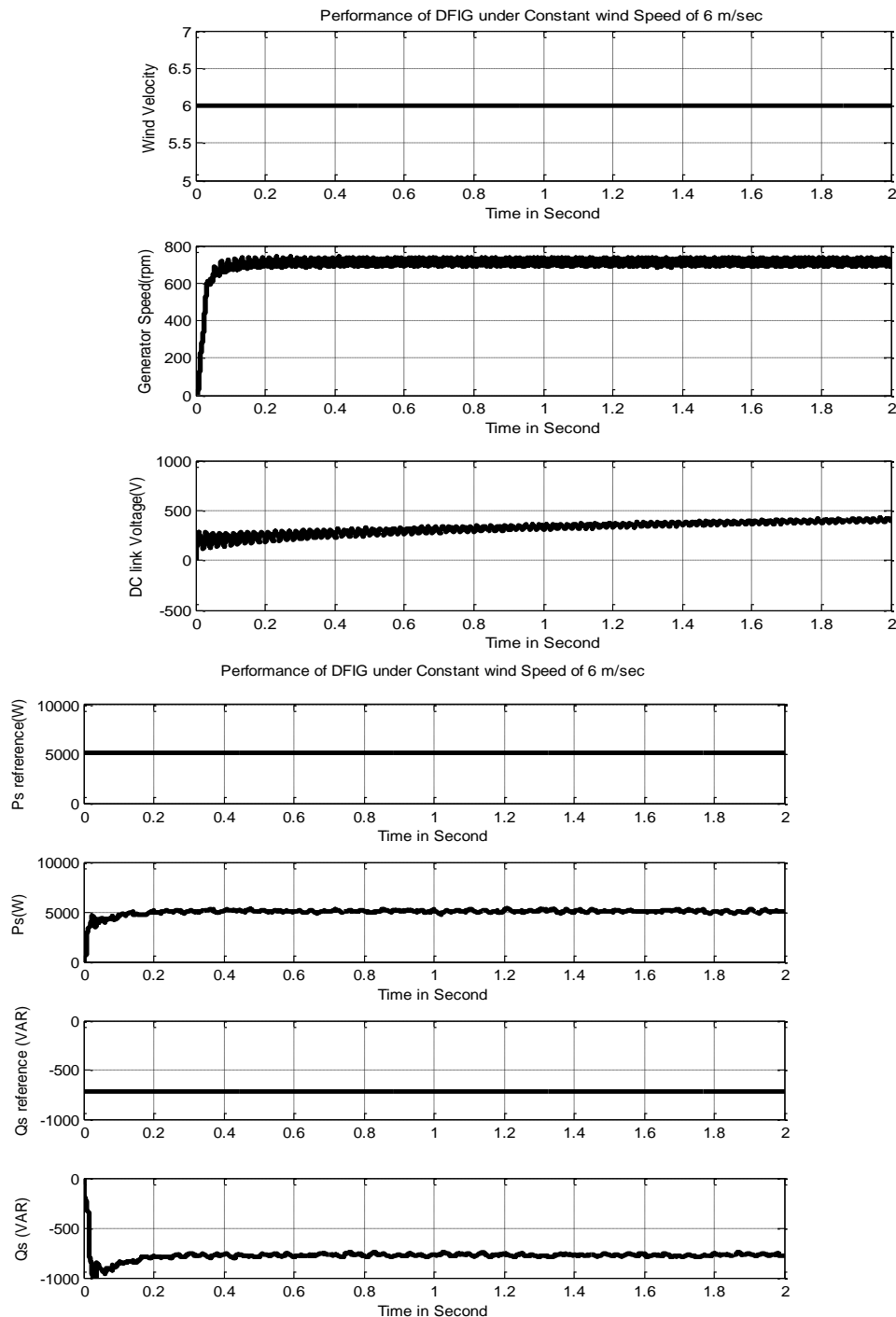


Figure 7.20: Performance of DFIG during constant wind velocity 6m/sec a) Wind Velocity b) Generator Speed c) DC link Voltage d) Reference stator Power e) Actual Stator power f) Reference Reactive Power g) Actual reactive Power

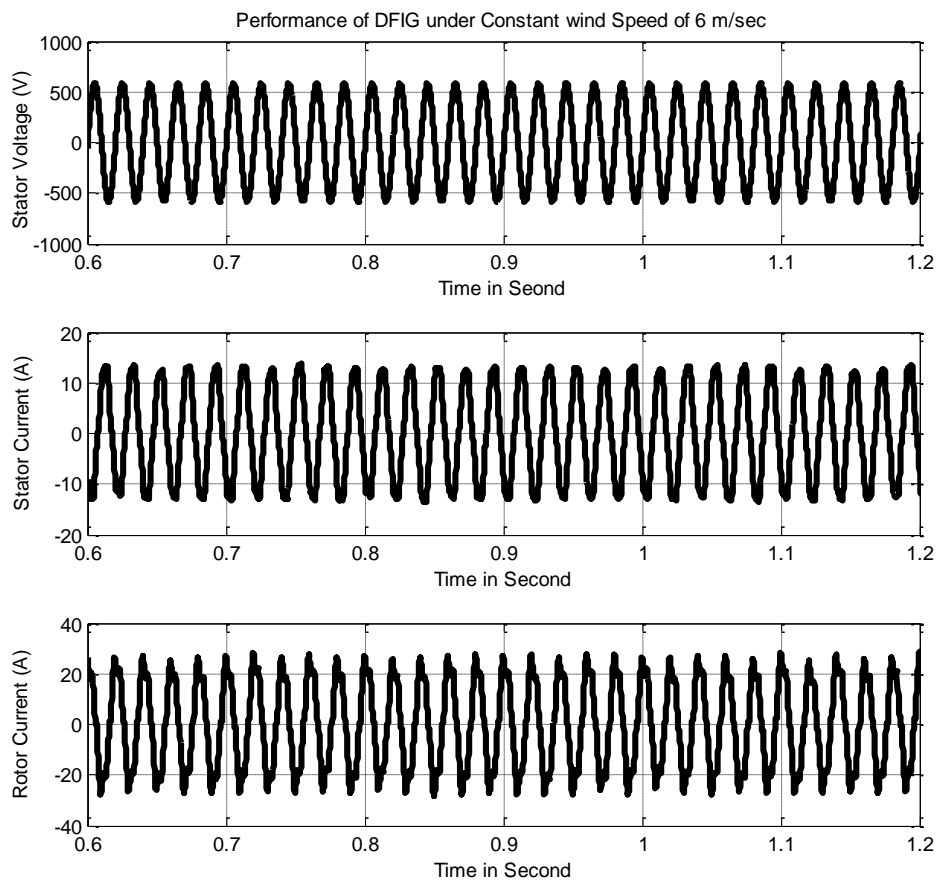


Figure7.21: Performance of DFIG during constant wind velocity 6m/sec a) Supply Voltage b) Supply current c) Rotor Current

Observations-

- The Active Power Tracks the reference Active Power More closely
- Oscillations in the Active and Reactive Power are much less Compared to PI and PR Controller.
- DC link Voltage is almost stable with fewer oscillations.
- Oscillation in Rotor Current is much less.
- The Stator Voltage and Stator current are almost in Phase giving reactive Power control

7.5.2 Performance of DFIG for Step Variation of wind Speed from (5 m/sec to 7m/sec)

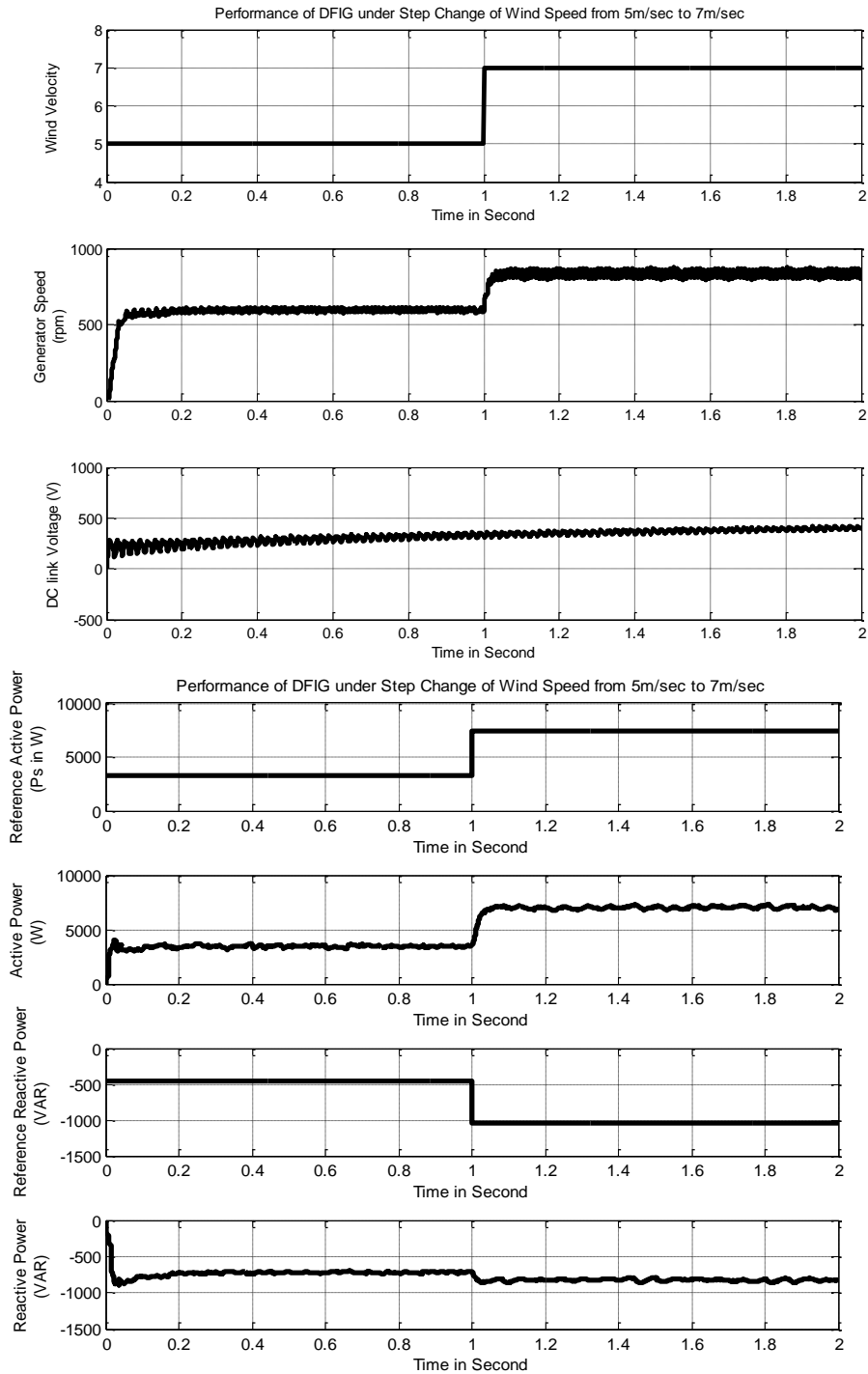


Figure 7.22: Performance of DFIG during step change in wind velocity 5m/sec to 7m/sec
a) Wind Velocity b) Generator Speed c) DC link Voltage d) Reference stator Power e) Actual Stator power f) Reference Reactive Power g) Actual reactive Power

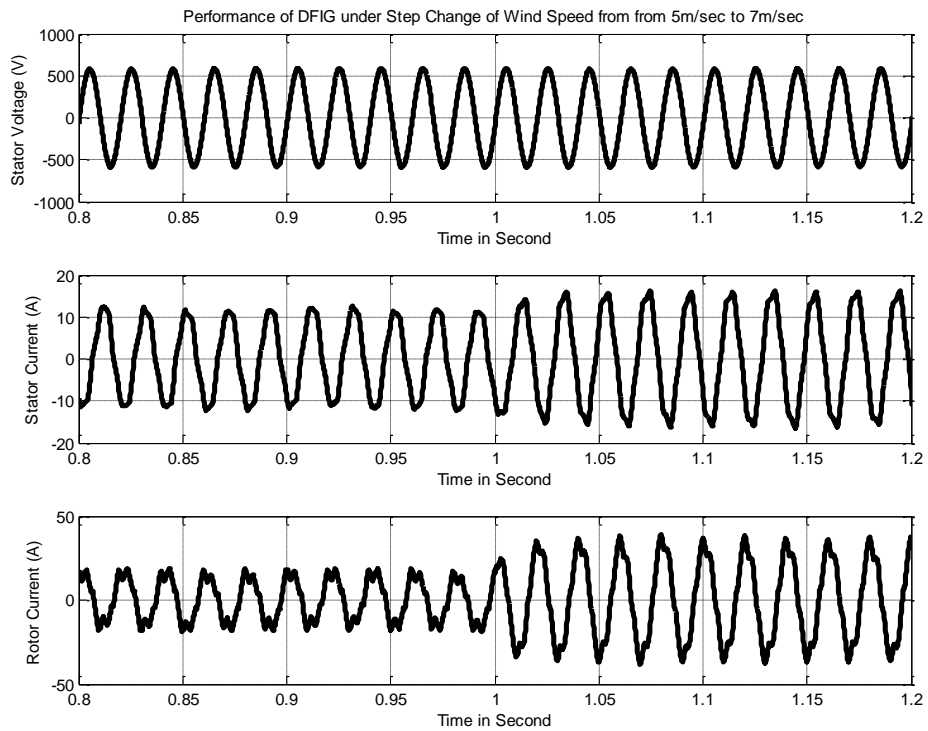


Figure7.23: Performance of DFIG during constant wind velocity step change in wind velocity 5m/sec to 7m/sec a) Supply Voltage b) Supply current c) Rotor Current

Observation-

- DC link Voltage is almost stable with Less Oscillations
- Oscillations in Rotor Current is much less
- The Stator Voltage and Stator current are almost in Phase giving reactive Power control
- The Active Power Tracks the reference Active Power More closely
- Oscillations in the Active and Reactive Power are much less Compared to PI and PR Controller

7.5.3 Performance of DFIG for Ramp Variation of wind Speed from (5 m/sec to 7m/sec)

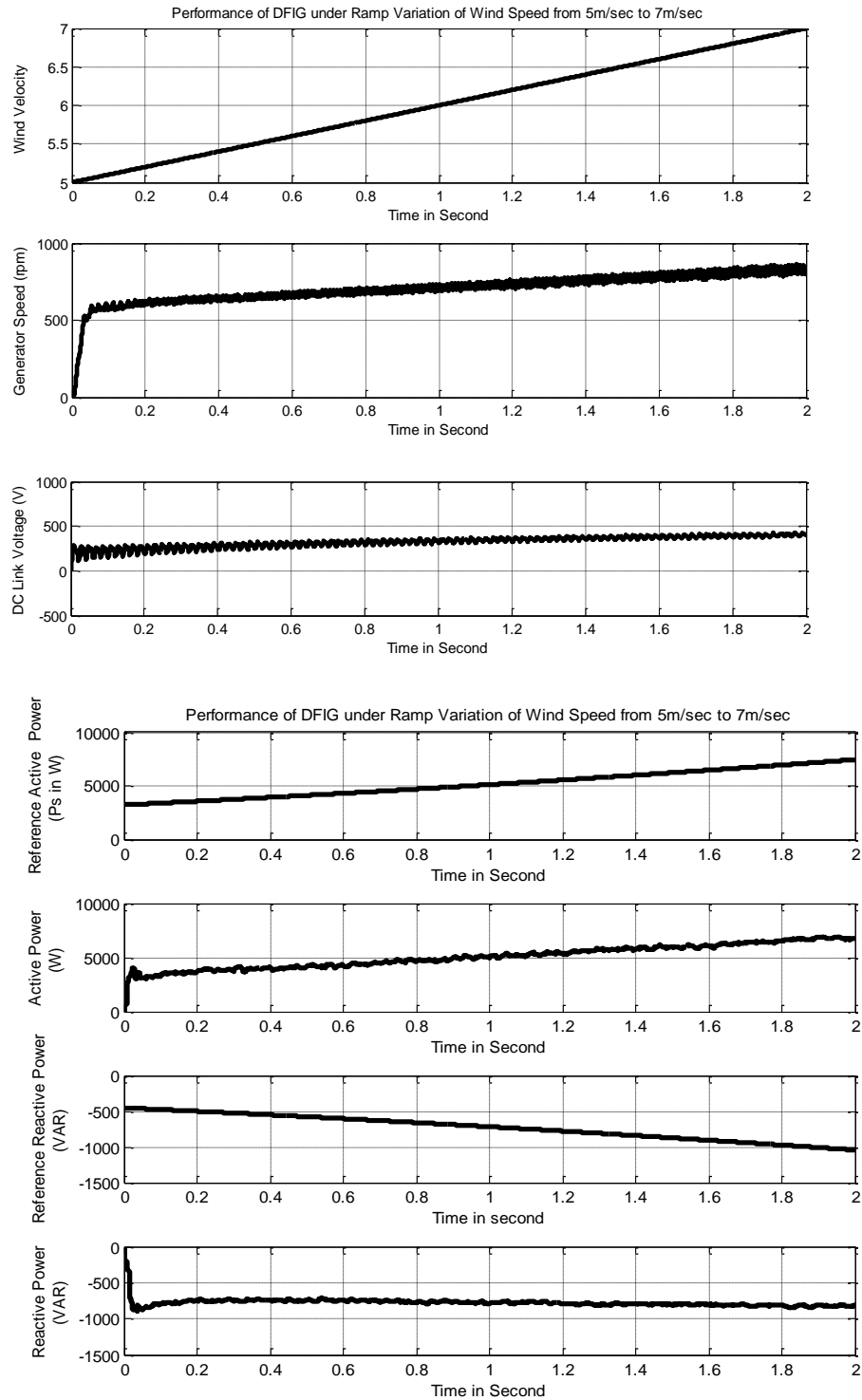


Figure 7.24: Performance of DFIG during step change in wind velocity 5m/sec to 7m/sec a) Wind Velocity b) Generator Speed c) DC link Voltage d) Reference stator Power e) Actual Stator power f) Reference Reactive Power g) Actual reactive Power.

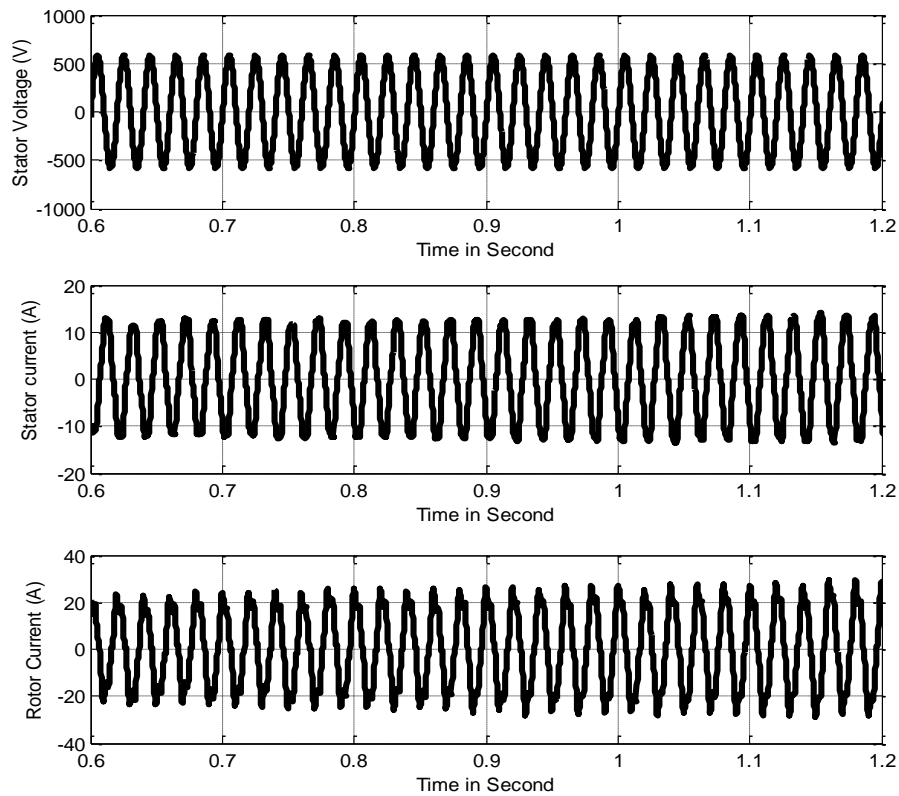


Figure7.25: Performance of DFIG during constant wind velocity step change in wind velocity 5m/sec to 7m/sec a) Supply Voltage b) Supply current c) Rotor Current

Observations-

- The Active Power Tracks the reference Active Power more closely
- Oscillations in the Active and Reactive Power are much less Compared to PI and PR Controller.
- DC link Voltage is almost Stable with Less Oscillations
- Oscillations in Rotor Current is much Less
- The Stator Voltage and Stator current are almost in Phase giving reactive Power control

7.6 Performance Characteristics of DFIG during Unsymmetrical Faults for (Line to Line Fault)

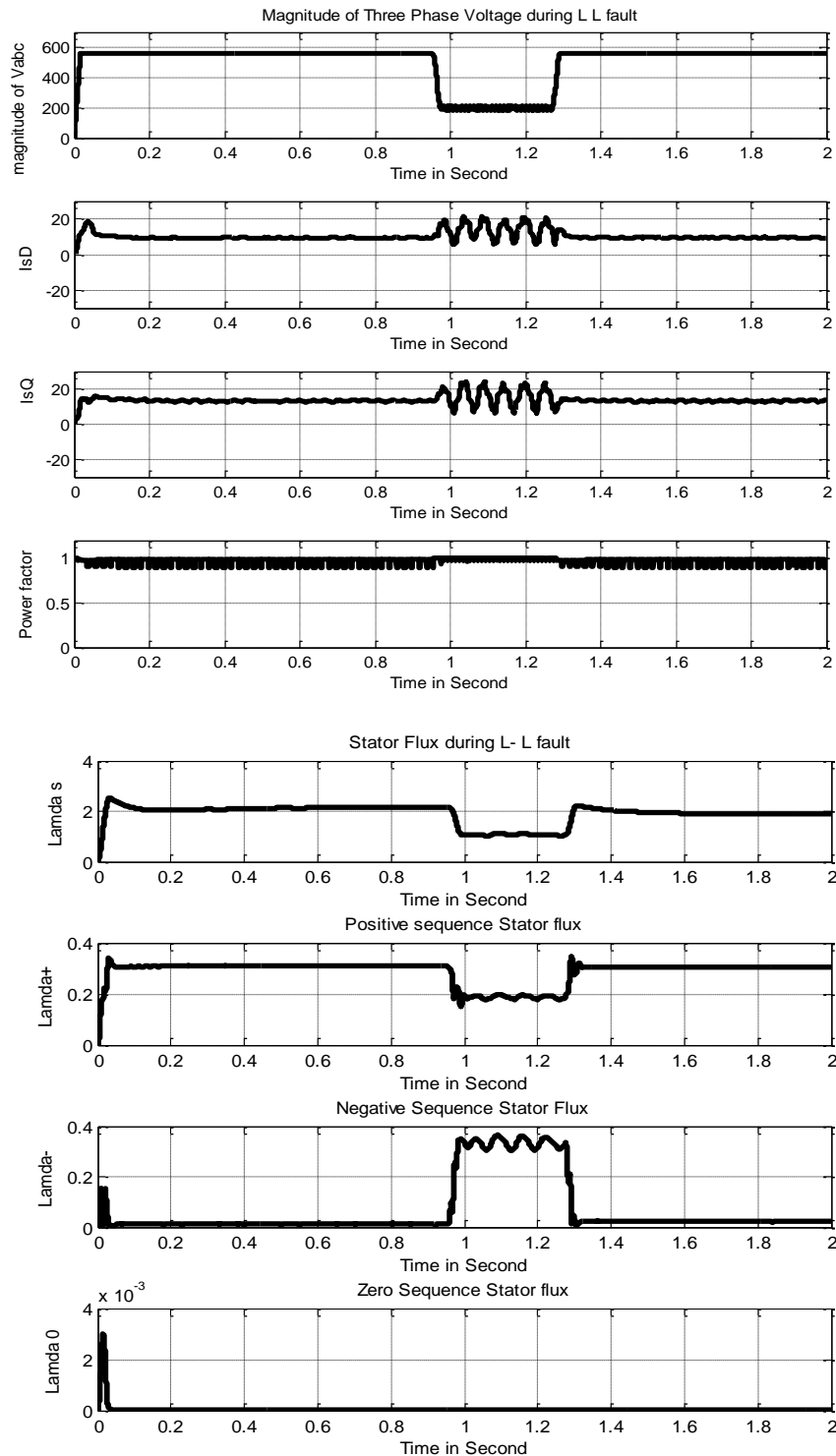


Figure 7.26: Performance of DFIG showing a) Voltage magnitude b),c) d and q axis rotor current d)Power factor on GSC side e)Stator flux f),g) h) positive, negative and zero sequence Stator flux.

7.6.1 Performance Characteristics of DFIG during Unsymmetrical Faults(Line to Line) fault using PI controller

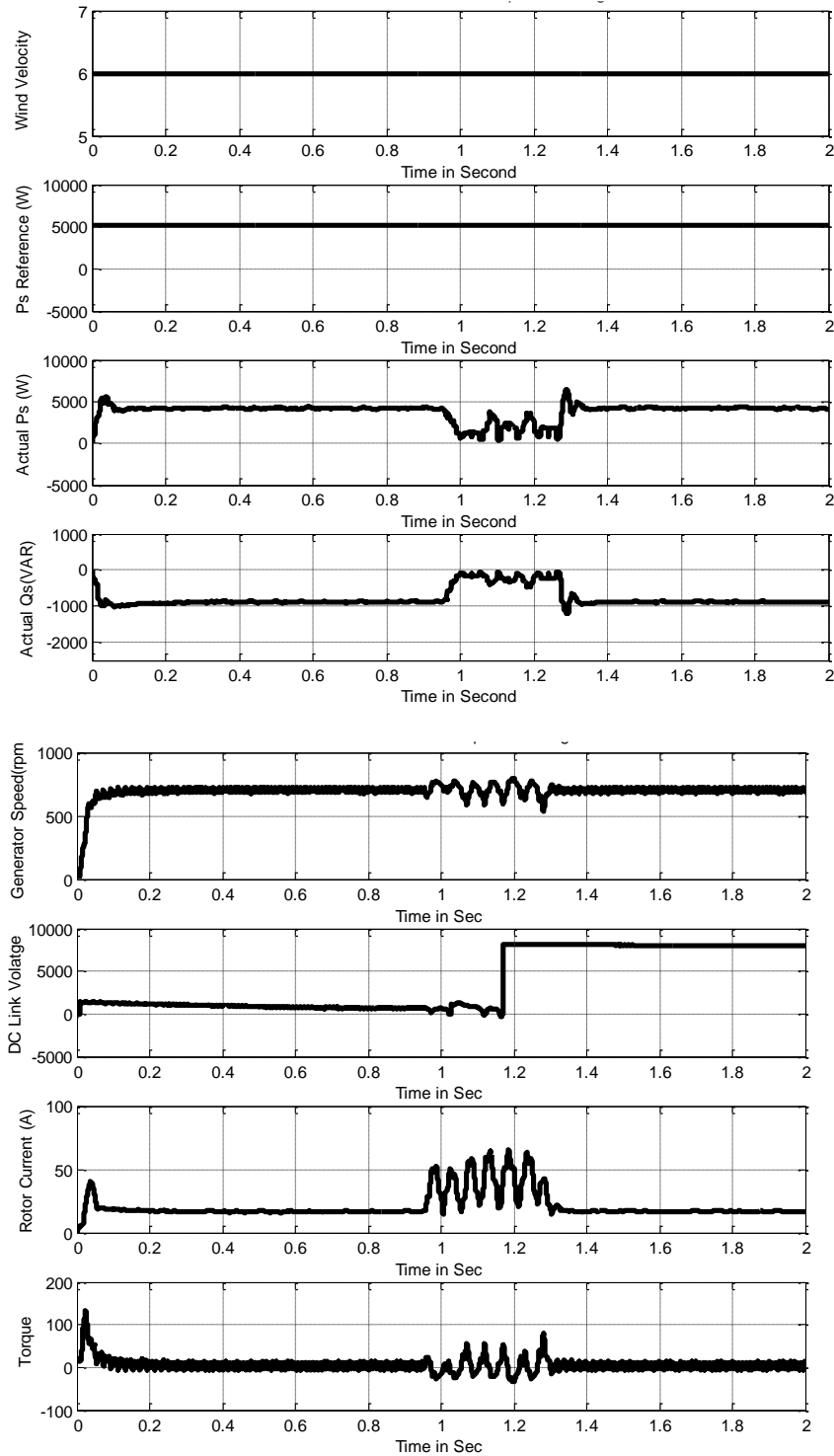


Figure 7.27: Performance of DFIG showing a) Wind Velocity b) Optimum Stator Power c) Actual Stator Power d) Actual reactive Power e) Generator Speed f) DC Link Voltage g) Rotor current h) Electromagnetic torque.

7.6.2 Performance of DFIG Using ANN Controller

7.6.2.1 Performance of DFIG For constant Speed 6m/sec for Line to Line fault during Neural Network

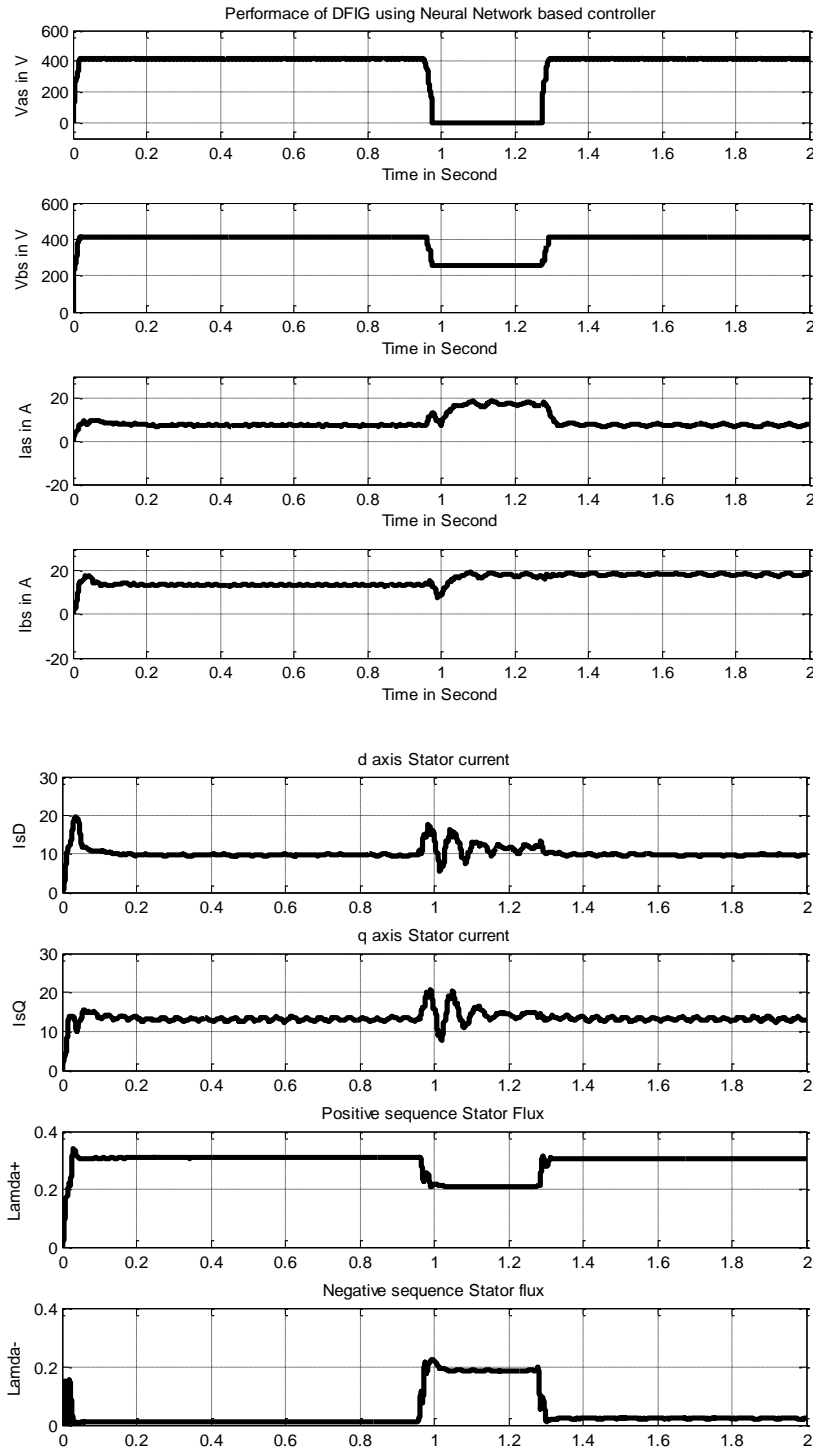


Figure 7.28: Performance of DFIG showing a) Voltage and Current magnitude b) d and q axis rotor current c) positive, negative sequence Stator flux.

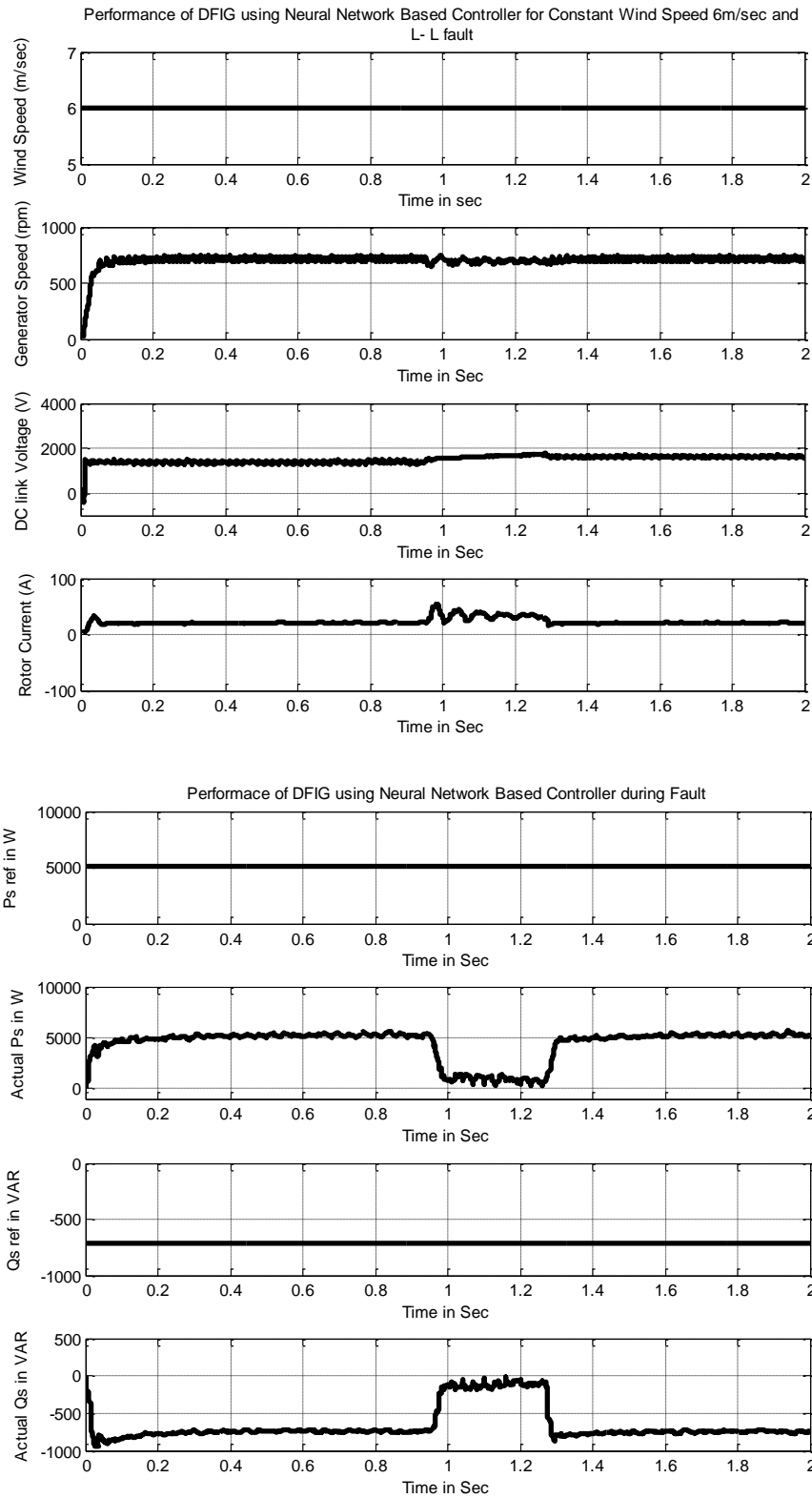


Figure 7.29: Performance of DFIG showing a) Wind Velocity b) Generator Speed c) DC Link Voltage d) Rotor Current e) Optimum Power f) Actual Stator power g) Reference reactive power h) Actual reference power

7.6.2.2 Performance of DFIG for Step change in Speed 5m/sec to 7m/sec for Line to Line fault during Neural Network

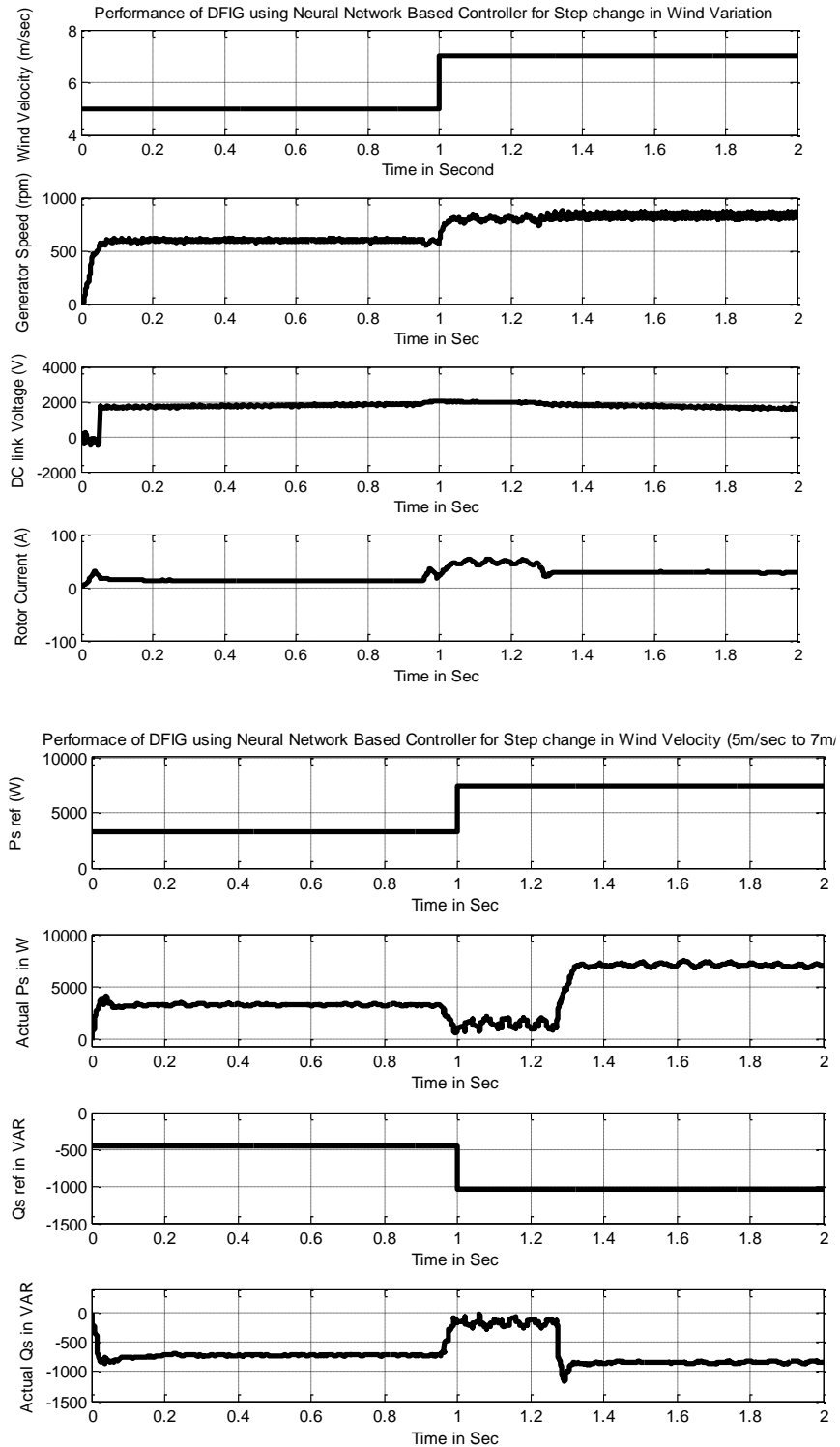


Figure 7.30: Performance of DFIG showing a) Wind Velocity b) Generator Speed c) DC Link Voltage d) Rotor Current e) Optimum Power f) Actual Stator power g) Reference reactive power h) Actual reference power.

7.6.2.3 Performance of DFIG for Ramp change in Speed for Line to Line fault during Neural Network

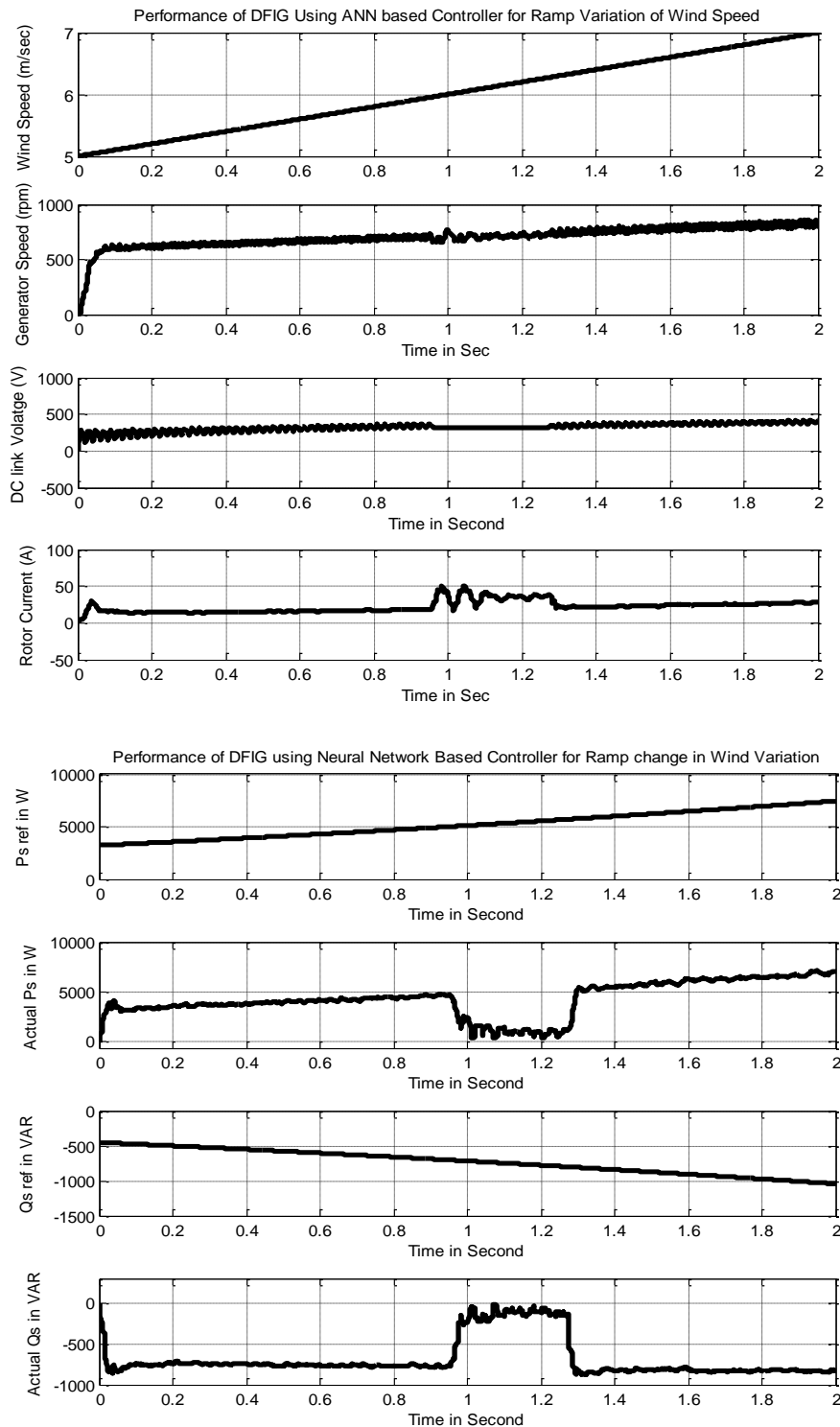


Figure 7.31: Performance of DFIG showing a) Wind Velocity b) Generator Speed c) DC Link Voltage d) Rotor Current e) Optimum Power f) Actual Stator power g) Reference reactive power h) Actual reference power

Observation:

With the aid of neural network based controller the following points were observed-

1. The generated active stator power oscillations during fault are reduced
2. Rotor current transients during fault is reduced.
3. The stator current transients are reduced to great extend.
4. The negative sequence flux is controlled using ANN controller.
5. The DC link Voltage is almost fixed during and after fault.
6. The pulsations in generator speed is also reduced.

7.6.3 Performance Characteristics of DFIG during Unsymmetrical Faults for (Line to Ground Fault)

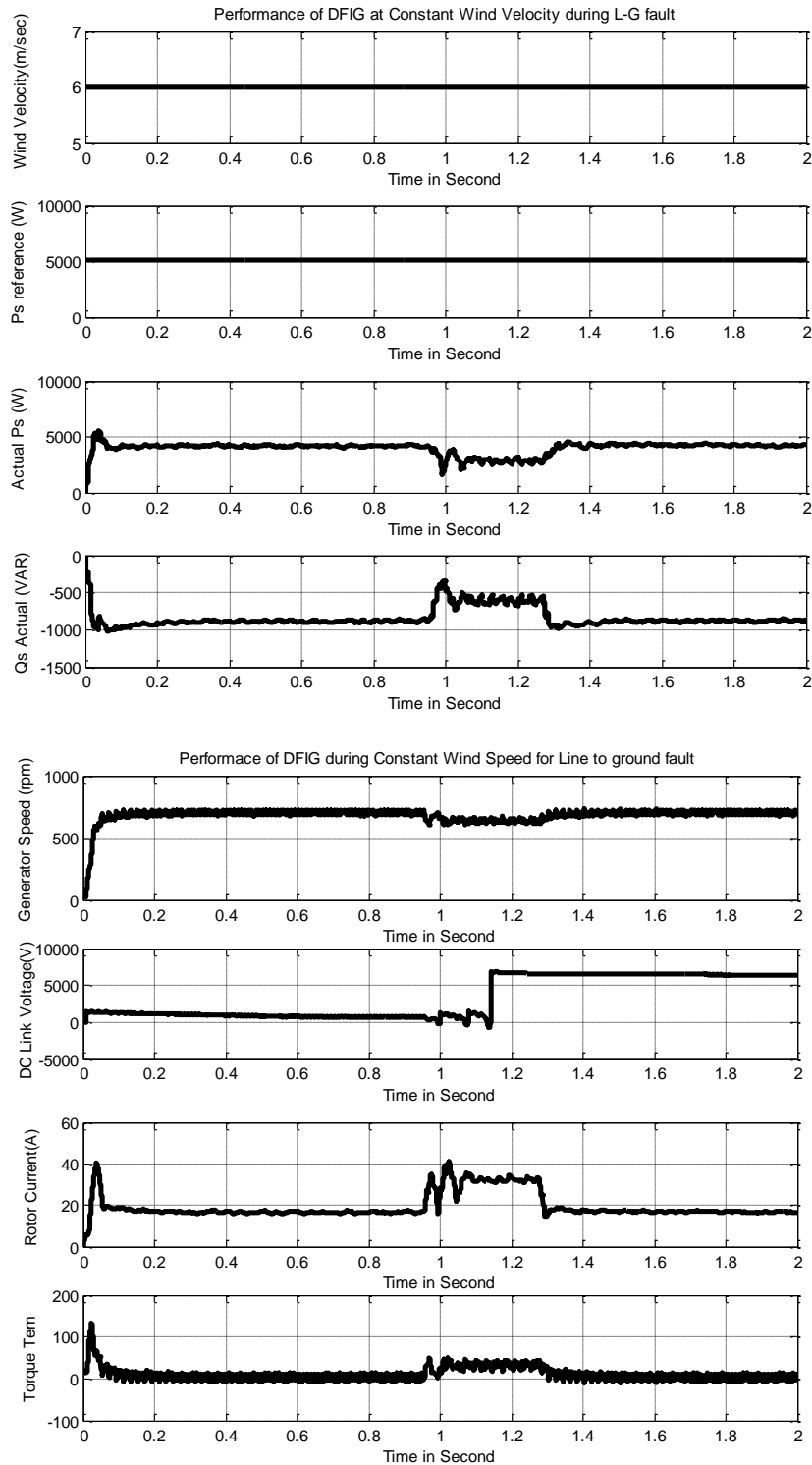


Figure 7.25: Performance of DFIG showing a) Wind Velocity b) Optimum Stator Power c) Actual Stator Power d) Actual reactive Power e) Generator Speed f) DC Link Voltage g) Rotor current h) Electromagnetic torque.

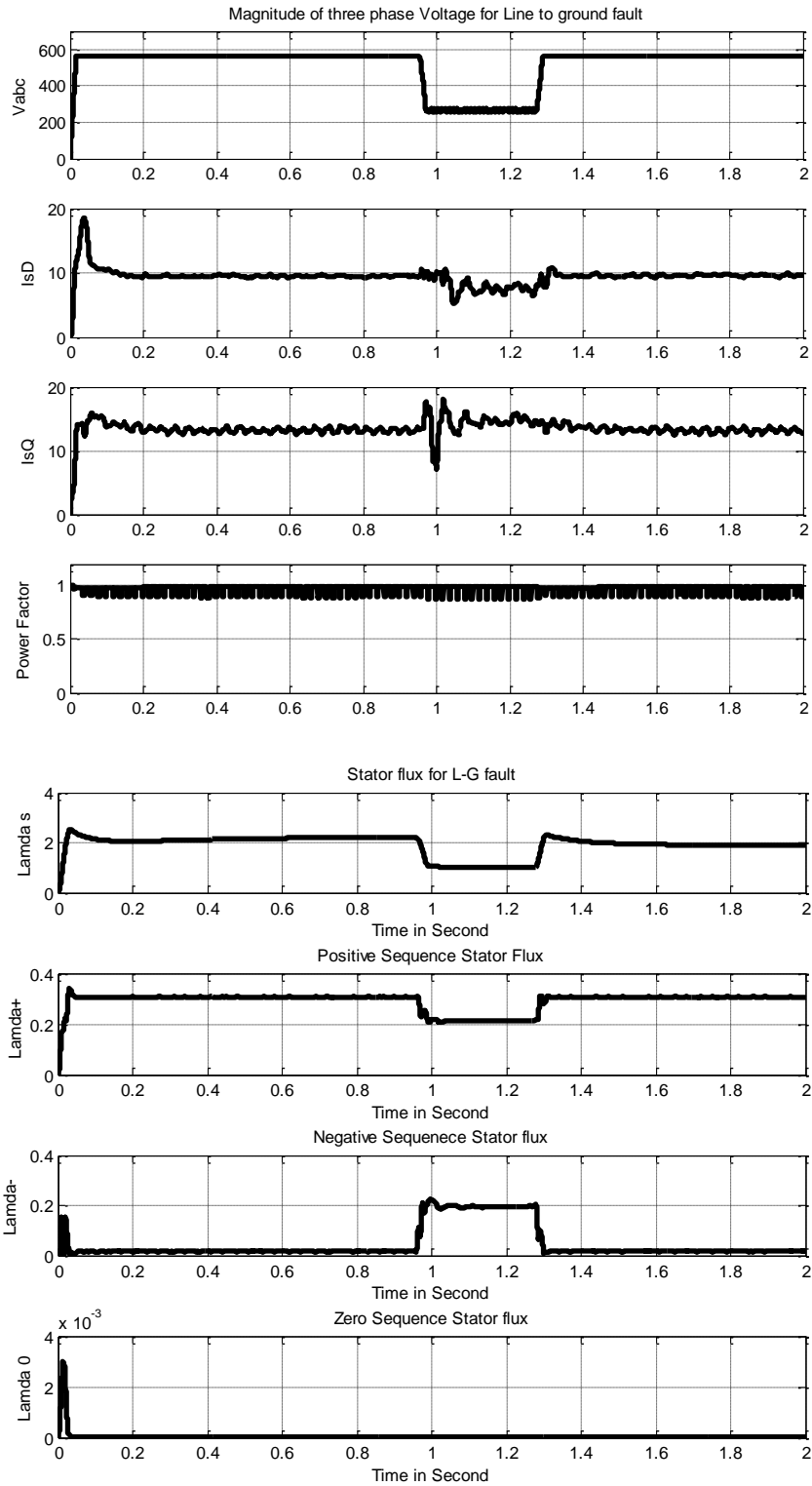


Figure7.26: Performance of DFIG showing a) Voltage magnitude b),c) d and q axis rotor current d)Power factor on GSC side e)Stator flux f,g) h) positive, negative and zero sequence Stator flux.

7.6.3.1 Performance of DFIG during LG Fault for Constant Speed (6m/sec) using Neural Network Based Controller

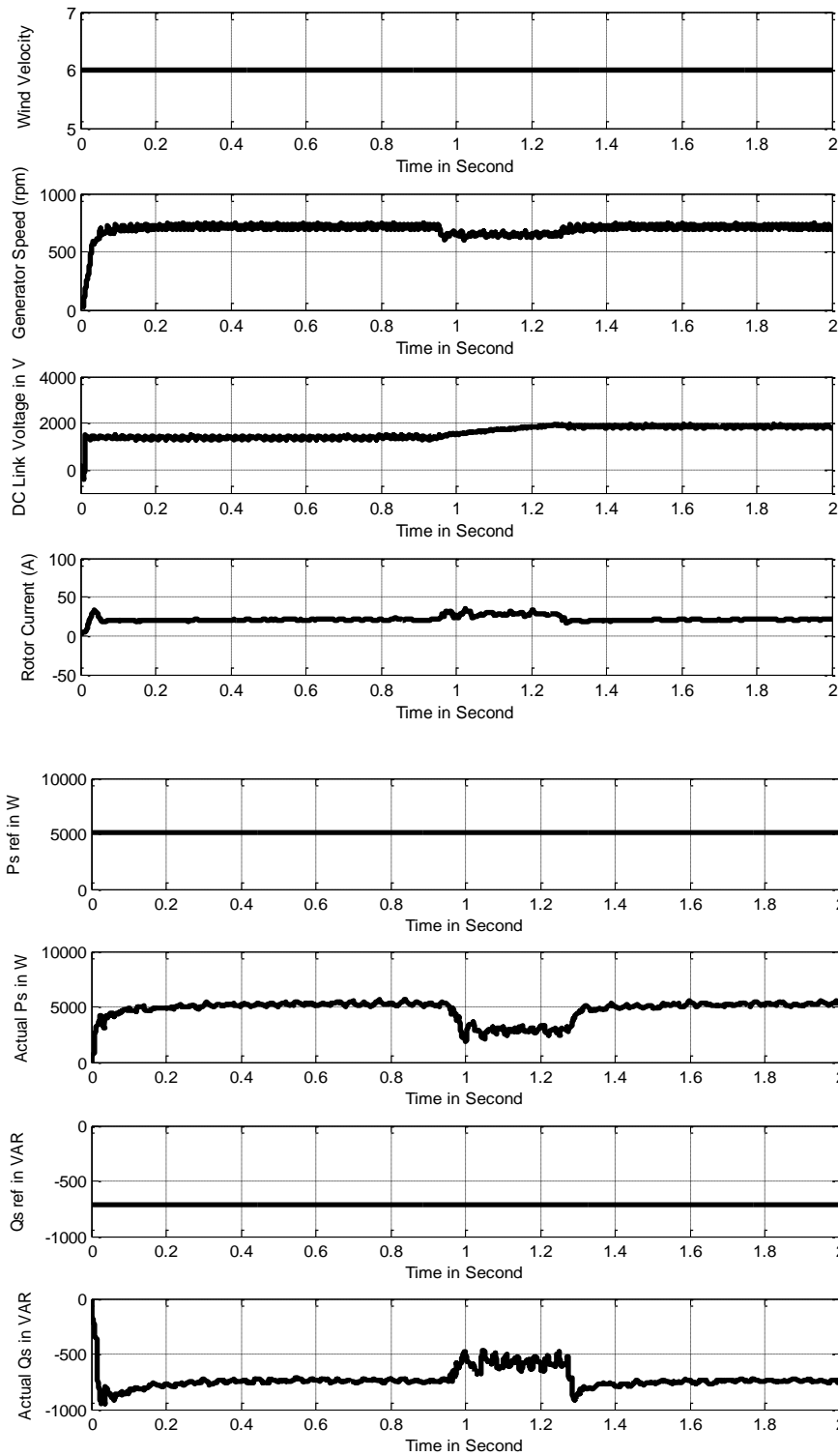


Figure 7.30: Performance of DFIG showing a) Wind Velocity b) Generator Speed c) DC Link Voltage d) Rotor Current e) Optimum Power f) Actual Stator power g) Reference reactive power h) Actual reference power

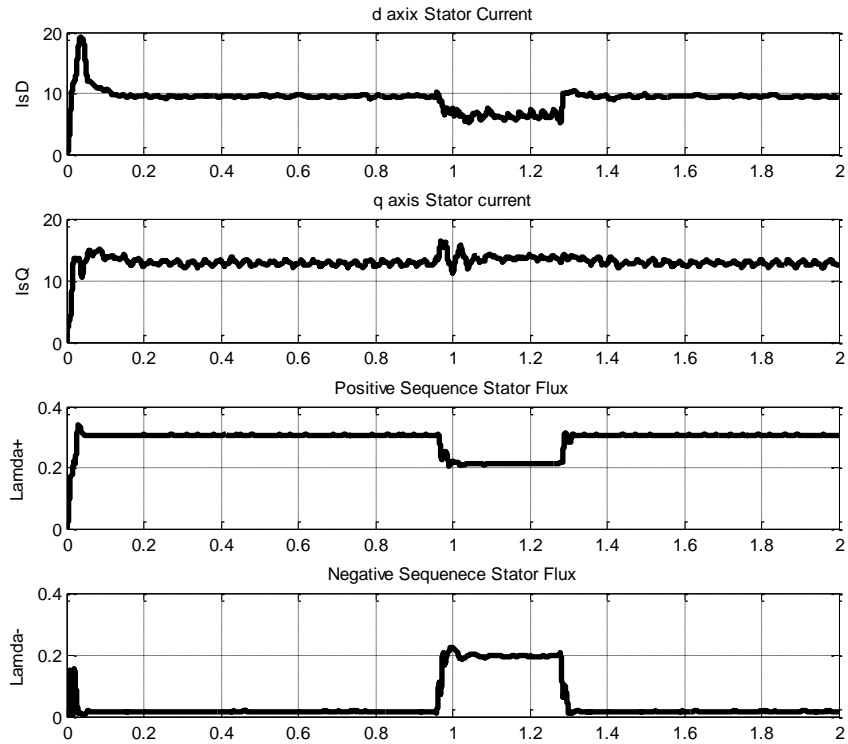
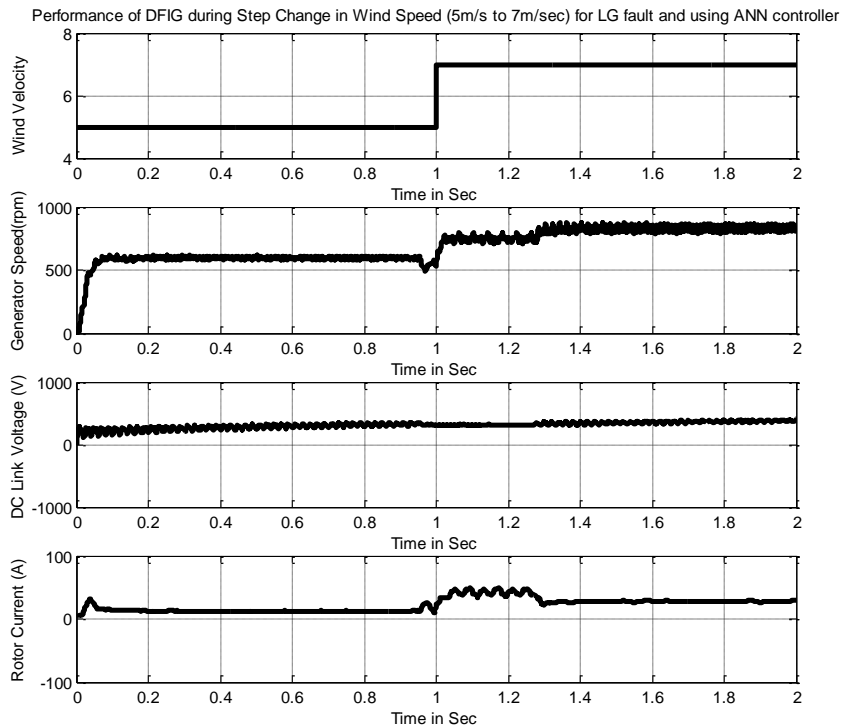


Figure 7.31 Performance of DFIG showing a)d and q axis stator current b)positive and negative sequence stator flux.

7.6.3.2 Performance of DFIG during LG Fault for Step change in Speed using Neural Network Based Controller



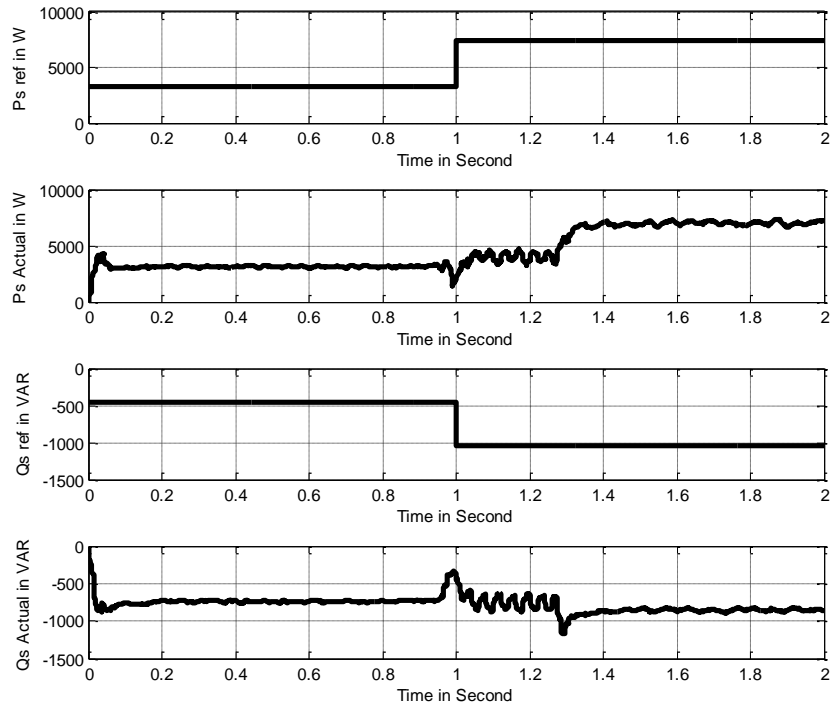
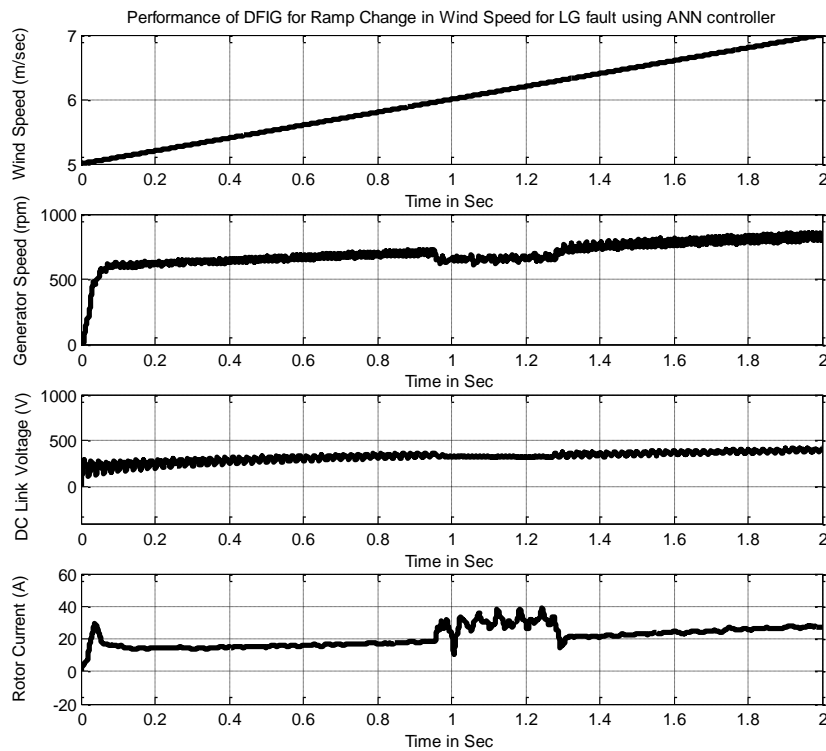


Figure 7.32: Performance of DFIG showing a) Wind Velocity b) Generator Speed c) DC Link Voltage d) Rotor Current e) Optimum Power f) Actual Stator power g) Reference reactive power h) Actual reference power

7.6.3.3 Performance of DFIG during LG Fault for Ramp change in Speed using Neural Network Based Controller



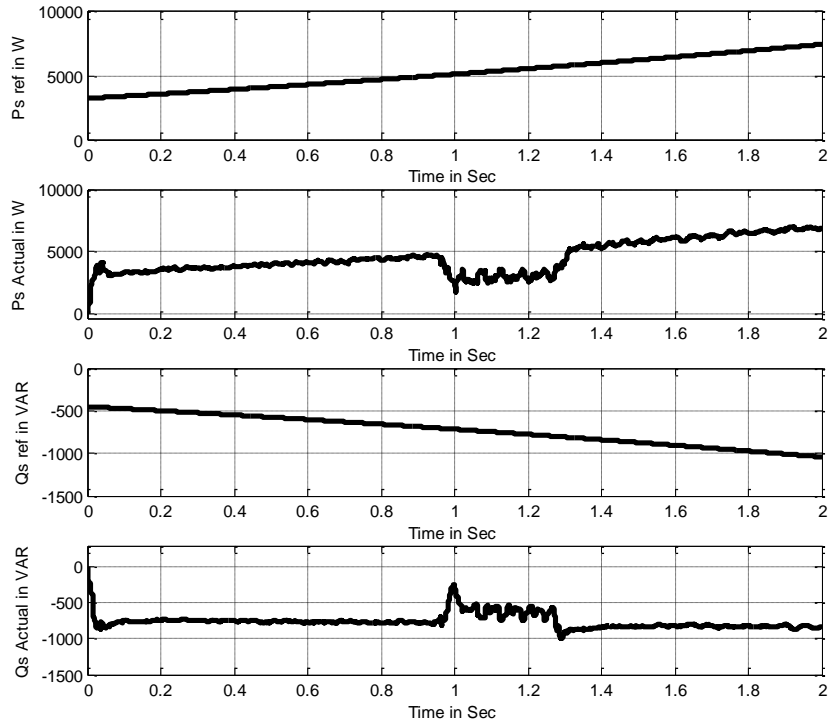
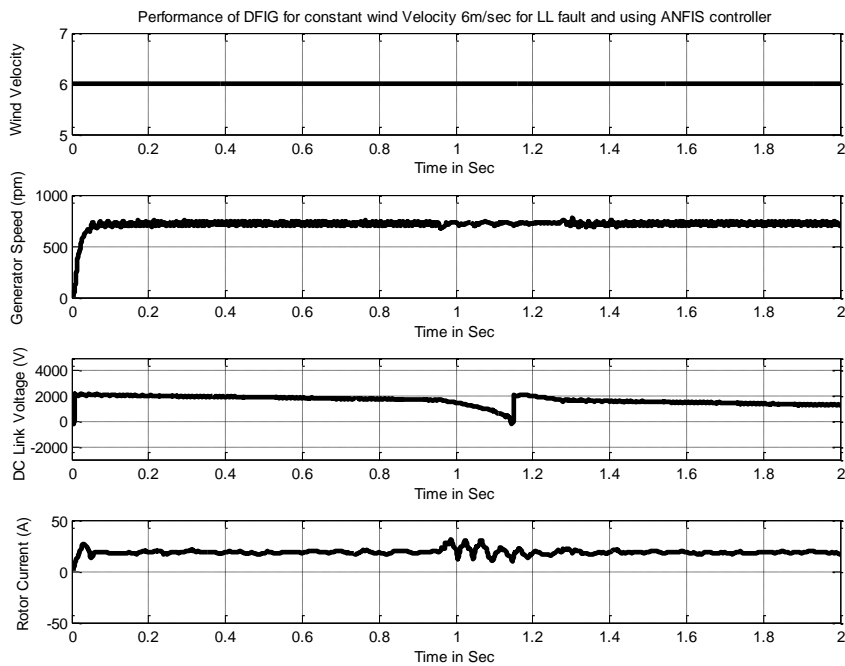


Figure 7.33: Performance of DFIG showing a) Wind Velocity b)Generator Speed c) DC Link Voltage d) Rotor Current e) Optimum Power f) Actual Stator power g) Reference reactive power h)Actual reference power

7.7 Performance of DFIG Using ANFIS Controller

7.7.1 Performance of DFIG during (L-L) Fault for Constant wind Speed



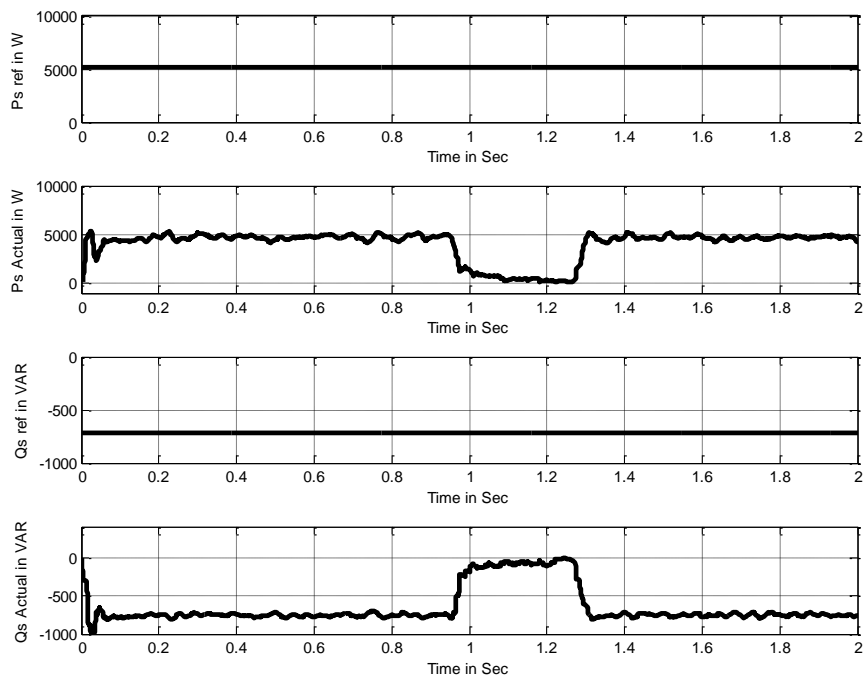
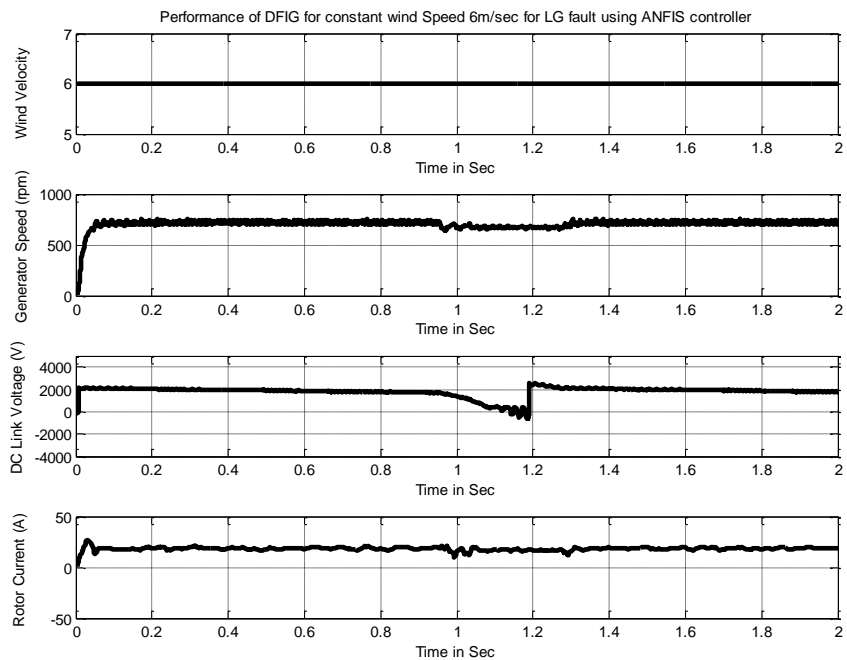


Figure 7.34: Performance of DFIG showing a) Wind Velocity b)Generator Speed c) DC Link Voltage d) Rotor Current e) Optimum Power f) Actual Stator power g) Reference reactive power h)Actual reference power

7.7.2 Performance of DFIG during Line to Ground Fault for Constant wind Speed using ANFIS Controller



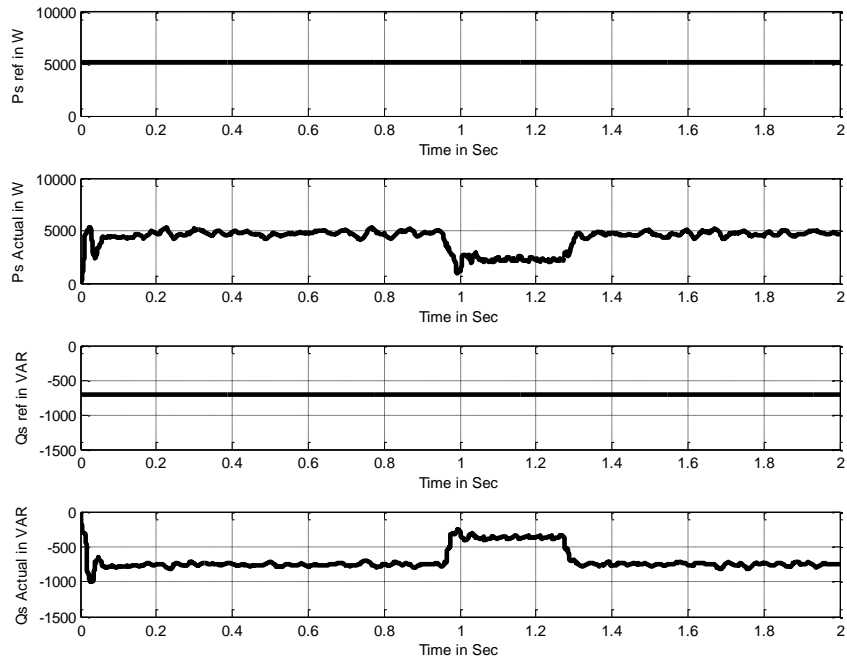
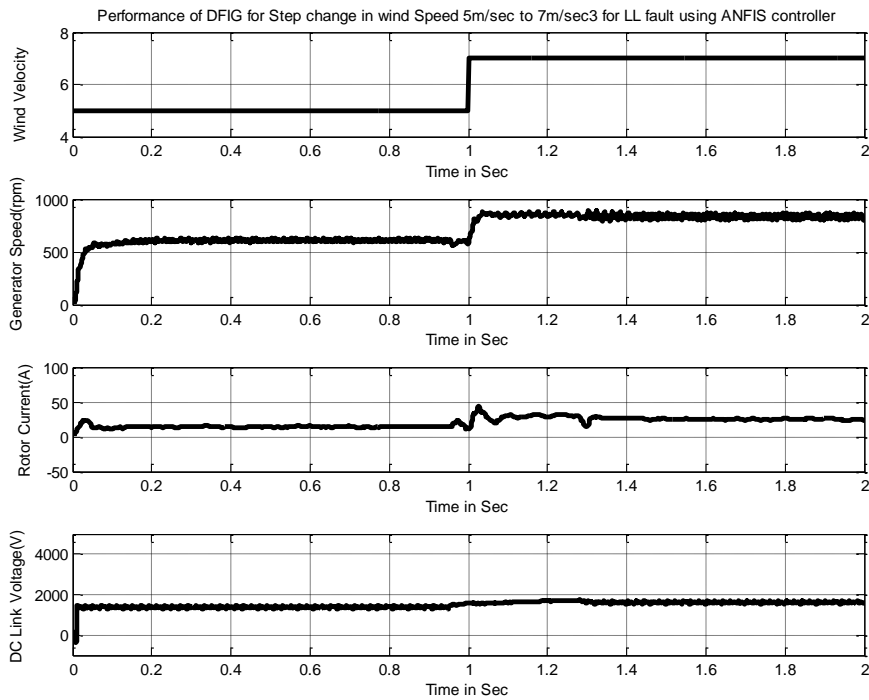


Figure 7.35: Performance of DFIG showing a) Wind Velocity b)Generator Speed c) DC Link Voltage d) Rotor Current e) Optimum Power f) Actual Stator power g) Reference reactive power h)Actual reference power

7.7.3 Performance of DFIG during Line to Line Fault for Step change in wind Speed using ANFIS Controller



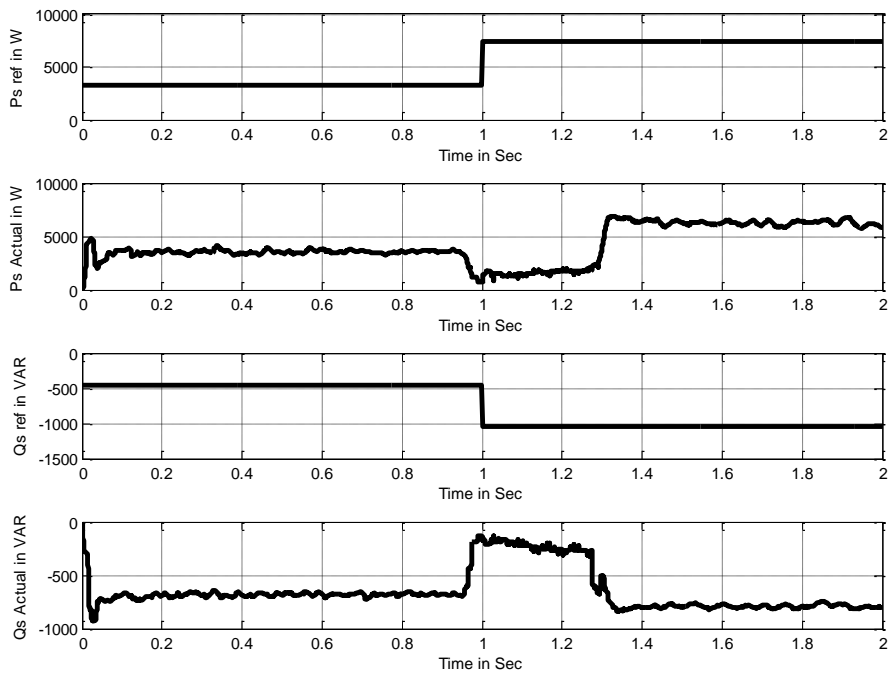
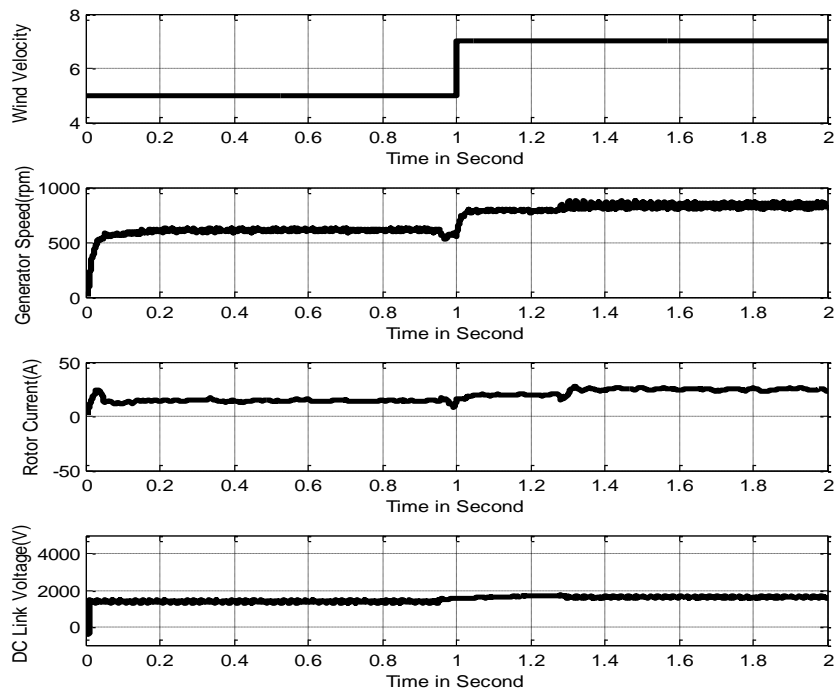


Figure 7.36: Performance of DFIG showing a) Wind Velocity b)Generator Speed c) DC Link Voltage d) Rotor Current e) Optimum Power f) Actual Stator power g) Reference reactive power h)Actual reference power

7.7.4 Performance of DFIG during Line to Ground Fault for Step change in wind Speed using ANFIS Controller



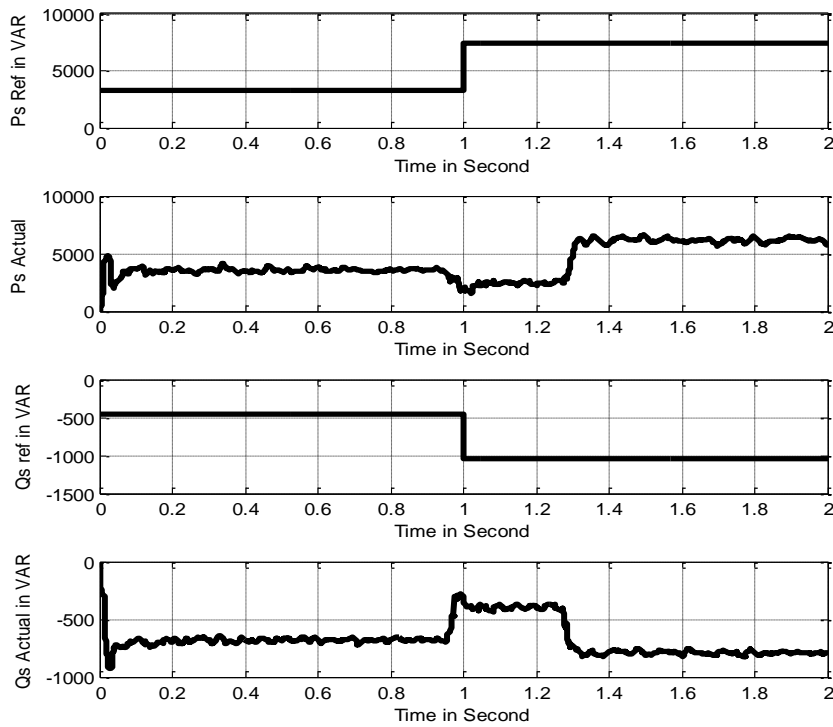
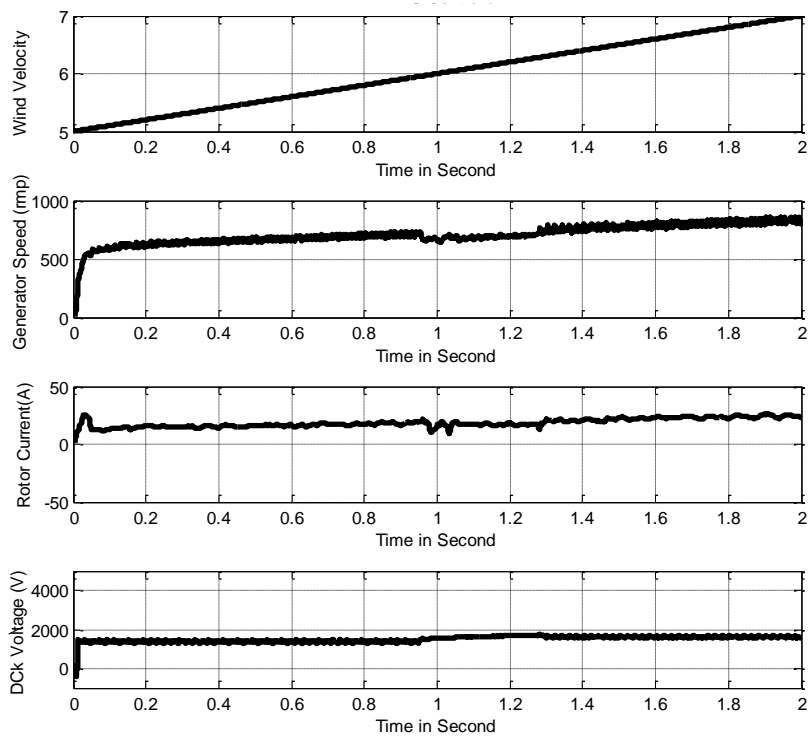


Figure 7.37: Performance of DFIG showing a) Wind Velocity b)Generator Speed c) DC Link Voltage d) Rotor Current e) Optimum Power f) Actual Stator power g) Reference reactive power h)Actual reference power

7.7.5 Performance of DFIG during Line to Ground Fault for Ramp change in wind Speed using ANFIS Controller



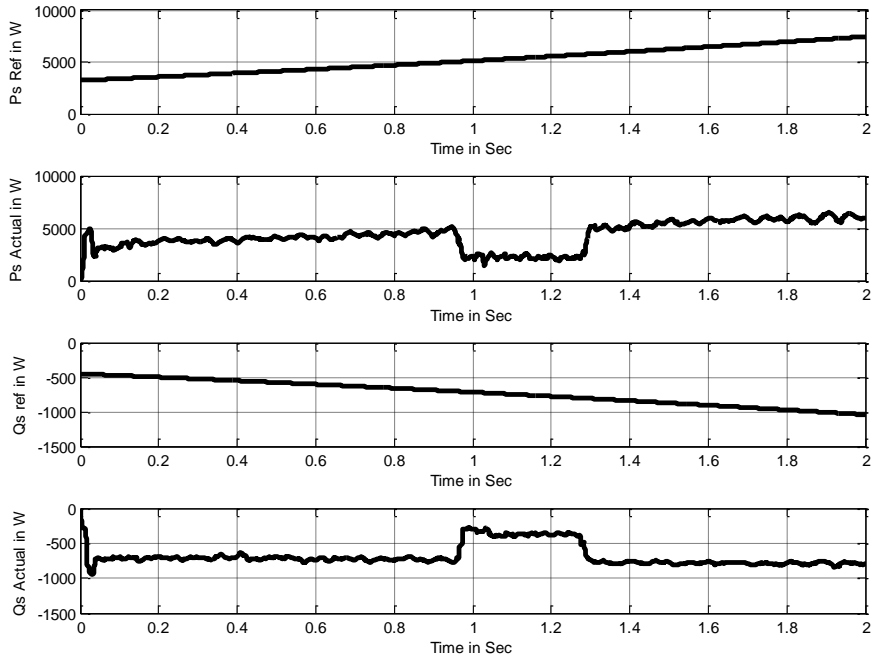
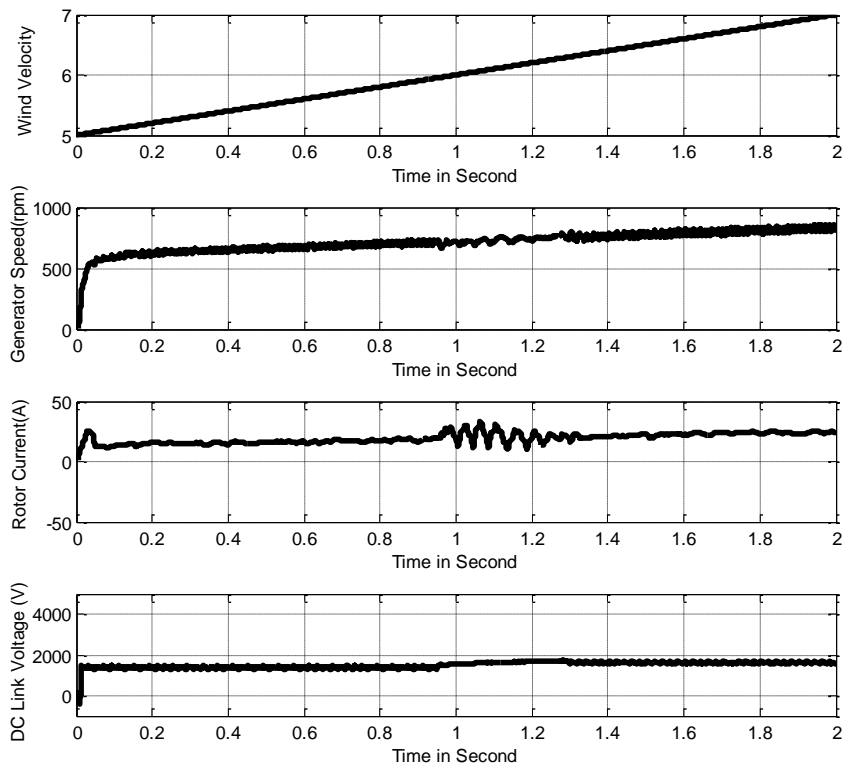


Figure 7.38: Performance of DFIG showing a) Wind Velocity b)Generator Speed c) DC Link Voltage d) Rotor Current e) Optimum Power f) Actual Stator power g) Reference reactive power h)Actual reference power.

7.7.6 Performance of DFIG during Line to Line Fault for ramp change in wind Speed using ANFIS Controller



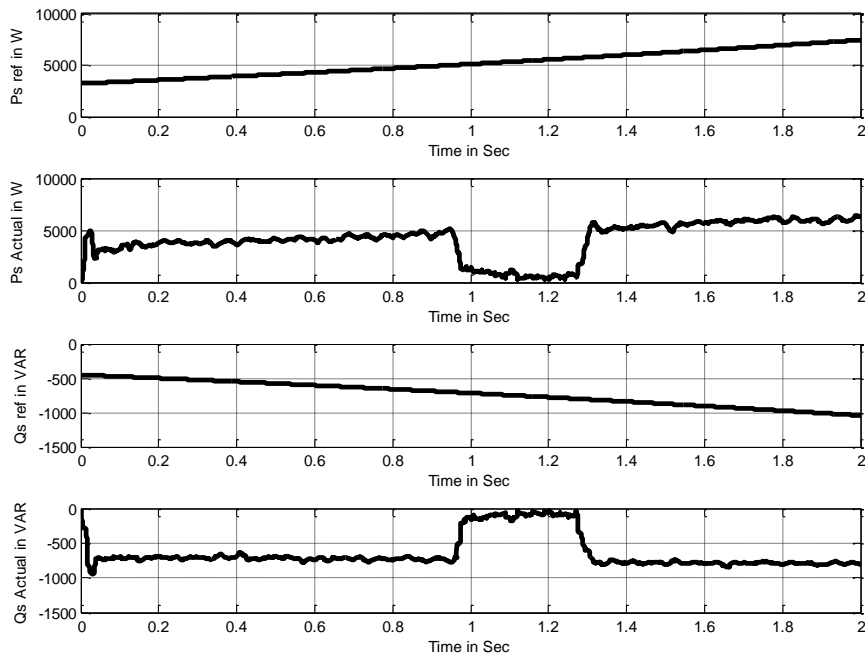
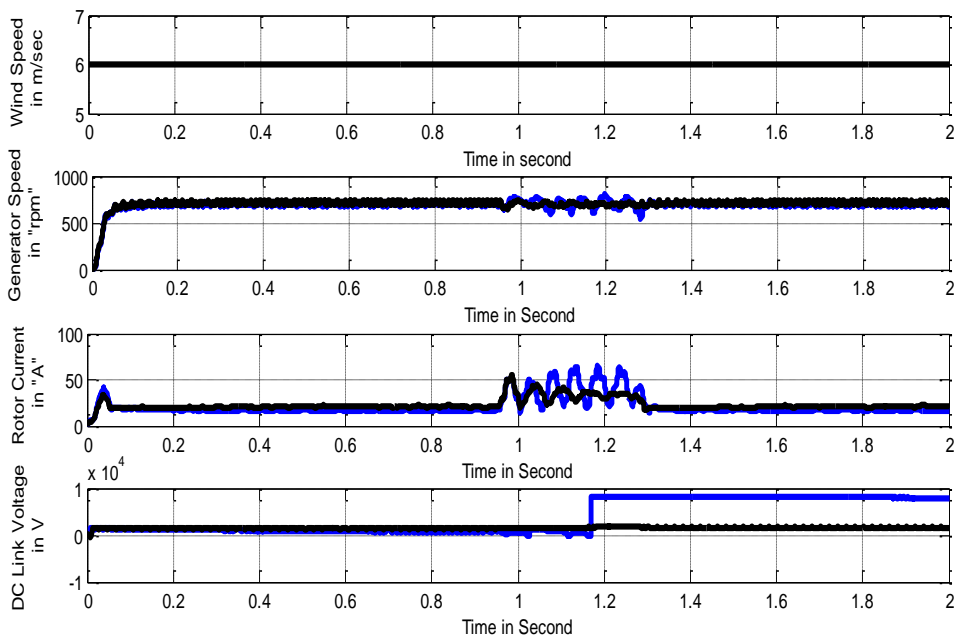


Figure 7.38: Performance of DFIG showing a) Wind Velocity b)Generator Speed c) DC Link Voltage d) Rotor Current e) Optimum Power f) Actual Stator power g) Reference reactive power h)Actual reference power.

7.8 Comparative Analysis of PI Controller and Neural Network Controller(black line –ANN controller, Blue line-PI controller)

7.8.1 During Line to Line Fault at Constant Wind Velocity (6m/sec)



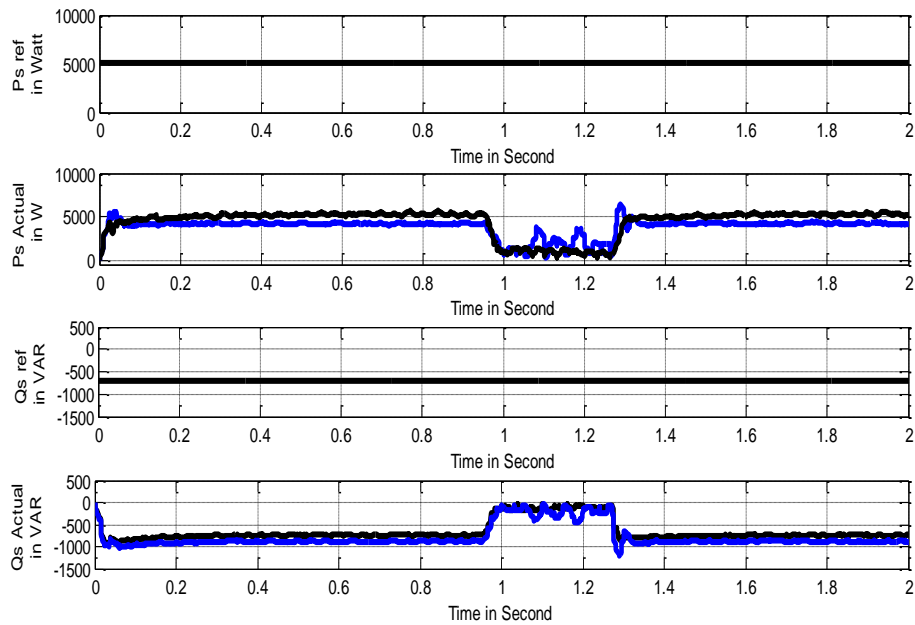
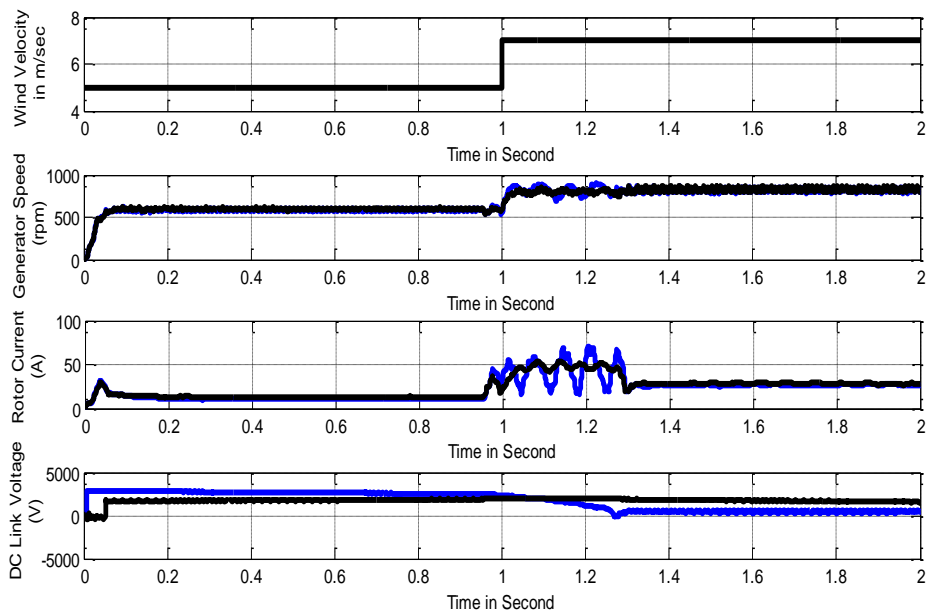


Figure 7.39: Comparative analysis of performance of DFIG showing comparison of a) Wind Velocity b)Generator rotor Speed c) Rotor current d) DC link Voltage e) Reference active Power during fault using PI and ANN Controller f)Actual stator active power g)reference stator reactive power and h) actual reactive power.

7.8.2 Performance during Line to Line Fault for Step Change of Wind Velocity (5m/sec to 7m/sec)



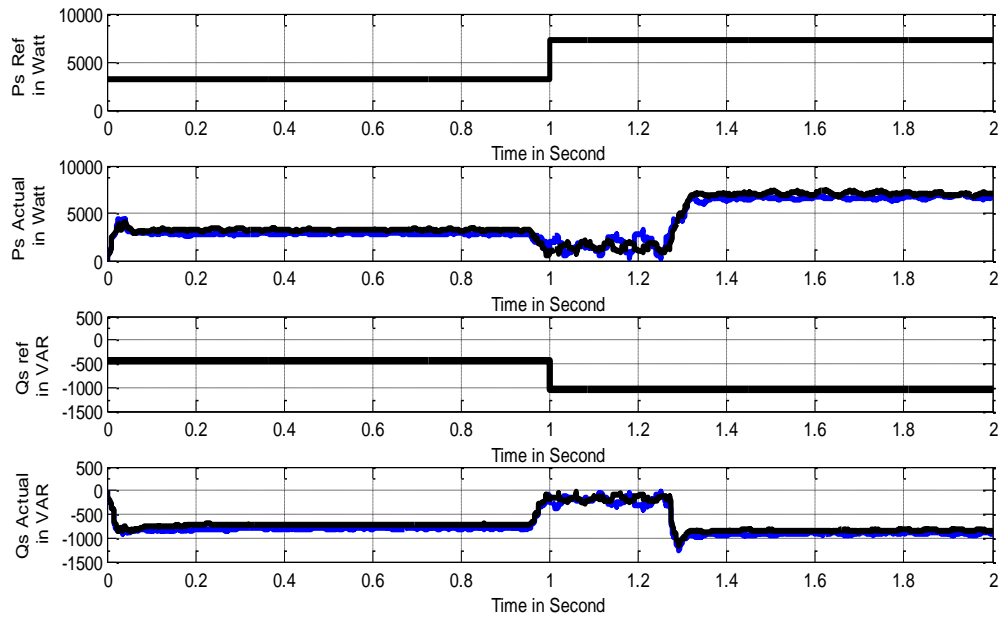
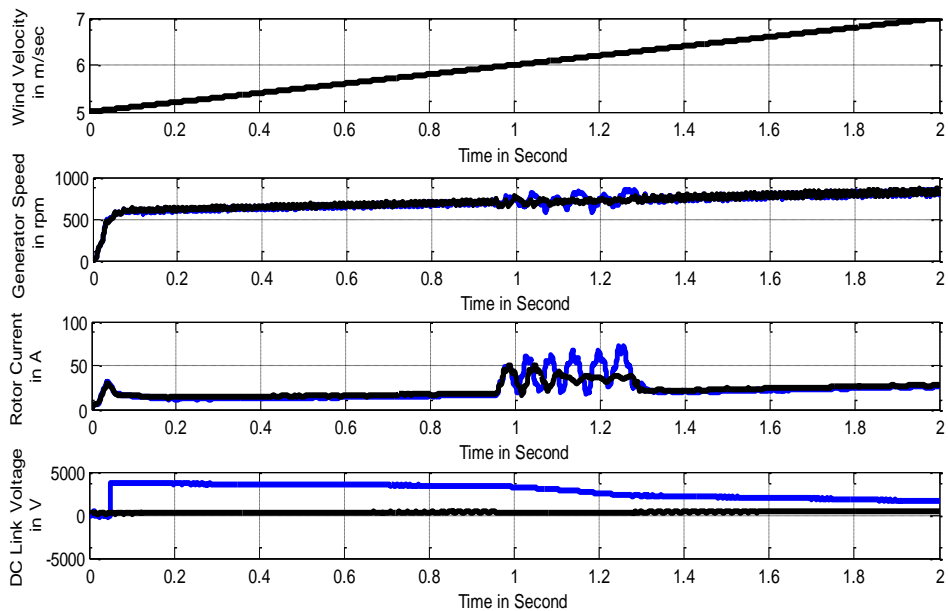


Figure 7.39: Comparative analysis of performance of DFIG showing comparison of a) Wind Velocity b)Generator rotor Speed c) Rotor current d) DC link Voltage e) Reference active Power during fault using PI and ANN Controller f)Actual stator active power g)reference stator reactive power and h) actual reactive power.

7.8.3 Performance during (L-L) ramp change of Wind Velocity (5m/sec to 7m/sec)



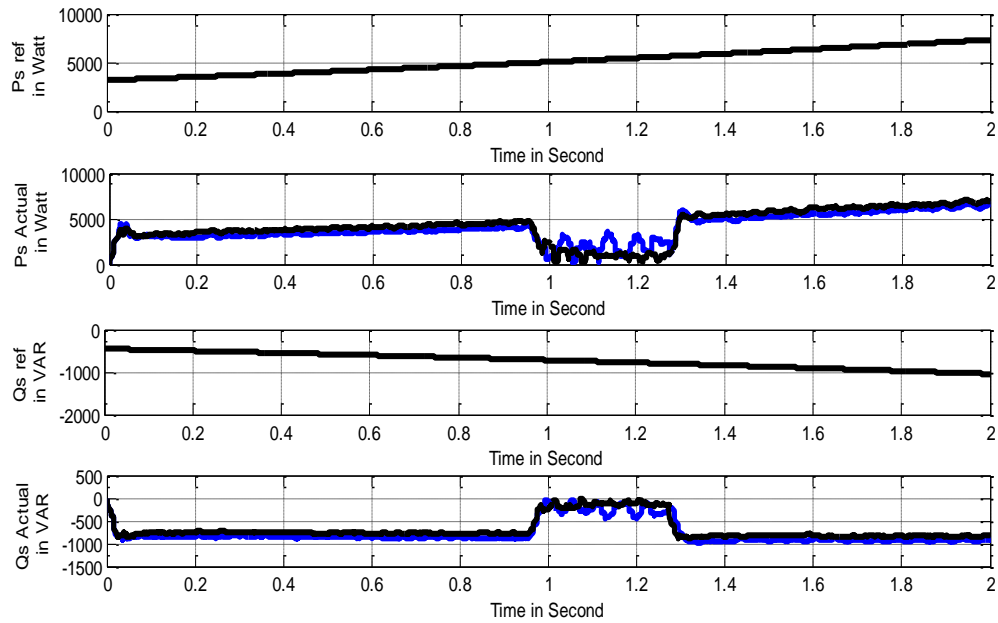


Figure 7.40: Comparative analysis of performance of DFIG showing comparison of a) Wind Velocity b) Generator rotor Speed c) Rotor current d) DC link Voltage e) Reference active Power during fault using PI and ANN Controller f) Actual stator active power g) reference stator reactive power and h) actual reactive power.

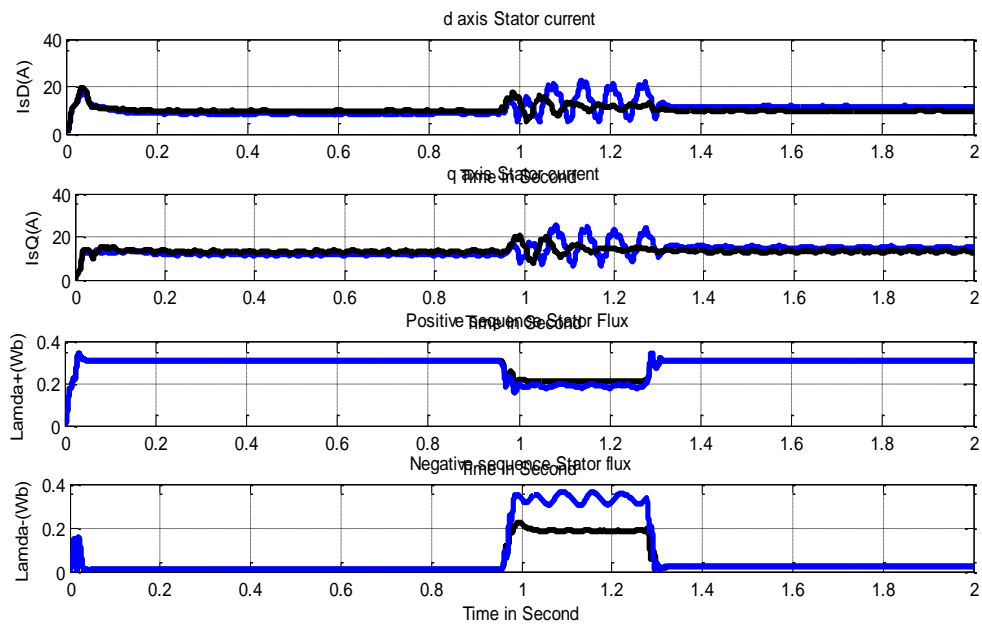


Figure 7.41: Comparative analysis of performance of DFIG showing comparison of a) d and q axis stator current b) Positive and Negative Sequence stator flux.

Observation:

It is observed that the negative sequence flux reduced to a great extent by the aid of an ANN controller. The fluctuations in Stator current is also reduced to a great extent. The comparative analysis of the performance of DFIG shows that the Neural Network controller reduces the

transients in Rotor current, Stator Active Power, DC link Voltage, Generator Speed to a great extend as compared to the Conventional PI controller.

7.9 Comparative Analysis of Performance between ANFIS Controller and Neural Network based Controller.(blue-ANFIS controller, Black-ANN controller)

7.9.1 Performance Comparison at Constant Wind Velocity(6m/sec) for (LL fault)

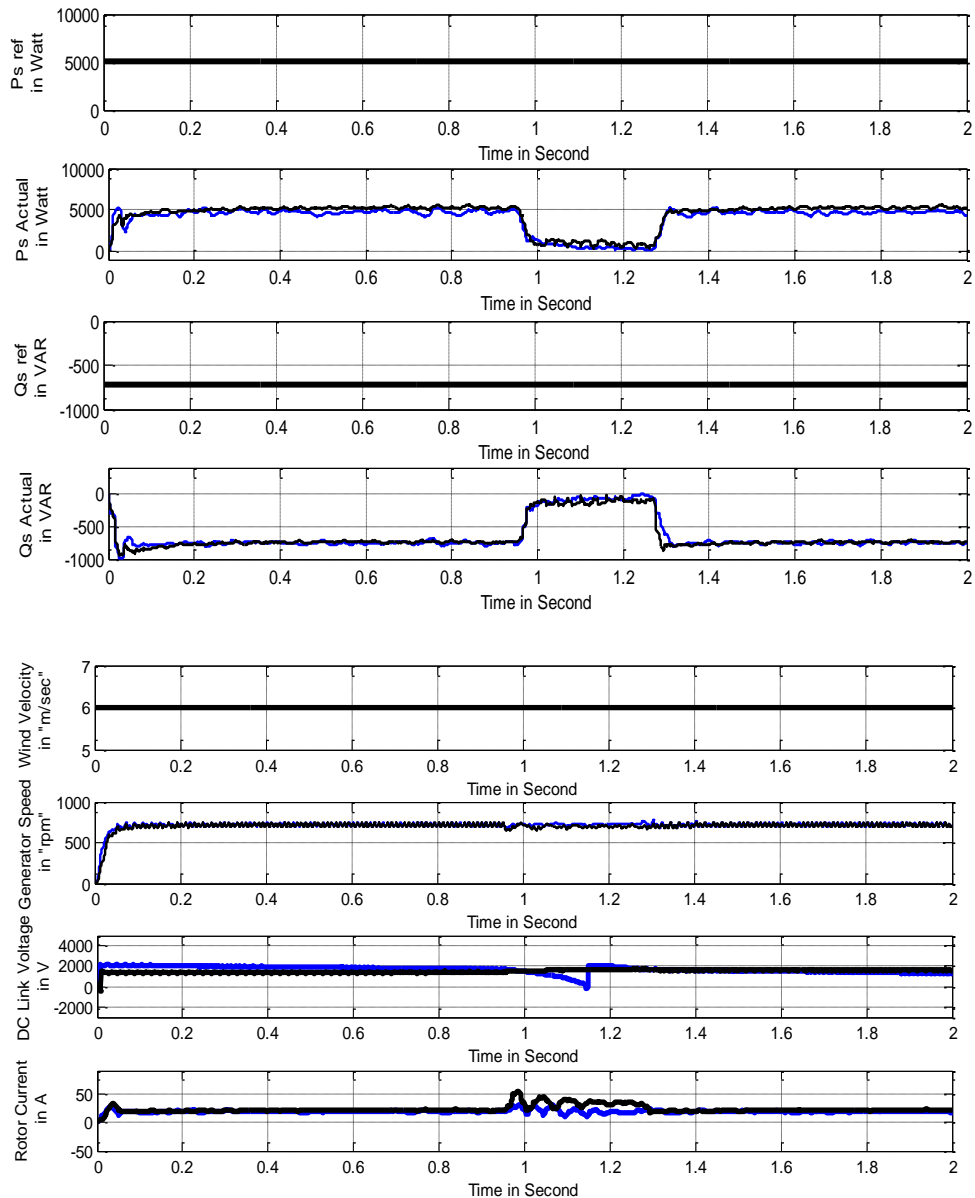


Figure 7.42: Comparative analysis of performance of DFIG showing comparison of a) Wind Velocity b)Generator rotor Speed c) Rotor current d) DC link Voltage e) Reference active Power during fault using PI and ANN Controller f)Actual stator active power g)reference stator reactive power and h) actual reactive power.

7.9.2 Performance Comparison of DFIG for Step change of Wind Velocity (5m/sec to 7m/sec) (Line to Line Fault)

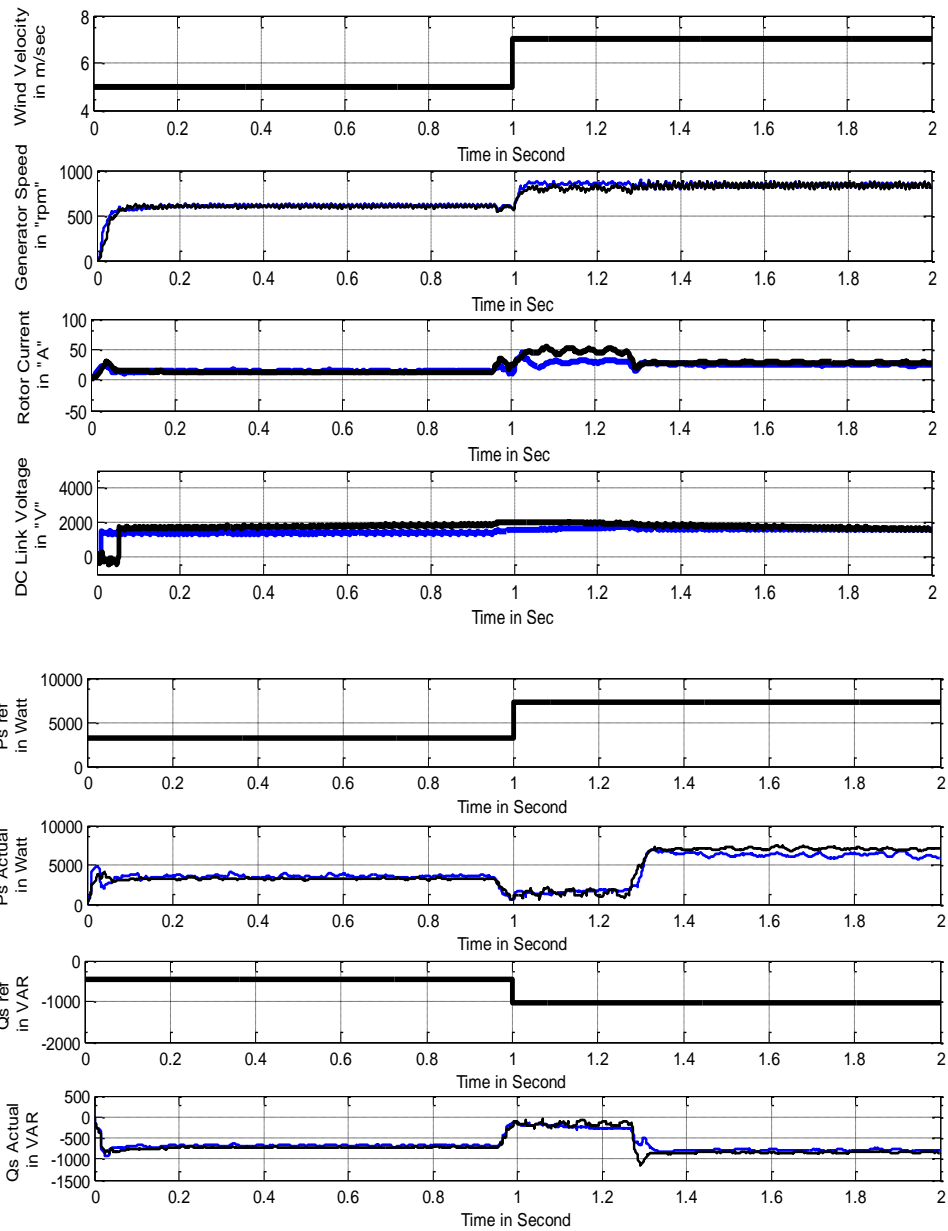


Figure 7.43: Comparative analysis of performance of DFIG showing comparison of a) Wind Velocity b) Generator rotor Speed c) Rotor current d) DC link Voltage e) Reference active Power during fault using PI and ANN Controller f) Actual stator active power g) reference stator reactive power and h) actual reactive power.

7.9.3 Performance Comparison of DFIG for Ramp change of wind Velocity (5m/se to 7m/sec) (LL fault)

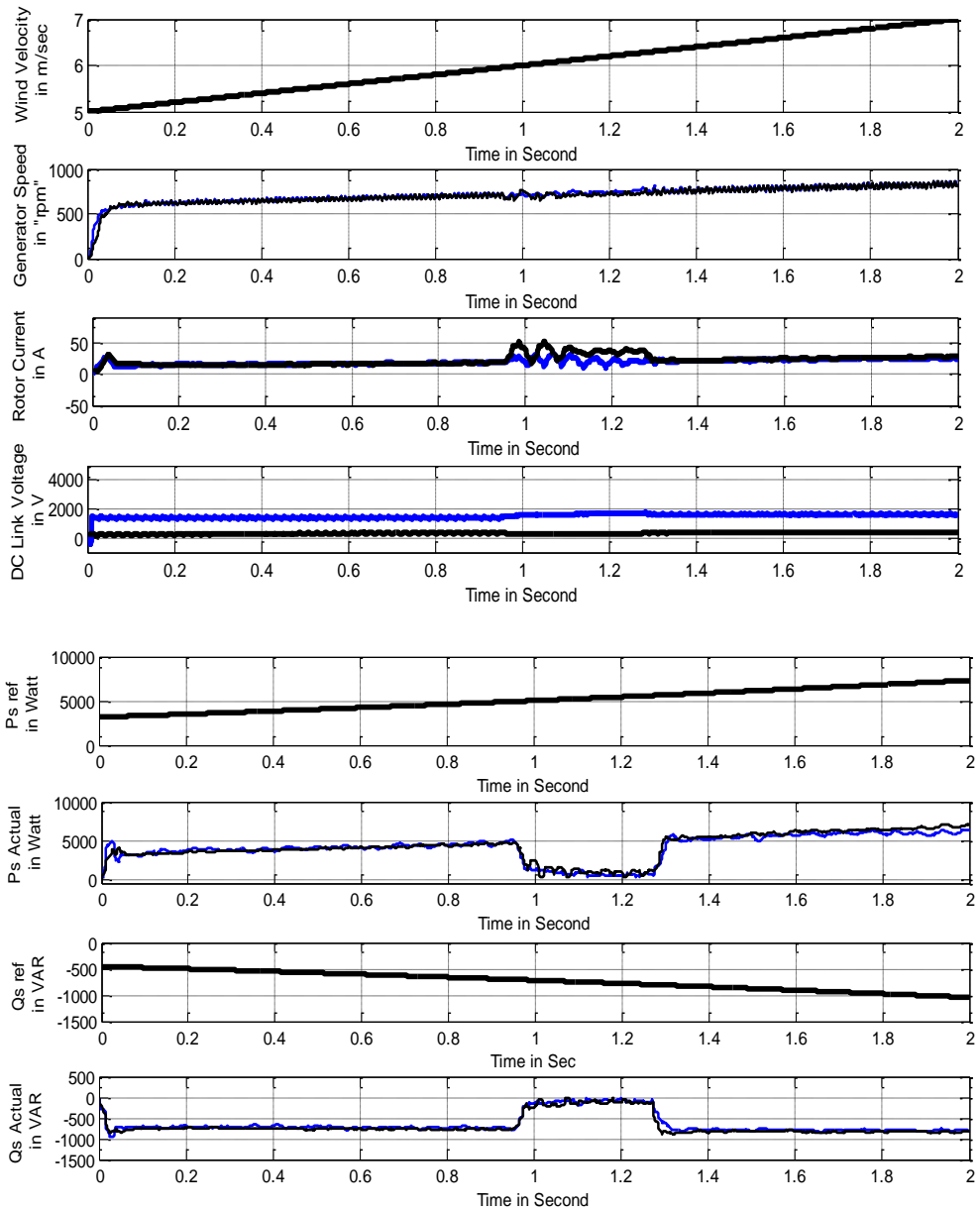


Figure 7.42: Comparative analysis of performance of DFIG showing comparison of a) Wind Velocity b)Generator rotor Speed c) Rotor current d) DC link Voltage e) Reference active Power during fault using PI and ANN Controller f)Actual stator active power g)reference stator reactive power and h) actual reactive power.

7.10 Performance Comparison between PI Controller and Neural Network based Controller (LG fault)

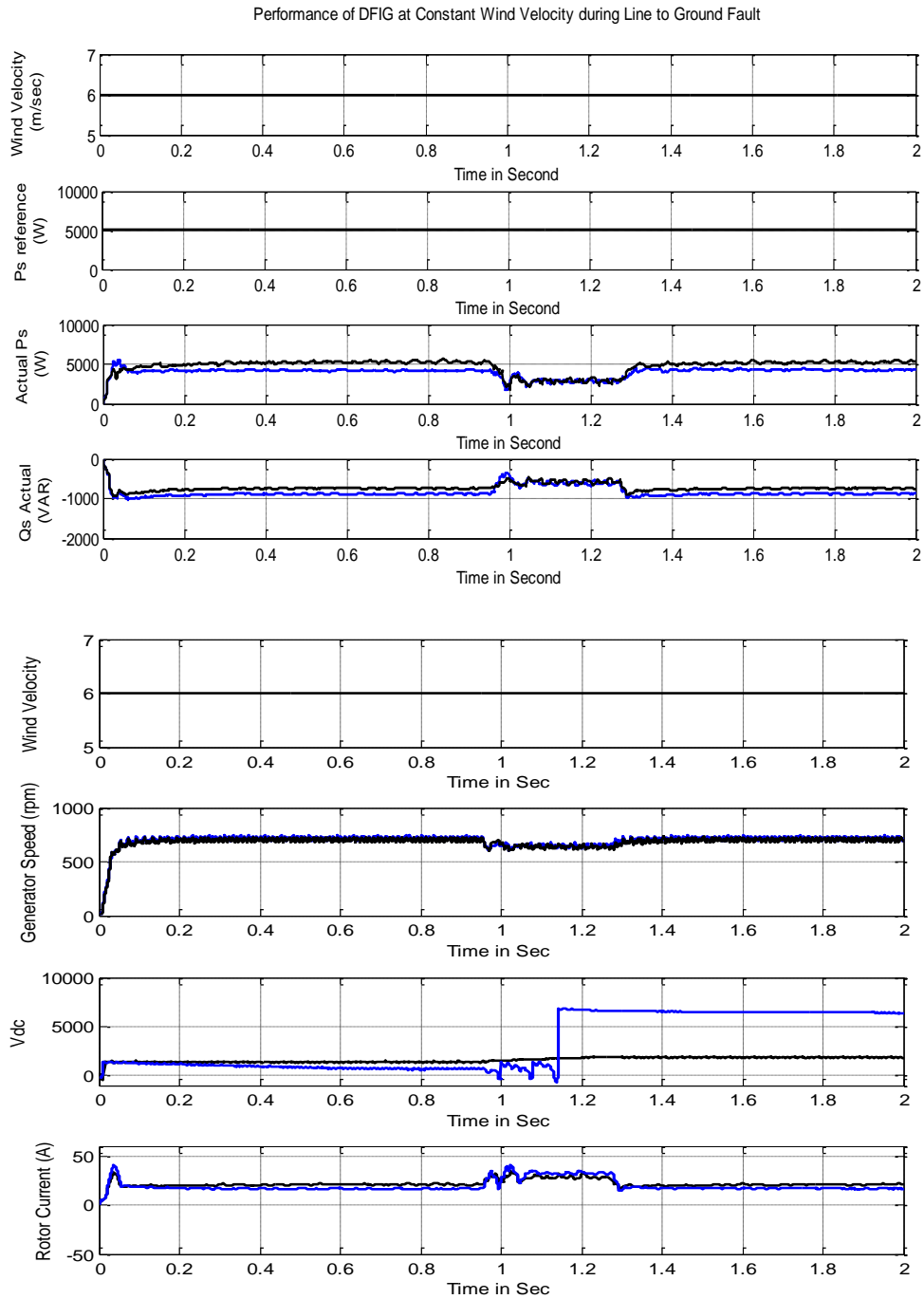


Figure 7.43: Comparative analysis of performance of DFIG showing comparison of a) Wind Velocity b) Generator rotor Speed c) Rotor current d) DC link Voltage e) Reference active Power during fault using PI and ANN Controller f) Actual stator active power g) reference stator reactive power and h) actual reactive power.

OBSERVATIONS:

- A fault is created from 0.9 sec to 1.3 sec where $V_a=0$
- During fault Active Power reduces and there is great fluctuations
- DC link Voltage increases
- There is fluctuation in generator Speed
- Rotor Current increases and fluctuates

7.11 Performance of DFIG during Symmetrical Voltage dips of 15% using ANN controller

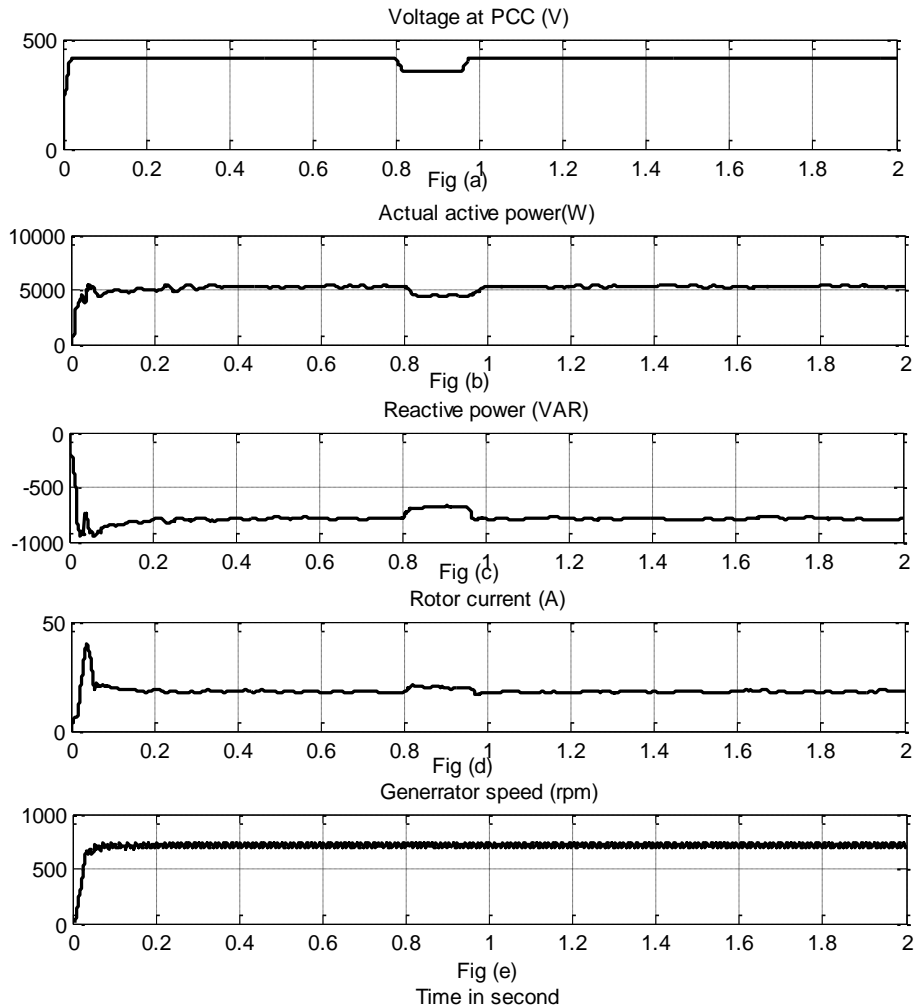


Figure 7.44: Response of DFIG using ANN controller for 15% symmetrical voltage dip showing i) Voltage at PCC ii) stator active power iii) stator reactive power iv) rotor current v) generator speed vi) DC link voltage

This system was studied for both PI and ANN controllers. Both PI controller and ANN controller response was almost stable for this voltage dip. The response for ANN controller is only presented. During fault the active power decreases (fig b). The reactive power increases to feed to the grid (fig c). Rotor current increases slightly (fig d) and generator speed is almost constant (fig e).

7.12 Performance of DFIG for symmetrical voltage dips of 85% using PI controller

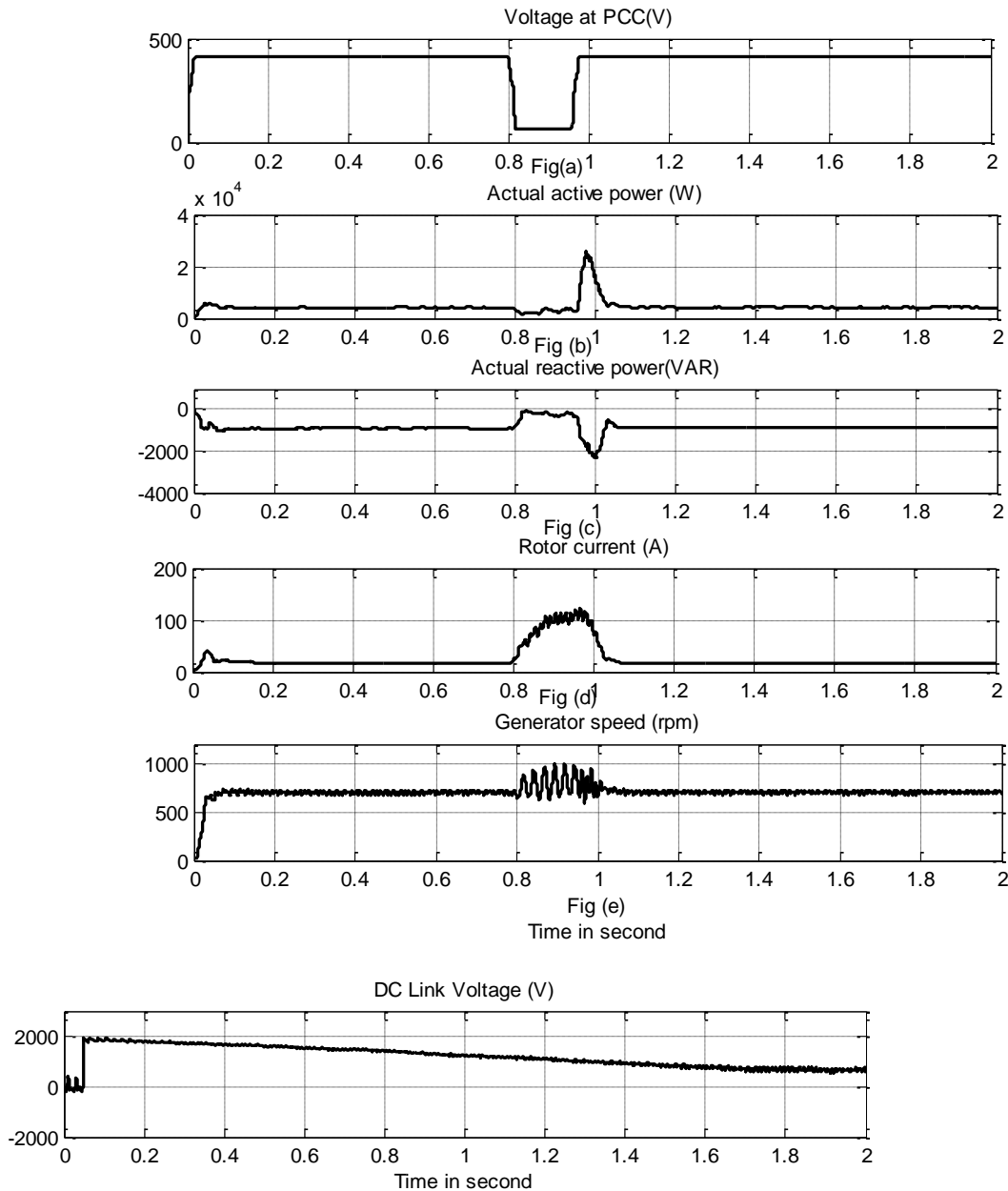


Figure 7.45: Response of DFIG using PI controller for 85% symmetrical voltage dip showing i) Voltage at PCC ii) stator active power iii) stator reactive power iv) rotor current v) generator speed vi) DC link voltage

Observation:-The response of actual stator active power shows immensely increased transients level (fig b). According to grid codes the active power generation reduces and is proportional to the voltage available. Reactive power is feed to the grid during fault decreases (fig c). Rotor current exceeds 4 times the rated rotor current fig (d). Generator speed fluctuations also increase (e). This is due to the fact that when the stator voltage drops the flux reduces and negative sequence flux increases rotating in $-\omega_s$ which cuts the rotor conductor at twice the speed which

cause the rotor overcurrent and increase in generator speed. . DC link voltage takes time to stabilize to reference value (=550V) (fig f).

7.13 Performance of DFIG for symmetrical Voltage dip of 85% using ANN controller

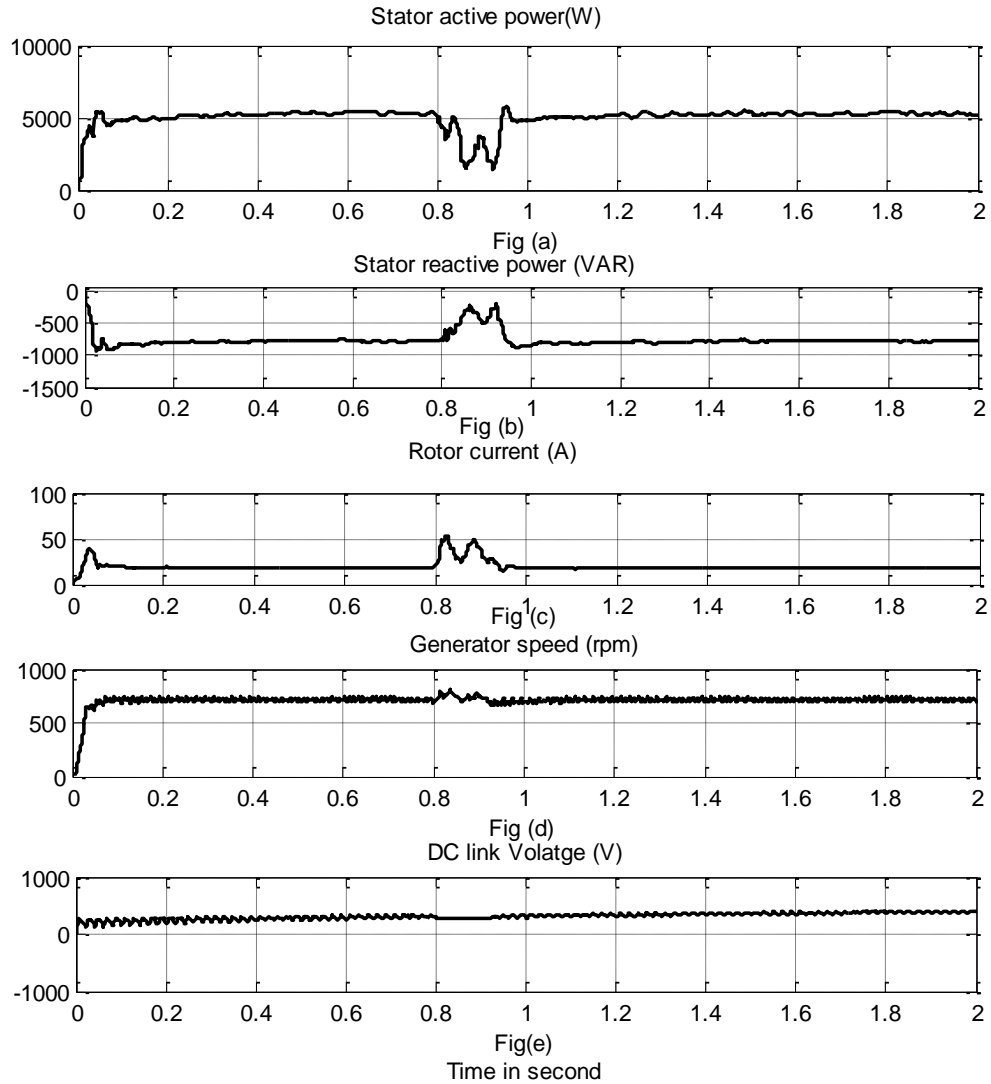


Figure 7.46: Response of DFIG using ANN controller for 85% symmetrical voltage dip i)stator active power ii) stator reactive power ii)rotor current iv)generator speed v)DC link voltage

Compared to figure (8.45) the performance improves to great extent. The sharp transients in generated active power reduce to permissible limit (fig a). During normal operation stator active power is tracking the reference active power (almost equals 5KW). The reactive power also increases to meet the grid requirement (fig b). It is evident from the response obtained that with the proposed intelligent controller as RSC is not disconnected so it will provide reactive power to the grid during fault and after the clearance of fault the voltage again restores back. The rotor overcurrent is limited 2 times the rated rotor current (fig c). The generator speed fluctuation

decreases to safe limit (fig d). DC link voltage is almost constant within 2.5 of rated value (fig e).

7.14 Performance of DFIG for symmetrical Voltage dip of 85% using ANFIS controller

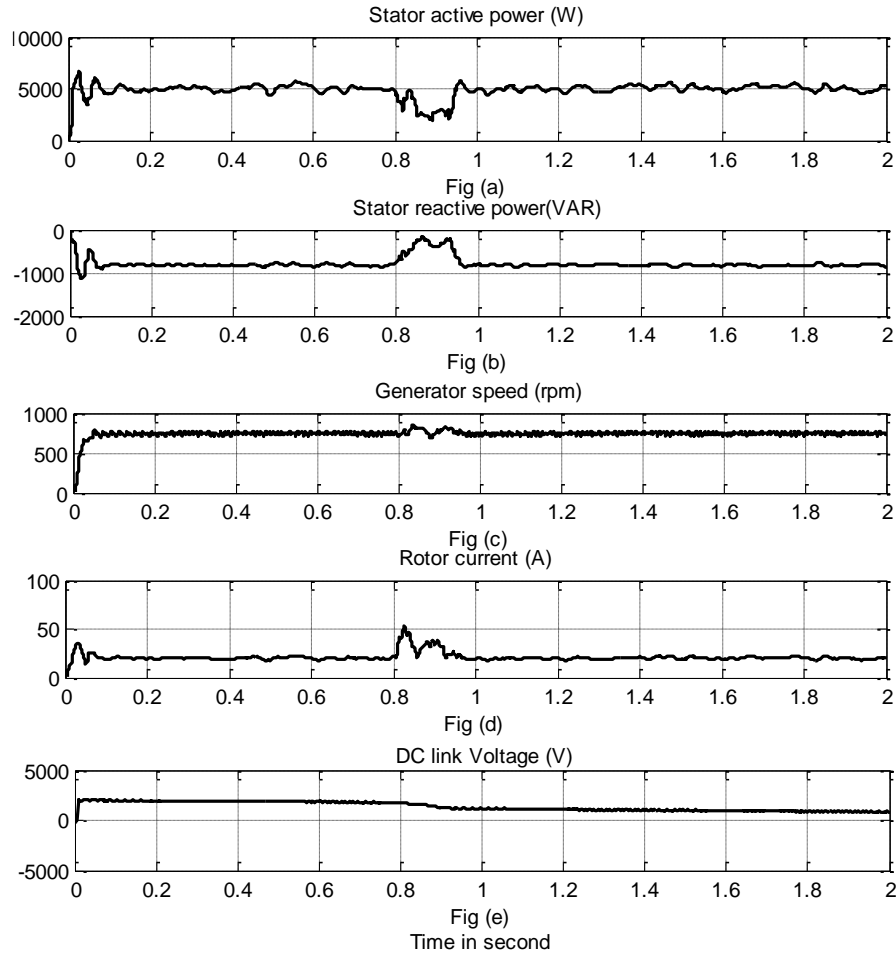


Figure (7.47) shows the generated response of DFIG for 85% symmetrical voltage dip using ANFIS controller showing i)stator active power ii) stator reactive power ii)rotor current iv)generator speed v)DC link voltage.

Observation: - Using ANFIS controller the stator active power fluctuations reduces during fault (fig a). The reactive power requirement is improved (fig b).Generator speed fluctuations are reduced considerably (fig c).The rotor overcurrent is further decreased with compared to ANN controller (fig d). DC link voltage is almost constant (fig e).

7.15 Performance Response of DFIG during Single Line to ground fault using PR Controller

Observation-

- Active Power fluctuation reduces and restore to its reference level
- DC link Voltage remains almost Constant during Faults
- Rotor Current Fluctuation is also less
- Generator Speed fluctuation also reduces.

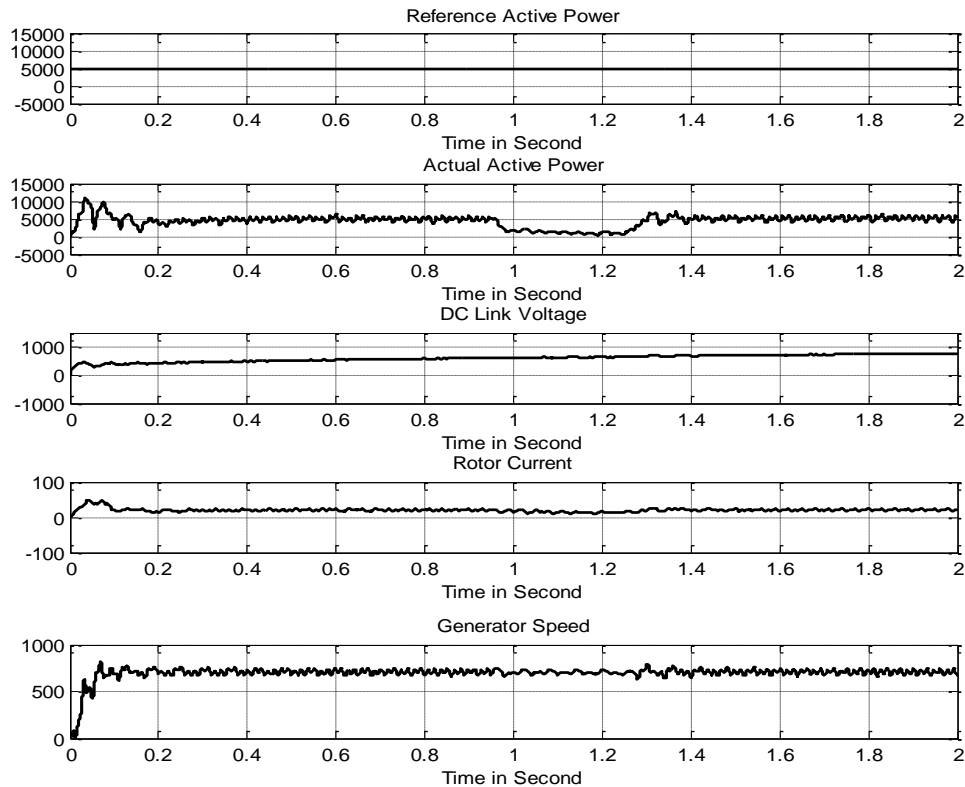


Figure 7.48: Performance of DFIG using PR controller showing a) reference stator active power b) actual stator active power c) DC link Voltage d) rotor current e) generator speed.

Table 7.1: Comparative data analysis

Parameters during Fault	PI Controller	ANN Controller	ANFIS Controller
Maximum Rotor Current	65.2708 A	54.64 A	33.58 A
Maximum Sator current	Ia = 25.7036 A Ib=29.2653 A Ic= 36.8640 A	27.2005 26.6870 29.1981	25.23A 20.68A 29.9A
Negative Sequence flux	0.345	0.2	0.349
THD	37%	10.5%	16%

7.16 Discussion

In DFIG configuration, the stator is directly connected to the grid. The effect of an abrupt drop of the grid voltage will directly appear on the stator terminals of DFIG. As the voltage is reduced the positive sequence flux also reduces. According to the law of constant flux, additional negative-sequence and transient DC flux components in the stator flux will appear to guarantee the total stator flux constancy. This negative sequence flux rotates in opposite direction unlike positive sequence flux and hence cuts the rotor conductors in twice the speed, resulting in a large EMF induction in the rotor circuit thereby causing rotor over-currents. This rotor overcurrent has to be pumped out to the grid by the DC link capacitor and GSC. But the entire current cannot be pumped out and hence DC link capacitor voltage increases. Besides this there are oscillations in electromagnetic torque, active power. According to IEC grid code there is also reactive power requirement to the grid during fault which has to be maintained by the WTDFIG. Thus this negative and DC component of stator flux has to be suppressed to eliminate its further effect.

A new method is proposed to control the rotor-side converter so that the rotor current contains components to oppose the undesired components in the stator-flux linkage. Fast observation of the stator-flux linkage components is essential to the control, which effectively constrains the rotor current given the voltage capability of the converter.

The rotor-side converter independently controls the active and reactive power flow by indirectly controlling the d and q axis rotor currents. An appropriate control of the rotor-side converter allows the magnetization of the generator through the rotor winding.

The grid-side converter keeps the DC voltage regulated and thus ensures the grid side converter operation with unity power factor, so the total reactive power exchange with the grid is made only through the stator of the generator and not through the rotor side. Otherwise there will be great voltage drop.

The system is designed and controlled with Neural Network based controller in such a way that the negative sequence component of the stator flux is reduced considerably to avoid its undesirable effect on the rotor side while keeping the positive-sequence component of the stator flux proportion to the positive-sequence component of the remaining grid flux to eliminate the transient DC flux component and to restrain the surplus active power flowing into the common dc link. As a result, in order to avoid the

appearance of the transient DC flux component and provide the required system response, the positive-sequence stator flux controller must be carefully tuned by controlling the reactive Power in the stator side using reactive power controller. The system is also tested with ANFIS controller.

The Neural Network controller improves the performance of DFIG during the grid fault conditions by controlling the active and reactive power of the DFIG during and after fault. As per the Indian grid codes Wind farm generators should have fault ride through capability by reducing the generated active power smoothly without pulsation and provide sufficient reactive power without drawing from the grid. The system is tested under unsymmetrical fault condition creating L-L and L-G fault. It is observed from the results that the stator active power is smoothly controlled. The pulsations that were present in generated active Power using PI controller are reduced to great extend. The rotor over current is also reduced. DC link Voltage is maintained almost constant (550 V) which tends to increase in case of PI controller. Less fluctuations and less overshoot in generated speed is also observed. If the performance of DFIG using both ANN and ANFIS controller are compared then it shows that with the aid of ANFIS controller the performance of DFIG becomes even better and smoother than the ANN controller during the fault ride through conditions. The harmonics in rotor current, active power, generator speed, and DC link voltage are greatly reduced giving a better performance. Also the generated active power tracks the reference power more closely for AI controlled controllers compared to the PI controller resulting in maximizing power supply in stator side. The negative sequence flux is sufficiently controlled which helps to control the over currents in rotor circuit.

Chapter 8

CONCLUSION

8.1 Conclusion

In this research work an AI technique based active and reactive power controller is proposed on rotor side converter (RSC) and voltage controller on grid side converter (GSC) to control the performance of doubly-fed induction generator (DFIG) under highly varying operating conditions especially during unsymmetrical faults. The conventional active and reactive Power PI controllers on the RSC and PI DC link Voltage controller on GSC side have been replaced by the ANN and then ANFIS based controllers. The AI based controllers are trained using the input and output data obtained from the conventional PI controller for transient simulations carried out for a set of different operating conditions. This controller is tested for various wind and unsymmetrical fault conditions especially during line to line fault and Line to ground fault and also for symmetrical voltage drop of 15% and 85%. The ANN and ANFIS based active and reactive power controller is used in lieu of the conventional PI controller and a comparative analysis was also carried out using all the types of controllers. The analysis shows that the performance of the DFIG improves significantly using AI based controllers. The ANN controller trained in Levenberg–Marquardt back propagation algorithm significantly reduces the active power oscillations, electromagnetic torque oscillations, rotor over currents, Stator current fluctuations and maintain DC link voltage constant and power factor at unity. The ANN based controller also meet the grid codes of IEC by providing reactive power requirement to the grid during fault conditions. This is ensured by the fact that the reactive power exchange is done only on the stator side and not on the grid side converter. The system is then tested with ANFIS controller tuned with hybrid algorithm. The results show that ANFIS controller further reduces the rotor over-currents and stator active power fluctuations during faults.

8.2 FUTURE SCOPE

Other optimisation techniques such as Genetic Algorithm, Bacteria foraging technique etc can be used to design the controller and more smooth control of the wind driven DFIG can be expected. Hardware implementation can be done to test the simulated results. Results can be studied again by putting loads on the grid side.

References:

- Bimal K. (2002) Bose "Modern Power Electronics and AC Drives" printice Hall PTR. ISBN 0-13-016743-6.
- Chowdhury BH and Chellapilla S. (2006) Double-fed induction generator control for variable speed wind power generation. *Electric Power Systems Research* 76: 786-800.
- Ekanayake J, Holdsworth L and Jenkins N. (2003) Comparison of 5th order and 3rd order machine models for doubly fed induction generator (DFIG) wind turbines. *Electric Power Systems Research* 67: 207-215.
- Feng Y, Lin H, Ho S, et al. (2015) Overview of wind power generation in China: Status and development. *Renewable and Sustainable Energy Reviews* 50: 847-858.
- Flannery PS and Venkataramanan G. (2008) A fault tolerant doubly fed induction generator wind turbine using a parallel grid side rectifier and series grid side converter. *IEEE transactions on power electronics* 23: 1126-1135.
- Hasanien HM and Al-Ammar EA. (2012) Dynamic response improvement of doubly fed induction generator-based wind farm using fuzzy logic controller. *Journal of Electrical Engineering* 63: 281-288.
- He Y and Hu J. (2008) DFIG wind power generation systems during unbalanced network fault: Analysis and operation. *Electrical Machines and Systems, 2008. ICEMS 2008. International Conference on. IEEE*, 2331-2336.
- Hu J-b and He Y-k. (2007) Multi-frequency proportional-resonant (MFPR) current controller for PWM VSC under unbalanced supply conditions. *Journal of Zhejiang University-Science A* 8: 1527-1531.
- Hu J-b, He Y-k and Nian H. (2007) Enhanced control of DFIG-used back-to-back PWM VSC under unbalanced grid voltage conditions. *Journal of Zhejiang University-Science A* 8: 1330-1339.
- Hu J-b, Zhang W, Wang H-s, et al. (2009) Proportional integral plus multi-frequency resonant current controller for grid-connected voltage source converter under imbalanced and distorted supply voltage conditions. *Journal of Zhejiang University-Science A* 10: 1532-1540.
- Jabr HM, Lu D and Kar NC. (2011) Design and implementation of neuro-fuzzy vector control for wind-driven doubly-fed induction generator. *IEEE Transactions on Sustainable Energy* 2: 404-413.
- Karimi-Davijani H, Sheikholeslami A, Livani H, et al. (2009) Fuzzy logic control of doubly fed induction generator wind turbine. *World Applied Sciences Journal* 6: 499-508.
- Kusagur A, Kodad S and Ram BVS. (2010) Modeling, design & simulation of an adaptive neuro-fuzzy inference system (ANFIS) for speed control of induction motor. *International Journal of Computer Applications* 6: 29-44.
- Le V, Li X, Li Y, et al. (2016) An innovative control strategy to improve the fault ride-through capability of DFIGs based on wind energy conversion systems. *Energies* 9: 69.
- Lima FK, Luna A, Rodriguez P, et al. (2010) Rotor voltage dynamics in the doubly fed induction generator during grid faults. *IEEE transactions on power electronics* 25: 118-130.
- Ling Y. (2016) The fault ride through technologies for doubly fed induction generator wind turbines. *Wind Engineering* 40: 31-49.
- López J, Gubía E, Olea E, et al. (2009) Ride through of wind turbines with doubly fed induction generator under symmetrical voltage dips. *IEEE Transactions on Industrial Electronics* 56: 4246-4254.

- Mishra J, Hore D and Rahman A. (2011) Fuzzy logic based improved active and reactive power control operation of DFIG for wind power generation. *Power Electronics and ECCE Asia (ICPE & ECCE), 2011 IEEE 8th International Conference on*. IEEE, 654-661.
- Mokryani G, Siano P, Piccolo A, et al. (2012) A fuzzy logic controller to increase fault ride-through capability of variable speed wind turbines. *Applied Computational Intelligence and Soft Computing 2012*: 7.
- Pena R, Clare J and Asher G. (1996) Doubly fed induction generator using back-to-back PWM converters and its application to variable-speed wind-energy generation. *IEE Proceedings-Electric Power Applications* 143: 231-241.
- Phan V-T and Lee H-H. (2010) Enhanced proportional-resonant current controller for unbalanced stand-alone DFIG-based wind turbines. *Journal of Electrical Engineering and Technology* 5: 443-450.
- Seman S, Niiranen J and Arkkio A. (2006) Ride-through analysis of doubly fed induction wind-power generator under unsymmetrical network disturbance. *IEEE Transactions on Power Systems* 21: 1782-1789.
- Slootweg J, Polinder H and Kling W. (2001) Dynamic modelling of a wind turbine with doubly fed induction generator. *Power Engineering Society Summer Meeting, 2001*. IEEE, 644-649.
- Tapia A, Tapia G, Ostolaza JX, et al. (2003) Modeling and control of a wind turbine driven doubly fed induction generator. *IEEE Transactions on energy conversion* 18: 194-204.
- Vas P. (1990) *Vector control of AC machines*: Oxford University Press, USA.
- Vrionis TD, Koutiva XI and Vovos NA. (2014) A genetic algorithm-based low voltage ride-through control strategy for grid connected doubly fed induction wind generators. *IEEE Transactions on Power Systems* 29: 1325-1334.
- Wang Y and Xu L. (2007) Control of DFIG-based wind generation systems under unbalanced network supply. *Electric Machines & Drives Conference, 2007. IEMDC'07. IEEE International*. IEEE, 430-435.
- Wang Y, Xu L and Williams B. (2009) Compensation of network voltage unbalance using doubly fed induction generator-based wind farms. *IET Renewable Power Generation* 3: 12-22.
- Wessels C, Gebhardt F and Fuchs FW. (2011) Fault ride-through of a DFIG wind turbine using a dynamic voltage restorer during symmetrical and asymmetrical grid faults. *IEEE transactions on power electronics* 26: 807-815.
- Wu Z, Zhu C and Hu M. (2013) Improved control strategy for DFIG wind turbines for low voltage ride through. *Energies* 6: 1181-1197.
- Xiang D, Ran L, Tavner PJ, et al. (2006) Control of a doubly fed induction generator in a wind turbine during grid fault ride-through. *IEEE Transactions on energy conversion* 21: 652-662.
- Xu L. (2008) Coordinated control of DFIG's rotor and grid side converters during network unbalance. *IEEE transactions on power electronics* 23: 1041-1049.
- Xu L and Wang Y. (2007) Dynamic modeling and control of DFIG-based wind turbines under unbalanced network conditions. *IEEE Transactions on Power Systems* 22: 314-323.
- Yan Y, Wang M, Song Z-F, et al. (2012) Proportional-resonant control of doubly-fed induction generator wind turbines for low-voltage ride-through enhancement. *Energies* 5: 4758-4778.
- Yang L, Xu Z, Ostergaard J, et al. (2012) Advanced control strategy of DFIG wind turbines for power system fault ride through. *IEEE Transactions on Power Systems* 27: 713-722.
- Yao J, Li Q, Chen Z, et al. (2013) Coordinated control of a DFIG-based wind-power generation system with SGSC under distorted grid voltage conditions. *Energies* 6: 2541-2561.

- Yasa Y, Isen E, Sozer Y, et al. (2013) Analysis of doubly fed induction generator wind turbine system during one phase-to-ground fault. *Power Electronics and Applications (EPE), 2013 15th European Conference on*. IEEE, 1-8.
- Zarei ME and Asaei B. (2013) Combined vector control and direct power control methods for DFIG under normal and unbalanced and distorted grid voltage conditions. *Power Electronics, Drive Systems and Technologies Conference (PEDSTC), 2013 4th*. IEEE, 107-112.
- Zheng X and Guo D. (2011) A Novel Ride-through Control Strategy of DFIG Wind Generator under Grid Voltage Dip. *JOURNAL OF INFORMATION & COMPUTATIONAL SCIENCE* 8: 579-591.
- Zhou P, He Y and Sun D. (2009a) Improved direct power control of a DFIG-based wind turbine during network unbalance. *IEEE transactions on power electronics* 24: 2465-2474.
- Zhou Y, Bauer P, Ferreira JA, et al. (2009b) Operation of grid-connected DFIG under unbalanced grid voltage condition. *IEEE Transactions on energy conversion* 24: 240-246.

APPENDIX A

Rating of the Wind Turbine:

Power = 7.5 KW

Radius, R = 3.24 m.

Rated rotational speed=296 rpm.

Inertia, J = 7.5 Kg m²

Gear box ratio = 3

Damping coefficient = 0.01 Nm rad⁻¹

Air density, Row= 1.06 Kg/m³.

APPENDIX B

Wound rotor induction machine:

Power=7.5KW.

Stator voltage=415 V.

Rotor Voltage=440 V.

Rated stator current=19 A.

Rated rotor current=11 A.

$R_s=1.06$ ohm

$R_r=0.0399$ ohm

$L_s = 0.2065H$

$L_0 = 0.0664H$ (Referred to the rotor)

$L_r = 0.0810H$ (Referred to the rotor)

$L_m=0.0664$ ohm;

No. of poles, $p = 6$

Rated speed=1000 rpm.

Cut in wind speed =4m/s

Rated wind speed=7m/s

$X_{ls}=0.0300$ ohm;

$X_{lr}=0.3492$ ohm;

$X_m=2.3161$ ohm;

$L_{ls}=0.1401$ ohm;

$L_{lr}=0.0146$ ohm;

$R_g=0.1$ ohm;

*$C=2.4*10^{-3}$ F;*

*$L_g=12*10^{-3}$ H;*

General turn ratio, $n=0.3806$;

